SENSITIVITY CALCULATIONS FOR CONSERVATION LAWS WITH APPLICATION TO DISCONTINUOUS FLUID FLOWS

Justin Ronald Appel

Dissertation submitted to the Faculty of the
Virginia Polytechnic Institute and State University
in partial fulfillment of the requirements for the degree of

Doctor of Philosophy
in
Mathematics

Max D. Gunzburger, Chair
John A. Burns
Eugene M. Cliff
Terry L. Herdman
Janet S. Peterson

March 14, 1997
Blacksburg, Virginia

Keywords: Sensitivity Analysis, Numerical Analysis, Conservation Laws

Sensitivity Calculations for Conservation Laws with Application to Discontinuous Fluid Flows

Justin R. Appel

(ABSTRACT)

Flow sensitivities are the derivatives of the variables that describe the fluid flow with respect to the parameters that determine the fluid flow. Sensitivities are of interest in their own right and are also of use in flow optimization, control and design and in the calculation of perturbed flows. Problems arise in all sensitivity calculation methods in the presence of discontinuities and other complexities such as shock waves, contact discontinuities and rarefaction waves that commonly occur in super and hypersonic inviscid, compressible fluid flows. Flow sensitivities are calculated using finite difference quotients, automatic differentiation and the sensitivity equation method for a variety of numerical methods. Explanations for the inaccuracies arising in the numerical approximations and implications these inaccuracies have on different applications are discussed. Possible corrections for the inaccuracies are outlined.

This work received support from the Office of Naval Research under grant number N00014-93-1-1004, the Commonwealth of Virginia's Center for Innovative Technology and AeroSoft, Inc.

To my loving wife Jennifer,

may we grow old together.

ACKNOWLEDGEMENTS

I would like to thank the Office of Naval Research, the Commonwealth of Virginia's Center for Innovative Technology and AeroSoft, Inc. for providing support the last five years making this dissertation possible. I would also like to thank the Interdisciplinary Center for Applied Mathematics (ICAM) and the Air Force Center for Optimal Design And Control (CODAC) for the resources necessary to complete my research as well as a friendly working environment.

I would like to thank several specific people who supported me along the way:

- My friend and colleague John Burkardt, who made various attempts to help me retain my sanity throughout my graduate career and endured long discussions of sensitivities, ADIFOR and other trials of life.
- My parents Ron and Nancy Appel, who instilled in me the value of education and provided continual support and encouragement. They never asked, "Are you ever going to get a real job?", even though I know it came to mind and always urged me to excel at everything I attempted.
- My committee members, John Burns, Gene Cliff, Terry Herdman, and Janet Peterson, who freely offered their mathematical and scientific expertise and encouraged me at various steps throughout my career.

I would especially like to take this opportunity to thank my advisor Max Gunzburger who always believed in me and my mathematical abilities even though there were times I did not. He was always there to provide support and guidance as I encountered many different problems. I will always be grateful for the knowledge he has passed on to me and his friendship.

Finally, I would like to thank my wife, Jennifer Deang, who provided the encouragement, patience, love and strength for me to continue. She suffered through my mild paranoia and major stress with a continual smile even while preparing a dissertation of her own. This dissertation is as much a tribute to her strengths as it is to my abilities.

Contents

List of Figures

List of Tables

Chapter 1

Introduction

The seemingly straightforward task of approximating a perturbed flow solution using a base flow and a flow sensitivity is, in many senses, a very complex problem due to constraints imposed on the computational cost and accuracy of the method. Additionally, the presence of shock waves, contact discontinuities and rarefaction waves, all occurring in inviscid compressible fluid flows, increase the difficulty of the problem. The following work is an extension of research on the calculation of perturbed flows. It includes generalizations to hyperbolic equations and linear discontinuous coefficient hyperbolic equations. Similarly, generalizations have been made to other application areas such as optimization and control with the realization that improvements in the perturbed flow calculation process will also enhance other areas. The focus and research has been on the definition, calculation, approximation and utilization of flow sensitivities in discontinuous fluid flows.

1.1 Sensitivity Analysis

Flow sensitivities, in the most general sense, are nonstandard derivatives. They are the derivatives of the output solution with respect to the input parameters. Sensitivities are considered nonstandard because the input parameters are usually implicit parameters such as wing shape or forebody bluntness as opposed to more standard spatial and temporal derivatives. Although these ideas seem fairly standard, Example 1 demonstrates a fundamental difference to the classical spatial derivatives.

Example 1 (Flow Sensitivity) *Calculate the flow sensitivity of the fluid flow with respect to the shape of the domain.*

Although this seems arbitrary, it is the basis for nearly every aerodynamic shape optimization problem. The example at hand is much too general and has no quantitative method to describe the shape of the domain. A revised Example 2 is given below.

Example 2 (Revised Flow Sensitivity) *Consider a cylinder of radius, r, that has a* 90° *turn and fluid flowing through it with an inflow velocity given by u_{inflow}. Calculate the flow sensitivity of the fluid flow,* $\mathbf{U}$*, through the tube with respect to both the radius, r, and the inflow velocity profile,* i.e.*, calculate the following two quantities:*

$$\begin{aligned} \frac{\partial \mathbf{U}}{\partial r} &= \textit{Derivative of the solution with respect to the cylinder radius} \\ \frac{\partial \mathbf{U}}{\partial u_{inflow}} &= \textit{Derivative of the solution with respect to the inflow velocity.} \end{aligned}$$

The revised example gives a much clearer idea of flow sensitivities and their complex nature. Sensitivities are important because they give information about what variables are changing, where these variables are changing and finally how they are changing or the rate of change of each variable with respect to different parameters. There are many methods of calculating sensitivities and also many possible applications for flow sensitivities.

Sensitivity calculation methods include finite difference quotient methods; semi-analytic methods such as automatic differentiation; and the sensitivity equation method, as well as others. These different methods can all be characterized into either a "discretize-then-differentiate" or the "differentiate-then-discretize" class. Due to the strengths and weaknesses of the different sensitivity calculation methods, there are factions in the research arena supporting each of the methods. Hence, several prominent methods will be considered in the coming chapters. Sensitivity calculation methods will be discussed in detail in Chapter 2 and Chapter 5 and applied to different fluid flow problems in Chapter 3, Chapter 5, Chapter 6 and Chapter 9. The context in which sensitivities are used has a big influence on the determination of which type of sensitivity calculation method is appropriate. For this reason, three different applications of sensitivities are considered in the context of fluid flow. First, the flow sensitivities are used in an optimization or control type setting. These problems can usually be written as a minimization problem and the flow sensitivities are used to help determine the gradient of a cost functional. Second, flow sensitivities are used in a Taylor approximation to determine perturbed flows. The flow solution at nearby values of the parameters that determine the flow can be approximated using a base flow and the flow sensitivities with respect to these parameters. Finally, flow sensitivities are used as informational tools. Flow sensitivities provide information about

what, where and when certain parameters most affect the flow solution. Each of these application areas is discussed further using practical examples in Chapter 3. It is important to note that this is not an exhaustive study of sensitivity calculation methods or their applications. For example, consider the adjoint method [11, 12, 13, 26, 38] for optimization which calculates all "sensitivities" via the adjoint equations at once. This method becomes more efficient as the number of design parameters increases and should be considered in any optimization involving many design parameters. Unfortunately, not every method can be considered. The studies within will focus on sensitivity calculation methods in which the sensitivities are calculated by differentiating either the continuous or discrete system of fluid flow equations.

1.2 Inviscid Compressible Fluid Flow

Fluid flow which is nonviscous and compressible is present in many situations and applications. The flow is modeled by the Euler equations which are some of the most studied equations in mathematics and science. Consequently, there is a great deal of theory and work done on these equations. The fact that the Euler equations are computationally simpler and cheaper to solve than the Navier-Stokes equations has made them a staple, now and in the years to come, in the computational fluid dynamics realm [23, 24]. The Euler equations are both interesting and difficult as they are hyperbolic partial differential equations for supersonic flows and hence their solutions contain discontinuities and complexities in the fluid flow such as shock waves, contact discontinuities and rarefaction waves. In particular, at super and hypersonic speeds, the flow solutions can have shock waves and contact discontinuities. There has been much work on hyperbolic equations and the numerical implications of the discontinuities that arise [14, 28, 47], but there is little theory about the effects these discontinuities can have on perturbed flow calculations, optimization and control problems and the underlying flow sensitivities. Due to the longevity and continual use of inviscid compressible fluid flow, it is reasonable to require optimization, control, and perturbed flow calculation methods to conform to and utilize the discontinuous nature of the flow.

1.3 Sensitivities and Discontinuous Flows

In Section 1.1 and Section 1.2, the usefulness and importance of both sensitivity analysis and discontinuous fluid flow has been made apparent. In fact, there are numerous examples where each area has made a significant impact, such as shape optimization and CFD for

aerodynamics. The focus of this research is that area which lies at the intersection of sensitivities and discontinuous flow, *i.e.*, the calculation of flow sensitivities for discontinuous fluid flows.

The calculation of sensitivities in the presence of discontinuities is an interesting and difficult problem. Most of the recent research has focused on the definition and calculation of sensitivities in general with relatively little focus on discontinuities. The sensitivity equation method has recently been studied by Appel *et al.* [1], Borggaard [7] and Borggaard *et al.* [8] among others. In theses cases, the discontinuities have been ignored, *i.e.*, the same algorithm is applied throughout the computational domain and differentiation occurs across the discontinuity. Burkardt [10] applied the sensitivity equation method to the Navier-Stokes equations, which do not have discontinuous flows, via shape optimization. It should be noted that the above authors received good results in this manner, but the question of how these discontinuities affect the optimizations still remains.

Likewise, the semi-analytic method has been studied by Taylor *et al.* [43, 44, 45], Taylor and Newman [35, 36], Eyi and Lee [18] and Baysal [3] in the design and optimization realm for computational fluid dynamics for both the Euler and Navier-Stokes equations. Bischof *et al.* [4, 5, 6] have also done work in the semi-analytic methods with their development of automatic differentiation methods such as ADIFOR and ADIC [4, 5, 6]. Again, in most of the work, the focus has been on the definition and calculation of sensitivities and not on the discontinuities arising in the higher speed flows. The semi-analytic methods rely on the differentiation of the discrete flow equations. Although the exact equations involve discontinuities in the flow solution, these discontinuities become "continuous" smears in the discrete space. Therefore, the belief by the semi-analytic community is that the differentiation occurring across these smeared discontinuities is generally all right and may even be preferred since it provides an approximation to the exact discrete sensitivities.

Taylor *et al.* [42] and Burgreen [9] have used the semi-analytic sensitivities for the calculation of perturbed flows and considered the effects of the discontinuities on these calculations. Likewise, it should be noted that Narducci [33] and Narducci *et al.* [34] have incorporated discontinuities in a design optimization problem. Cliff, Heinkenschloss, and Shenoy [11, 12] have also considered a flow optimization via the adjoint method where the shock position is used as an explicit parameter in the cost functional and have proven existence and differentiability results. In general, there has been many applications of flow sensitivities involving discontinuous flow, but little has been done to understand the effects these discontinuities have on the applications. For completeness, Jameson and Reuther [26, 38] and Cliff *et al.* [11, 12, 13] should be mentioned for their work in the area of adjoint methods for optimization-based design using discontinuous fluid flow.

The present research intersects the above work by studying the effects of discontinuities

on both the calculation of flow sensitivities and their applications. The goal is to develop sensitivity calculation methods that will automatically take into account discontinuities without knowing *a priori* their position or speed through the fluid flow. There are several steps in this process. The first is to understand the influence of discontinuities on the sensitivity calculation methods and the second is the development of robust numerical methods for calculating flow sensitivities. The present research will address both of these steps.

1.4 Generalizations and Other Applications

The argument has been made for studying flow sensitivities in the presence of discontinuities in fluid flows. It is important to note that the research herein is not only relevant to the Euler equations and inviscid compressible fluid flow applications, but can be extended to any physical application in which the solution is modeled by systems of hyperbolic conservation laws.

Physical applications modeled by systems of hyperbolic conservation laws include traffic flow, open-channel flow, two-phase flow through porous media, reactive flow, shallow water flow, detonation waves, magneto-hydrodynamics and petroleum reservoir simulation [21, 28]. It is conceivable that sensitivities could be calculated for any of these physical applications. These sensitivities could then be used in an optimization using the solution as a constraint or in the calculation of a perturbed solution in the same manner as described for the Euler equations. The sensitivities can also be used to help gain an understanding of the physical processes modeled by the conservation laws. Hence, even though the focus of the research is on flow sensitivities for inviscid compressible fluid flow, the results have implications to many areas in science and engineering.

Chapter 2

Sensitivity Background Material

2.1 Definition of a Sensitivity

In many settings it is important to know how much the solution of a system of equations varies or changes when certain parameters that affect the solution are altered or, how "*sensitive*" the solution is with respect to certain parameters. For example, how will changing the width of an airfoil effect the flow over the airfoil, *i.e.*, will small changes in the width of the airfoil cause small or large changes in the flow and at what locations throughout the domain. Sensitivities for a system of equations are defined to be the partial derivatives of the output variables describing the solution of the system of equations with respect to the input variables that determine the solution of the system of equations. The input variables are usually thought of as parameters and can be explicit or implicit in nature. In the context of fluid flow, flow sensitivities are the partial derivatives of the variables that describe the flow with respect to the parameters that determine the flow. For example, the sensitivity of flow over an airfoil could be calculated with respect to the angle of attack of the airfoil or the width of the airfoil. In each case, the parameter is a single number describing the attack angle or the airfoil width. Although sensitivities can be used in a variety of settings and problems, the focus of this work is in the context of fluid flow. The results can be easily transferred to different problems and disciplines making the obvious changes in language and governing equations. Thus, other examples are foregone and the discussion is concentrated on flow sensitivities.

Sensitivities play an integral part in the optimization and control process and are gaining strength in other areas as well. (See Chapter 3) One of the biggest issues involving flow sensitivities is how the derivatives are defined and computed. Several prominent method-

ologies have been developed to calculate flow sensitivities.

2.2 Sensitivity Methodologies

Consider a two-dimensional fluid flow problem where the flow is inviscid, but compressible, *i.e.*, flow over an airfoil cross section at supersonic speeds. The fluid flow is governed by the two-dimensional Euler Equations, Eq. 2.1, of fluid dynamics.

$$\frac{\partial \mathbf{U}}{\partial t} + \frac{\partial \mathbf{F}}{\partial x} + \frac{\partial \mathbf{G}}{\partial y} = \mathbf{0} \tag{2.1}$$

where

$$\mathbf{U} = \begin{bmatrix} \rho \\ m \\ n \\ e \end{bmatrix}, \quad \mathbf{F} = \begin{bmatrix} m \\ P + \rho u^2 \\ mv \\ u(P+e) \end{bmatrix}, \quad \mathbf{G} = \begin{bmatrix} n \\ nu \\ P + \rho v^2 \\ v(P+e) \end{bmatrix}$$

and where ρ = density, m = x-component of momentum, n = y-component of momentum, (u, v) = velocity in Cartesian coordinates (x, y), e = total energy and P = static pressure. The variables are related by an equation of state which, for a perfect gas is

$$e = \frac{P}{(\gamma - 1)} + \frac{1}{2}\rho(u^2 + v^2) \tag{2.2}$$

where $u = \frac{m}{\rho}$, $v = \frac{n}{\rho}$, and γ is the ratio of specific heats. The fluid flow problem will also involve boundary conditions which depend on the specific problem being solved. In most cases, the exact solution to the Euler equations is not known and approximations are found by numerically solving [32] the discrete Euler equations, Eq. 2.3.

$$\nabla_t^h \mathbf{U}^h + \nabla_x^h \mathbf{F}^h + \nabla_y^h \mathbf{G}^h = \mathbf{0} \tag{2.3}$$

where

$$\mathbf{U}^h = \begin{bmatrix} \rho^h \\ m^h \\ n^h \\ e^h \end{bmatrix}, \quad \mathbf{F}^h = \begin{bmatrix} m^h \\ P^h + \rho^h (u^h)^2 \\ m^h v^h \\ u^h (P^h + e^h) \end{bmatrix}, \quad \mathbf{G}^h = \begin{bmatrix} n^h \\ n^h u^h \\ P^h + \rho^h (v^h)^2 \\ v^h (P^h + e^h) \end{bmatrix}$$

and where ∇_t^h, ∇_x^h, and ∇_y^h represent the discretizations of the t, x, and y derivatives, respectively. These discretizations will depend on the specific finite difference, finite volume, or finite element scheme used to approximate the flow solution. The discrete variables ρ^h, m^h, n^h, u^h,v^h, e^h, and P^h are defined at the discrete set of points

$$(x_i, y_j), \qquad \begin{array}{ll} x_i = i\Delta x & i = 0, 1, 2, \ldots, N \\ y_j = j\Delta y & j = 0, 1, 2, \ldots, M. \end{array}$$

Again, the discrete variables are related by a discrete equation of state,

$$e^h = \frac{P^h}{(\gamma - 1)} + \frac{1}{2}\rho^h((u^h)^2 + (v^h)^2) \tag{2.4}$$

where $u^h = \frac{m^h}{\rho^h}$, $v^h = \frac{n^h}{\rho^h}$, and γ is the ratio of specific heats.

Consider calculating the sensitivity of the flow with respect to a single parameter, α. The flow sensitivity with respect to the parameter is denoted by $\frac{\partial \mathbf{U}}{\partial \alpha} = \mathbf{U}_\alpha$. Currently, there are several different views on how the flow sensitivities should be defined and computed.

The calculation of sensitivities can be broken into two different classes. The first is the "discretize-then-differentiate" approach. In this class of methods, the discrete equations for the approximate flow solution $\mathbf{U}^h$ are differentiated with respect to a parameter α to determine a discrete set of equations for the approximate sensitivity $(\mathbf{U}^h)_\alpha$. The second class of sensitivities is the "differentiate-then-discretize" approach. In this class of methods, the original system of continuous partial differential equations for the flow solution $\mathbf{U}$ are differentiated with respect to a parameter α to get a new system of linear partial differential equations for the approximate sensitivities $\mathbf{U}_\alpha$. The initial conditions and boundary conditions for the fluid flow must also be differentiated with respect to the parameter α to calculate the flow sensitivity. This system can then be discretized to solve for the sensitivities, $(\mathbf{U}_\alpha)^h$. For example, the system of PDE's for the sensitivities can be discretized and solved in the same manner as the original system of PDE's for the flow, or the system can be solved using a new linear equation solver. In general, the sensitivity calculation methodologies are not consistent, *i.e.*, $(\mathbf{U}_\alpha)^h \neq (\mathbf{U}^h)_\alpha$, although each methodology is preferred in certain circumstances. This will be discussed in greater detail in Section 2.4.

2.2.1 "Discretize-then-Differentiate" Sensitivities

There are at least three different sensitivity calculation methods that approximate the sensitivities of the discrete equations, $(\mathbf{U}^h)_\alpha$. The first is a finite difference quotient approach, the second is a semi-analytic approach, and the third is an automatic differentiation approach. Each of these three methods will be discussed here in detail and in subsequent chapters they will be applied to fluid flow problems.

Finite Difference Quotient Sensitivities

The finite difference approach in effect approximates the sensitivities using a finite difference quotient approximation. First, the approximate fluid flow $\mathbf{U}^h$ is calculated at a particular

value of the parameter α. The parameter is then perturbed by an amount $\Delta\alpha$ and the approximate fluid flow is again calculated at $\alpha + \Delta\alpha$. The sensitivity, $(\mathbf{U}^h)_\alpha$ can then be approximated by applying a standard finite difference quotient approximation such as the forward difference in Eq. 2.5,

$$(\mathbf{U}^h)_\alpha = \frac{\partial(\mathbf{U}^h)}{\partial\alpha} \approx \frac{\mathbf{U}^h(\alpha + \Delta\alpha) - \mathbf{U}^h(\alpha)}{\Delta\alpha}. \tag{2.5}$$

It is obvious that by perturbing the parameter α in a different manner the sensitivity could be approximated using a different finite difference quotient such as a central or backward difference. Also, higher order sensitivities can be calculated using the appropriate higher order difference quotient.

Finite difference sensitivities are desirable in many different settings because they can be easily implemented and calculated. Flow sensitivities with respect to multiple parameters require extra time and work. Consider calculating the flow sensitivities with respect to each of the parameters α_1, α_2, ..., α_N. The finite difference approach requires a different finite difference quotient for each of the N sensitivities, $\mathbf{U}_{\alpha_1}$, $\mathbf{U}_{\alpha_2}$, ..., $\mathbf{U}_{\alpha_N}$, *i.e.*,

$$(\mathbf{U}^h)_{\alpha_j} \approx \frac{\mathbf{U}^h(\alpha_1, \ldots, \alpha_j + \Delta\alpha_j, \ldots, \alpha_N) - \mathbf{U}^h(\alpha_1, \ldots, \alpha_j, \ldots, \alpha_N)}{\Delta\alpha_j}, \qquad j = 1, \ldots, N. \tag{2.6}$$

Hence, the N sensitivities require $N + 1$ flow solutions and N finite difference quotients using the simple forward difference method. If the number N is large, this can become a cumbersome and time consuming task. In a more complex quotient, the number of flow solutions increases. For example, in the central difference quotient $2N + 1$ flow solutions are required for the N sensitivities.

Semi-Analytic Sensitivities

The semi-analytic method for calculating the sensitivities differentiates the discrete numerical scheme with respect to a parameter, α, to derive a new numerical scheme for the sensitivities, $(\mathbf{U}^h)_\alpha$ [7]. Consider the simple initial value problem,

$$\begin{aligned} y'(x) &= \beta y(x), \\ y(0) &= \hat{y}_0. \end{aligned} \tag{2.7}$$

If the x-domain is broken up into M uniform intervals of width Δx, then the problem can be discretized and solved for $y_j^h \approx y((j-1)\Delta x)$ using the following numerical scheme,

$$y_{j+1}^h = y_j^h + \beta\Delta x y_j^h, \tag{2.8}$$

$$y_0^h = \hat{y}_0. \tag{2.9}$$

The semi-analytic approach to calculate the sensitivity with respect to β differentiates this numerical scheme to derive a new scheme for the discrete sensitivity.

$$s_{j+1}^h = s_j^h + \Delta x y_j^h + \beta \frac{\partial \Delta x}{\partial \beta} y_j^h + \beta \Delta x s_j^h \tag{2.10}$$

where

$$s_j^h \approx s((j-1)\Delta x) \approx \frac{\partial y((j-1)\Delta x)}{\partial \beta} = (y_j^h)_\beta.$$

Although this may seem like a practical approach, the implementation of the flow sensitivity scheme is usually cumbersome and inefficient since most numerical schemes for the flow equations are large and complicated. This method may also introduce mesh sensitivities that are neither physically relevant to the problem nor easy to implement. If the resulting differentiation can be calculated and implemented correctly by hand, certain aspects of the problem allow for efficient calculation of flow sensitivities [7]. Taylor *et al.* [43, 44, 45] have produced an efficient implementation for the multidimensional Euler equations. However, in most cases this implementation is foregone to the automatic differentiation methods such as ADIFOR.

Automatic Differentiation Sensitivities

The third method for calculating sensitivities is the automatic differentiation approach. This method automates the semi-analytic approach using a computational method. The idea is to use a computer program such as Automatic Differentiation of Fortran (ADIFOR) or Automatic Differentiation of C (ADIC) [4, 5, 6, 22], which will, in effect, differentiate the approximate flow simulation code via the chain rule. The idea is that the semi-analytic approach, whether calculated by hand or using automatic differentiation will calculate the "exact" discrete sensitivity of the discrete flow solution while the finite difference sensitivity will only provide an approximation to it. Of course as $\Delta\alpha \to 0$, the finite difference sensitivity will approach the automatic differentiation sensitivity. The automatic differentiation approach has recently gained much attention with its hands off approach to calculating sensitivities. With a rudimentary knowledge of sensitivities and a basic knowledge of the flow simulation code and a computer language, sensitivities are easily calculated. Again, the calculation of sensitivities with respect to multiple parameters, α_1, α_2, ..., α_N, requires additional work, *i.e.*, the automatic differentiation creates a new numerical subroutine for each parameter, α_j, that must be solved.

2.2.2 "Differentiate-then-Discretize" Sensitivities

In this class there is basically one method, the Sensitivity Equation Method. The idea is to differentiate the continuous fluid flow equations with respect to a parameter, α, to derive a new set of continuous equations for the sensitivity variables. The continuous boundary and initial conditions must also be differentiated with respect to α. These equations are then discretized and solved for the sensitivities $(\mathbf{U}_\alpha)^h$. The sensitivity equation method is first demonstrated using the simple initial value problem, Eq. 2.7, and will be differentiated with respect to β. The continuous sensitivity equations and initial conditions for the initial value problem are given by

$$\begin{aligned} s'(x) &= y(x) + \beta s(x), \\ s(0) &= \frac{\partial \hat{y}_0}{\partial \beta} \end{aligned} \tag{2.11}$$

where $s(x) = \frac{\partial y(x)}{\partial \beta}$. The sensitivities can now be approximated by discretizing Eq. 2.11.

The sensitivity equation method approach will also be demonstrated using the Euler equations, Eq. 2.1, and will be differentiated with respect to an implicit parameter α. The resulting continuous sensitivity equations for the Euler equations are given in Eq. 2.12.

$$\frac{\partial \mathbf{S}}{\partial t} + \frac{\partial \mathbf{F}^s}{\partial x} + \frac{\partial \mathbf{G}^s}{\partial y} = \mathbf{0} \tag{2.12}$$

where

$$\mathbf{S} = \frac{\partial \mathbf{U}}{\partial \alpha} = \begin{bmatrix} \partial\rho/\partial\alpha \\ \partial m/\partial\alpha \\ \partial n/\partial\alpha \\ \partial e/\partial\alpha \end{bmatrix} = \begin{bmatrix} \rho_\alpha \\ m_\alpha \\ n_\alpha \\ e_\alpha \end{bmatrix},$$

$$\mathbf{F}^s = \begin{bmatrix} m_\alpha \\ P_\alpha + \rho_\alpha u^2 + \rho u u_\alpha \\ m_\alpha v + m v_\alpha \\ u_\alpha(P+e) + u(P_\alpha + e_\alpha) \end{bmatrix}, \quad \mathbf{G}^s = \begin{bmatrix} n_\alpha \\ n_\alpha u + n u_\alpha \\ P_\alpha + \rho_\alpha v^2 + \rho v v_\alpha \\ v_\alpha(P+e) + v(P_\alpha + e_\alpha) \end{bmatrix}$$

and where ρ_α = the sensitivity of the density with respect to α, m_α = the sensitivity of the x-component of momentum with respect to α , n_α = the sensitivity of the y-component of momentum with respect to α, (u_α, v_α) = the sensitivity of velocity with respect to α, e_α = the sensitivity of total energy with respect to α and P_α = the sensitivity of the static pressure with respect to α. The sensitivities are related by differentiating the equation of state, which results in

$$e_\alpha = \frac{P_\alpha}{(\gamma - 1)} + \frac{1}{2}\rho_\alpha(u^2 + v^2) + \rho(u u_\alpha + v v_\alpha) \tag{2.13}$$

where $u_\alpha = \frac{m_\alpha \rho - m\rho_\alpha}{\rho^2}$, $v_\alpha = \frac{n_\alpha \rho - n\rho_\alpha}{\rho^2}$. Again, the boundary and/or initial conditions for the specific problem at hand would also have to be differentiated. It is important to note that the flow sensitivities depend on the fluid flow. In other words, the continuous sensitivity equations and the continuous flow equations are coupled, *i.e.*, the continuous sensitivity equations can not be solved without first knowing the solution of the continuous flow equations. Once these continuous sensitivity equations have been derived, they can be discretized and solved in any manner. Since the sensitivity equations are linear in the sensitivity variables, they can be solved very efficiently and cheaply with a linear equation solver. On the other hand, if it is not desirable to write a linear equation solver, then the equations can be solved using the same nonlinear equation solver as the flow equations with very few changes since the equations, Eq. 2.1 and Eq. 2.12, have similar forms. It is expected that the sensitivity equations will converge very quickly using the nonlinear solver due to their linearity.

Again, the problem of calculating flow sensitivities with respect to multiple implicit parameters, α_1, α_2, ..., α_N, is considered. It should be obvious that the differentiation of the continuous Euler equations, Eq. 2.1, will result in an identical set of continuous sensitivity equations for each parameter, α_j, assuming the parameters are implicit. The continuous sensitivity equations for the different parameters are given in Eq. 2.14.

$$\frac{\partial \mathbf{S}_j}{\partial t} + \frac{\partial \mathbf{F}^{s_j}}{\partial x} + \frac{\partial \mathbf{G}^{s_j}}{\partial y} = \mathbf{0} \tag{2.14}$$

where

$$\mathbf{S}_j = \frac{\partial \mathbf{U}}{\partial \alpha_j} = \begin{bmatrix} \partial\rho/\partial\alpha_j \\ \partial m/\partial\alpha_j \\ \partial n/\partial\alpha_j \\ \partial e/\partial\alpha_j \end{bmatrix} = \begin{bmatrix} \rho_{\alpha_j} \\ m_{\alpha_j} \\ n_{\alpha_j} \\ e_{\alpha_j} \end{bmatrix},$$

$$\mathbf{F}^{s_j} = \begin{bmatrix} m_{\alpha_j} \\ P_{\alpha_j} + \rho_{\alpha_j} u^2 + \rho u u_{\alpha_j} \\ m_{\alpha_j} v + m v_{\alpha_j} \\ u_{\alpha_j}(P+e) + u(P_{\alpha_j} + e_{\alpha_j}) \end{bmatrix}, \quad \mathbf{G}^{s_j} = \begin{bmatrix} n_{\alpha_j} \\ n_{\alpha_j} u + n u_{\alpha_j} \\ P_{\alpha_j} + \rho_{\alpha_j} v^2 + \rho v v_{\alpha_j} \\ v_{\alpha_j}(P+e) + v(P_{\alpha_j} + e_{\alpha_j}) \end{bmatrix}.$$

The only change in the continuous sensitivity equations for each implicit parameter is the differentiation of the continuous boundary and initial conditions. Consequently, if this is related to linear partial differential equations, it can be seen that one must solve multiple linear systems $A\mathbf{x} = \mathbf{b_j}$. In each system the coefficient matrix A is identical and only the right hand sides, $\mathbf{b}_j$, differ. Hence, the systems can be solved very efficiently using a single matrix LU-factorization and N forward and back solves if the matrix A is available. It is in this realm that the computational efficiency of the sensitivity equation method becomes truly transparent.

It should be noted that if each parameter, α_j, appears explicitly in the system of equations, then the different flow sensitivities will result in different continuous sensitivity equations. Again, the continuous sensitivity equations for the explicit parameters will be linear and are computationally cheap to solve, but the single matrix factorization structure is lost. In practice, most parameters are implicit and the focus will be on these parameters. All results still hold for explicit parameters, but there will be a small rise in the cost of the sensitivity equation method.

2.3 Sensitivity Methodology Cost Comparison

When comparing the different sensitivity calculation methods, one of the largest factors is the computational cost of each method. In this section, a heuristic argument relating the cost of each method is given. The first method is the finite difference approach. It has already been noted that to calculate N sensitivities a minimum of $N + 1$ flow solutions must be calculated. If the flow solution is small and easy to calculate, then this may not be a big factor, but in many large computational fluid dynamics problems, a single solution requires hours of CPU time. In this setting, if N gets even moderately large, then the finite difference approach can become computationally inefficient depending on the computational hardware available.

The second method to consider is the semi-analytic approach. Since it is difficult to implement correctly for complicated schemes, the focus is solely on automatic differentiation. As with the finite difference approach, the semi-analytic approach derives a new subroutine for each different sensitivity by differentiating the flow code. This results in $N + 1$ independent subroutines that must be solved. The flow solution is calculated once and the different sensitivities are calculated using N different subroutines that are of approximately the same cost as the flow scheme. Hence, the automatic differentiation approach is of approximately the same cost as the finite difference approach [4, 5, 6, 22]. In both the automatic differentiation and the finite difference approaches, the cost is independent of whether or not the parameter is implicit or explicit in nature.

The final method is the sensitivity equation method. In this method two different examples will be considered. First, consider the example where the flow sensitivities with respect to N explicit parameters are desired. After deriving the continuous sensitivity equations, there are N different equations that must be solved along with the flow solution. The difference here is that each equation is linear. This is in contrast to the flow equations which in general will be nonlinear. Utilizing the linearity of the continuous sensitivity equations allows the sensitivities to be calculated at less cost than either the finite difference approach or the

semi-analytic approach. Now consider an example where the flow sensitivities with respect to N implicit parameters are desired. This is different because there is now only one set of equations for all sensitivities. The only thing that will change is the initial and boundary conditions. In this situation, one must solve N linear equations with only the right hand side changing for each system. If this property is utilized, then the N sensitivities can be calculated with one LU-matrix factorization and N forward and back solves.

Although the sensitivity equation method is the most computationally efficient, it may not give a consistent sensitivity as will be discussed in the Section 2.4. The finite difference method and the automatic differentiation method are the easiest to implement, but are more costly than the sensitivity equation method on most practical problems. It should be noted that this is simply a heuristic argument. In practice, the size of the problem, the complexity of the code and the computational hardware available will determine the trade off between computational costs, implementational costs and consistency issues.

2.4 Consistency of Sensitivities Derivatives

As mentioned in earlier sections, there are some consistency issues in the sensitivity methodologies, *i.e.*, in general $(\mathbf{U}^h)_\alpha \neq (\mathbf{U}_\alpha)^h$. The real question that is being asked is do the operations of differentiation and discretization commute? It has been shown that in most cases, these two different operations will not commute [7, 10]. The next question is which sensitivity is the "*correct*" sensitivity? This will depend upon the problem. Consider an optimization problem that optimizes the numerical solution of the discrete constraint equations. In this case, the sensitivity of the discrete flow $(\mathbf{U}^h)_\alpha$ is the desired and correct sensitivity to use, *i.e.*, it provides an approximation of the derivative of the discrete flow. In most practical applications, it is the sensitivity of the discrete solution that is required. As is seen in Section 2.3, these sensitivities may be very expensive to calculate. The sensitivity of the continuous solution $(\mathbf{U}_\alpha)^h$, on the other hand, provides a computationally efficient approximation to this sensitivity, but provides an approximation to the continuous flow as opposed to the discrete flow. It has been shown that in many cases if the grid size is small enough, then the sensitivity equation method provides a "*good*" enough approximation to the discrete sensitivity for use in optimization [1, 7, 8, 10]. Hence, it can be desirable to use the sensitivity equation method even though it will provide inconsistent derivatives due to its computational efficiency. In the calculation of perturbed flows and for use as informational tools, it is the approximation of the continuous sensitivities, $(\mathbf{U}_\alpha)^h$ that is desired. There are also certain computational issues that make the sensitivity equation method a more desirable approach for use in perturbed flows as will be discussed in Section 3.5 and Chapter 9.

In certain applications and conditions such as discontinuous fluid flow, both $(\mathbf{U}_\alpha)^h$ and $(\mathbf{U}^h)_\alpha$ provide insufficient approximations of the true discretized sensitivities. These problems are the purpose and focus of this research.

Chapter 3

Flow Sensitivity Applications

3.1 Mathematical Significance of Sensitivities

Flow sensitivities, *i.e.*, the derivatives of the variables that describe the flow with respect to parameters that determine the flow, are useful in at least three settings. First, they are interesting in their own right since they tell the engineer or scientist what, when, and where these parameters most influence the flow. Second, they can be used in a Taylor approximation or some other like setting to determine perturbed flows, *i.e.*, given the flow variables and their sensitivities at specified values of the parameters, one can determine approximations to the flow variables at nearby values of the parameters. Certain methods for computing the sensitivities result in the determination of the perturbed flow at much less cost compared to doing a full-fledged flow solution at the new value of the parameters. Taylor *et al.* [42] and Burgreen [9] both in the presence of discontinuities and gave examples of how the discontinuity affects the approximation. Third, flow sensitivities can be used within an optimization setting to help determine the gradient of the objective functional with respect to the parameters that participate in the optimization process. This is an ever growing area that has recently received much attention [3]. Some of the major contributors include Bischof [6], Taylor and Newman [35, 36], Taylor *et al.* [43, 44, 45], Lee [18], Borggaard [7], Borggaard *et al.* [8], Burkardt [10] and Appel *et al.* [1]. In most cases, the discontinuities have been ignored; however, Narducci, Grossman, and Haftka [34] and Cliff, Heinkenschloss and Shenoy [11, 12] have considered designs in which the shock location must be taken into account. In optimizations where the objective function is highly discontinuous it is probably preferable to use a nongradient-based optimization technique such as a direct search method [16, 27]. The emphasis should be made here on highly discontinuous objective functions such as a noisy objective function where the gradient would be some-

what meaningless [20] as opposed to an inviscid compressible airfoil optimization involving a single shock in which the gradient points in the right direction almost everywhere [1]. Direct search methods are very robust but converge at a much slower rate and are usually too slow to solve optimization problems with large numbers of parameters.

In each of the above applications, difficulties arise in the calculation and use of sensitivities for flows with discontinuities. Clearly, the importance and usefulness of flow sensitivities in optimization-based design has been demonstrated [3]. However, for sensitivities to be a truly powerful tool in the other two contexts there will need to be improvements made on how the sensitivities are defined, computed, and utilized. Such improvements will also result in better performance of the optimization process. This research is thus devoted to the understanding of flow sensitivities in general and not only to optimization-based design.

3.2 Flow Sensitivities as Informational Tools

The first application of flow sensitivities to be discussed is that of an informational tool. To illustrate, a simple supersonic ramp is considered and flow sensitivities are calculated with respect to the inflow Mach number. The flow solution is calculated at an inflow Mach number of $M = 1.6$ and a ramp angle of $14.03°$. The sensitivity with respect to the inflow Mach number is then found by calculating the flow solution at a inflow Mach number of $M + \Delta M = 1.65$, and performing the forward difference approximation,

$$\frac{\partial \mathbf{U}}{\partial M} = \frac{\mathbf{U}(x, y, M + \Delta M) - \mathbf{U}(x, y, M)}{\Delta M}.$$

The sensitivity of the flow density with respect to the inflow Mach number, $\frac{\partial \rho}{\partial M}$, is given in Fig. 3.1. All flow solutions were calculated on a 30×40 grid using *ErICA* [33] and nondimensionalized by standard reference quantities. If viewed as an informational tool, Fig. 3.1 tells the engineer that the shock wave is the most sensitive part of the flow with respect to the inflow Mach number. Although the shock is the most sensitive part of the flow, the approximate flow sensitivities are inaccurate due to numerical calculation problems involving discontinuities. If the flow sensitivities are calculated across a discontinuity in the flow, like shock waves, then current sensitivity calculation methods will incorrectly approximate the "exact" continuous sensitivities. These flow sensitivity calculation problems in the presence of discontinuities are the focus of this work and will be discussed later. The sensitivities also tell the engineer that the pre- and post-shock regions are areas of constant sensitivity with the pre-shock region being more sensitive with respect to the inflow Mach number than the post-shock region, as would be expected. This is just a simple example, but the benefits of knowing where, when, and how the flow will change with respect to certain parameters are numerous.

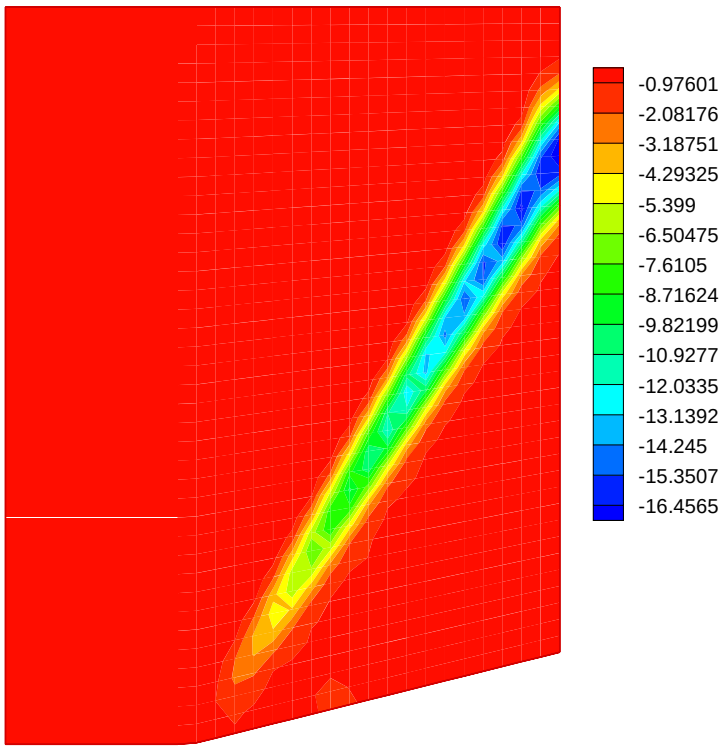

Figure 3.1: Sensitivity of the flow density with respect to inflow Mach number.

3.3 Calculation of Perturbed Flows

The second application of flow sensitivities is the calculation of perturbed flows where the same supersonic ramp example is used. An approximation to a perturbed flow can be calculated using a Taylor approximation method. The flow sensitivity with respect to the inflow Mach number is calculated using a forward difference. In this application, the flow at a nearby inflow Mach number is calculated using the flow sensitivity with respect to the inflow Mach number and a base flow at a fixed inflow Mach number. The perturbed flow solution is then found from the following Taylor approximation

$$\mathbf{U}(x, y; M + \Delta M) \approx \mathbf{U}(x, y; M) + \Delta M \frac{\partial \mathbf{U}}{\partial M}(x, y; M),$$

where $M = 1.6$ and $\Delta M = 0.1$ and is shown in Fig. 3.2. The flow sensitivity of the flow density is shown in Fig. 3.1.

Likewise, the Taylor approximation is shown versus the solution calculated at $M = 1.7$ without using a Taylor approximation in Fig. 3.3. The error in the Taylor series approximation can be estimated numerically by first calculating the flow solution at the inflow Mach number of $M + \Delta M$ which will be called the calculated solution. Then, one has to check the absolute value of the difference between this calculated solution and the approximate perturbed flow calculation at each grid point. The error in the perturbed flow density has been calculated and is shown in Fig. 3.4.

The error in the perturbed flow calculation is the largest in the shock region due mainly to two reasons. The first is the inaccurate calculation of the sensitivities across the shock wave which will be discussed later. The second is the incorrect placement of the shock wave by the Taylor approximation. When the parameter M is varied, the position of the shock wave, in general, will also vary. To correctly calculate a perturbed flow using sensitivities, the sensitivity of the shock position with respect to the parameter M must be calculated. This idea will be discussed later in Chapter 9. Before perturbed flow calculations using sensitivities can become truly useful, this problem must be remedied.

If the above problems can be corrected in an efficient manner, then the use of sensitivities to calculate perturbed flows can become a very useful tool. In calculating the above flow sensitivities using a finite difference approximation, at least one more flow solution was required, which would appear to make the calculation of perturbed flows inefficient. The flow sensitivities were only calculated in this manner to present a sample of their potential usefulness. In a different setting, a less costly method such as the sensitivity equation method could be used and the computational savings would be significant. At the present time, sensitivities used for calculating perturbed flows and as informational tools provide

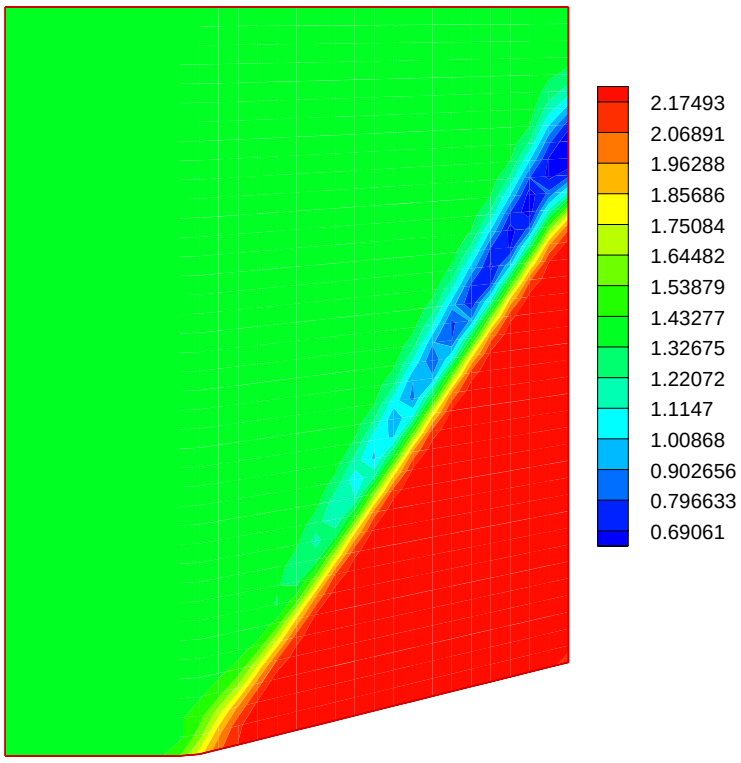

Figure 3.2: Calculation of perturbed flow density using sensitivities in a Taylor approximation.

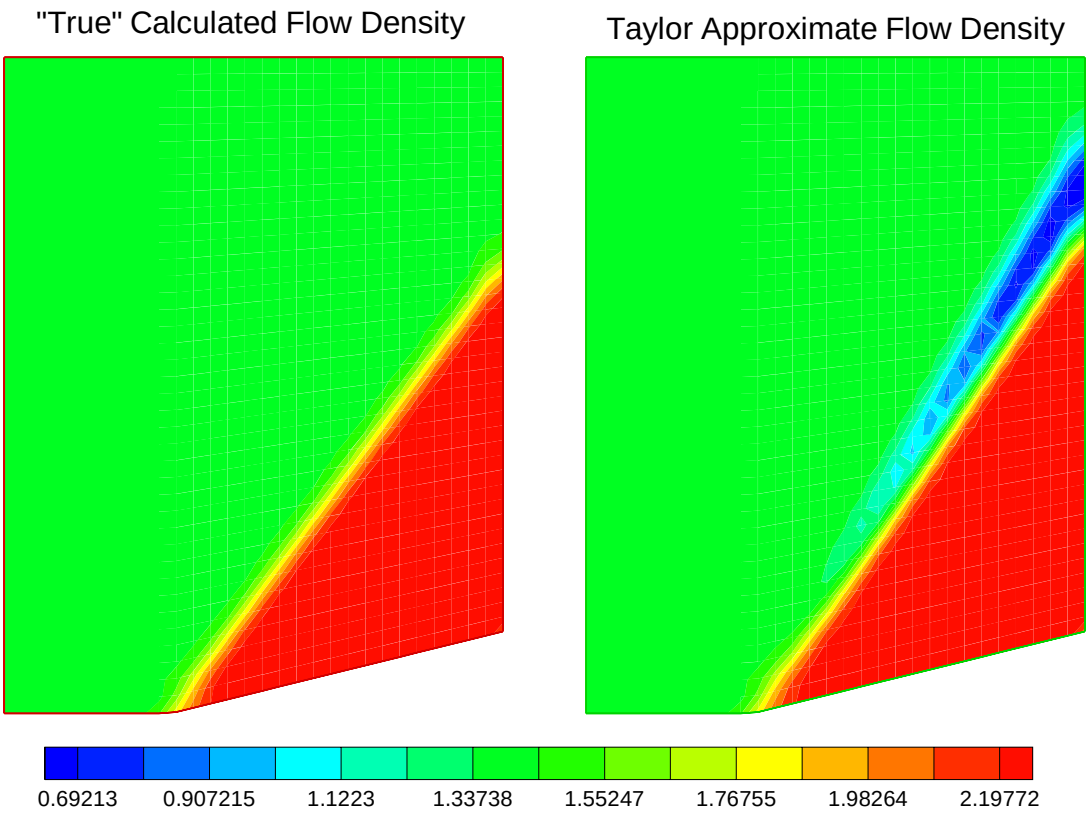

Figure 3.3: Comparison of perturbed flow density and calculated flow density.

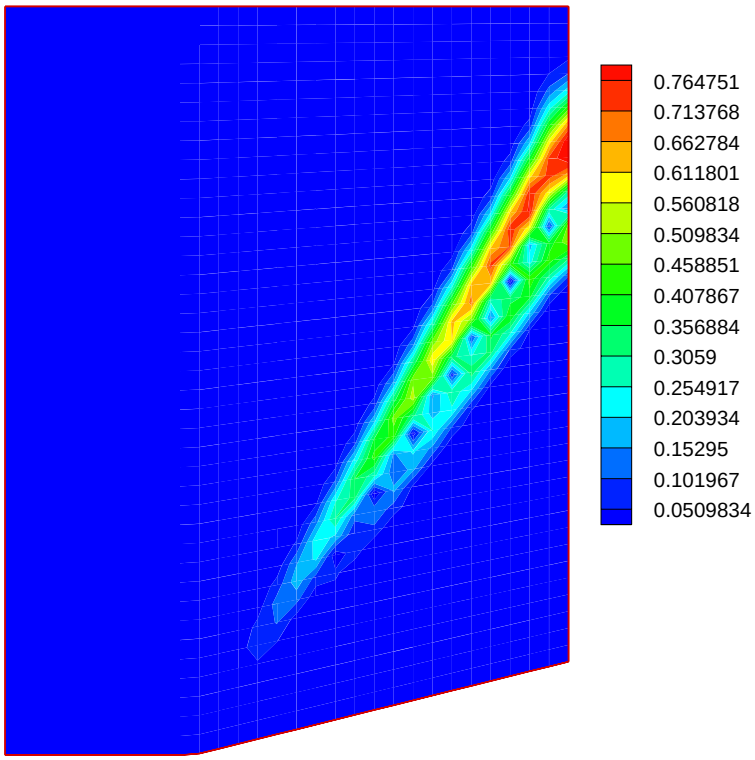

Figure 3.4: Error between perturbed flow density and calculated flow density.

accurate and efficient methods provided the flows are not discontinuous. It is this realm of flow sensitivities in discontinuous flow that is approached here.

3.4 Sensitivities in Optimization

The advances in computational efficiency and in the modeling capabilities of fluid flows has increased the use and need for computational fluid dynamics in aerodynamical design methods. Thus, optimization and control is the current area in which sensitivities have the most impact on aerodynamical design.

The structure of a flow-optimization problem involves objectives that express the goals of the flow optimization. These goals must be analytically expressed as the minimization or maximization of a cost functional. There are also constraints upon the flow. The nature of the flow is expressed in terms of a specific set of governing equations, in this case, the Euler equations. Finally, there is a set of design parameters that are to be used to meet the objectives.

In many of the problems, it is desirable to use a gradient-based optimization procedure such as a trust-region algorithm [15]. For this optimization procedure, it is necessary to calculate the gradient of the cost functional with respect to the design parameters. For example, consider the following flow matching cost functional and gradient of the cost functional where $\hat{\mathbf{U}}$ describes the target flow, $\mathbf{U}$ describes the test flow and Γ describes the computational area in which the flows are matched which is independent of α_k. The cost functional is given by

$$\mathcal{J} = \frac{1}{2}\int_{\Gamma} \left|\mathbf{U} - \hat{\mathbf{U}}\right|^2 \, d\Gamma. \tag{3.1}$$

The gradient with respect to the design variables is then

$$\frac{\partial \mathcal{J}}{\partial \alpha_k} = G = \int_{\Gamma} (\mathbf{U} - \hat{\mathbf{U}}) \cdot \frac{\partial \mathbf{U}}{\partial \alpha_k} \, d\Gamma. \tag{3.2}$$

It is easy to see that the gradient is defined in terms of the sensitivity variables, $\frac{\partial \mathbf{U}}{\partial \alpha_k}$. Hence, the optimization procedure must include a calculation of the flow sensitivities at each step.

Of course, many optimization procedures require the use of a linear approximation to both the constraints and the cost functional. The linear approximant can be defined using the concept of Fréchet derivatives and hence, the Fréchet differentiability of the constraints and the cost functional must be established. Knowing the flow sensitivities with respect to the parameters, α_j, is sufficient to calculate the directional or Gateaux derivatives of the

cost functional along each of the coordinate α_j-axis, but, in general, does not imply Fréchet differentiability. To ensure proper convergence of the optimizer, Fréchet differentiability must also be established. (See Cliff *et al.* [12])

3.4.1 Perfect-Gas Optimization on an Unstructured Grid

In this section, a flow optimization application to inviscid compressible flow is discussed where the Euler equations are solved numerically using an unstructured grid [2]. The unstructured grid approach allows grid elements of different sizes and orientations to make up the grid. This can provide more accurate approximations than the structured approach which requires the elements to follow a regular pattern and orientation. The problem is to design a forebody simulator. The simulator is used to approximate the flow distortion produced by the forward-fuselage on the engine inlet flow since the entire forebody cannot be accommodated in a wind tunnel. The challenge is to design a simulator at a restricted size that will produce the same flow profile [25].

The objective is to match the flow variables at a cross-sectional reference plane by choosing the simulator shape and the free-stream velocity or Mach number. The state variables are the flow variables, $\mathbf{U}$, of the Euler equations, Eq. 3.3.

$$\frac{\partial \mathbf{U}}{\partial t} + \frac{\partial \mathbf{F}}{\partial x} + \frac{\partial \mathbf{G}}{\partial y} = 0 \tag{3.3}$$

where

$$\mathbf{U} = \begin{bmatrix} \rho \\ m \\ n \\ e \end{bmatrix}, \quad \mathbf{F} = \begin{bmatrix} m \\ P + \rho u^2 \\ mv \\ u(P+e) \end{bmatrix}, \quad \mathbf{G} = \begin{bmatrix} n \\ nu \\ P + \rho v^2 \\ v(P+e) \end{bmatrix}$$

in which ρ =density, P =static pressure, (u, v) = velocity in Cartesian coordinates (x, y), and e is the total energy. This energy is related to the other variables by an equation of state which, for a perfect gas, is

$$e = \frac{P}{(\gamma - 1)} + \frac{1}{2}\rho(u^2 + v^2). \tag{3.4}$$

There are three design parameters, denoted by α, which include the inflow Mach number, and two parameters that determine the shape of the forebody. The cost functional $\mathcal{J}$ depends on the flow solution and also depends on the design parameters. This flow matching cost functional is given by

$$\mathcal{J} = \frac{1}{2}\int_{\Gamma} \left|\mathbf{U} - \hat{\mathbf{U}}\right|^2 d\Gamma \tag{3.5}$$

where the integration is performed over the cross-sectional reference plane, Γ, which is independent of α and $\hat{\mathbf{U}}$ is the target solution. It should be noted that the flow solution for the forebody simulator problem is a steady-state solution, *i.e.* constant throughout time and hence the cost functional is independent of time. The flow solution must satisfy the constraints which in this context are denoted by $g(\mathbf{U}, \alpha) = 0$ and are just the governing fluid-dynamic equations or Euler equations, Eq. 3.3. The minimization problem can be formally written as

Problem 1 (Forebody Minimization) *Find the design parameters α such that*

$$\mathcal{J}(\alpha) = \frac{1}{2} \int_{\Gamma} \left| \mathbf{U} - \hat{\mathbf{U}} \right|^2 d\Gamma \tag{3.6}$$

is minimized subject to $g(\mathbf{U}, \alpha) = 0$ where $\mathbf{U}$ is the test flow, $\hat{\mathbf{U}}$ is the target flow, and $g(\mathbf{U}, \alpha) = 0$ are the constraint equations, i.e.*, the two-dimensional Euler equations.*

In the two-dimensional version of this problem, the forebody simulator is completely defined by four points of a cubic Bezier curve, Eq. 3.7.

$$\begin{aligned} x(s) &= \sum_{i=0}^{3} x_i B_{i,3}(s) \\ y(s) &= \sum_{i=0}^{3} y_i B_{i,3}(s) \\ B_{i,r} &= \begin{pmatrix} r \\ i \end{pmatrix} s^i (1-s)^{r-i}, \quad s \in [0,1] \end{aligned} \tag{3.7}$$

For purposes of demonstration, the sensitivity equation method will be used to design a forebody simulator that is constrained to be one-half of the length of a target forebody. Two points of the Bezier curve are used as end points while the other two points are used to define the curve's slope at these end points. Bezier curves are desirable because they provide a variety of designs using very few parameters. For the forebody-simulator problem, the beginning and ending points (x_0, y_0) and (x_3, y_3) are fixed as are the x location of the remaining points, x_1 and x_2. These locations are chosen to be $x_1/L = 0.2$ and $x_2/L = 0.6$. The y locations of these slope-defining points, y_1 and y_2, are two design parameters which completely define a cubic Bezier curve. Four possible forebody simulators corresponding to different sets of the design parameters are shown in Fig. 3.5. In each forebody the values of y_2 and y_3 are equal to 0.4 or 0.0. Note, the points y_1 and y_2 control the slope at each end of the forebody.

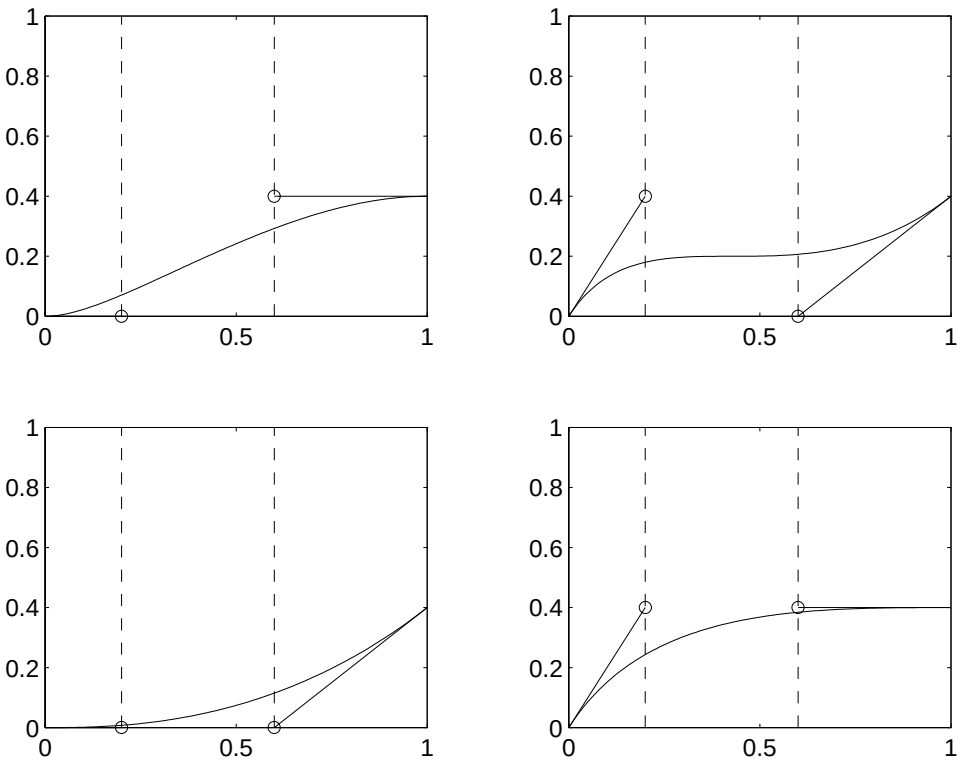

Figure 3.5: Forebody-simulator configurations corresponding to four different pairs of design parameters. The left circle denotes the point (x_1, y_1) and the right circle denotes the point (x_2, y_2). The vertical dashed lines (- -) denote the lines $x_1 = 0.2$ and $x_2 = 0.6$.

A version of this problem was studied by Borggaard [7]. Here, AeroSoft's $\mathcal{UGASP}$ code is used on an unstructured mesh [2, 32]. The cost function measures the difference between the computed flow and a target flow, integrated over the outflow plane:

$$\mathcal{J} = \frac{1}{2}\int_{\Gamma} \left|\mathbf{U} - \hat{\mathbf{U}}\right|^2 \, d\Gamma.$$

The gradient with respect to each design variable is then

$$\frac{\partial \mathcal{J}}{\partial \alpha_k} = G = \int_{\Gamma} (\mathbf{U} - \hat{\mathbf{U}}) \cdot \frac{\partial \mathbf{U}}{\partial \alpha_k} \, d\Gamma.$$

The computational geometry for the problem is described by a trapezoidal domain with the forebody removed as in Figs. 3.6, 3.7, and 3.8. The boundary conditions are specified in the following way: 1) inflow conditions are applied on the left side and slanted top portion, 2) a simple first order extrapolation outflow is specified for the right side, 3) tangency is applied on the curved forebody, and 4) a symmetry condition is applied on the horizontal boundary preceding the forebody.

The target-flow profile is generated by setting the free-stream velocity equivalent to an inflow Mach number of $M_\infty = 2.0$, while the Bezier curve is described by

$$\begin{aligned}
(x_0, y_0) &= (0.0, 0.0)\, m \\
(x_1, y_1) &= (0.2, \mathbf{0.2})\, m \\
(x_2, y_2) &= (1.1, \mathbf{0.3})\, m \\
(x_3, y_3) &= (2.0, 0.4)\, m.
\end{aligned}$$

where the coordinates are given in meters.

The initial, shortened forebody is described by the following control points

$$\begin{aligned}
(x_0, y_0) &= (0.0, 0.0)\, m \quad \text{fixed} \\
(x_1, y_1) &= (0.2, \mathbf{0.2})\, m \quad x_2 \text{ fixed} \\
(x_2, y_2) &= (0.6, \mathbf{0.3})\, m \quad x_3 \text{ fixed} \\
(x_3, y_3) &= (1.0, 0.4)\, m \quad \text{fixed}.
\end{aligned}$$

The third design parameter, the free-stream velocity, initially corresponds to the flight Mach number of $M_\infty = 2.0$, and has the value $U_\infty = 658.97\ m/s$. Hence, the initial three design parameters are given by

$$\begin{aligned}
\alpha_1^0 &= 658.97 m/s = \text{free-stream velocity} \\
\alpha_2^0 &= 0.2m = y_1\text{- Bezier point} \\
\alpha_3^0 &= 0.3m = y_2\text{- Bezier point.}
\end{aligned} \tag{3.8}$$

The final design is obtained using a trust-region algorithm when one of three conditions are met: 1) the gradient has reduced four orders of magnitude, 2) the design variables fail to change in the fourth significant digit, or 3) the objective function fails to change. After convergence, the optimization yields the following design parameters:

$$\begin{aligned} \alpha_1^{final} &= 655.65 m/s = \text{free-stream velocity} \\ \alpha_2^{final} &= 0.41549 m = y_1\text{- Bezier point} \\ \alpha_3^{final} &= 0.27854 m = y_2\text{- Bezier point.} \end{aligned} \tag{3.9}$$

The design forebody is described by the following Bezier points

$$\begin{aligned} (x_0, y_0) &= (0.0, 0.0)\, m \\ (x_1, y_1) &= (0.2, \mathbf{0.41549})\, m \\ (x_2, y_2) &= (0.6, \mathbf{0.27854})\, m \\ (x_3, y_3) &= (1.0, 0.4)\, m. \end{aligned}$$

The target flow, initial flow and optimal design flow and unstructured meshes are shown in Figs. 3.6, 3.7, and 3.8, respectively.

Problem 1 shows how flow sensitivities easily lend themselves to aerodynamic optimization. It should be noted that the shock wave at the front of the forebody has been ignored in the optimization process by applying the same algorithm throughout the domain. It is unclear what effect this has on the optimization process. In the optimization at hand, the optimizer was able to move towards a minimum, but undoubtably the shock hindered the gradient and hence the optimization process. Consider the graph of the flow sensitivity in Fig. 3.9. In this plot it is easy to see a large spike at the shock wave. The spike at hand should be a single point representing a δ-function and thus each point in the spike represents an inaccurate continuous sensitivity at that point. It is unclear whether this spike is necessary in the optimization as it represents an approximation to the exact discrete sensitivity or if its removal will greatly speed up the optimization. This idea is explored further in Chapter 6 where optimizations are performed using finite difference sensitivities, sensitivity equation method sensitivities and exact continuous sensitivities. The finite difference and the sensitivity equation method sensitivities involve large spikes at the discontinuities, but the exact continuous sensitivities will not involve spikes.

3.5 Sensitivity Methodology and Applications

With an understanding of some possible applications, it is important to understand how the sensitivity methodology fits into these applications. The first thing to consider is the

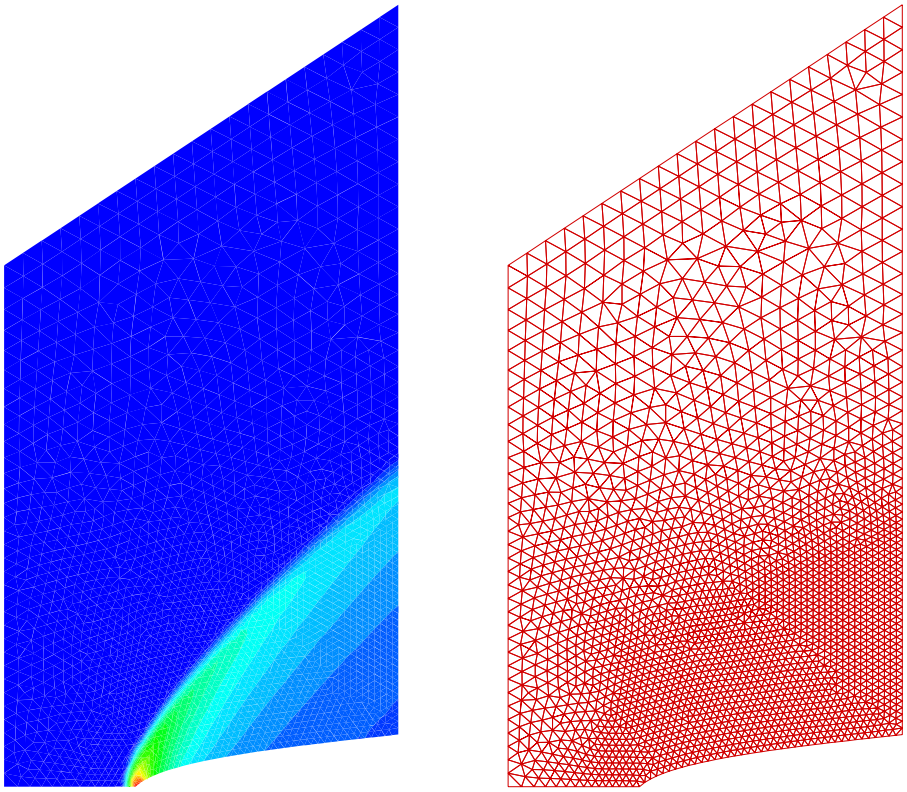

Figure 3.6: Target flow and mesh for the forebody simulator on an unstructured mesh.

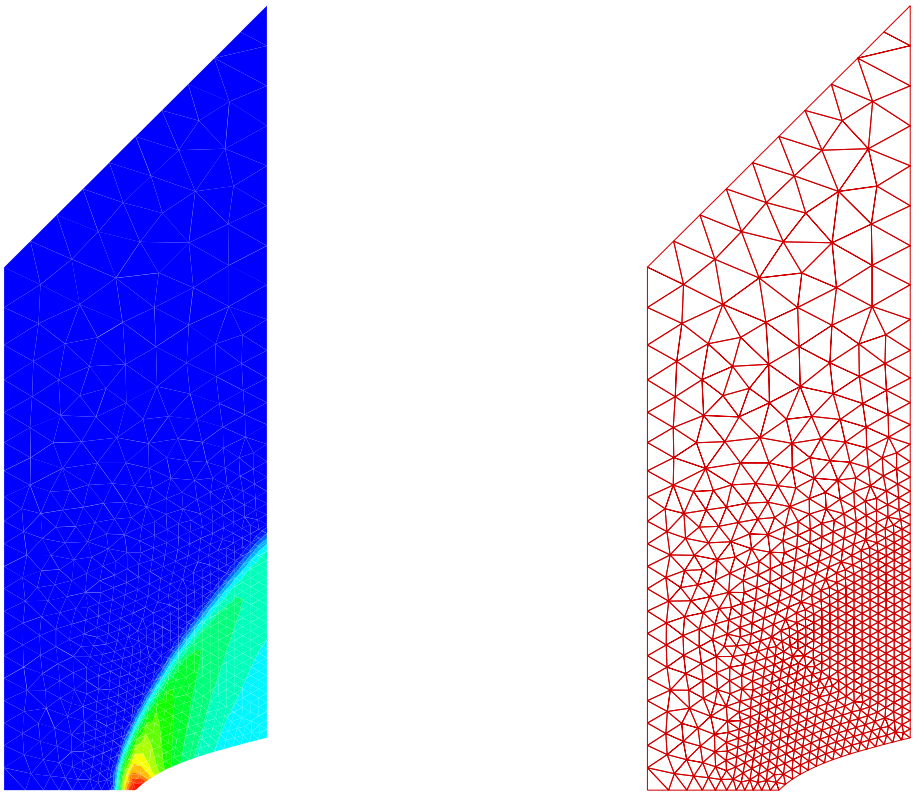

Figure 3.7: Initial flow and mesh for the forebody simulator on an unstructured mesh.

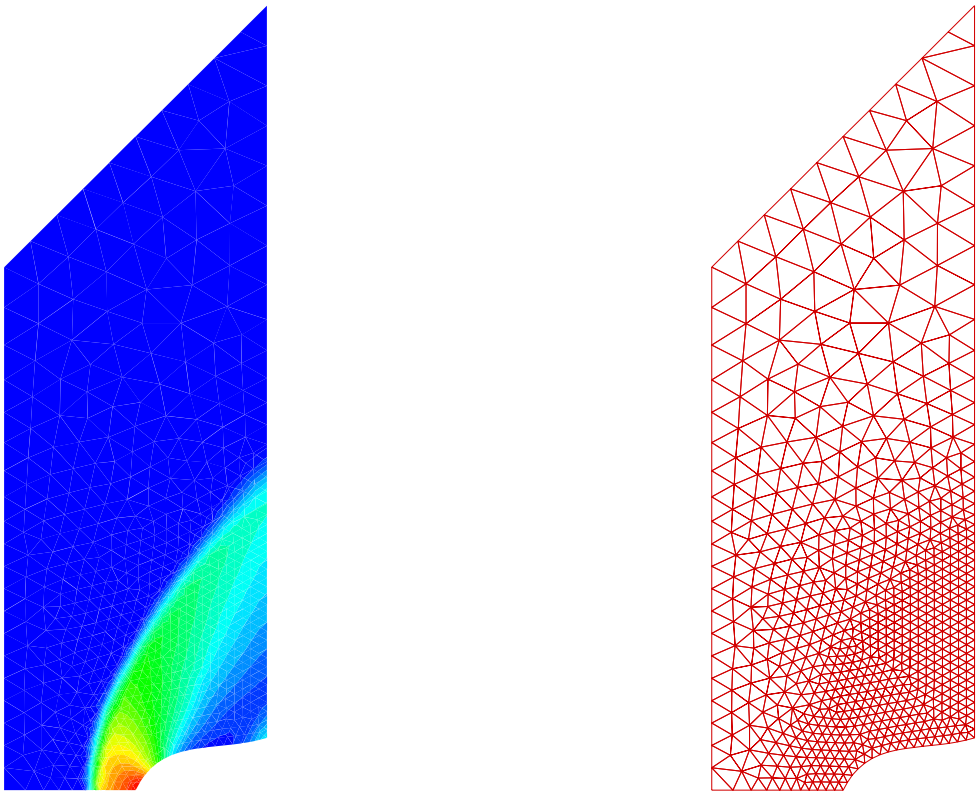

Figure 3.8: Optimal flow and mesh for the forebody simulator on an unstructured mesh.

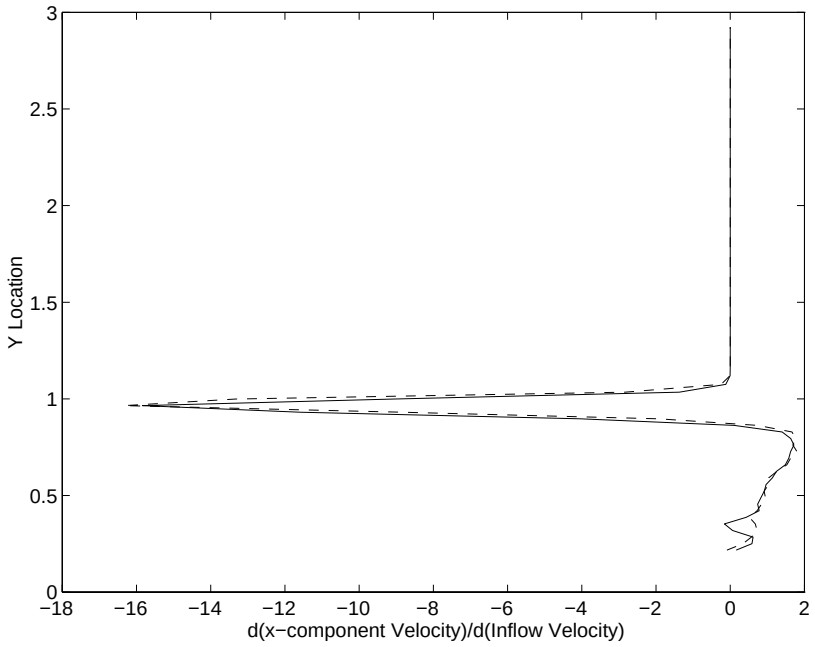

Figure 3.9: Flow sensitivity of the x-component of the velocity with respect to the inflow or free-stream velocity at the outlet reference plane Γ. The solid line (—) denotes a finite difference sensitivity and a dashed (- -) line denotes the sensitivity equation method sensitivity.

use of sensitivities as informational tools. In this case, the engineer or scientist must decide if they want information about the continuous solution or the discrete solution. This will dictate whether or not to use the "discretize-then-differentiate" or the "differentiate-then-discretize" sensitivity. The number of different sensitivities will also dictate which method to use as it will have an effect on the total cost based on the cost per sensitivity. Finally, the complexity of the flow problem will affect the cost and help to dictate which method to use.

The next application to consider is perturbed flow calculations. It is this application that clearly brings to the front the sensitivity equation method. For example, if a finite difference sensitivity is used to calculate a single perturbed flow, then more work has been done to approximate the perturbed flow than if it had just been recalculated. In the case where the sensitivities are used to calculate a single perturbed flow, it is more cost efficient to use the sensitivity equation method than to use the other two methods. If a single sensitivity is used to calculate multiple perturbed flows, then the finite difference and automatic differentiation methods can be computationally efficient depending on the

number of sensitivities and on the number of perturbed flows.

Finally, the idea of optimization based design is considered. In this context, the "discretize-then-differentiate" sensitivity is desired for consistency, but the finite difference method and the automatic differentiation method may become very costly if too many sensitivities are required for the optimization. For this reason, the sensitivity equation method maybe used although it may not give a consistent sensitivity. This problem is usually remedied using a more robust optimizer such as trust-region method [15] and the cost efficiency in the sensitivity calculation will easily offset this. In order to be complete, it should be mentioned that if the design requires a large number of design sensitivities, then a method such as the adjoint method which calculates all the "sensitivities" at once must be considered and may even be more efficient [26].

If cost requirements are not an issue, which is not usually the case, then the easiest method should be used. The easiest and quickest method to implement is probably the finite difference method. The sensitivity equation and the automatic differentiation methods are second depending on if one has a knowledge of the flow code or mathematics.

3.6 Overview of Problems in Sensitivities

In Chapter 5, and Chapter 7 some of the current problems in calculating flow sensitivities in the context of discontinuous and complex flows, *i.e.*, fluid flows that contain shocks, contact discontinuities, and rarefaction waves are discussed. These physical and numerical phenomena present many different problems in the calculation of flow sensitivities that currently make their use in the calculation of perturbed flows impractical and hamper their use in optimization and the information that they provide in their own right.

One of the largest problems is the computational costs of the methods. Due to the cost incurred in calculating each flow sensitivity, perturbed flows are rarely calculated via these sensitivities. Likewise, these costs can force the use of the adjoint method to calculate gradients when many parameters are present in the optimization process [26, 38].

Another problem is at the discontinuity in the flow. At this point, the derivative or sensitivity does not exist in the classical sense, *i.e.*, there is not enough smoothness to define a classical derivative. Instead, there is a δ-function at points of the discontinuity of the flow. Although this is fine in a theoretical sense, it causes many problems numerically. In the discrete setting, the δ-function becomes smeared out over many grid points and becomes a large spike as in Fig. 3.9. These spikes cause multiple problems in flow sensitivity applications and will be considered in the following chapters.

Chapter 4

Fluid Flow Problems

4.1 Introduction

In this chapter, the Riemann problem or shock tube problem of gas dynamics is described in detail. This example problem will be used in later chapters to discuss flow sensitivities and the numerical methods used to calculate flow sensitivities. The chapter includes discussions of the problem, the analytical solution and the numerical solutions of the problem. The problem is chosen because it is the simplest one-dimensional inviscid flow problem, yet still retains all of the "*important*" aspects of more complex fluid flow problems.

4.2 One-Dimensional Riemann Problem

The Riemann problem from gas dynamics [14, 28, 31, 40] will be used in the calculation of the sensitivities as it contains many "troublesome" aspects present in typical flow solutions, including shock waves, rarefaction waves and contact discontinuities. The physical problem is a tube containing two different gases separated by a thin diaphragm. The two gases have different pressures and densities. If the diaphragm is instantaneously broken the gas at a higher density and pressure will flow into the gas of lower density and pressure. The problem is to model this flow. The flow is governed by the one-dimensional equations of gas dynamics, *i.e.*, the one-dimensional Euler equations, which can be written in conservation law form as

$$\mathbf{U}_t + \mathbf{F}(\mathbf{U})_x = \mathbf{0} \tag{4.1}$$

$$\mathbf{U}(x,0) = h(x) = \begin{cases} \begin{bmatrix} \rho_4 \\ m_4 \\ e_4 \end{bmatrix} & x < c = \text{Diaphragm position} \\ \begin{bmatrix} \rho_1 \\ m_1 \\ e_1 \end{bmatrix} & x > c = \text{Diaphragm position} \end{cases} \tag{4.2}$$

where

$$\mathbf{U} = \begin{bmatrix} \rho \\ m \\ e \end{bmatrix}, \qquad \mathbf{F}(\mathbf{U}) = \begin{bmatrix} m \\ (\frac{m^2}{\rho}) + P \\ (\frac{m}{\rho})(e+P) \end{bmatrix}$$

and where ρ is the density, u is the velocity, $m = \rho u$ is momentum, P is the pressure, and e is the internal energy per unit volume. The variables are related by the equation of state, which for a perfect gas is

$$e = \rho\epsilon + \frac{1}{2}\rho u^2, \tag{4.3}$$

where ϵ is the internal energy per unit mass and $\epsilon = \frac{P}{(\gamma_i - 1)\rho}$ with γ_i the ratio of specific heats in the ith subregion. The equations can also be written in nonconservation law form as

$$\mathbf{U}_t + A(\mathbf{U})\mathbf{U}_x = \mathbf{0}, \tag{4.4}$$

where $A(\mathbf{U})$ is given by

$$A(\mathbf{U}) = \begin{bmatrix} 0 & 1 & 0 \\ -(3-\gamma_i)\frac{u^2}{2} & (3-\gamma_i)u & \gamma_i - 1 \\ (\gamma_i - 1)u^3 - \frac{\gamma_i u e}{\rho} & \frac{\gamma_i e}{\rho} - \frac{3}{2}(\gamma_i - 1)u^2 & \gamma_i u \end{bmatrix}. \tag{4.5}$$

The problem is defined on the region $\Omega = [-\infty, \infty] \times [0, T]$. Initially, both fluids are at rest and are at different pressures and densities defined by $P_4 > P_1$, $\rho_4 > \rho_1$, and $u_4 = u_1 = 0$ with each P_i, ρ_i, u_i defined on a different subregion. The exact initial conditions used in the calculations are given in Fig. 4.1. Note, the ratio of specific heats, γ_i, is taken as 1.4 in all the Riemann problem calculations.

4.3 Solution of the Riemann Problem

The solution of the 1-D Riemann problem has five distinct regions as seen in Fig. 4.2 and Fig. 4.3; region (1) Low pressure and density region (2) Area between shock and contact

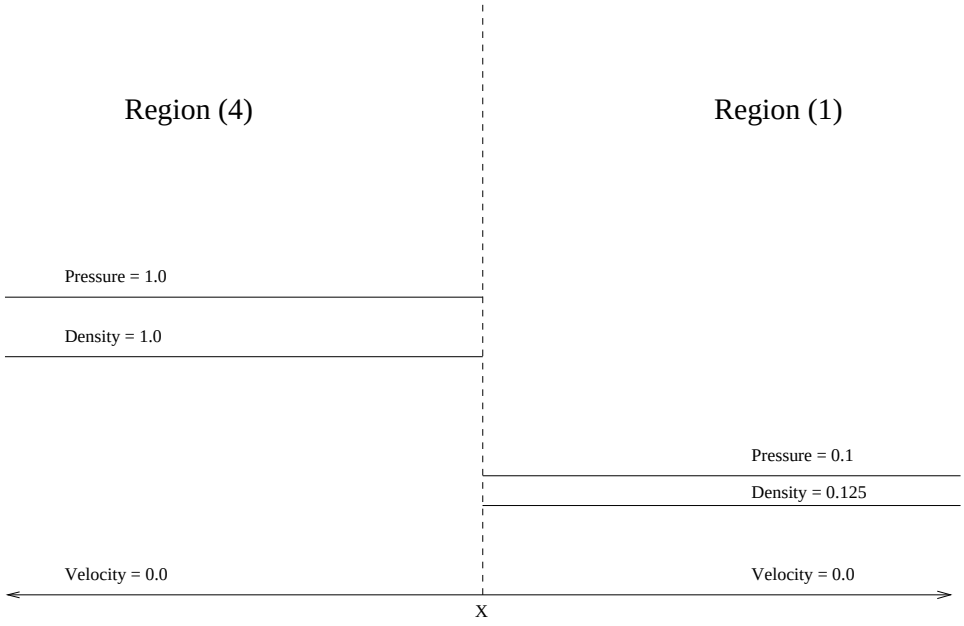

Figure 4.1: Initial conditions for the 1-D Riemann problem

discontinuity, region (3) Area between contact discontinuity and rarefaction wave, region(R) Rarefaction wave and region (4) High pressure and density region. The exact solution can be solved for explicitly as a function of x and t in each region [24, 31] and is given by the following equations

$$\begin{bmatrix} P \\ \rho \\ u \end{bmatrix} = \begin{cases} \begin{bmatrix} P_4 \\ \rho_4 \\ u_4 \end{bmatrix} = \begin{bmatrix} P_{High} \\ \rho_{High} \\ u_{High} \end{bmatrix}, & x < -a_4 t + c \\ \begin{bmatrix} P_R \\ \rho_R \\ u_R \end{bmatrix} = \begin{bmatrix} P_R \\ \rho_R \\ u_R \end{bmatrix}, & -a_4 t + c \leq x \leq \left(\frac{\gamma_4+1}{2} u_3 - a_4\right) t + c \\ \begin{bmatrix} P_3 \\ \rho_3 \\ u_3 \end{bmatrix} = \begin{bmatrix} P_2 \\ \rho_3 \\ u_2 \end{bmatrix}, & \left(\frac{\gamma_4+1}{2} u_3 - a_4\right) t + c \leq x \leq u_2 t + c \\ \begin{bmatrix} P_2 \\ \rho_2 \\ u_2 \end{bmatrix} = \begin{bmatrix} \phi \\ \rho_2 \\ u_2 \end{bmatrix}, & u_2 t + c < x < a_1 \left(\frac{\gamma_1-1}{2\gamma_1} + \frac{\gamma_1+1}{2\gamma_1}\frac{P_2}{P_1}\right)^{\frac{1}{2}} t + c \\ \begin{bmatrix} P_1 \\ \rho_1 \\ u_1 \end{bmatrix} = \begin{bmatrix} P_{Low} \\ \rho_{Low} \\ u_{Low} \end{bmatrix}, & a_1 \left(\frac{\gamma_1-1}{2\gamma_1} + \frac{\gamma_1+1}{2\gamma_1}\frac{P_2}{P_1}\right)^{\frac{1}{2}} t + c \leq x \end{cases} \tag{4.6}$$

where $a_i^2 = \frac{\gamma_i P_i}{\rho_i}$ and where ϕ is given implicitly by

$$\frac{P_4}{P_1} = \frac{\phi}{P_1}\left(1 - \frac{(\gamma_4 - 1)(a_1/a_4)(\phi/P_1 - 1)}{\sqrt{2\gamma_1}\sqrt{2\gamma_1 + (\gamma_1+1)(\phi/P_1 - 1)}}\right)^{\frac{-2\gamma_4}{\gamma_4 - 1}}. \tag{4.7}$$

The remaining variables, ρ_2, u_2, and ρ_3, are defined by

$$\rho_2 = \rho_1 \frac{P_2}{P_1}\left(\frac{1 + \frac{\gamma_1 - 1}{\gamma_1 + 1}\frac{P_1}{P_2}}{1 + \frac{\gamma_1 - 1}{\gamma_1 + 1}\frac{P_2}{P_1}}\right) \tag{4.8}$$

$$u_2 = a_1\left(\frac{P_2}{P_1} - 1\right)\sqrt{\frac{2/\gamma_1}{(\gamma_1+1)\frac{P_2}{P_1} + (\gamma_1 - 1)}} \tag{4.9}$$

$$\rho_3 = \rho_4\left(\frac{P_3}{P_4}\right)^{\frac{1}{\gamma_4}} \tag{4.10}$$

and in the rarefaction wave, the quantities P_R, ρ_R, and u_R, are given by

$$P_R = P_4\left(1 - \frac{\gamma_4 - 1}{2}\frac{u_R}{a_4}\right)^{\frac{2\gamma_4}{\gamma_4 - 1}} \tag{4.11}$$

$$\rho_R = \rho_4\left(1 - \frac{\gamma_4 - 1}{2}\frac{u_R}{a_4}\right)^{\frac{2}{\gamma_4 - 1}} \tag{4.12}$$

$$u_R = \left(\frac{u_3 - u_4}{\frac{\gamma_4+1}{2}u_3}\right)\left(\frac{x - c}{t}\right) + \frac{a_4 u_3 - (a_4 - \frac{\gamma_4+1}{2}u_3)u_4}{\frac{\gamma_4+1}{2}u_3}. \tag{4.13}$$

The solution at time $t = 0.148$ and for $0 \le x \le 1$ is plotted in Fig. 4.3.

4.4 Numerical Methods for the Riemann Problem

The Riemann problem is solved using three different numerical schemes. The first is a two-step Lax-Wendroff finite difference scheme described in Sod [40],

$$\begin{aligned} \mathbf{U}_{i+\frac{1}{2}}^{n+\frac{1}{2}} &= \frac{1}{2}\left(\mathbf{U}_{i+1}^n + \mathbf{U}_i^n\right) - \frac{\Delta t}{2\Delta x}\left(\mathbf{F}_{i+1}^n - \mathbf{F}_i^n\right), \\ \hat{\mathbf{U}}_i^{n+1} &= \mathbf{U}_i^n - \frac{\Delta t}{\Delta x}\left(\mathbf{F}_{i+\frac{1}{2}}^{n+\frac{1}{2}} - \mathbf{F}_{i-\frac{1}{2}}^{n+\frac{1}{2}}\right). \end{aligned} \tag{4.14}$$

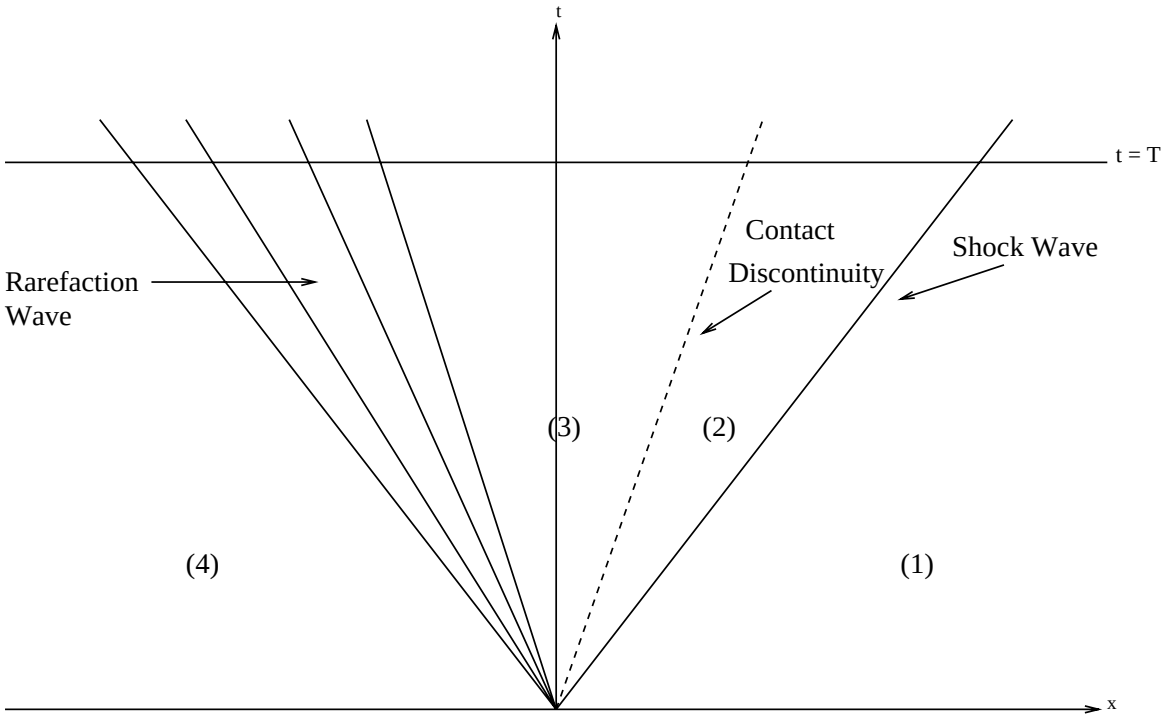

Figure 4.2: Solution of 1-D Riemann problem at t=T

The second is the Godunov finite difference scheme described in Sod [40],

$$\begin{aligned} \mathbf{U}_{i+\frac{1}{2}}^{n+\frac{1}{2}} &= \frac{1}{2}\left(\mathbf{U}_{i+1}^{n}+\mathbf{U}_{i}^{n}\right)-\frac{\Delta t}{\Delta x}\left(\mathbf{F}_{i+1}^{n}-\mathbf{F}_{i}^{n}\right), \\ \hat{\mathbf{U}}_{i}^{n+1} &= \mathbf{U}_{i}^{n}-\frac{\Delta t}{\Delta x}\left(\mathbf{F}_{i+\frac{1}{2}}^{n+\frac{1}{2}}-\mathbf{F}_{i-\frac{1}{2}}^{n+\frac{1}{2}}\right). \end{aligned} \tag{4.15}$$

Both the two-step Lax-Wendroff scheme and the Godunov scheme have the post processing artificial viscosity term of Lapidus [40] added to the approximate solution. Let $\hat{\mathbf{U}}_i^{n+1}$ be the approximate solution at the next time step. The solution with the Lapidus artificial viscosity is described by

$$\mathbf{U}_{i}^{n+1}=\hat{\mathbf{U}}_{i}^{n+1}+\frac{\nu\Delta t}{\Delta x}\Delta'\left[|\Delta'\hat{\mathbf{U}}_{i+1}^{n+1}|\cdot\Delta'\hat{\mathbf{U}}_{i+1}^{n+1}\right], \tag{4.16}$$

where $\Delta'\hat{\mathbf{U}}_i^n=\hat{\mathbf{U}}_i^n-\hat{\mathbf{U}}_{i-1}^n$, and ν is an adjustable constant.

The final scheme is the Roe scheme as described in LeVeque [28],

$$\mathbf{U}_{i}^{n+1}=\mathbf{U}_{i}^{n}-\frac{\Delta t}{\Delta x}\left(\mathbf{F}_{i+\frac{1}{2}}^{*}-\mathbf{F}_{i-\frac{1}{2}}^{*}\right), \tag{4.17}$$

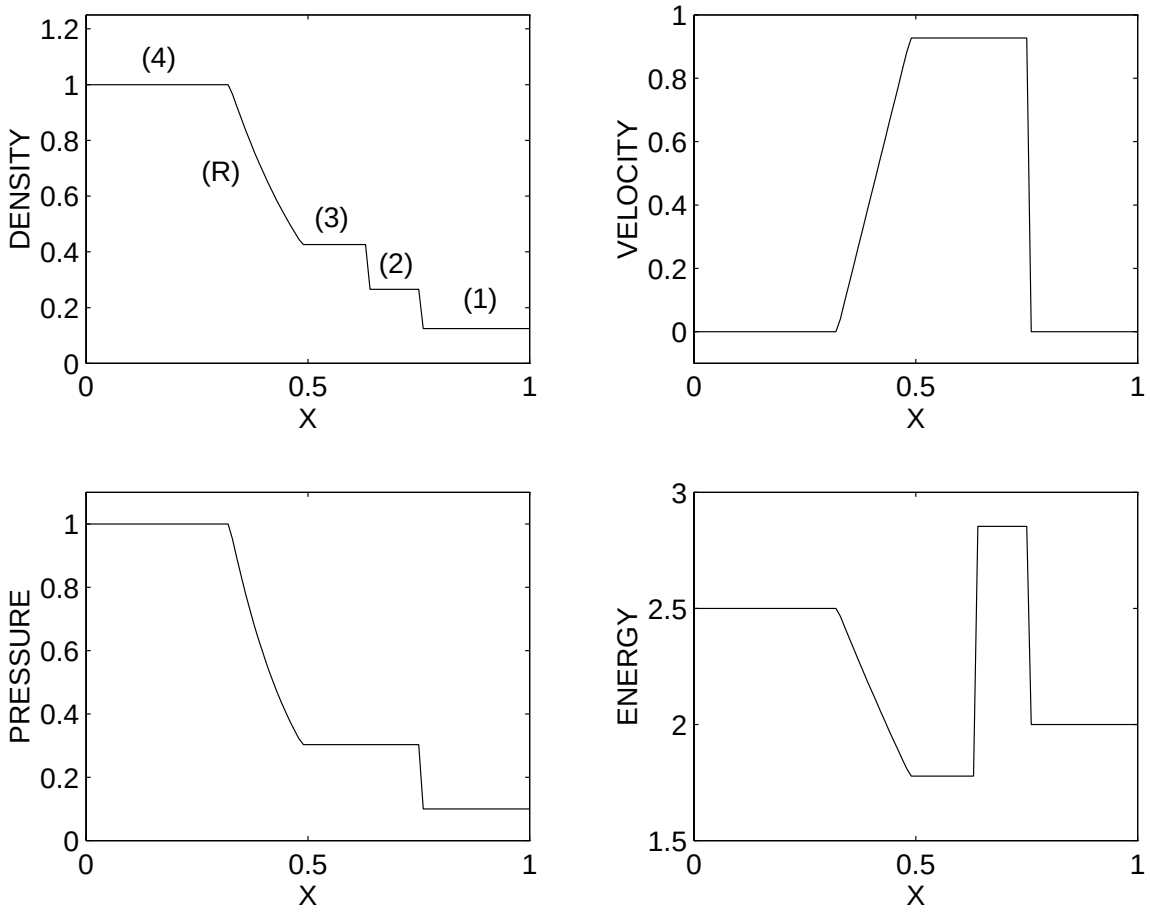

Figure 4.3: Exact solution of 1-D Riemann problem at t=0.148

where $\mathbf{F}^* = \frac{1}{2}(\mathbf{F}_i + \mathbf{F_{i+1}}) - \frac{1}{2}\sum_j |\bar{\lambda_j}|\partial w_j \bar{\mathbf{r}}_j$ and where $\bar{\lambda_j}$ and $\bar{\mathbf{r}}_j$ are the eigenvalues and eigenvectors of the rho-averaged Jacobian matrix $\bar{A}(\mathbf{U}_i, \mathbf{U}_{i+1})$ and ∂w_j are scalars defining the waves. The Roe scheme is based on solving the simpler constant coefficient linear system of conservation laws

$$\mathbf{U}_t + \bar{A}(\mathbf{U}_i, \mathbf{U}_{i+1})\mathbf{U}_x = \mathbf{0} \tag{4.18}$$

between each of the grid points. The rho-averaged Jacobian, $\bar{A}(\mathbf{U}_i, \mathbf{U}_{i+1})$, is calculated by rewriting the Jacobian in terms of the density, ρ; velocity, u; and enthalpy, $H = \left(\frac{e+P}{\rho}\right)$. These variables are then replaced by an average weighted by the square root of the densities [24], *i.e.*,

$$\bar{u}_{i+\frac{1}{2}} = \frac{(u\sqrt{\rho})_{i+1} + (u\sqrt{\rho})_i}{\sqrt{\rho_{i+1}} + \sqrt{\rho_i}}.$$

The sonic entropy fix of Harten and Hyman [28] is added to the Roe scheme which allows the formation of rarefaction waves in the solution. The second-order superbee flux-limiter method has also been added. Flux-limiters hybridize a high order flux, $\mathbf{F}_H$, that works well in smooth regions and a lower order flux, $\mathbf{F}_L$, that works well near discontinuities. The hybrid flux is given by

$$\mathbf{F}(\mathbf{U}) = F_L(\mathbf{U}) + \Phi(\mathbf{U})\left[\mathbf{F}_H(\mathbf{U}) - \mathbf{F}_L(\mathbf{U})\right] \tag{4.19}$$

where $\Phi(\mathbf{U})$ is the limiter. If the solution is smooth then $\Phi(\mathbf{U})$ should be near one and near a discontinuity $\Phi(\mathbf{U})$ should be near zero [28]. The higher and lower order fluxes used and the limiting function $\Phi(\mathbf{U})$ will determine the specific type of flux-limiter. The specifics for the second-order flux limiter can be found in LeVeque [28] or Hirsch [24]. The Roe calculations were performed using CLAWPACK routines [29].

The flow solutions have been calculated using the three different numerical schemes discussed above. The spatial grid size was $\Delta x = 0.01$ and the temporal grid size was $\Delta t = 0.001$. The numerical solutions are given for the Lax-Wendroff, Godunov and Roe schemes in Fig. 4.4, Fig. 4.5, and Fig. 4.6 respectively.

These numerical solutions have been calculated on a fairly fine grid. The discontinuities become more smeared out as the grid spacing becomes larger. For this reason, a graph of the solutions using a coarse, medium and fine grid on a single graph are shown for the Lax-Wendroff, Godunov and Roe schemes in Fig. 4.7, Fig. 4.8 and Fig. 4.9, respectively. The grid spacing for the coarse grid is $\Delta t = 0.004$ and $\Delta x = 0.04$ while the grid spacing for the medium grid is $\Delta t = 0.002$ and $\Delta x = 0.02$.

The figures clearly show that the most accurate solution is achieved with the fine grid. This can be shown by comparing these flow solutions to the exact flow solution. The fine grid solution is plotted versus the exact flow in Fig. 4.10, Fig. 4.11 and Fig. 4.12 for the Lax-Wendroff, Godunov and Roe methods respectively.

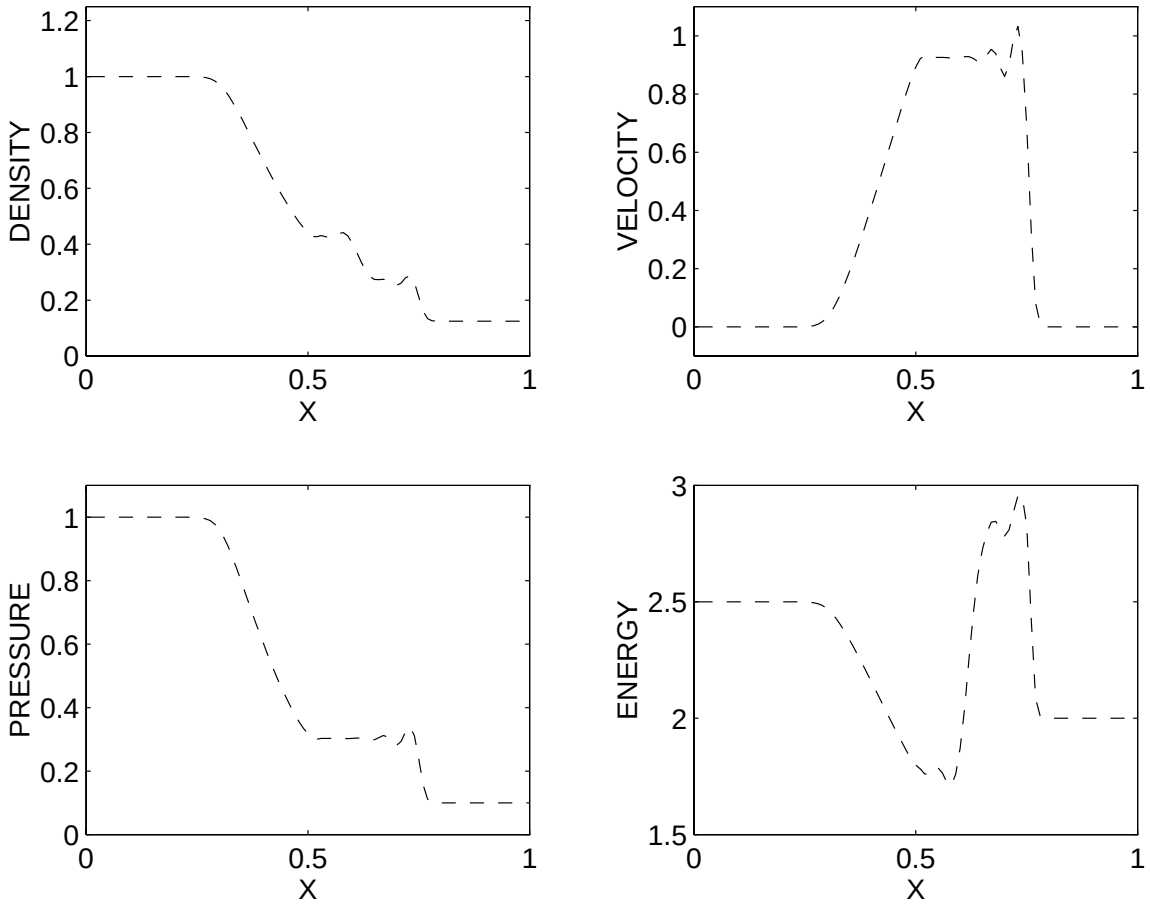

Figure 4.4: Riemann problem flow solution using the Lax-Wendroff method on a fine grid.

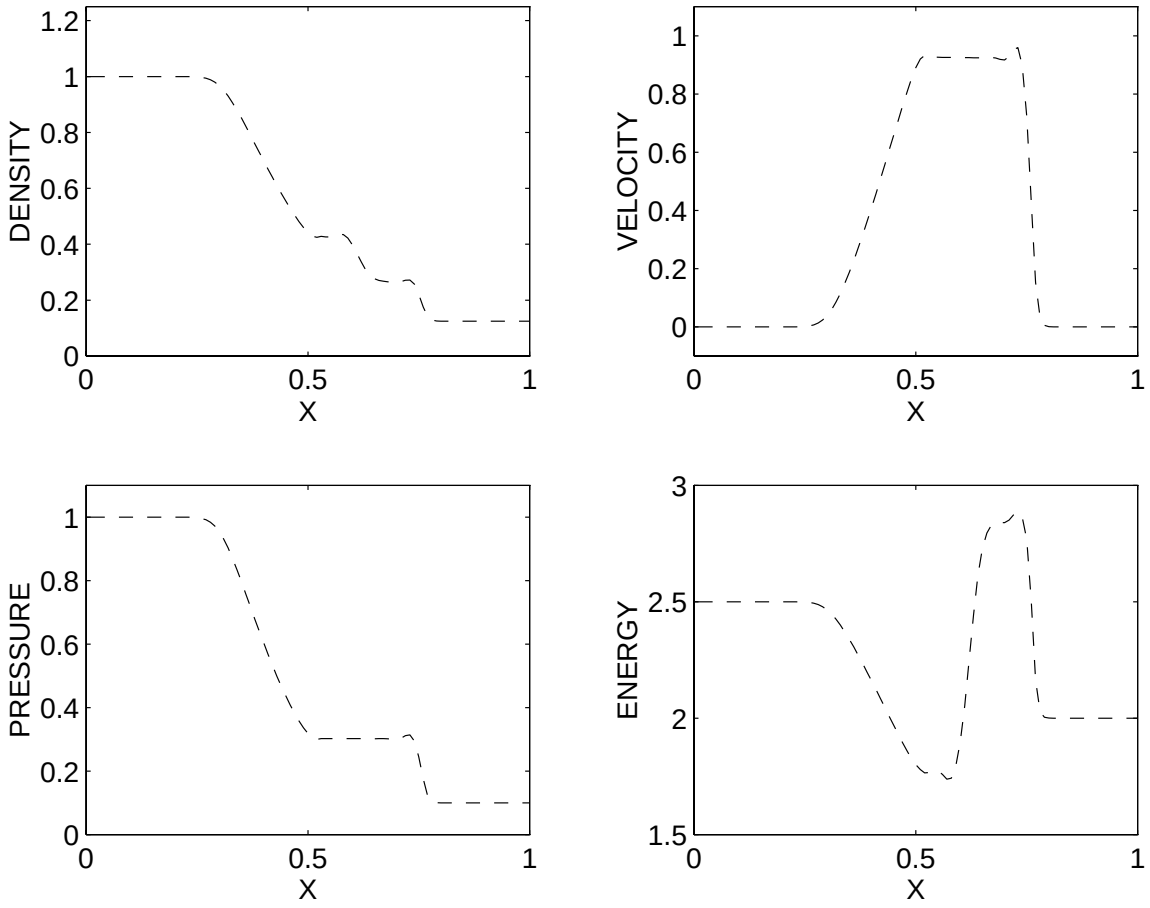

Figure 4.5: Riemann problem flow solution using the Godunov method on a fine grid.

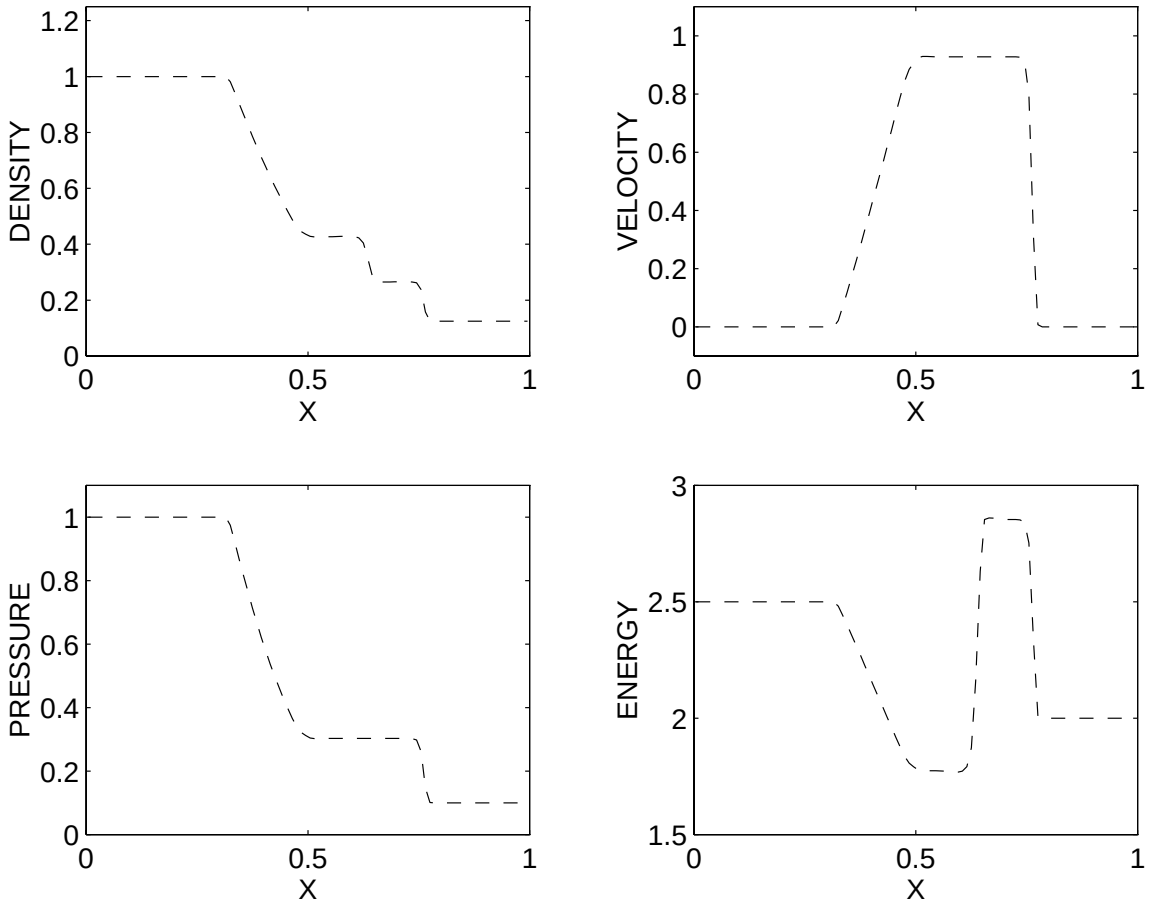

Figure 4.6: Riemann problem flow solution using the Roe method on a fine grid.

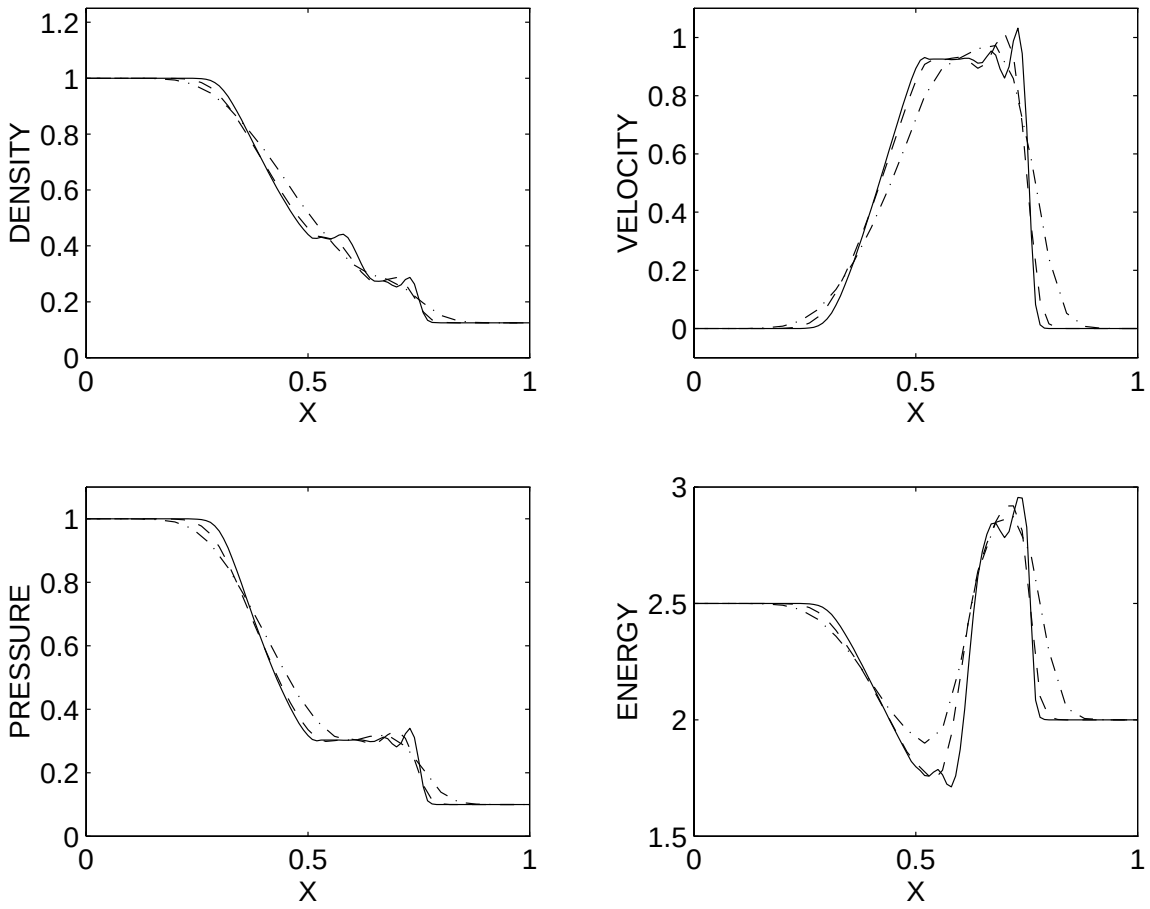

Figure 4.7: Comparison of different grid spacings for the Lax-Wendroff method. A solid line denotes the (—) fine grid, a dashed line denotes the (- -) medium grid, and a dot-dash line denotes the (·-·) coarse grid.

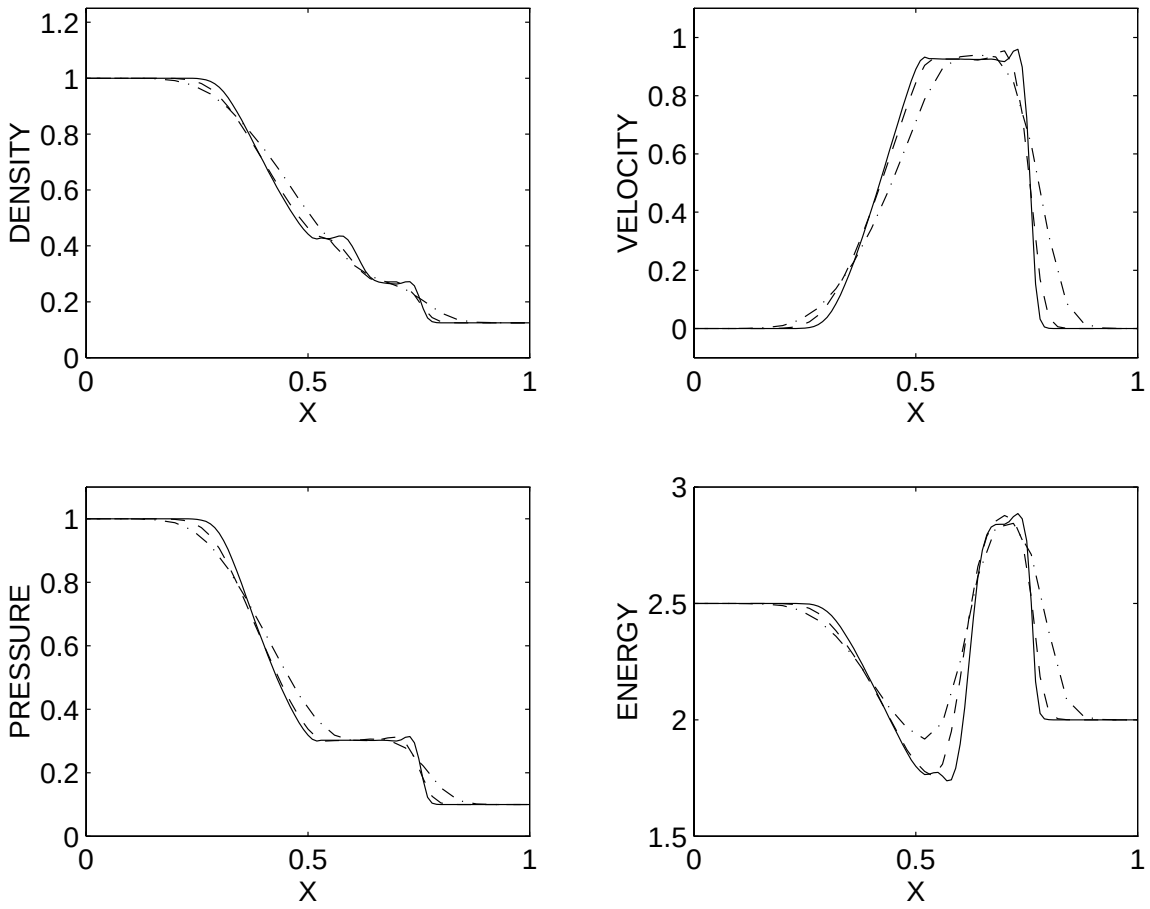

Figure 4.8: Comparison of different grid spacings for the Godunov method. A solid line denotes the (—) fine grid, a dashed line denotes the (- -) medium grid, and a dot-dash line denotes the (·-·) coarse grid.

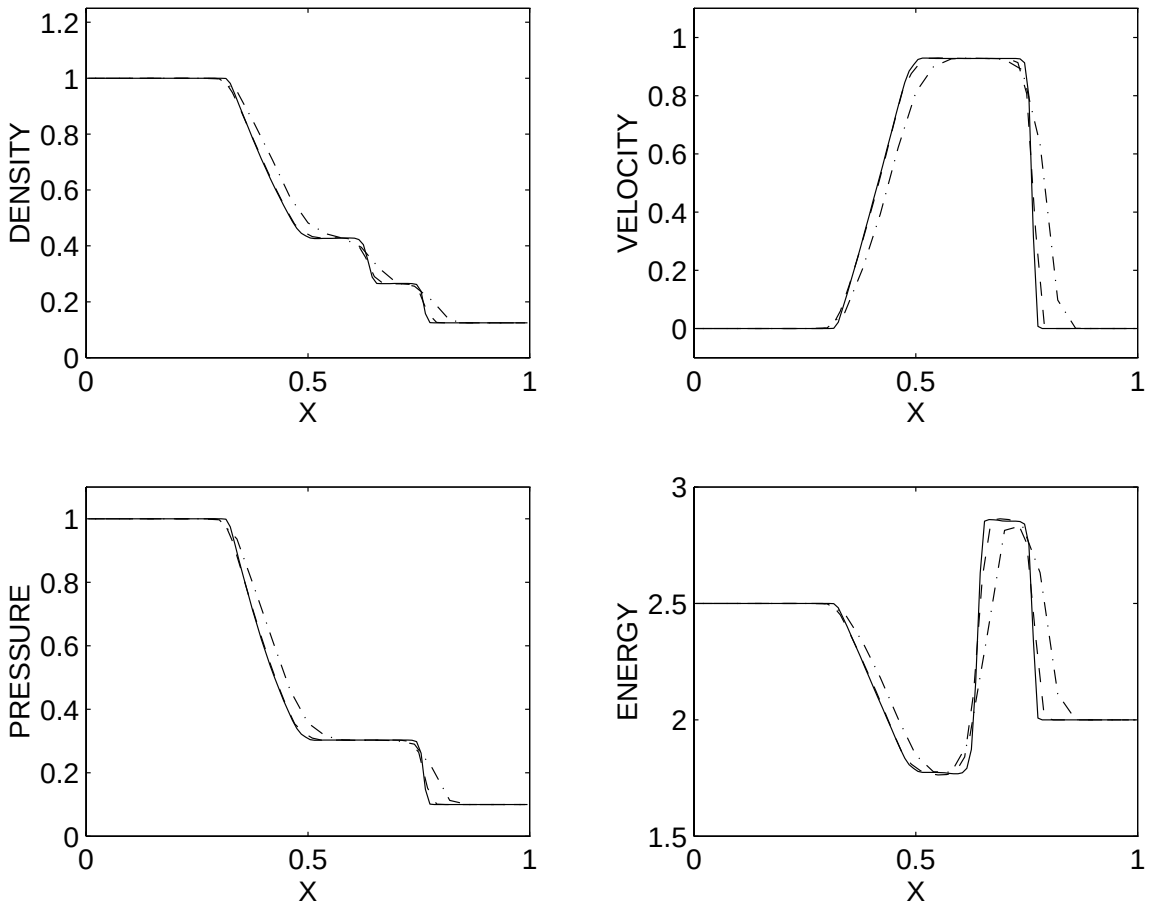

Figure 4.9: Comparison of different grid spacings for the Roe method. A solid line denotes the (—) fine grid, a dashed line denotes the (- -) medium grid, and a dot-dash line denotes the (·-·) coarse grid.

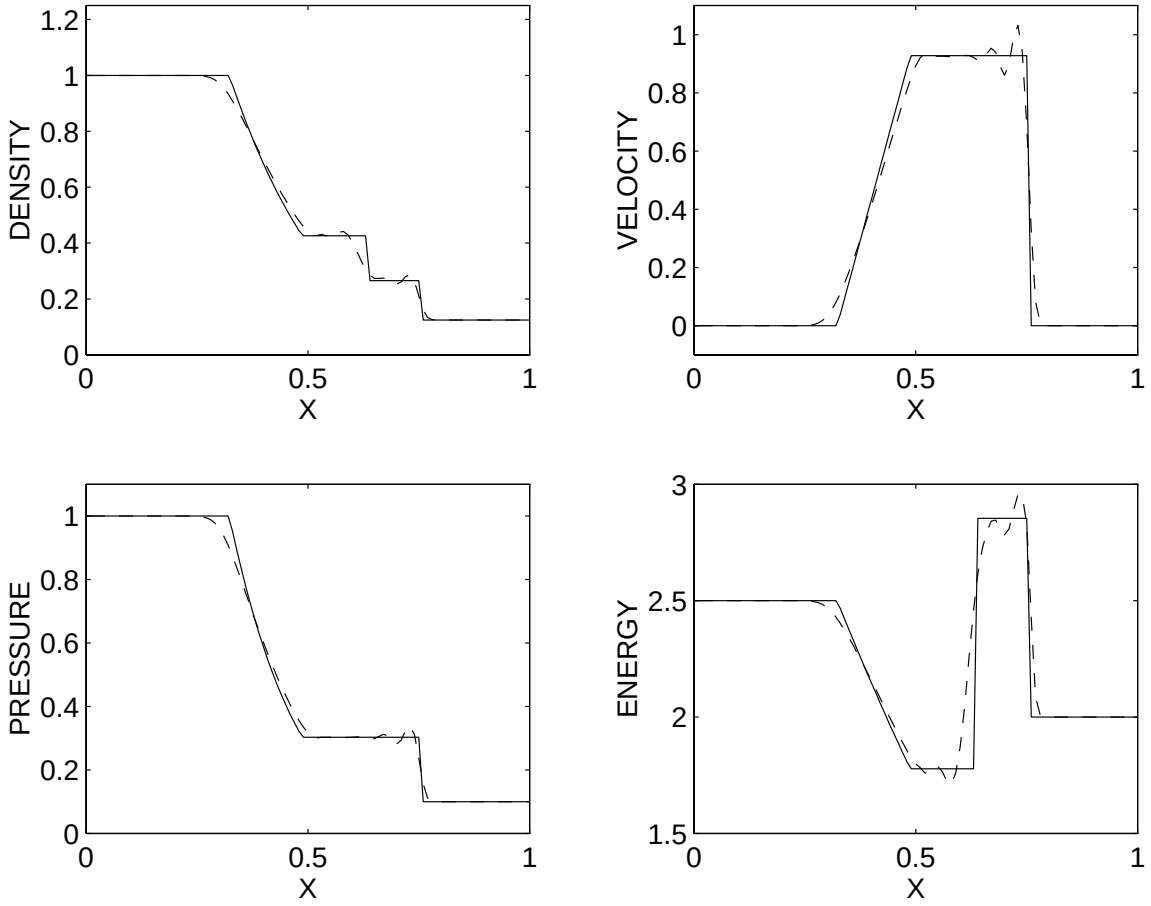

Figure 4.10: Comparison of the Lax-Wendroff fine grid solution (- -) to the exact solution (—).

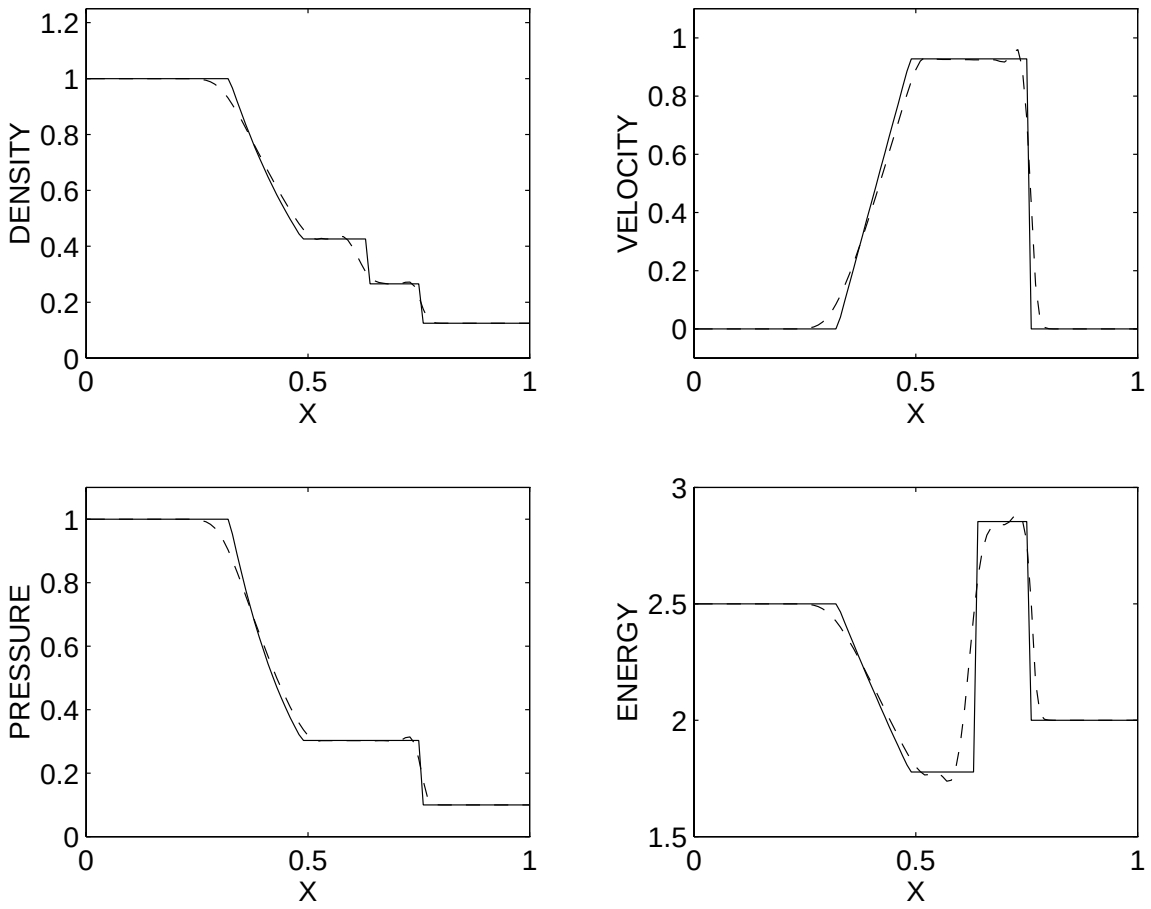

Figure 4.11: Comparison of the Godunov fine grid solution (- -) to the exact solution (—).

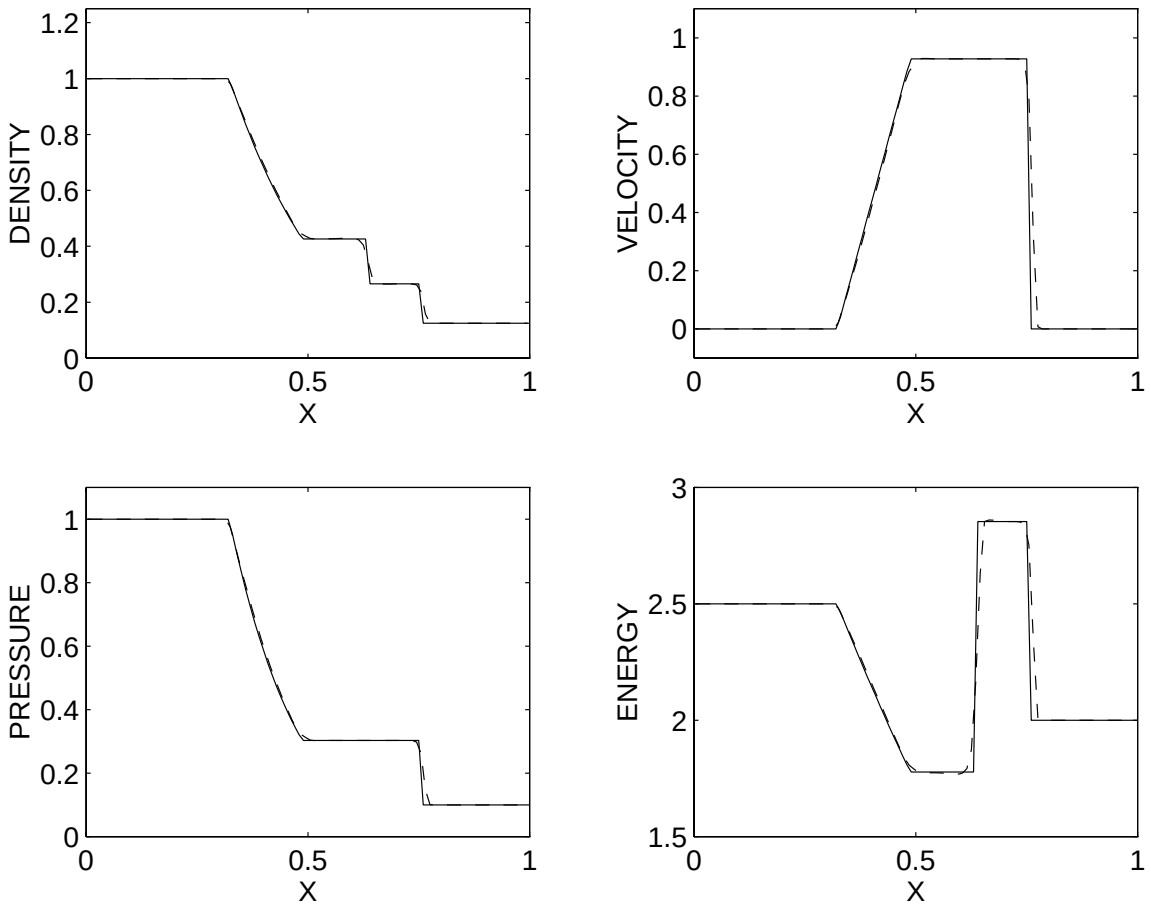

Figure 4.12: Comparison of the Roe fine grid solution (- -) to the exact solution (—).

4.5 Conclusions

It is clear that each of the numerical methods do a nice job of approximating the exact solution for a fine grid. It can also be seen that as the grid size increases, *i.e.*, the grid gets coarser, the numerical approximation of the discontinuities becomes more smeared out. Since the flow sensitivities are coupled to the flow solution, it is expected that the resolution of the approximate flow solution will have a direct effect on the approximate sensitivity calculation. Two things of note arise from the above graphs. The first is the sharp capture of the discontinuities by the Roe scheme, *i.e.*, shock waves and contact discontinuities are captured in just a couple of grid points as opposed to the Lax-Wendroff and Godunov methods. This is expected using the second order superbee limiters as opposed to the artificial viscosity. The artificial viscosity term attempts to add some diffusion to the solutions of the Lax-Wendroff and Godunov methods and helps them capture the discontinuities but the Roe method still does a better job.

The second thing to note is the oscillations in the post-shock region for the Lax-Wendroff method. This behavior is expected and described in LeVeque [28] due to the dispersive nature of the method. One possible remedy is to increase the size of the time step, Δt. This has the result of a smoother, less oscillatory flow solution. After increasing Δt, the solution for a coarse, medium and fine grid on a single graph is shown in Fig. 4.13. The grid spacing is $\Delta t = 0.0164444$ and $\Delta x = 0.04$ for the coarse grid; $\Delta t = 0.0082222$ and $\Delta x = 0.02$ for the medium grid; and $\Delta t = 0.004$ and $\Delta x = 0.01$ for the fine grid. Clearly, the larger time step, Δt, reduces the magnitude of the oscillations near the discontinuity. Again, the fine grid solution using the larger time step is compared to the exact flow solution in Fig. 4.14. It is easy to see that the Lax-Wendroff approximate flow solution for the larger time step in Fig. 4.14 is a better approximation to the exact solution than the smaller time step solution shown in Fig. 4.10.

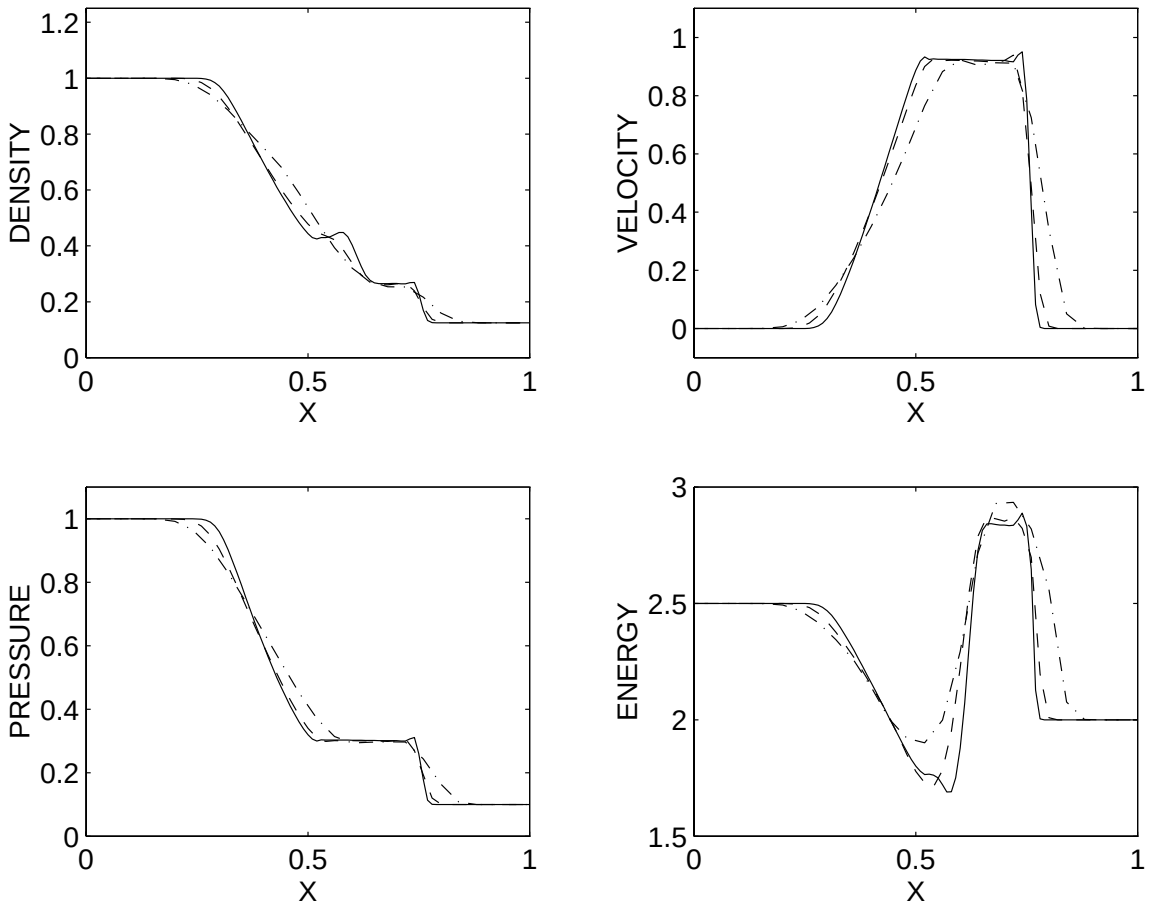

Figure 4.13: Comparison of different grid spacings for the Lax-Wendroff method using a larger time step than in Fig. 4.7. A solid line denotes the (—) fine grid, a dashed line denotes the (- -) medium grid, and a dot-dash line denotes the (·-·) coarse grid.

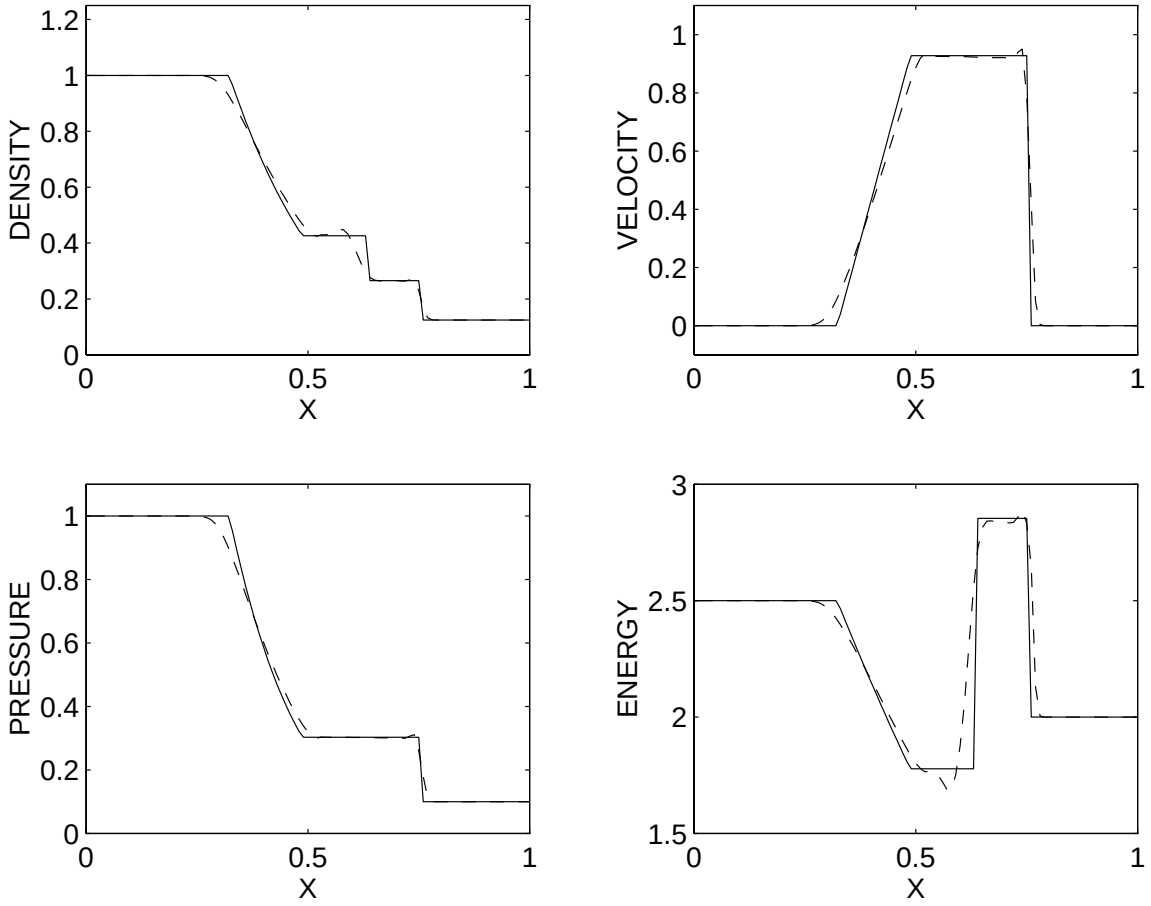

Figure 4.14: Comparison of the Lax-Wendroff fine grid solution (- -) to the exact solution (—) using a larger time step.

Chapter 5

Sensitivity Calculations for the Riemann Problem

5.1 Sensitivity Calculations

In optimization, or in calculating perturbed flows, it becomes important to calculate the sensitivity of the flow with respect to a parameter α. In the next few sections, the sensitivity of the Riemann flow problem with respect to $\alpha = P_4$, the initial high pressure, is calculated. The sensitivities are calculated using finite difference quotients, automatic differentiation and the sensitivity equation method for the Lax-Wendroff, Godunov, and Roe numerical schemes. The finite difference sensitivities are calculated using the forward difference quotient,

$$(\mathbf{U}^h)_\alpha \approx \frac{\mathbf{U}^h(\alpha + \Delta\alpha) - \mathbf{U}^h(\alpha)}{\Delta\alpha}, \tag{5.1}$$

where $\Delta\alpha = 0.1$. The automatic differentiation sensitivity is calculated using the software package ADIFOR [4, 5, 6]. The sensitivity equation method differentiates the continuous Euler Equations and boundary conditions with respect to P_4 to derive a new set of continuous sensitivity equations that can then be solved using one of the numerical methods mentioned above. It will also be necessary to compare these results to the *exact* sensitivities and thus, the exact continuous sensitivities will also be calculated. Since the exact solution is known, Eq. 4.6, it can be differentiated with respect to P_4 to find the exact continuous sensitivity of the fluid flow with respect to P_4.

5.2 Exact Continuous Sensitivities of the 1-D Riemann Problem

The solution of the 1-D Riemann problem has five distinct regions as seen in Fig. 4.2 and Fig. 4.3. Hence, the solution can be differentiated in each region to calculate the exact continuous sensitivity of the flow in that region with respect to the variable P_4. It is important to note that the differentiation is not across shocks or contact discontinuities. If the differentiation had occurred across these phenomena, then a δ-function would result. Likewise, since a corner exists at both ends of the rarefaction wave, it is not possible to take a two sided derivative at this point and one can only rely on a one sided derivative. This will have the effect of introducing a jump discontinuity in the sensitivities at both ends of the rarefaction wave. The exact continuous sensitivity equation should hold everywhere in the domain except at the point where the discontinuity occurs and as one sided limits at the ends of the rarefaction waves. After differentiation, the exact continuous sensitivity of the flow with respect to P_4 as a function of x and t is given by the Eq. 5.2.

$$\begin{bmatrix} \frac{\partial P}{\partial P_4} \\ \frac{\partial \rho}{\partial P_4} \\ \frac{\partial u}{\partial P_4} \end{bmatrix} = \begin{cases} \begin{bmatrix} \frac{\partial P_4}{\partial P_4} \\ \frac{\partial \rho_4}{\partial P_4} \\ \frac{\partial u_4}{\partial P_4} \end{bmatrix} = \begin{bmatrix} 1 \\ 0 \\ 0 \end{bmatrix}, & x < -a_4 t + c \\ \begin{bmatrix} \frac{\partial P_R}{\partial P_4} \\ \frac{\partial \rho_R}{\partial P_4} \\ \frac{\partial u_R}{\partial P_4} \end{bmatrix} = \begin{bmatrix} P_R' \\ \rho_R' \\ u_R' \end{bmatrix}, & -a_4 t + c \leq x < \left(\frac{\gamma_4+1}{2} u_3 - a_4\right) t + c \\ \begin{bmatrix} \frac{\partial P_3}{\partial P_4} \\ \frac{\partial \rho_3}{\partial P_4} \\ \frac{\partial u_3}{\partial P_4} \end{bmatrix} = \begin{bmatrix} P_2' \\ \rho_3' \\ u_3' \end{bmatrix}, & \left(\frac{\gamma_4+1}{2} u_3 - a_4\right) t + c \leq x \leq u_2 t + c \\ \begin{bmatrix} \frac{\partial P_2}{\partial P_4} \\ \frac{\partial \rho_2}{\partial P_4} \\ \frac{\partial u_2}{\partial P_4} \end{bmatrix} = \begin{bmatrix} \phi' \\ \rho_2' \\ u_3' \end{bmatrix}, & u_2 t + c < x < a_1 \left(\frac{\gamma_1-1}{2\gamma_1} + \frac{\gamma_1+1}{2\gamma_1}\frac{P_2}{P_1}\right)^{\frac{1}{2}} t + c \\ \begin{bmatrix} \frac{\partial P_1}{\partial P_4} \\ \frac{\partial \rho_1}{\partial P_4} \\ \frac{\partial u_1}{\partial P_4} \end{bmatrix} = \begin{bmatrix} 0 \\ 0 \\ 0 \end{bmatrix}, & a_1 \left(\frac{\gamma_1-1}{2\gamma_1} + \frac{\gamma_1+1}{2\gamma_1}\frac{P_2}{P_1}\right)^{\frac{1}{2}} t + c \leq x \end{cases} \tag{5.2}$$

where $a_i^2 = \frac{\gamma_i P_i}{\rho_i}$ and the equation for ϕ' is found by differentiating the implicit equation

$$\frac{P_4}{P_1} = \frac{\phi}{P_1}\left(1 - \frac{(\gamma_4 - 1)\left(\frac{a_1}{a_4}\right)\left(\frac{\phi}{P_1} - 1\right)}{\sqrt{2\gamma_1}\sqrt{2\gamma_1 + (\gamma_1+1)\left(\frac{\phi}{P_1} - 1\right)}}\right)^{\frac{-2\gamma_4}{\gamma_4 - 1}}$$

for ϕ with respect to P_4 and solving for ϕ'. This equation is not considered here due to it's complexity and length, but it can be derived using a little calculus and is explicit in ϕ'. The other variables, ρ_2', ρ_3', and u_3' are given by

$$\begin{aligned}\rho_2' &= \rho_1\left(\frac{P_2'}{P_1}\right)\left(\frac{1+\frac{\gamma_1-1}{\gamma_1+1}\frac{P_1}{P_2}}{1+\frac{\gamma_1-1}{\gamma_1+1}\frac{P_2}{P_1}}\right) \\ &+ \rho_1\left(\frac{P_2}{P_1}\right)\left(\frac{\gamma_1-1}{\gamma_1+1}\right)\left(\frac{(\frac{-P_1}{P_2^2}P_2')(1+\frac{\gamma_1-1}{\gamma_1+1}\frac{P_2}{P_1})-(1+\frac{\gamma_1-1}{\gamma_1+1}\frac{P_1}{P_2})\frac{P_2'}{P_1}}{(1+\frac{\gamma_1-1}{\gamma_1+1}\frac{P_2}{P_1})^2}\right) \qquad (5.3)\end{aligned}$$

$$\rho_3' = \rho_4\left(\frac{1}{\gamma_4}\right)\left(\frac{P_3}{P_4}\right)^{\frac{1-\gamma_4}{\gamma_4}}\left(\frac{P_3'P_4-P_3}{P_4^2}\right) \qquad (5.4)$$

$$u_3' = \frac{2a_4'}{\gamma_4-1}\left(1-\left(\frac{P_3}{P_4}\right)^{\frac{\gamma_4-1}{2\gamma_4}}\right)-\left(\frac{a_4}{\gamma_4}\right)\left(\frac{P_3}{P_4}\right)^{\frac{-\gamma_4-1}{2\gamma_4}}\left(\frac{P_3'P_4-P_3}{P_4^2}\right) \qquad (5.5)$$

with $a_4' = \frac{1}{2}(\frac{\gamma_4 P_4}{\rho_4})^{-\frac{1}{2}}(\frac{\gamma_4}{\rho_4})$.

In the rarefaction wave, the sensitivity variables, P_R', ρ_R', and u_R' are given by

$$P_R' = \left(1-\frac{\gamma_4-1}{2}\frac{u_R}{a_4}\right)^{\frac{2\gamma_4}{\gamma_4-1}} - P_4\gamma_4\left(1-\frac{\gamma_4-1}{2}\frac{u_R}{a_4}\right)^{\frac{2\gamma_4+1}{\gamma_4-1}}\left(\frac{u_R'a_4-u_Ra_4'}{a_4^2}\right) \qquad (5.6)$$

$$\rho_R' = -\rho_4\left(1-\frac{\gamma_4-1}{2}\frac{u_R}{a_4}\right)^{\frac{3-\gamma_4}{\gamma_4-1}}\left(\frac{u_R'a_4-u_Ra_4'}{a_4^2}\right) \qquad (5.7)$$

$$u_R' = \frac{2u_4u_3'}{(\gamma_4+1)u_3^2}\left(\frac{x-c}{t}\right)+\frac{a_4'u_3^2-a_4'u_4u_3+a_4u_4u_3'}{(\gamma_4+1)u_3^2}. \qquad (5.8)$$

The sensitivity with respect to the parameter P_4 has been calculated at time $t = 0.148$ and for $0 \le x \le 1$ and is graphed in Fig. 5.1. It is important to remember that the exact solution will have a δ-function at both the shock wave and the contact discontinuity which is not shown in Fig. 5.1. The question now arises about the consistency of the approximate sensitivity calculation methods, *i.e.*, how close do the approximate methods come to the exact continuous sensitivity and the exact discrete sensitivities? This idea will be considered further in the coming sections. The δ-functions will play an important role in the numerical approximations of the flow sensitivities. Although the δ-function is a single point, the numerical schemes have a difficult time approximating this function and the δ-function becomes a "δ-spike" spread out over several grid points. The loss of important information can be attributed to this spike.

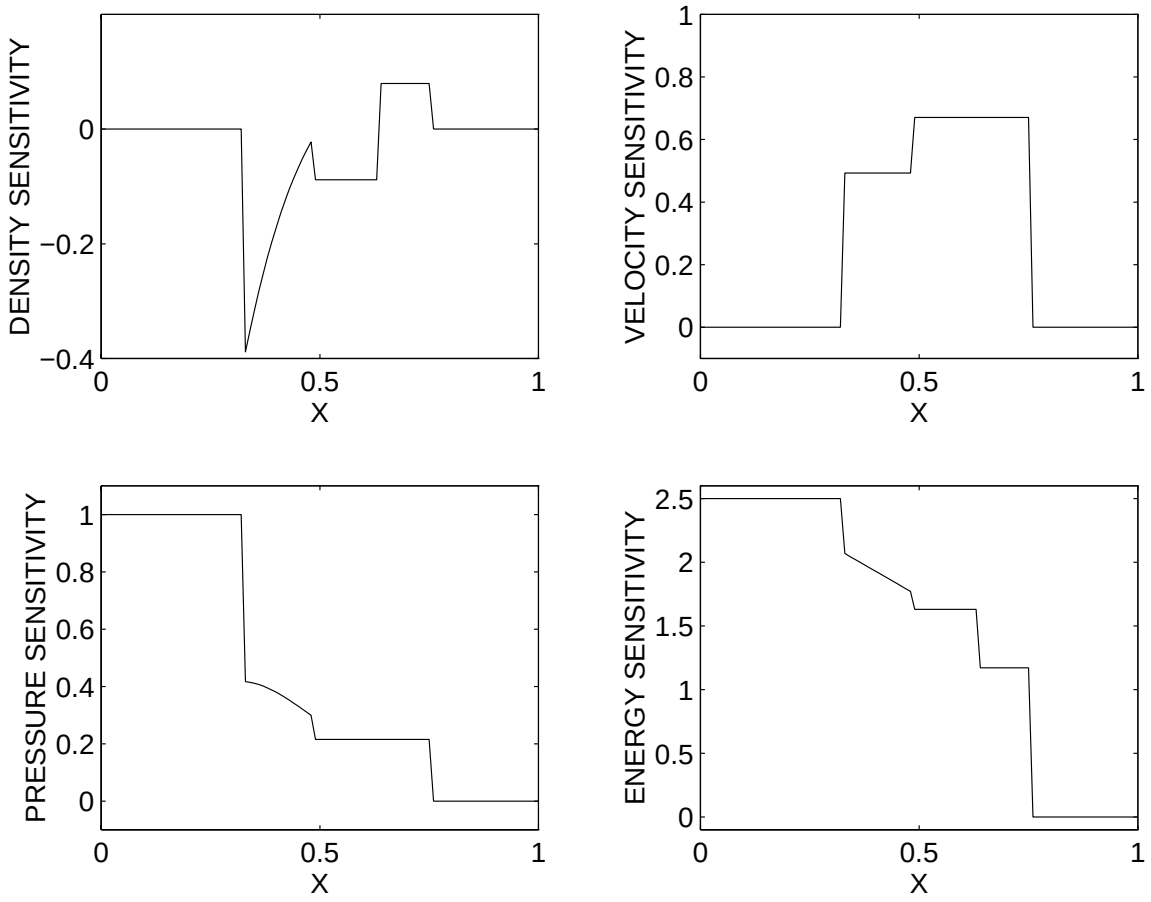

Figure 5.1: Exact continuous sensitivity with respect to P_4 at t=0.148.

5.3 Continuous Sensitivity Equations

The continuous sensitivity equations for the sensitivity equation method are derived by differentiating the original continuous flow equations, Eq. 4.1, and initial conditions, Eq. 4.2, with respect to P_4. The continuous sensitivity equations can be written in conservation law form as

$$\mathbf{S}_t + \left[\frac{\partial \mathbf{F}}{\partial P_4}(\mathbf{U})\right]_x = \mathbf{0} \tag{5.9}$$

where

$$\frac{\partial \mathbf{F}}{\partial P_4}(\mathbf{U}) = \mathbf{F^s}(\mathbf{U},\mathbf{S}) = \begin{bmatrix} m' \\ \frac{2mm'}{\rho} - \frac{m^2}{\rho^2}\rho' + P' \\ (\frac{m'}{\rho} - \frac{m}{\rho^2}\rho')(e+P) + (\frac{m}{\rho})(e'+P') \end{bmatrix}$$

$$\mathbf{S} = \begin{bmatrix} \rho' = \frac{\partial \rho}{\partial P_4} \\ m' = \frac{\partial m}{\partial P_4} \\ e' = \frac{\partial e}{\partial P_4} \end{bmatrix}$$

and where $m' = \rho' u + \rho u'$ and $e' = \frac{P'}{\gamma - 1} + \frac{1}{2}\rho' u^2 + \rho u u'$. The initial conditions for the system are given by

$$\mathbf{S}(x,0) = \begin{cases} \begin{bmatrix} 0 \\ 0 \\ \left(\frac{1}{\gamma_4 - 1}\right) \end{bmatrix} & x \le c \\ \begin{bmatrix} 0 \\ 0 \\ 0 \end{bmatrix} & x > c. \end{cases} \tag{5.10}$$

As is discussed in Section 7.1, the continuous sensitivity equations, Eq. 5.9, only hold within each of the regions (1-4) and (R) and do not hold across the shock, the contact discontinuity, or even at the two ends of the rarefaction wave because the flux function, $\mathbf{F}(\mathbf{U})$ is nondifferential at these points.

5.4 Numerical Methods for the Continuous Sensitivity Equations

The continuous sensitivity equations are solved using three different numerical schemes. The first is a two-step Lax-Wendroff finite difference scheme described in Sod [40],

$$\mathbf{S}_{i+\frac{1}{2}}^{n+\frac{1}{2}} = \frac{1}{2}\left(\mathbf{S}_{i+1}^{n} + \mathbf{S}_{i}^{n}\right) - \frac{\Delta t}{2\Delta x}\left(\mathbf{F}^{\mathbf{s}n}_{i+1} - \mathbf{F}^{\mathbf{s}n}_{i}\right),$$

$$\hat{\mathbf{S}}_i^{n+1} = \mathbf{S}_i^n - \frac{\Delta t}{\Delta x}\left(\mathbf{F^s}_{i+\frac{1}{2}}^{n+\frac{1}{2}} - \mathbf{F^s}_{i-\frac{1}{2}}^{n+\frac{1}{2}}\right). \tag{5.11}$$

The second is the Godunov finite difference scheme also described in Sod [40],

$$\begin{aligned}\mathbf{S}_{i+\frac{1}{2}}^{n+\frac{1}{2}} &= \frac{1}{2}\left(\mathbf{S}_{i+1}^n + \mathbf{S}_i^n\right) - \frac{\Delta t}{\Delta x}\left(\mathbf{F^s}_{i+1}^{n} - \mathbf{F^s}_{i}^{n}\right),\\ \hat{\mathbf{S}}_i^{n+1} &= \mathbf{S}_i^n - \frac{\Delta t}{\Delta x}\left(\mathbf{F^s}_{i+\frac{1}{2}}^{n+\frac{1}{2}} - \mathbf{F^s}_{i-\frac{1}{2}}^{n+\frac{1}{2}}\right).\end{aligned} \tag{5.12}$$

Both the two-step Lax-Wendroff scheme and the Godunov scheme have the post processing artificial viscosity term of Lapidus [40] added to the approximate solution. Let $\hat{\mathbf{S}}_i^{n+1}$ be the approximate solution at the next time step without artificial viscosity, then the solution with the Lapidus artificial viscosity, $\mathbf{S}_j^{n+1}$, is given by Eq. 5.13.

$$\mathbf{S}_i^{n+1} = \hat{\mathbf{S}}_i^{n+1} + \frac{\nu\Delta t}{\Delta x}\Delta'\left[|\Delta'\hat{\mathbf{S}}_{i+1}^{n+1}| \cdot \Delta'\hat{\mathbf{S}}_{i+1}^{n+1}\right], \tag{5.13}$$

where $\Delta'\hat{\mathbf{S}}_i^n = \hat{\mathbf{S}}_i^n - \hat{\mathbf{S}}_{i-1}^n$, and ν is an adjustable constant.

The Roe scheme for the continuous sensitivity requires the development of a new numerical scheme. Two ideas were instrumental in the development of the new Roe scheme for the continuous sensitivity equations. The first idea is that the scheme should be easy to implement and the second idea is that the scheme should retain as much of the original structure as possible. With this in mind, the nonconservation law form of the continuous sensitivity equations is

$$\begin{aligned}\mathbf{S}_t + \frac{\partial \mathbf{F^s}(\mathbf{U},\mathbf{S})}{\partial \mathbf{U}}\mathbf{U}_x + \frac{\partial \mathbf{F^s}(\mathbf{U})}{\partial \mathbf{S}}\mathbf{S}_x &= \mathbf{0}\\ \mathbf{S}_t + \frac{\partial \mathbf{F^s}(\mathbf{U})}{\partial \mathbf{S}}\mathbf{S}_x &= -\frac{\partial \mathbf{F^s}(\mathbf{U},\mathbf{S})}{\partial \mathbf{U}}\mathbf{U}_x\end{aligned} \tag{5.14}$$

where $\frac{\partial \mathbf{F^s}(\mathbf{U})}{\partial \mathbf{S}} = A(\mathbf{U})$ is the same Jacobian as in the flow equations and is given by

$$A(\mathbf{U}) = \begin{bmatrix} 0 & 1 & 0 \\ -(3-\gamma)\frac{u^2}{2} & (3-\gamma)u & \gamma-1 \\ (\gamma-1)u^3 - \frac{\gamma u e}{\rho} & \frac{\gamma e}{\rho} - \frac{3}{2}(\gamma-1)u^2 & \gamma u \end{bmatrix} \tag{5.15}$$

and $\frac{\partial \mathbf{F^s}(\mathbf{U},\mathbf{S})}{\partial \mathbf{U}} =$

$$\begin{bmatrix} 0 & 0 & 0 \\ (\gamma-3)\frac{m m_\alpha}{\rho^2} - (\gamma-3)\frac{m^2\rho_\alpha}{\rho^3} & -(\gamma-3)\frac{m_\alpha}{\rho} + (\gamma-3)\frac{m\rho_\alpha}{\rho^2} & 0 \\ \frac{-\gamma m_\alpha e - \gamma m e_\alpha}{\rho^2} + \frac{2\gamma m e\rho_\alpha + 3(\gamma-1)m^2 m_\alpha}{\rho^3} & \frac{\gamma e_\alpha}{\rho} - \frac{\gamma e\rho_\alpha + 3(\gamma-1)m m_\alpha}{\rho^2} & \frac{\gamma m_\alpha}{\rho} - \frac{\gamma m\rho_\alpha}{\rho^2} \\ -3(\gamma-1)\frac{m^3\rho_\alpha}{\rho^4} & +3(\gamma-1)\frac{m^2\rho_\alpha}{\rho^3} & \end{bmatrix}. \tag{5.16}$$

It should be noted that an equivalent form to Eq. 5.14 is given in Eq. 5.17 and either form is acceptable.

$$\mathbf{S}_t + A(\mathbf{U})\mathbf{S}_x = -A(\mathbf{U})_x\mathbf{S} \tag{5.17}$$

In the implementation of the Roe scheme for the continuous sensitivity equations, the preservation of as much of the original structure as possible is desired. Hence, the continuous flow equations for the Roe scheme are treated as a conservation law with a source term. This can be solved using a splitting approach, in which one alternates between solving the homogeneous equation

$$\mathbf{S}_t + A(\mathbf{U})\mathbf{S}_x = \mathbf{0} \tag{5.18}$$

and the equation

$$\mathbf{S}_t = -\frac{\partial \mathbf{F^s}(\mathbf{U},\mathbf{S})}{\partial \mathbf{U}}\mathbf{U}_x. \tag{5.19}$$

The method employed uses "Strang splitting" [41] where a single time step, Δt, of Eq. 5.14 is solved by first solving Eq. 5.19 over half a time step, $\Delta t/2$. Then these results are used to solve Eq. 5.18 over a full time step and finally Eq. 5.19 is solved again over a half time step. This method is appealing because Eq. 5.18 is identical to the nonconservation form of the Euler equations, Eq. 4.4. Thus it can be solved using the same eigenvalues and eigenvectors as the flow equations. The only change is that the sensitivity variables, $\mathbf{S}$, must be projected onto the eigenvectors as opposed to the flow variables being projected. The source equation, Eq. 5.19, is solved using the following discretization,

$$\mathbf{S}_i^{n+\frac{1}{2}} = \mathbf{S}_i^n - \frac{\Delta t}{\Delta x}\frac{\partial \mathbf{F^s}(\mathbf{U}_i^n,\mathbf{S}_i^n)}{\partial \mathbf{U}}\left(\mathbf{U}_i^j - \mathbf{U}_{i-1}^j\right). \tag{5.20}$$

The obvious desirability of the method is that given a Roe code to calculate the flow solution, it can be easily modified to calculate the flow sensitivities.

It is important to note that the continuous sensitivity equations for high speed flows are linear hyperbolic equations with discontinuous coefficients. There seems to be little literature on the numerical solution of these types of equations. LeVeque and Zhang [30] present one approach, but assumptions require that the discontinuity is at a fixed location throughout time. This does not apply to the Riemann problem or most other problems in aerodynamics.

5.5 Approximate Sensitivity Calculations

The sensitivities have been calculated using finite differences, ADIFOR, and the sensitivity equation method using the three numerical schemes described above. For the finite

difference sensitivity, both the flow at the original value of the parameter, α, and the perturbed value, $\alpha+\Delta\alpha$ are solved using the the same numerical scheme for the flow equations and then the forward difference quotient is calculated. For the automatic differentiation sensitivities, the program ADIFOR is applied to each numerical scheme to derive a new FORTRAN code that will calculate both the flow solution and the automatic differentiation flow sensitivity.

In the first set of graphs, the sensitivities are calculated using a fine grid. The spatial grid size is $\Delta x = 0.01$ and the temporal grid size is $\Delta t = 0.001$. The numerical solutions of the different sensitivity calculation methods for the Lax-Wendroff, Godunov, and Roe schemes are given versus the exact continuous sensitivities in Fig. 5.2, Fig. 5.3, and Fig. 5.4 respectively. The grid spacing can have an effect on the accuracy of the sensitivity calculations and the flow solution calculation as seen previously in Chapter 4. Hence, the Lax-Wendroff sensitivities are calculated for both a coarse and medium grid and are graphed versus the exact continuous sensitivities in Fig. 5.5 and Fig. 5.6. The Godunov sensitivities are calculated for both a coarse and medium grid and are graphed versus the exact continuous sensitivities in Fig. 5.7 and Fig. 5.8. Finally, the Roe sensitivities are calculated for both a coarse and medium grid and are graphed versus the exact continuous sensitivities in Fig. 5.9 and Fig. 5.10. The grid spacing is $\Delta t = 0.002$ and $\Delta x = 0.02$ for the medium grid and $\Delta t = 0.004$ and $\Delta x = 0.04$ for the coarse grid. Clearly, there is good agreement between all the sensitivity calculation methods. Therefore, the method or numerical scheme may not be that important and the easiest and cheapest method should be used. But there are still many problems with the sensitivities in the presence of flow discontinuities.

Again, the grid spacing can have an affect on the accuracy of the Lax-Wendroff method flow solution inducing oscillations. Since the sensitivity equations are coupled with the fluid flow equations, the oscillations in the flow will produce inaccuracies in the approximate sensitivity calculations. This can again be corrected using a larger time step, Δt. The Lax-Wendroff sensitivities are calculated for coarse, medium and fine grid for the larger Δt and plotted versus the exact continuous sensitivities in Fig. 5.11, Fig. 5.12 and Fig. 5.13 respectively. The grid spacing is $\Delta t = 0.004$ and $\Delta x = 0.01$ for the fine grid, $\Delta t = 0.0082222$ and $\Delta x = 0.02$ for the medium grid, and $\Delta t = 0.0164444$ and $\Delta x = 0.04$ for the coarse grid.

5.6 Conclusions

The complexities in the flow, *i.e.*, the shock waves, contact discontinuities and rarefaction waves, and the grid spacing have a large impact on the accuracy of the sensitivity calculation

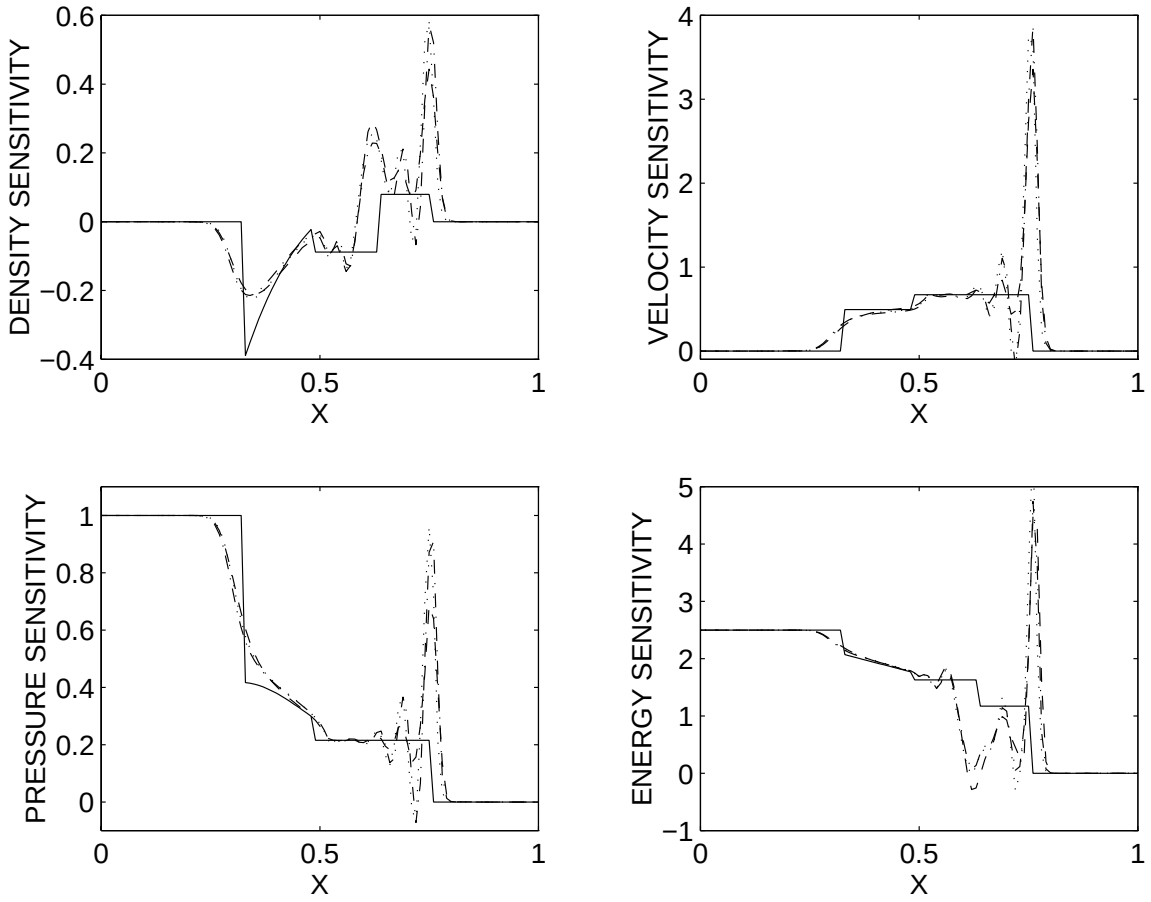

Figure 5.2: Comparison of the three different sensitivity calculation methods using the Lax-Wendroff numerical scheme versus the exact sensitivity. A dotted line ($\cdots$) denotes the ADIFOR sensitivity, a dot-dash line ($\text{-}\cdot\text{-}$) denotes the finite difference sensitivity, a dashed line (- -) denotes the sensitivity equation method sensitivity, and a solid line (—) denotes the exact sensitivity.

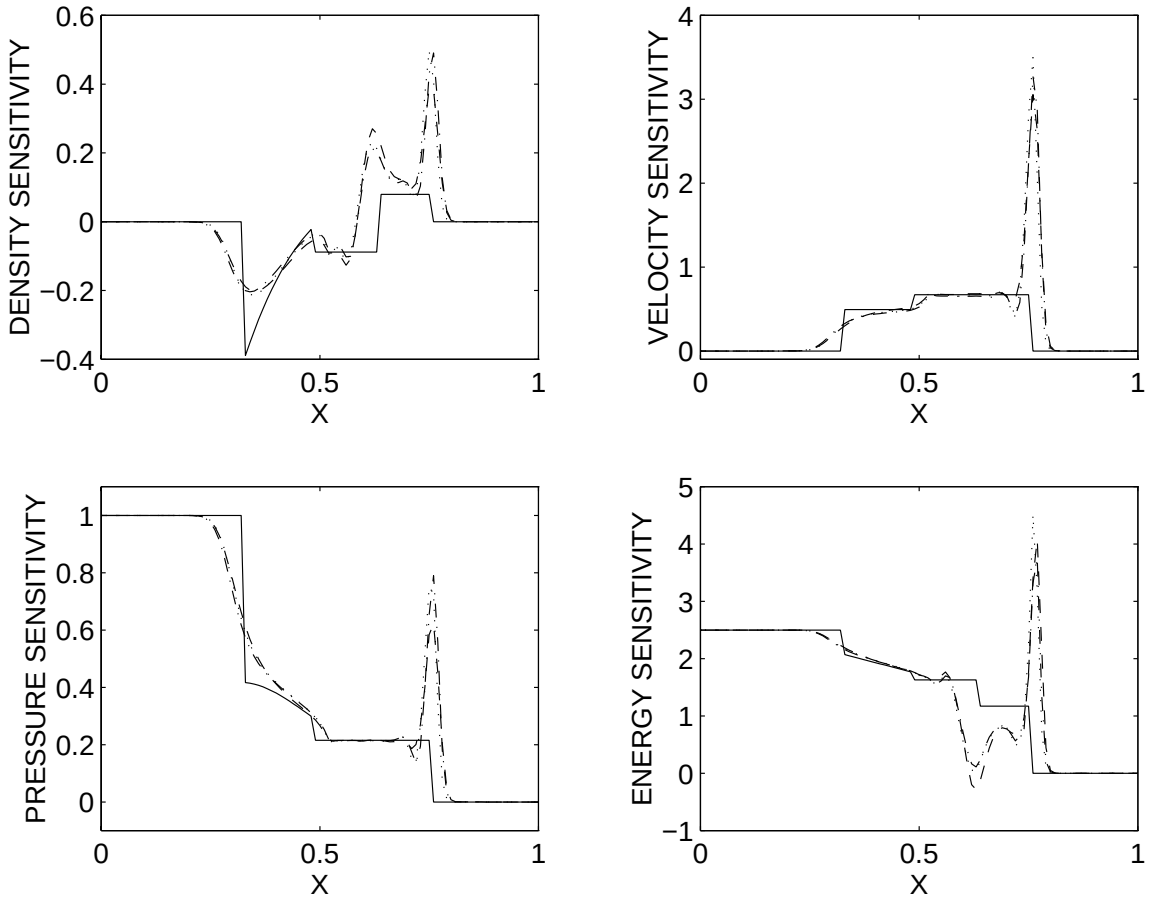

Figure 5.3: Comparison of the three different sensitivity calculation methods using the Godunov numerical scheme versus the exact sensitivity. A dotted line ($\cdots$) denotes the ADIFOR sensitivity, a dot-dash line ($\text{-}\cdot\text{-}$) denotes the finite difference sensitivity, a dashed line (- -) denotes the sensitivity equation method sensitivity, and a solid line (—) denotes the exact sensitivity.

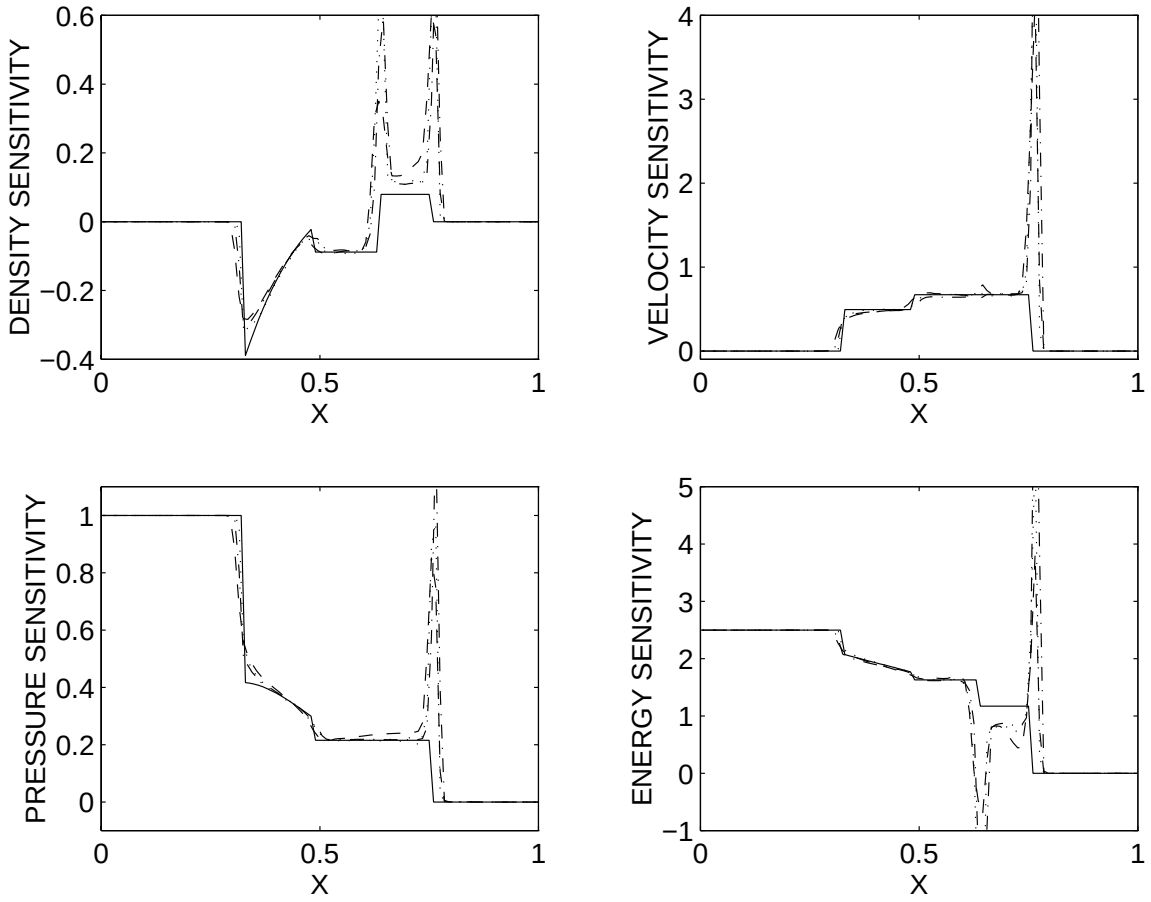

Figure 5.4: Comparison of the three different sensitivity calculation methods using the Roe numerical scheme versus the exact sensitivity. A dotted line (· · ·)denotes the ADIFOR sensitivity, a dot-dash line (·-·) denotes the finite difference sensitivity, a dashed line (- -) denotes the sensitivity equation method sensitivity, and a solid line (—) denotes the exact sensitivity.

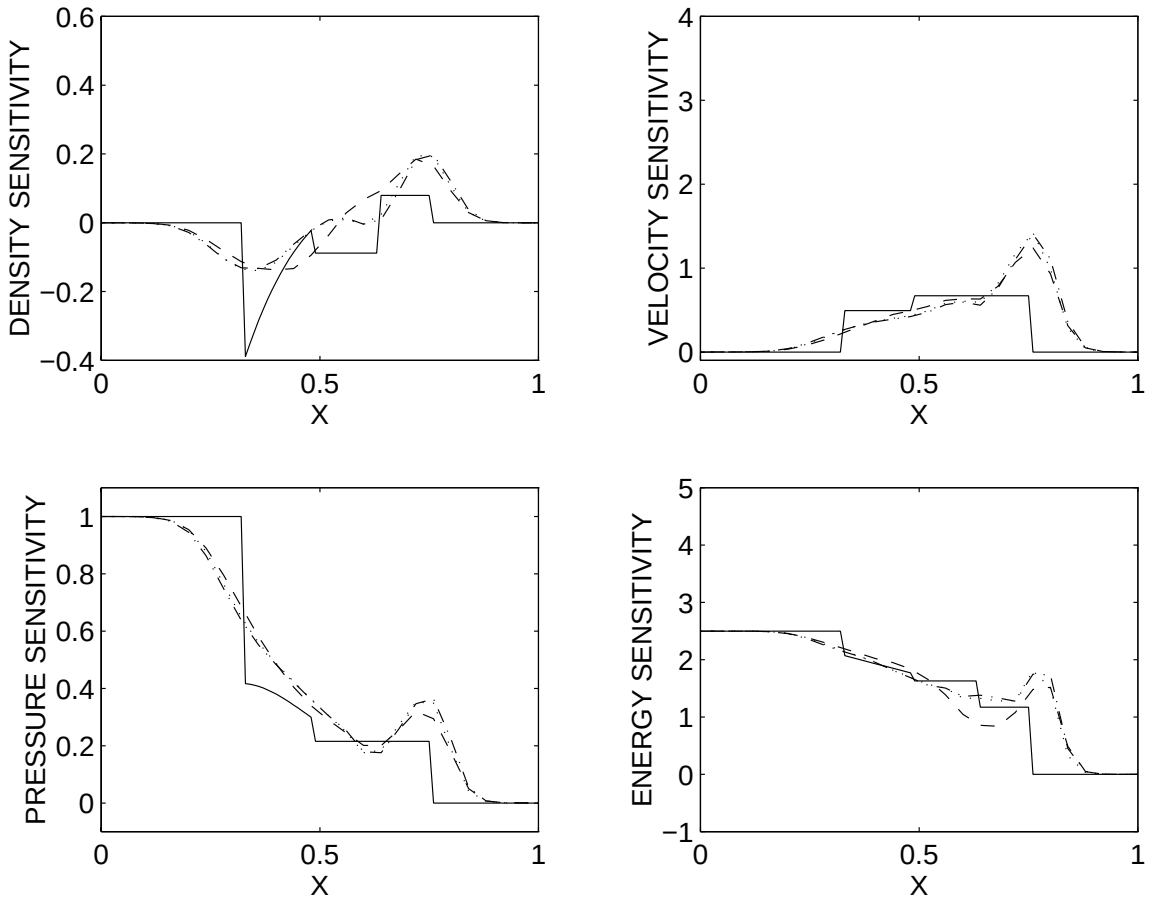

Figure 5.5: Comparison of the three different sensitivity calculation methods using the Lax-Wendroff numerical scheme on a coarse grid versus the exact sensitivity. A dotted line ($\cdots$) denotes the ADIFOR sensitivity, a dot-dash line ($\cdot$-$\cdot$) denotes the finite difference sensitivity, a dashed line (- -) denotes the sensitivity equation method sensitivity, and a solid line (—) denotes the exact sensitivity.

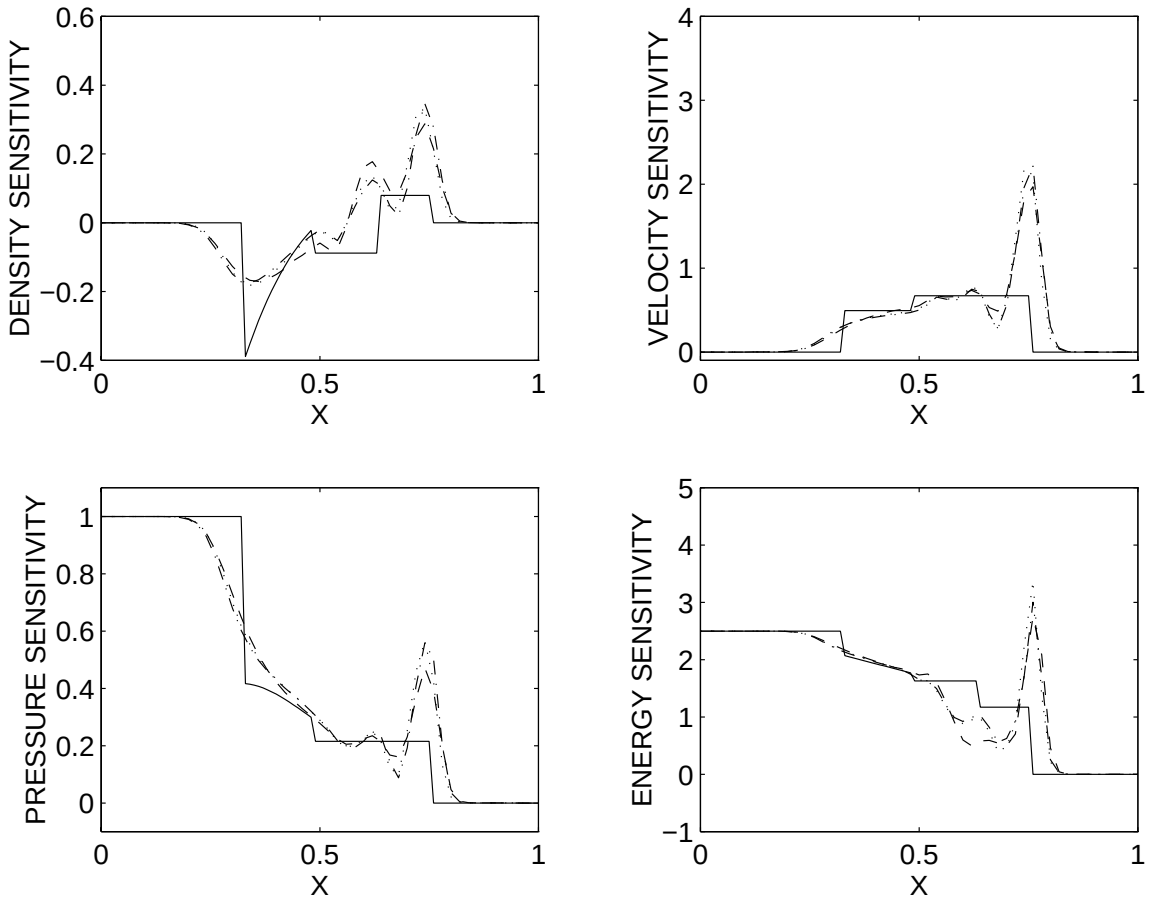

Figure 5.6: Comparison of the three different sensitivity calculation methods using the Lax-Wendroff numerical scheme on a medium grid versus the exact sensitivity. A dotted line ($\cdots$) denotes the ADIFOR sensitivity, a dot-dash line ($\cdot$-$\cdot$) denotes the finite difference sensitivity, a dashed line (- -) denotes the sensitivity equation method sensitivity, and a solid line (—) denotes the exact sensitivity.

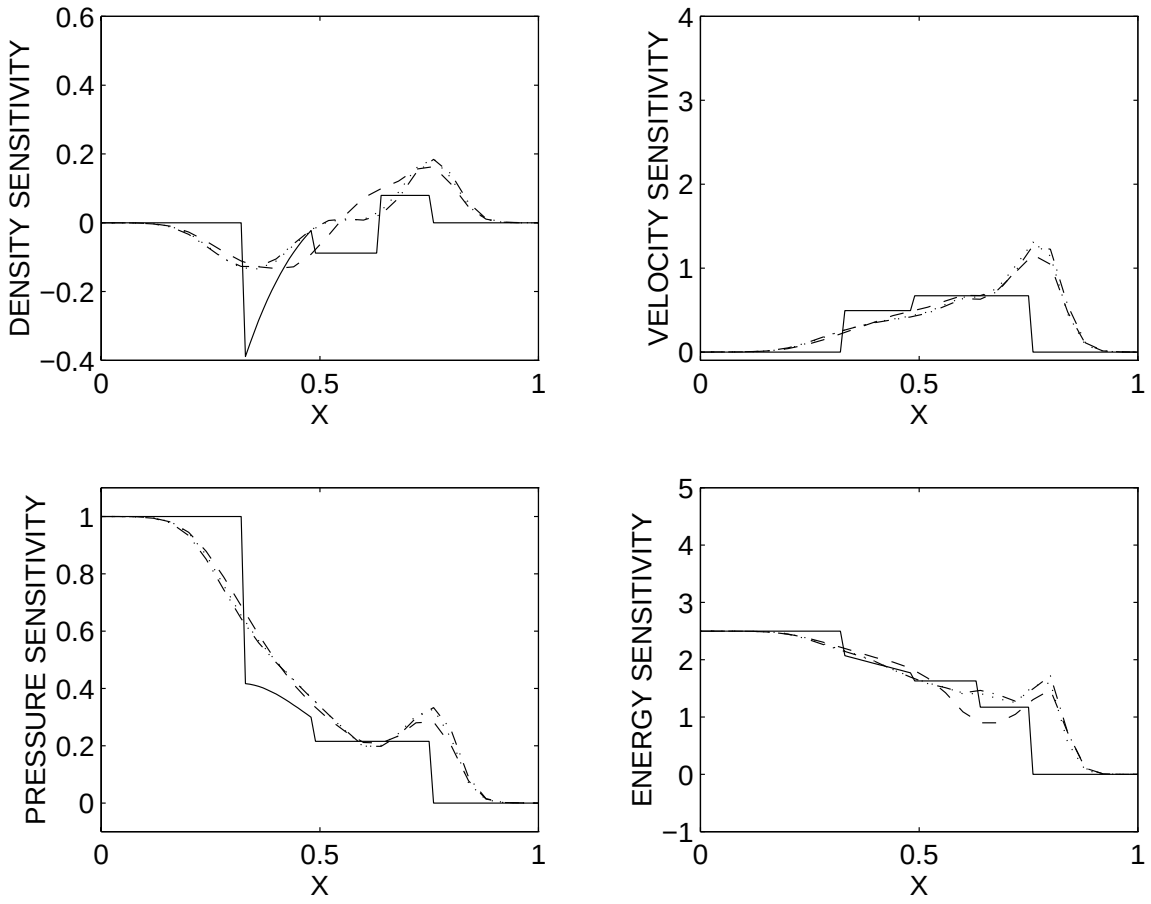

Figure 5.7: Comparison of the three different sensitivity calculation methods using the Godunov numerical scheme on a coarse grid versus the exact sensitivity. A dotted line ($\cdots$) denotes the ADIFOR sensitivity, a dot-dash line ($-\cdot-$) denotes the finite difference sensitivity, a dashed line (- -) denotes the sensitivity equation method sensitivity, and a solid line (—) denotes the exact sensitivity.

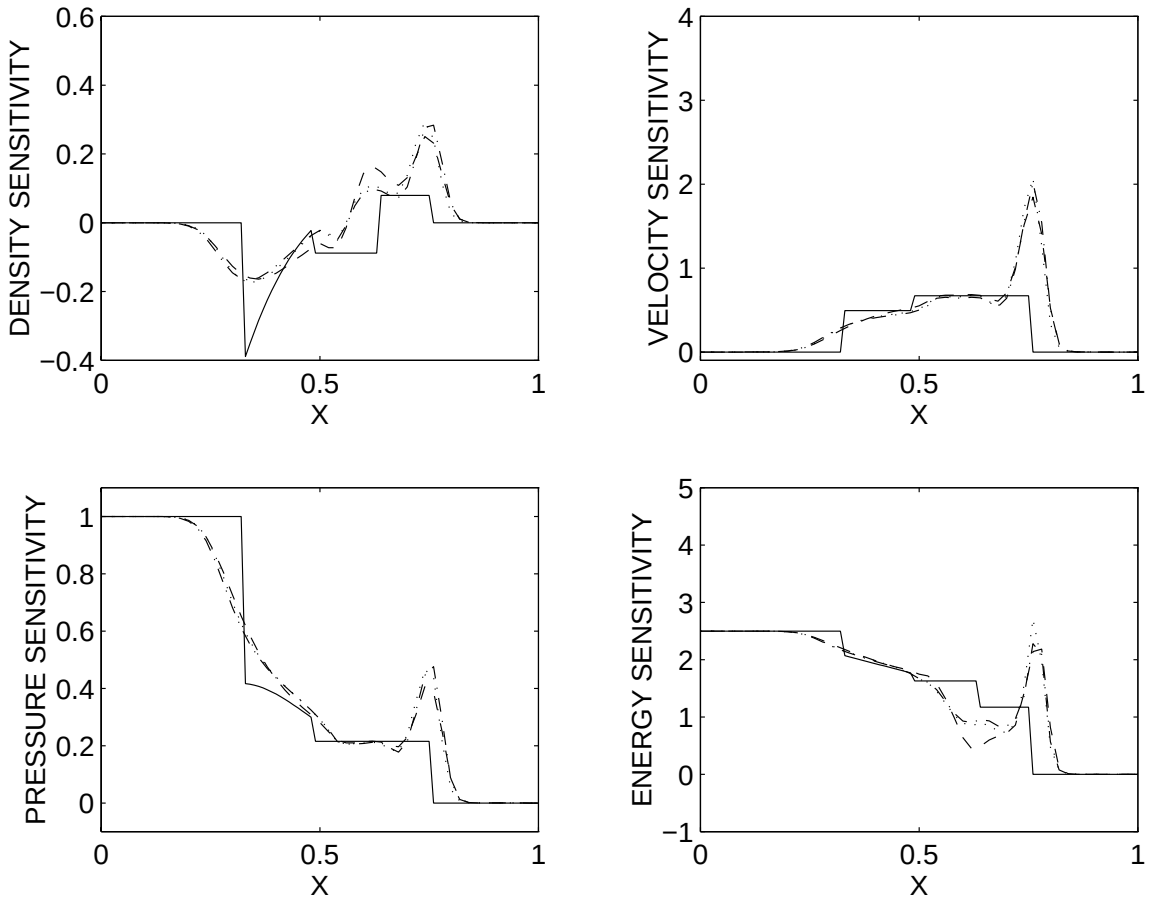

Figure 5.8: Comparison of the three different sensitivity calculation methods using the Godunov numerical scheme on a medium grid versus the exact sensitivity. A dotted line ($\cdots$) denotes the ADIFOR sensitivity, a dot-dash line ($\text{-}\cdot\text{-}$) denotes the finite difference sensitivity, a dashed line (- -) denotes the sensitivity equation method sensitivity, and a solid line (—) denotes the exact sensitivity.

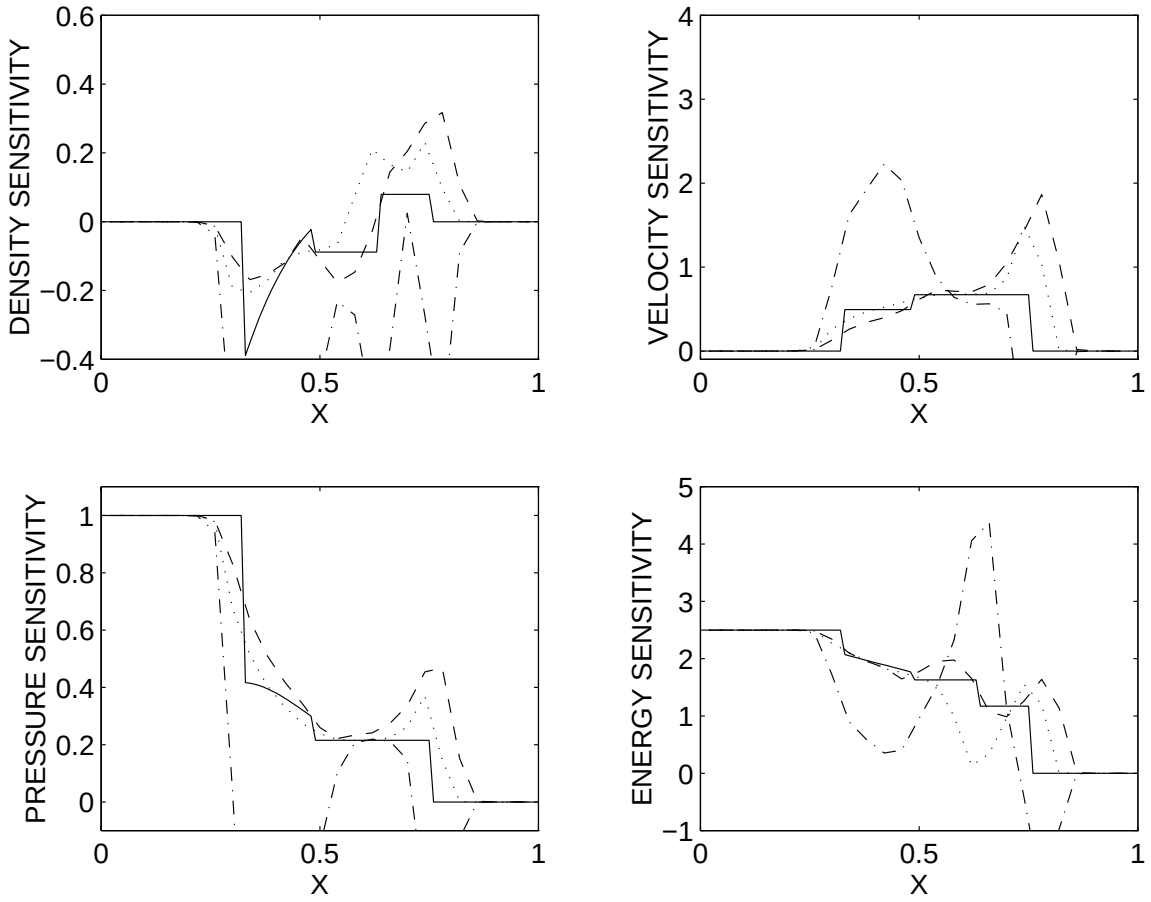

Figure 5.9: Comparison of the three different sensitivity calculation methods using the Roe numerical scheme on a coarse grid versus the exact sensitivity. A dotted line ($\cdots$) denotes the ADIFOR sensitivity, a dot-dash line ($\cdot$-$\cdot$) denotes the finite difference sensitivity, a dashed line (- -) denotes the sensitivity equation method sensitivity, and a solid line (—) denotes the exact sensitivity.

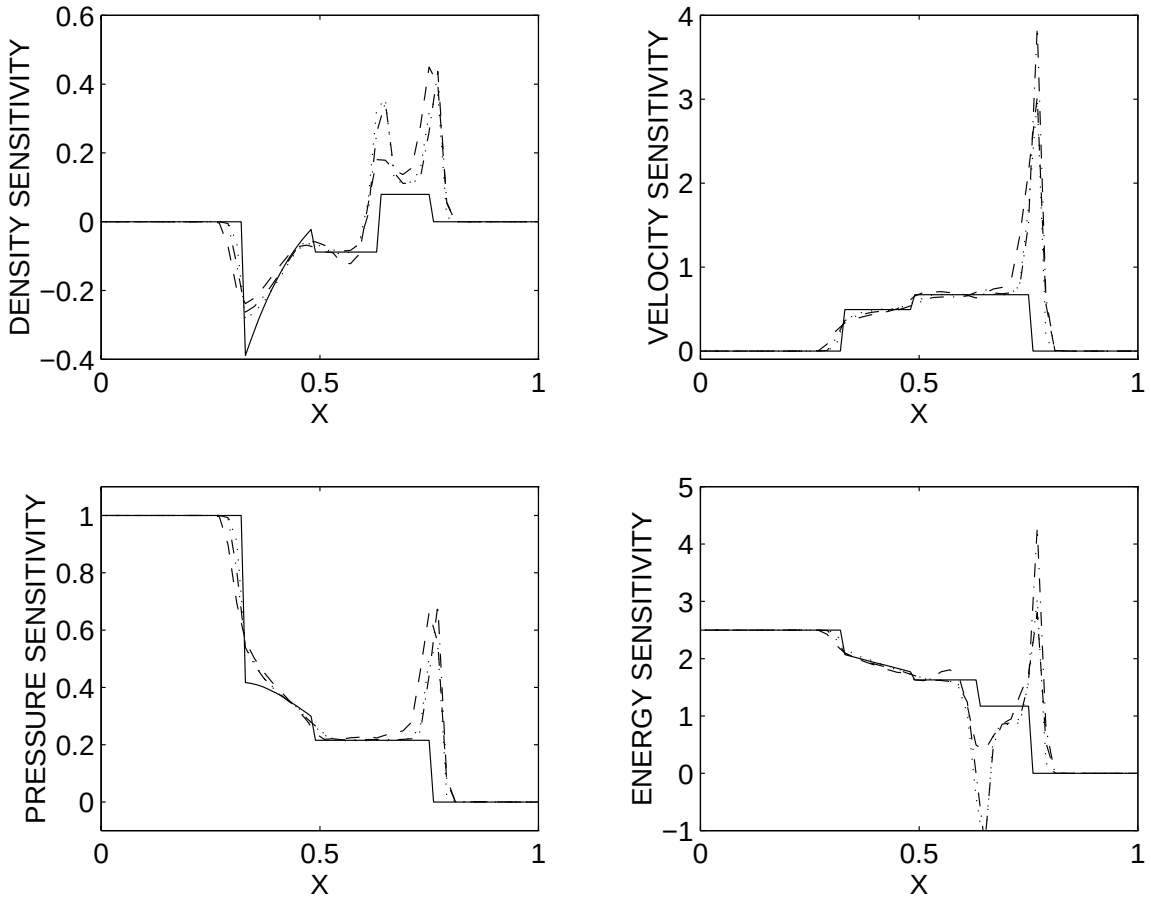

Figure 5.10: Comparison of the three different sensitivity calculation methods using the Roe numerical scheme on a medium grid versus the exact sensitivity. A dotted line ($\cdots$) denotes the ADIFOR sensitivity, a dot-dash line ($-\cdot-$) denotes the finite difference sensitivity, a dashed line (- -) denotes the sensitivity equation method sensitivity, and a solid line (—) denotes the exact sensitivity.

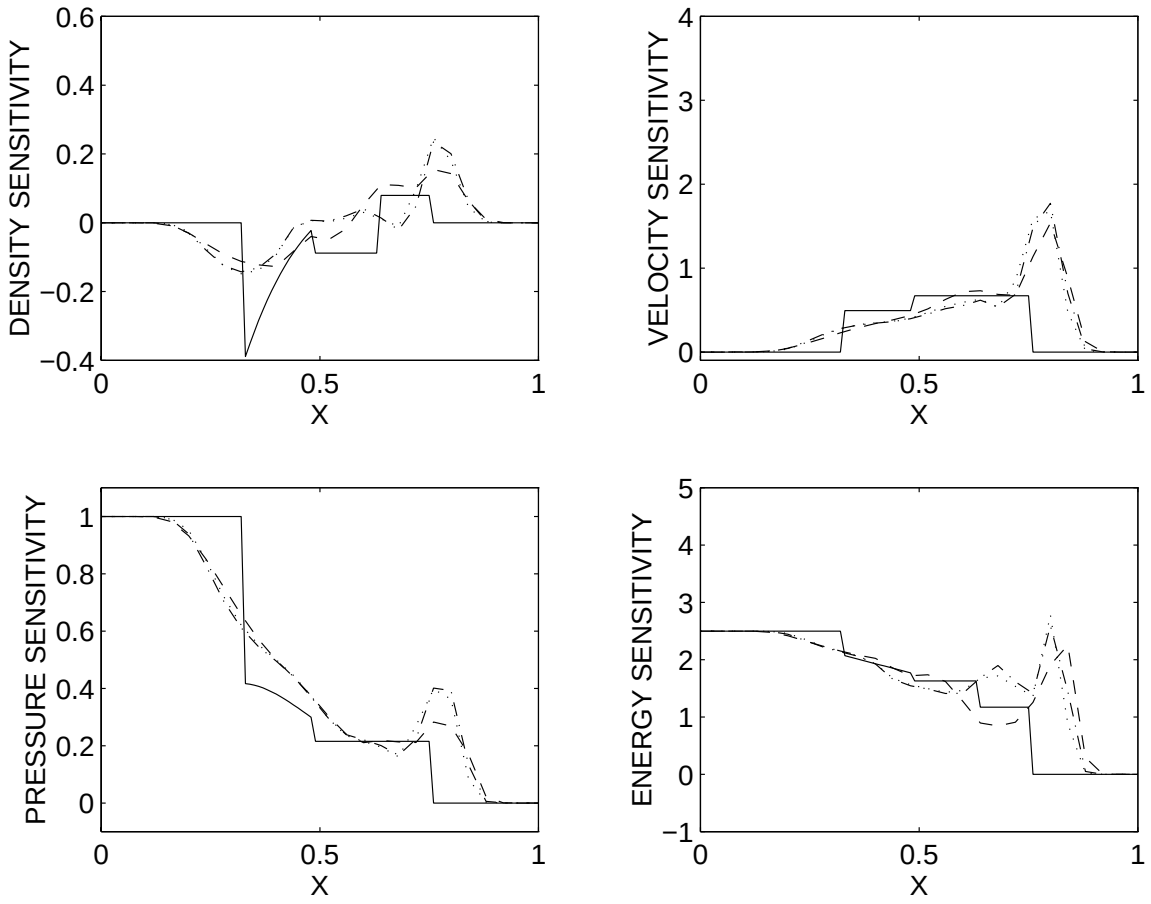

Figure 5.11: Comparison of the three different sensitivity calculation methods using the Lax-Wendroff numerical scheme versus with a larger time step the exact sensitivity on a coarse grid. A dotted line ($\cdots$) denotes the ADIFOR sensitivity, a dot-dash line ($\text{-}\cdot\text{-}$) denotes the finite difference sensitivity, a dashed line (- -) denotes the sensitivity equation method sensitivity, and a solid line (—) denotes the exact sensitivity.

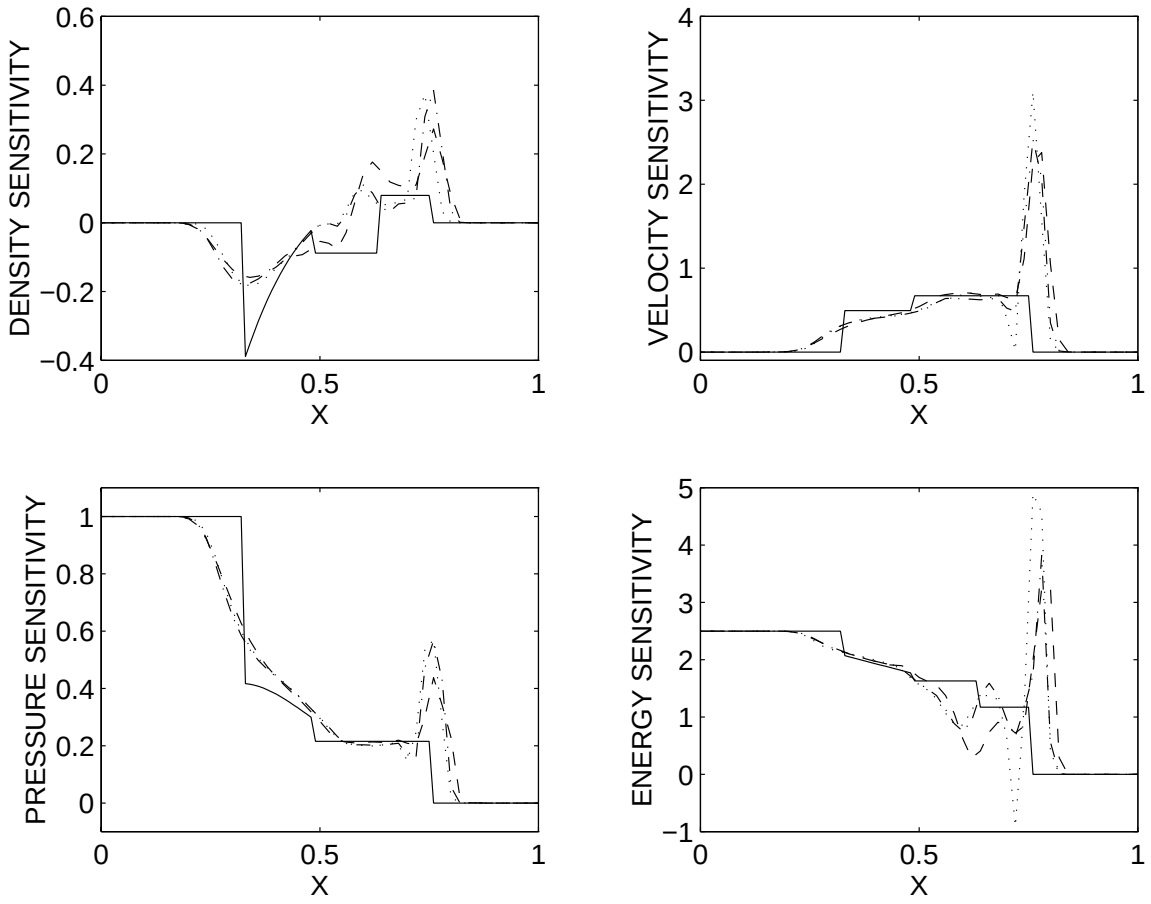

Figure 5.12: Comparison of the three different sensitivity calculation methods using the Lax-Wendroff numerical scheme with a larger time step versus the exact sensitivity on a medium grid. A dotted line ($\cdots$) denotes the ADIFOR sensitivity, a dot-dash line ($\cdot$-$\cdot$) denotes the finite difference sensitivity, a dashed line (- -) denotes the sensitivity equation method sensitivity, and a solid line (—) denotes the exact sensitivity.

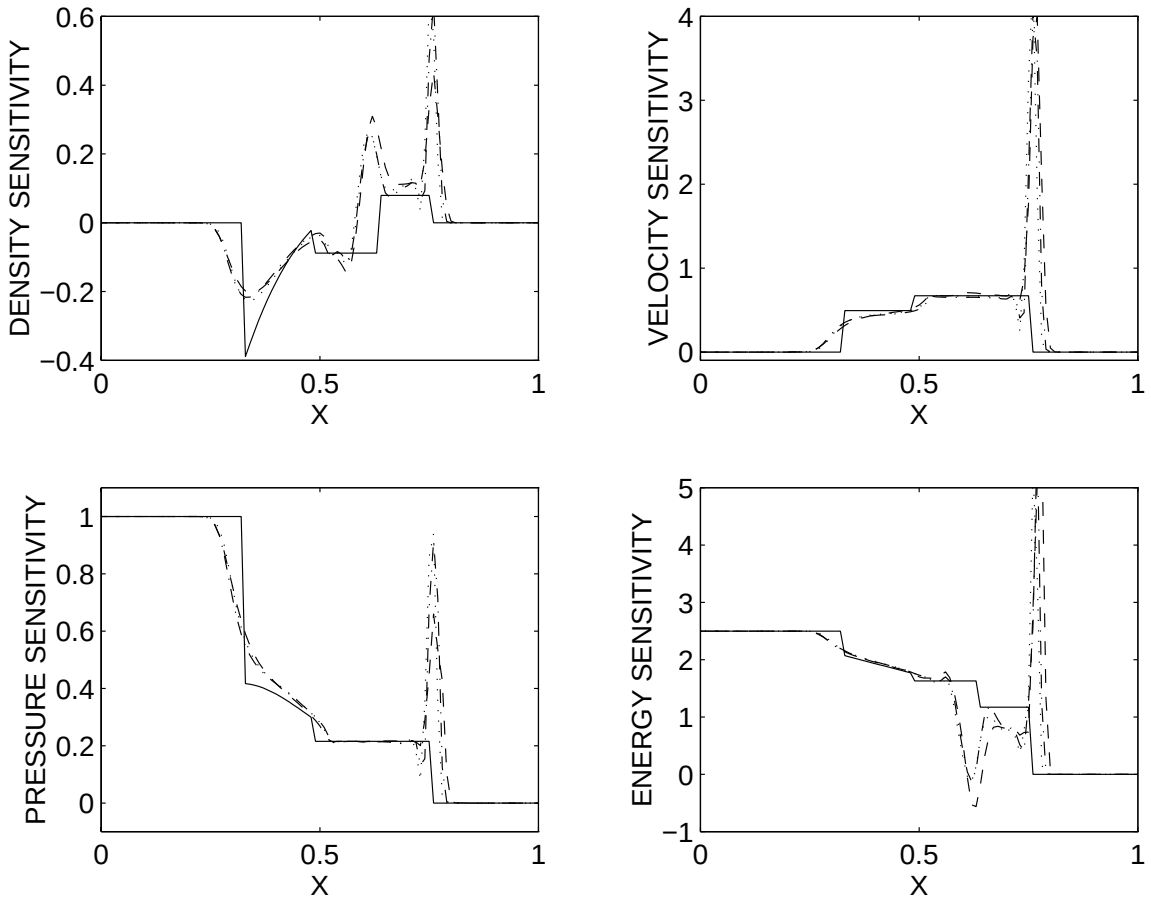

Figure 5.13: Comparison of the three different sensitivity calculation methods using the Lax-Wendroff numerical scheme with a larger time step versus the exact sensitivity on a fine grid. A dotted line ($\cdots$) denotes the ADIFOR sensitivity, a dot-dash line ($\cdot$-$\cdot$) denotes the finite difference sensitivity, a dashed line (- -) denotes the sensitivity equation method sensitivity, and a solid line (—) denotes the exact sensitivity.

methods. It is interesting to note that all the sensitivity calculation methods give virtually indistinguishable results for the medium and fine grids. Consider for example, Fig. 5.2, Fig. 5.3, and Fig. 5.4. In each of these graphs, it is difficult to distinguish between the three different methods except in the regions where large spikes occur. There are differences in the sensitivities based upon the grid sizing and the numerical methods, but if the grid size and numerical method remains fixed there is little difference between the different sensitivity calculation methods. For example, the sensitivities calculated using the Roe scheme on a fine grid, Fig. 5.4, are a better approximation to the exact sensitivities than the sensitivities calculated using the Lax-Wendroff method on either the fine grid, Fig. 5.2, or medium grid, Fig. 5.6, but each of the three sensitivity calculation methods are almost identical to each other in each of the above graphs.

It is hard to make a comparison between the three methods on the coarse grids. In Fig. 5.9, the finite difference sensitivity has become unstable. Although it looks as if it is trying to approximate the exact sensitivities, large oscillations occur at the discontinuities.

The results for the fine and medium grids are quite interesting. Even though two different methodologies are used to approximate the flow sensitivities, the results are nearly identical. In Section 2.4, the inconsistency of the sensitivity equation method sensitivities and the semi-analytic sensitivities was discussed. The above results imply that these inconsistencies arise mainly in the area around the spikes and are negligible elsewhere. It will be shown in Chapter 7 that these spikes are due largely to errors in the sensitivity approximation methods. Hence, it is reasonable to expect that if the spikes can be eliminated, then the different sensitivity methodologies can become interchangeable in many applications.

As far as the numerical methods are concerned, the Roe scheme does the best job of approximating the exact continuous sensitivities followed by the Godunov scheme and the Lax-Wendroff scheme. These are the expected results since the Roe scheme does the best job of approximating the exact flow solution followed by the Godunov and Lax-Wendroff schemes, respectively. It is interesting to note that even though the approximate flow solution using the Roe scheme on a fine grid is very close to the exact flow solution in Fig. 4.12, the sensitivities calculated using the Roe scheme on a fine grid are not very close to the exact continuous sensitivities in the region between the shock wave and the contact discontinuity in Fig. 5.4. This is due in a large part to the spikes arising at both the shock wave and the contact discontinuity.

The final observation is that all the different sensitivity calculation methods incurred problems at the shock wave, contact discontinuity and the rarefaction wave. At the shock wave and contact discontinuity, large spikes arose as the methods attempted to approximate the δ-function at that point. If the grid was coarse, then the spikes were small humps and much of the flow sensitivity information was effectively lost. If the grid was refined, then

the spikes became thinner but grew in magnitude. The flow sensitivities of the rarefaction wave involve jump discontinuities at both ends. In all the methods, these jumps were not captured very accurately unless the grid was refined and a better numerical scheme such as the Roe scheme was used. An interesting thing is that the discontinuities in flow sensitivities were not captured with the same accuracy that the discontinuities in the flow solution were captured using the equivalent methods and grids.

Chapter 6

Optimization Using Exact Continuous Sensitivities

6.1 Riemann Problem Optimizations

In this chapter, another flow optimization is considered using the Riemann or shock tube problem from gas dynamics. The Riemann problem is important to study in an optimization context because it involves shock waves, contact discontinuities and rarefaction waves in the flow solution. The Riemann problem is considered here only in an optimization context. It was discussed in detail in Chapter 4. The optimizations will involve several flow matching problems. The idea is to match a desired flow at a specific time, t_0, by altering the initial conditions of the problem. The initial conditions that can be altered are the pressure and density to the left and right of the diaphragm. In the optimizations below, the design parameter is chosen to be the initial left pressure, P_4. The initial left density, the initial right pressure and the initial right density are kept fixed throughout the optimization procedure. The cost functional for the desired optimization is given by

$$\mathcal{J} = \frac{1}{2} \int_{\Gamma} \left| \mathbf{U}(t_0; P_4) - \hat{\mathbf{U}}(t_0) \right|^2 d\Gamma,$$

where $\hat{\mathbf{U}}(t_0)$ is the target solution, $\mathbf{U}(t_0; P_4)$ is the test flow and Γ is the computational area along the tube. In the above cost functional, both the target and test flows have been evaluated at a specific time, $t = t_0$. In this optimization, there is only one design parameter, P_4 and only the gradient of the cost functional with respect to P_4, $\frac{\partial \mathcal{J}}{\partial P_4}$, is needed. The

gradient of the cost functional with respect to P_4 is then defined by

$$\frac{\partial \mathcal{J}}{\partial P_4} = G = \int_\Gamma (\mathbf{U}(t_0; P_4) - \hat{\mathbf{U}}(t_0)) \cdot \frac{\partial \mathbf{U}(t_0; P_4)}{\partial P_4} \, d\Gamma.$$

The test flow for each P_4^i must satisfy the one-dimensional Euler equations, Eq. 4.1, where P_4^i denotes the value of the design parameter at the ith optimization iteration. The corresponding flow matching optimization can then be stated in Problem 2.

Problem 2 (Riemann Problem Optimization) *Find the initial left pressure, P_4 such that*

$$\mathcal{J} = \frac{1}{2} \int_\Gamma \left| \mathbf{U}(t_0; P_4) - \hat{\mathbf{U}}(t_0) \right|^2 \, d\Gamma \tag{6.1}$$

is minimized subject to $h(\mathbf{U}, P_4) = 0$ where $\mathbf{U}(t_0; P_4)$ is the test flow, $\hat{\mathbf{U}}(t_0)$ is the target flow and $h(\mathbf{U}, P_4) = 0$ are the one-dimensional Euler equations and initial conditions, Eq. 4.1 and Eq. 4.2.

The optimizations will be calculated using an unconstrained minimization package written by Gay [19], published as ACM TOMS Algorithm 611. The source code is publicly available through **netlib** [17]. Algorithm 611 is a BFGS model/trust region method for unconstrained minimization. Details about the algorithm can be found in Gay [19] and the BFGS model/trust region is discussed in Dennis and Schnabel [15]. Algorithm 611 was applied using the subroutine SUMSL which requires the user to supply both the cost functional and the gradient of the cost functional and the default tolerances were used. The algorithm terminates upon relative cost functional convergence, absolute cost functional convergence, or design parameter convergence. The default tolerances used were near the machine precision. This optimization requires the gradient and thus, the flow sensitivities with respect to the design parameter, P_4, must be calculated. Likewise, the cost functional and gradient must be approximated at each iteration of the optimization. The cost functional and gradient will be calculated using a simple scaled one-point quadrature rule since most of the flow is constant. The approximate cost functional is calculated from

$$\mathcal{J}^h \approx \frac{1}{2\Delta x} \sum_{j=0}^{xdim} \Delta x \left| \mathbf{U}_j^h(t_0; P_4^i) - \hat{\mathbf{U}}(x_j, t_0) \right|^2 \tag{6.2}$$

where Γ is broken up into $xdim$ equal intervals of length Δx, $\mathbf{U}_j^h(t_0; P_4^i)$ is the approximate flow solution at the point $(x_j, t_0; P_4^i) = (j\Delta x, t_0; P_4^i)$, P_4^i is the value of the design parameter at the ith iteration of the optimization. The target flow is known and does not have to be approximated at each of the grid points. Thus, $\hat{\mathbf{U}}(x_j, t_0)$ is the target flow evaluated at the

point $(j\Delta x, t_0)$. The approximate gradient of the cost functional is calculated from

$$\frac{\partial \mathcal{J}^h}{\partial P_4} \approx \frac{1}{2\Delta x} \sum_{j=0}^{xdim} \Delta x \left(\mathbf{U}_j^h(t_0; P_4^i) - \hat{\mathbf{U}}(x_j, t_0) \right) \cdot \frac{\partial \mathbf{U}^h}{\partial P_4}(x_j, t_0; P_4^i). \tag{6.3}$$

In the Section 3.4.1, it was mentioned that the discontinuities arising in the flow create spikes in the approximate flow sensitivities (See Fig. 3.9). The impact of the spikes on the optimization process is unknown. This idea will be explored in the following optimizations. In these optimization problems, the flow sensitivities with respect to the initial left pressure, P_4, are calculated using the finite difference method and the sensitivity equation method. These methods both create large spikes at the discontinuities, which in this case are the shock wave and the contact discontinuity. The optimizations using the finite difference sensitivities and the sensitivity equation method sensitivities will be compared with optimizations using the exact continuous sensitivities. Since the exact solution to the Riemann problem is known and given analytically, this solution can be differentiated with respect to the design parameter to calculate the exact continuous sensitivities. These sensitivities do not contain spikes at the discontinuities and were discussed in detail in Chapter 5 for the Riemann problem. As a matter of completeness, it should be noted that the numerical method used to calculate both the flow solutions and the flow sensitivities was the two-step Lax-Wendroff method with Lapidus artificial viscosity.

6.1.1 Optimization Verification

The first set of optimizations to consider is a verification problem. The target solution is picked as an attainable solution. Hence, if the cost functional, gradient and flow sensitivities are calculated correctly, the optimization should choose a design flow that is identical to the target flow and the cost functional at this design flow should be zero. For this case, the target solution is generated by setting $P_4 = 1.0$ and calculating the approximate numerical flow solution. After the optimization has finished, the design parameter should be $P_4^{final} = 1.0$ and the cost functional should be $\mathcal{J}(P_4^{final}) = 0.0$. Optimizations were performed using the three different sensitivity calculation methods and two different initial guesses, $P_4^0 = 3.0$ and $P_4^0 = 0.3$. The optimization results are given in Tables 6.1-6.6.

In each of the six optimizations, Tables 6.1-6.6, the correct design parameter, $P_4^{final} = 1.0$ and a zero, to round off error, cost functional was achieved. Thus, the verification of the optimization routines is complete. It is interesting to point out that in Table 6.3 and Table 6.6, where optimizations using the exact continuous sensitivities were used, the gradient was at least two orders of magnitude larger than the gradients in the optimizations

Table 6.1: Optimization using finite difference sensitivities on a fine grid where the target flow was the approximate numerical solution at $P_4 = 1.0$ and the initial guess was $P_4^0 = 3.0$.

Its.	Cost Func. Evals.	Cost Func. $\mathcal{J}^h(P_4^i)$	Grad. Evals.	Grad. $\frac{\partial \mathcal{J}^h}{\partial P_4}$	P_4^i
0	1	0.7604583D+03	1	0.7741857D+03	0.3000000D+01
1	2	0.1910870D+03	2	0.3756920D+03	0.2000000D+01
2	3	0.6944935D+00	3	0.2421071D+02	0.1057219D+01
3	4	0.1265700D-01	4	-0.3278520D+01	0.9922789D+00
4	5	0.1230884D-06	5	0.1022381D-01	0.1000024D+01
5	6	0.1738015D-14	6	-0.6288935D-06	0.1000000D+01
6	7	0.1274080D-14	7	0.1638653D-12	0.1000000D+01

Table 6.2: Optimization using sensitivity equation method sensitivities on a fine grid where the target flow was the approximate numerical solution at $P_4 = 1.0$ and the initial guess was $P_4^0 = 3.0$.

Its.	Cost Func. Evals.	Cost Func. $\mathcal{J}^h(P_4^i)$	Grad. Evals.	Grad. $\frac{\partial \mathcal{J}^h}{\partial P_4}$	P_4^i
0	1	0.7604583D+03	1	0.7411822D+03	0.3000000D+01
1	3	0.5111618D+01	2	-0.6487529D+02	0.8430300D+00
2	4	0.5874897D-01	3	0.6893130D+01	0.1016633D+01
3	5	0.3564307D-06	4	-0.1702267D-01	0.9999590D+00
4	6	0.2352337D-11	5	0.4370977D-04	0.1000000D+01
5	7	0.1274187D-14	6	0.2692180D-09	0.1000000D+01
6	8	0.1274181D-14	7	0.1055926D-12	0.1000000D+01
7	9	0.1274181D-14	8	0.5729014D-13	0.1000000D+01
8	10	0.1274181D-14	8	0.5729014D-13	0.1000000D+01

using the other sensitivities, Tables 6.1-6.2 and Tables 6.4-6.5. It is also interesting to note that the optimizations using the exact continuous sensitivities seemed to converge slightly faster than the optimizations using the other sensitivities. These points, as well as others, will be considered in Section 6.1.2 and Section 6.2.

6.1.2 Optimization Using a Nonattainable Target Flow

Although these optimizations are interesting, it is also necessary to perform some calculations where the design flow and parameter is not known *a priori* to the optimization process. This means a design flow that gives a zero cost functional may not be achievable.

Table 6.3: Optimization using exact continuous sensitivities on a fine grid where the target flow was the approximate numerical solution at $P_4 = 1.0$ and the initial guess was $P_4^0 = 3.0$.

Its.	Cost Func. Evals.	Cost Func. $\mathcal{J}^h(P_4^i)$	Grad. Evals.	Grad. $\frac{\partial \mathcal{J}^h}{\partial P_4}$	P_4^i
0	1	0.7604583D+03	1	0.7184442D+03	0.3000000D+01
1	3	0.3274222D+02	2	-0.1488089D+03	0.5902929D+00
2	4	0.3011793D-02	3	0.1376074D+01	0.1003766D+01
3	5	0.1067282D-06	4	-0.8196260D-02	0.9999776D+00
4	6	0.3358130D-13	5	0.4531869D-05	0.1000000D+01
5	7	0.1274874D-14	6	0.1484010D-10	0.1000000D+01

Table 6.4: Optimization using finite difference sensitivities on a fine grid where the target flow was the approximate numerical solution at $P_4 = 1.0$ and the initial guess was $P_4^0 = 0.3$.

Its.	Cost Func. Evals.	Cost Func. $\mathcal{J}^h(P_4^i)$	Grad. Evals.	Grad. $\frac{\partial \mathcal{J}^h}{\partial P_4}$	P_4^i
0	1	0.9203523D+02	1	-0.2551461D+03	0.3000000D+00
1	2	0.1837093D+02	2	0.1186508D+03	0.1300000D+01
2	3	0.6440810D-01	3	-0.7394222D+01	0.9825795D+00
3	4	0.3060066D-03	4	0.5097576D+00	0.1001200D+01
4	5	0.5128664D-10	5	-0.2086911D-03	0.9999995D+00
5	6	0.1274089D-14	6	0.1847105D-08	0.1000000D+01
6	7	0.1274080D-14	7	-0.9180310D-13	0.1000000D+01
7	8	0.1274080D-14	8	0.3539044D-13	0.1000000D+01
8	9	0.1274080D-14	8	0.3539044D-13	0.1000000D+01

The target flow for the next set of optimizations is taken to be the exact flow solution at $P_4 = 1.0$. Although this may appear to be the same optimization problem, it is inherently different. The exact flow solution involves sharp discontinuities and constant states in each of the flow regions except for the rarefaction wave. The approximate numerical solution will not exactly capture the states or the discontinuities. Evidence of this was seen and discussed in Chapter 4. The optimization procedure will try to find the design flow that best matches the exact flow at $P_4 = 1.0$. This may be, and in fact is not, the approximate numerical flow solution at $P_4 = 1.0$. Another thing to note is that the cost functional may or may not be a continuous function in the one-dimensional design space of the initial left pressure. Discontinuities or noise in the cost functional can cause many problems in the optimization procedure. The optimizations were performed using the three different sensitivity calculation methods and two different initial guesses, $P_4^0 = 3.0$ and $P_4^0 = 0.3$. The optimization results are given in Tables 6.7-6.12.

Table 6.5: Optimization using sensitivity equation method sensitivities on a fine grid where the target flow was the approximate numerical solution at $P_4 = 1.0$ and the initial guess was $P_4^0 = 0.3$.

Its.	Cost Func. Evals.	Cost Func. $\mathcal{J}^h(P_4^i)$	Grad. Evals.	Grad. $\frac{\partial \mathcal{J}^h}{\partial P_4}$	P_4^i
0	1	0.9203523D+02	1	-0.2573787D+03	0.3000000D+00
1	2	0.1837093D+02	2	0.1154340D+03	0.1300000D+01
2	3	0.1968784D-01	3	-0.4006835D+01	0.9903700D+00
3	4	0.1217087D-03	4	0.3145188D+00	0.1000757D+01
4	5	0.2473587D-09	5	0.4484259D-03	0.1000001D+01
5	6	0.1276256D-14	6	-0.5121905D-07	0.1000000D+01
6	7	0.1274181D-14	7	0.5729014D-13	0.1000000D+01

Table 6.6: Optimization using exact continuous sensitivities on a fine grid where the target flow was the approximate numerical solution at $P_4 = 1.0$ and the initial guess was $P_4^0 = 0.3$.

Its.	Cost Func. Evals.	Cost Func. $\mathcal{J}^h(P_4^i)$	Grad. Evals.	Grad. $\frac{\partial \mathcal{J}^h}{\partial P_4}$	P_4^i
0	1	0.9203523D+02	1	-0.2589840D+03	0.3000000D+00
1	2	0.1837093D+02	2	0.1086965D+03	0.1300000D+01
2	3	0.4059792D-02	3	0.1597502D+01	0.1004372D+01
3	4	0.2935802D-06	4	-0.1359380D-01	0.9999628D+00
4	5	0.1218196D-12	5	0.8733065D-05	0.1000000D+01
5	6	0.1274871D-14	6	0.4726679D-10	0.1000000D+01

In the optimizations, Tables 6.7-6.12, it is interesting that each of the different sensitivity calculation methods produced different values for the design parameter, P_4^{final}, and only the finite difference sensitivities produced the same final design parameter for the different initial guesses. It should also be noted that the finite difference method finds a design flow that gives the smallest value for the cost functional. The algorithm gave warnings during the optimization using both the sensitivity equation method sensitivities and the exact continuous sensitivities that the cost functional was noisy or discontinuous and that the tolerances were probably too small. Hence, the final iteration for these methods have multiple functional evaluations as the optimizer keeps reducing the step size to find a point where the cost functional is smaller than the predicted value, see Tables 6.8-6.9 and Tables 6.11-6.12. Likewise, the gradient in each of the optimizations is not zero. The gradient is the smallest for the finite difference method, but rather large for the sensitivity equation method and the exact continuous sensitivities. For these reasons, the cost functional is probably noisy and discontinuous with multiple local minimums. It is expected that the

Table 6.7: Optimization using finite difference sensitivities on a fine grid where the target flow was the exact flow solution at $P_4 = 1.0$ and the initial guess was $P_4^0 = 3.0$.

Its.	Cost Func. Evals.	Cost Func. $\mathcal{J}^h(P_4^i)$	Grad. Evals.	Grad. $\frac{\partial \mathcal{J}^h}{\partial P_4}$	P_4^i
0	1	0.7617346D+03	1	0.7745689D+03	0.3000000D+01
1	2	0.1916649D+03	2	0.3773000D+03	0.2000000D+01
2	3	0.1038909D+01	3	0.1819968D+02	0.1050266D+01
3	4	0.6791546D+00	4	-0.3035955D+01	0.1002132D+01
4	5	0.6682004D+00	5	-0.3011671D-01	0.1009013D+01
5	6	0.6681950D+00	6	0.8258742D-04	0.1009082D+01
6	7	0.6681950D+00	6	0.8258742D-04	0.1009082D+01

Table 6.8: Optimization using sensitivity equation method sensitivities on a fine grid where the target flow was the exact flow solution at $P_4 = 1.0$ and the initial guess was $P_4^0 = 3.0$.

Its.	Cost Func. Evals.	Cost Func. $\mathcal{J}^h(P_4^i)$	Grad. Evals.	Grad. $\frac{\partial \mathcal{J}^h}{\partial P_4}$	P_4^i
0	1	0.7617346D+03	1	0.7411927D+03	0.3000000D+01
1	3	0.6849734D+01	2	-0.7122699D+02	0.8343272D+00
2	4	0.7172827D+00	3	0.7323060D+01	0.1024197D+01
3	5	0.6698180D+00	4	-0.2680079D+00	0.1006496D+01
4	6	0.6691586D+00	5	0.5366698D-03	0.1007121D+01
5	15	0.6691586D+00	5	0.5366698D-03	0.1007121D+01

finite difference sensitivities should do a better job since they are approaching the exact discrete sensitivities of the approximate numerical flow solution as $\Delta P_4 \longrightarrow 0$. The sensitivity equation method and exact continuous sensitivities, on the other hand, are inconsistent sensitivities for the approximate numerical solution. These are not the sensitivities for the approximate flow solution but for the exact flow solution and hence, the gradients may be pointing slightly in the wrong direction. This idea was discussed in detail in Section 2.4. The small error in the gradients may be okay early in the optimization procedure, but as the optimizer closes in on the minimum this error can cause problems resulting in multiple cost functional evaluations, as is seen in Tables 6.8-6.9 and Tables 6.11-6.12. The optimizer projects a step size in the descent direction and if the cost functional does not decrease at this step, the optimizer will keep reducing the step size until a smaller cost functional is achieved. The multiple cost functional evaluations at the end of the optimizations, Tables 6.8-6.9 and Tables 6.11-6.12, are due to this effect. Again, the point should be made that the exact continuous sensitivities drive the optimizer faster to a minimum than the other sensitivities up until the point where design parameter gets very close to the mini-

Table 6.9: Optimization using exact continuous sensitivities on a fine grid where the target flow was the exact flow solution at $P_4 = 1.0$ and the initial guess was $P_4^0 = 3.0$.

Its.	Cost Func. Evals.	Cost Func. $\mathcal{J}^h(P_4^i)$	Grad. Evals.	Grad. $\frac{\partial \mathcal{J}^h}{\partial P_4}$	P_4^i
0	1	0.7617346D+03	1	0.7189655D+03	0.3000000D+01
1	3	0.3499220D+02	2	-0.1512721D+03	0.5856748D+00
2	4	0.6714634D+00	3	0.1873550D+01	0.1005353D+01
3	24	0.6714634D+00	3	0.1873550D+01	0.1005353D+01

Table 6.10: Optimization using finite difference sensitivities on a fine grid where the target flow was the exact flow solution at $P_4 = 1.0$ and the initial guess was $P_4^0 = 0.3$.

Its.	Cost Func. Evals.	Cost Func. $\mathcal{J}^h(P_4^i)$	Grad. Evals.	Grad. $\frac{\partial \mathcal{J}^h}{\partial P_4}$	P_4^i
0	1	0.9391989D+02	1	-0.2562724D+03	0.3000000D+00
1	2	0.1851528D+02	2	0.1183711D+03	0.1300000D+01
2	3	0.8053465D+00	3	-0.1083292D+02	0.9840434D+00
3	4	0.6685629D+00	4	0.6364151D+00	0.1010534D+01
4	5	0.6681962D+00	5	-0.7752518D-02	0.1009064D+01
5	6	0.6681950D+00	6	-0.3877456D-05	0.1009082D+01
6	7	0.6681950D+00	7	0.2319935D-10	0.1009082D+01
7	8	0.6681950D+00	7	0.2319935D-10	0.1009082D+01

mizer and the inconsistences cause problems. In a practical problem, the tolerances would be on the order of 10^{-6} to 10^{-8} as opposed to the machine precision, and the inconsistencies would have a smaller effect on the optimization.

6.1.3 Optimization on a Medium Grid

In the previous optimization, good results were achieved, but a fine grid was used. Another point to consider is the grid sizing. As the grid size decreases, the finite difference sensitivities and sensitivity equation method sensitivities become better approximations to the exact continuous sensitivities. The grid for the previous optimizations was a fine grid where $\Delta t = 0.001$ and $\Delta x = 0.01$. It is necessary to see how the optimization is affected as the grid size increases. The optimizations have been run again except that Δx was changed to $\Delta x = 0.02$, decreasing the number of grid points by half while Δt remained the same as $\Delta t = 0.001$. The next set of optimizations is again a verification problem. The target flow is the approximate numerical solution at $P_4 = 1.0$ on the medium grid and hence, a zero

Table 6.11: Optimization using sensitivity equation method sensitivities on a fine grid where the target flow was the exact flow solution at $P_4 = 1.0$ and the initial guess was $P_4^0 = 0.3$.

Its.	Cost Func. Evals.	Cost Func. $\mathcal{J}^h(P_4^i)$	Grad. Evals.	Grad. $\frac{\partial \mathcal{J}^h}{\partial P_4}$	P_4^i
0	1	0.9391989D+02	1	-0.2581464D+03	0.3000000D+00
1	2	0.1851528D+02	2	0.1150086D+03	0.1300000D+01
2	3	0.7341138D+00	3	-0.6597531D+01	0.9917940D+00
3	4	0.6683012D+00	4	0.5993952D+00	0.1008515D+01
4	27	0.6683012D+00	4	0.5993952D+00	0.1008515D+01

Table 6.12: Optimization using exact continuous sensitivities on a fine grid where the target flow was the exact flow solution at $P_4 = 1.0$ and the initial guess was $P_4^0 = 0.3$.

Its.	Cost Func. Evals.	Cost Func. $\mathcal{J}^h(P_4^i)$	Grad. Evals.	Grad. $\frac{\partial \mathcal{J}^h}{\partial P_4}$	P_4^i
0	1	0.9391989D+02	1	-0.2591193D+03	0.3000000D+00
1	2	0.1851528D+02	2	0.1090880D+03	0.1300000D+01
2	3	0.6747714D+00	3	0.1280803D+01	0.1003732D+01
3	19	0.6747714D+00	3	0.1280803D+01	0.1003732D+01

cost functional is achievable when $P_4^{final} = 1.0$. The results are shown in Tables 6.13-6.15, for an initial guess of $P_4^0 = 3.0$.

As before, in each of the different optimizations, Tables 6.13-6.15, the optimization is working correctly and a design flow with the final design parameter, $P_4^{final} = 1.0$ is achieved and results in a zero, to round off error, cost functional. Again the exact continuous sensitivities tend to drive the optimizer a little faster than the other sensitivities, but not as fast as the exact continuous sensitivities on a fine grid. In the medium grid, the discontinuities are more smeared out and the exact continuous sensitivities provide a gradient with more inconsistency.

6.1.4 Optimization Using a Nonattainable Target Flow and Medium Grid

It is necessary to perform optimizations where the target flow is not known *a priori* and may be unattainable. The target flow is the exact solution at $P_4 = 1.0$ and the medium size grid is used. These results are shown in Tables 6.16-6.18, for an initial guess of $P_4^0 = 3.0$.

Table 6.13: Optimization using finite difference sensitivities on a medium grid where the target flow was the approximate numerical solution at $P_4 = 1.0$ and the initial guess was $P_4^0 = 3.0$.

Its.	Cost Func. Evals.	Cost Func. $\mathcal{J}^h(P_4^i)$	Grad. Evals.	Grad. $\frac{\partial \mathcal{J}^h}{\partial P_4}$	P_4^i
0	1	0.3843470D+03	1	0.3879058D+03	0.3000000D+01
1	2	0.9626979D+02	2	0.1904212D+03	0.2000000D+01
2	3	0.1262392D+00	3	0.7062038D+01	0.1035766D+01
3	4	0.1852330D-03	4	-0.2702814D+00	0.9986291D+00
4	5	0.3615417D-09	5	-0.3776205D-03	0.9999981D+00
5	6	0.8562071D-15	6	0.2715624D-07	0.1000000D+01
6	7	0.8543426D-15	7	-0.3742549D-14	0.1000000D+01

Table 6.14: Optimization using sensitivity equation method sensitivities on a medium grid where the target flow was the approximate numerical solution at $P_4 = 1.0$ and the initial guess was $P_4^0 = 3.0$.

Its.	Cost Func. Evals.	Cost Func. $\mathcal{J}^h(P_4^i)$	Grad. Evals.	Grad. $\frac{\partial \mathcal{J}^h}{\partial P_4}$	P_4^i
0	1	0.3843470D+03	1	0.3757689D+03	0.3000000D+01
1	3	0.1985483D+01	2	-0.2762699D+02	0.8574422D+00
2	4	0.1720533D-02	3	0.8141954D+00	0.1004178D+01
3	5	0.5268263D-07	4	-0.4505718D-02	0.9999769D+00
4	6	0.8545013D-15	5	-0.1200119D-07	0.1000000D+01
5	7	0.8543880D-15	6	-0.2232483D-13	0.1000000D+01

The optimizations in Tables 6.16-6.18, give similar results as their counterparts using fine grids. The reducing of the grid sizing may have reduced the noise in the cost functional, as the finite difference optimization, Table 6.16, and the sensitivity equation method optimization, Table 6.17, both reached approximately the same minimum. Also the exact continuous sensitivities show similar inconsistency problems at the end of the optimization, Table 6.18, where a minimum is achieved, but the gradient is still a fairly large positive number.

6.1.5 Optimizations Using Exact Flow and Sensitivities

Finally, optimizations are considered using the exact flow solution, Eq. 4.6 and the exact continuous sensitivities, Eq. 5.2. Although this is somewhat artificial in the sense that the exact flow solution is almost never known, it is important to include these optimizations for

Table 6.15: Optimization using exact continuous sensitivities on a medium grid where the target flow was the approximate numerical solution at $P_4 = 1.0$ and the initial guess was $P_4^0 = 3.0$.

Its.	Cost Func. Evals.	Cost Func. $\mathcal{J}^h(P_4^i)$	Grad. Evals.	Grad. $\frac{\partial \mathcal{J}^h}{\partial P_4}$	P_4^i
0	1	0.3843470D+03	1	0.3629513D+03	0.3000000D+01
1	3	0.1707470D+02	2	-0.7940095D+02	0.5762548D+00
2	4	0.1261453D-01	3	0.2105399D+01	0.1011310D+01
3	5	0.5137176D-06	4	0.1342400D-01	0.1000072D+01
4	6	0.6015357D-12	5	0.1452365D-04	0.1000000D+01
5	7	0.8545168D-15	6	-0.1030691D-09	0.1000000D+01
6	8	0.8545122D-15	7	-0.6800156D-14	0.1000000D+01
7	9	0.8545122D-15	7	-0.6800156D-14	0.1000000D+01

Table 6.16: Optimization using finite difference sensitivities on a medium grid where the target flow was the exact flow solution at $P_4 = 1.0$ and the initial guess was $P_4^0 = 3.0$.

Its.	Cost Func. Evals.	Cost Func. $\mathcal{J}^h(P_4^i)$	Grad. Evals.	Grad. $\frac{\partial \mathcal{J}^h}{\partial P_4}$	P_4^i
0	1	0.3844327D+03	1	0.3881078D+03	0.3000000D+01
1	2	0.9617700D+02	2	0.1905999D+03	0.2000000D+01
2	3	0.7226570D+00	3	0.4487945D+01	0.1034975D+01
3	4	0.6723033D+00	4	-0.1399204D+00	0.1011705D+01
4	5	0.6722527D+00	5	-0.7395187D-03	0.1012408D+01
5	6	0.6722527D+00	6	0.1388082D-06	0.1012412D+01
6	7	0.6722527D+00	6	0.1388082D-06	0.1012412D+01

completeness. The exact continuous sensitivities have been used in optimizations involving the approximate flow solution where they are known to provide inconsistent gradients. These optimizations should be compared to examples where the exact continuous sensitivities provide a consistent derivative, *i.e.*, optimizations using the exact flow solution. This will provide information about the optimization method and difficulty of the optimization problem since the approximation and inconsistency of the sensitivity calculations have been removed. Optimizations are performed using the same target flows, initial guesses, and grid sizing for comparison purposes.

Table 6.17: Optimization using sensitivity equation method sensitivities on a medium grid where the target flow was the exact flow solution at $P_4 = 1.0$ and the initial guess was $P_4^0 = 3.0$.

Its.	Cost Func. Evals.	Cost Func. $\mathcal{J}^h(P_4^i)$	Grad. Evals.	Grad. $\frac{\partial \mathcal{J}^h}{\partial P_4}$	P_4^i
0	1	0.3844327D+03	1	0.3762906D+03	0.3000000D+01
1	3	0.2822552D+01	2	-0.2892261D+02	0.8628339D+00
2	4	0.6731155D+00	3	0.6453517D+00	0.1015377D+01
3	5	0.6722665D+00	4	-0.1523810D-01	0.1012047D+01
4	6	0.6722614D+00	5	-0.4480023D-05	0.1012124D+01
5	7	0.6722614D+00	6	0.3182469D-10	0.1012124D+01
6	8	0.6722614D+00	6	0.3182469D-10	0.1012124D+01

Table 6.18: Optimization using exact continuous sensitivities on a medium grid where the target flow was the exact flow solution at $P_4 = 1.0$ and the initial guess was $P_4^0 = 3.0$.

Its.	Cost Func. Evals.	Cost Func. $\mathcal{J}^h(P_4^i)$	Grad. Evals.	Grad. $\frac{\partial \mathcal{J}^h}{\partial P_4}$	P_4^i
0	1	0.3844327D+03	1	0.3631611D+03	0.3000000D+01
1	3	0.1844788D+02	2	-0.7960897D+02	0.5758687D+00
2	4	0.6723010D+00	3	0.1574836D+01	0.1011722D+01
3	38	0.6723010D+00	3	0.1574836D+01	0.1011722D+01

Optimization Verification Using Exact Flow

The first optimization to perform using the exact flow is an optimization in which the target solution is attainable. This will verify the correctness of the optimization procedure, flow calculations and sensitivity calculations. For optimizations using the exact flow solution, an attainable target flow is the exact flow solution at $P_4 = 1.0$. This is just the opposite of the optimizations using the approximate flow solution for the obvious reasons. The results of the optimizations performed using the exact continuous sensitivities on a fine grid with initial guesses of $P_4^0 = 3.0$ and $P_4^0 = 0.3$ are given in Table 6.19 and Table 6.20, respectively. The results for the optimization using the exact flow and exact continuous sensitivities on a medium grid with an initial guess of $P_4^0 = 3.0$ are given in Table 6.21. In each of the optimizations, Tables 6.19-6.21, the optimizer achieved the correct minimum with little difficulty. The optimizer is developed for continuous functions and there is no guarantee that it will work well for flows having discontinuities. These optimizations seem to imply that, barring δ-spikes and inconsistencies, the optimizer is working "correctly" for discontinuous flows.

Table 6.19: Optimization using the exact flow and exact continuous sensitivities on a fine grid where the target flow was the exact flow solution at $P_4 = 1.0$ and the initial guess was $P_4^0 = 3.0$.

Its.	Cost Func. Evals.	Cost Func. $\mathcal{J}^h(P_4^i)$	Grad. Evals.	Grad. $\frac{\partial \mathcal{J}^h}{\partial P_4}$	P_4^i
0	1	0.7492669D+03	1	0.7146752D+03	0.3000000D+01
1	3	0.2092717D+02	2	-0.1118463D+03	0.6909207D+00
2	4	0.2109604D-02	3	0.1257872D+01	0.1003389D+01
3	5	0.1352248D-05	4	-0.3185273D-01	0.9999142D+00
4	6	0.9065711D-13	5	0.8215771D-05	0.1000000D+01
5	7	0.4550613D-15	6	0.5381436D-10	0.1000000D+01

Table 6.20: Optimization using the exact flow and exact continuous sensitivities on a fine grid where the target flow was the exact flow solution at $P_4 = 1.0$ and the initial guess was $P_4^0 = 0.3$.

Its.	Cost Func. Evals.	Cost Func. $\mathcal{J}^h(P_4^i)$	Grad. Evals.	Grad. $\frac{\partial \mathcal{J}^h}{\partial P_4}$	P_4^i
0	1	0.9481299D+02	1	-0.2547852D+03	0.3000000D+00
1	2	0.1916550D+02	2	0.1076519D+03	0.1300000D+01
2	3	0.1628461D-02	3	0.1105184D+01	0.1002978D+01
3	4	0.1955180D-05	4	-0.3830118D-01	0.9998968D+00
4	5	0.1011884D-12	5	0.8682757D-05	0.1000000D+01
5	6	0.4550618D-15	6	0.6830682D-10	0.1000000D+01

Optimization Using a Nonattainable Target Flow and the Exact Flow

The next example to consider is optimizations using a target flow that is not attainable. The target flow for these optimizations is the approximate flow solution at $P_4 = 1.0$. This is a nonattainable target flow because it involves smeared discontinuities and the exact flow will only involve sharp discontinuities. The results of the exact flow optimizations using a nonattainable target flow on a fine grid with initial guesses of $P_4^0 = 3.0$ and $P_4^0 = 0.3$ are given in Table 6.22 and Table 6.23, respectively. The results for the exact flow optimization using a nonattainable target flow on a medium grid with an initial guess of $P_4^0 = 3.0$ are given in Table 6.24.

In each of the optimizations, Tables 6.22-6.24, the optimizer converged to approximately the same nonzero minimum cost functional. The optimization using the medium grid converged to a slightly different minimum than the optimizations using the fine grid as expected due

Table 6.21: Optimization using the exact flow and exact continuous sensitivities on a medium grid where the target flow was the exact flow solution at $P_4 = 1.0$ and the initial guess was $P_4^0 = 3.0$.

Its.	Cost Func. Evals.	Cost Func. $\mathcal{J}^h(P_4^i)$	Grad. Evals.	Grad. $\frac{\partial \mathcal{J}^h}{\partial P_4}$	P_4^i
0	1	0.3782064D+03	1	0.3606139D+03	0.3000000D+01
1	3	0.1391953D+02	2	-0.6458206D+02	0.6430741D+00
2	4	0.1048930D-03	3	0.1996991D+00	0.1001062D+01
3	5	0.1583964D-06	4	-0.7760715D-02	0.9999587D+00
4	6	0.1249060D-14	5	0.6184497D-06	0.1000000D+01
5	7	0.2241440D-15	6	0.1916101D-11	0.1000000D+01

Table 6.22: Optimization using the exact flow and exact continuous sensitivities on a fine grid where the target flow was the approximate flow solution at $P_4 = 1.0$ and the initial guess was $P_4^0 = 3.0$.

Its.	Cost Func. Evals.	Cost Func. $\mathcal{J}^h(P_4^i)$	Grad. Evals.	Grad. $\frac{\partial \mathcal{J}^h}{\partial P_4}$	P_4^i
0	1	0.7481828D+03	1	0.7141539D+03	0.3000000D+01
1	3	0.1920826D+02	2	-0.1110333D+03	0.6918938D+00
2	4	0.6873984D+00	3	0.9971463D+00	0.1002462D+01
3	5	0.6867869D+00	4	-0.2750797D-01	0.9996974D+00
4	6	0.6867666D+00	5	0.5577800D-05	0.9997716D+00
5	7	0.6867666D+00	5	0.5577800D-05	0.9997716D+00

to the smearing of the discontinuities. Again, even using a nonattainable target solution, the optimizer seems to be working correctly. These results imply that, even though there are discontinuities in the flow, the optimizer works correctly when a consistent gradient is used. This allows the optimizations with and without spikes to be compared without worrying about the optimization procedure itself.

6.2 Conclusions

The results of the optimizations, Tables 6.1-6.24, are very interesting. The optimizations in which the sensitivities did not involve spikes tended to move very quickly toward the minimizer and then slow down as it approaches the minimizer due to inconsistency problems. Although this is not an exhaustive study, the results clearly imply that sensitivities

Table 6.23: Optimization using the exact flow and exact continuous sensitivities on a fine grid where the target flow was the approximate flow solution at $P_4 = 1.0$ and the initial guess was $P_4^0 = 0.3$.

Its.	Cost Func. Evals.	Cost Func. $\mathcal{J}^h(P_4^i)$	Grad. Evals.	Grad. $\frac{\partial \mathcal{J}^h}{\partial P_4}$	P_4^i
0	1	0.9292398D+02	1	-0.2546500D+03	0.3000000D+00
1	2	0.1892282D+02	2	0.1072603D+03	0.1300000D+01
2	3	0.6884970D+00	3	0.1429085D+01	0.1003627D+01
3	4	0.6868085D+00	4	-0.5426856D-01	0.9996253D+00
4	5	0.6867666D+00	5	0.1575713D-04	0.9997717D+00
5	6	0.6867666D+00	5	0.1575713D-04	0.9997717D+00

Table 6.24: Optimization using the exact flow and exact continuous sensitivities on a medium grid where the target flow was the approximate flow solution at $P_4 = 1.0$ and the initial guess was $P_4^0 = 3.0$.

Its.	Cost Func. Evals.	Cost Func. $\mathcal{J}^h(P_4^i)$	Grad. Evals.	Grad. $\frac{\partial \mathcal{J}^h}{\partial P_4}$	P_4^i
0	1	0.3779453D+03	1	0.3604040D+03	0.3000000D+01
1	3	0.1218777D+02	2	-0.6412141D+02	0.6449975D+00
2	4	0.6876901D+00	3	0.6309577D+00	0.1000703D+01
3	5	0.6873891D+00	4	-0.1903435D-01	0.9972370D+00
4	6	0.6873662D+00	5	0.4714237D-05	0.9973385D+00
5	7	0.6873662D+00	5	0.4714237D-05	0.9973385D+00

without spikes speed up the optimization procedure. This increased speed diminishes as the grid size increases because the discontinuities become more smeared out and hence, the sensitivities without spikes are "more" inconsistent. In larger optimizations, a small decrease in the number of iterations or cost functional evaluations can make a large decrease in the computational cost and time. The most viable approach is probably to use the sensitivities without spikes in the optimization procedure for the first few iterations and then switch to a more consistent sensitivity. Clearly, the development of numerical schemes that approximate the flow sensitivities without spikes would be beneficial to the optimization process.

Chapter 7

Sensitivities and Discontinuous Flow

7.1 Flow Sensitivities and Discontinuities

7.1.1 Shock Waves

The calculation of flow sensitivities in the presence of shock waves is a difficult enterprise. In the sensitivity equation method, the automatic differentiation method, and the finite difference method, the discontinuities occurring at the shock wave or contact discontinuity must be dealt with.

Suppose that the flow is characterized by a single parameter α. Then, if the flow is described by a one-dimensional equation, the flow may be viewed as a function of x, t and α, *i.e.* $\mathbf{U}(x, t; \alpha)$. It is assumed that all calculations are examined at a specific time t_0. For a flow simulation, one would pick a particular value of α_0 for the parameter and then proceed to determine $\mathbf{U}$ as a function of x, *i.e.*, $\mathbf{U}(x, t_0; \alpha_0)$. If the location of the shock wave is denoted by x_s, then in general, if the value of the parameter is changed, the location of the shock wave changes so the shock location is a function of the parameter, $x_s = x_s(\alpha)$. Thus, at a particular value α_0, the shock location is given by $x_s(\alpha_0)$ as is sketched in Fig. 7.1. For a fixed value of the parameter $\alpha = \alpha_0$, the flow variable $\mathbf{U}(x, t_0; \alpha_0)$ is a discontinuous function of x, and certainly cannot be differentiated with respect to x at $x_s(\alpha_0)$. Likewise, if the value of x is fixed to, say $x = x_0$, then for at least some x_0, $\mathbf{U}(x_0, t_0; \alpha)$, viewed as a function of α is discontinuous and hence not differentiable with respect to α at $x_s(\alpha) = x_0$.

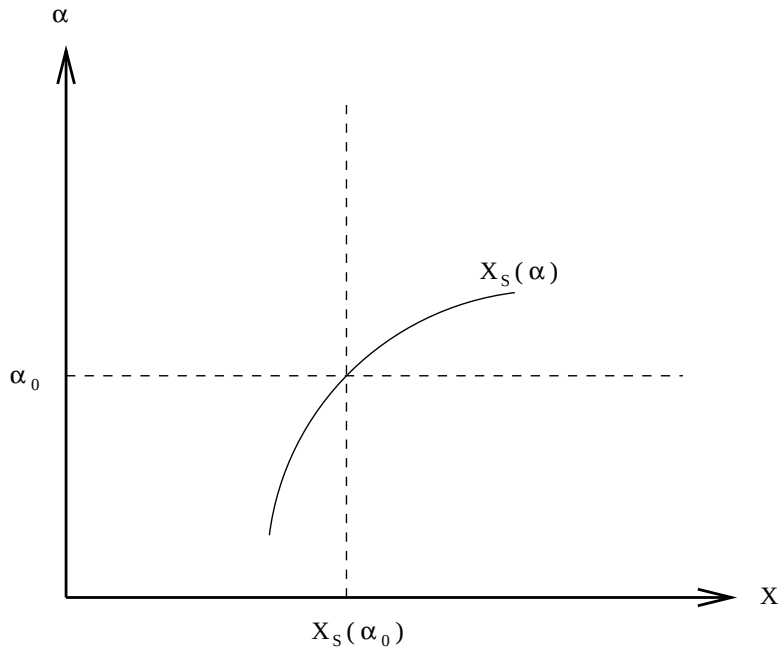

Figure 7.1: A shock wave in (x, α)-space. Flow variables are discontinuous when one crosses the shock wave $x_s(\alpha)$ at the point $(x_s(\alpha_0), \alpha_0)$ along either the horizontal or vertical dashed lines.

The conclusion that can be drawn from the above discussion is that, strictly speaking, flow sensitivity derivatives do not exist at shock waves in much the same way that spatial and temporal flow derivatives do not exist at those locations. In the calculation of flow sensitivities by all three numerical approaches, the presence of shock waves has been ignored, *i.e.*, the same algorithm has been applied at points in (x, α)-space where a shock wave is present as was applied at points where the flow is smooth. As a result, flow sensitivities with large spikes at the shock are obtained; these spikes approximate the δ-function which the exact flow sensitivities contain at that location.

To see how these spikes arise, consider the difference quotient approach to approximating sensitivities. The flow is computed at (x_1, t_0, α_1) and at $(x_1, t_0, \alpha_1 + \Delta\alpha)$ and the flow sensitivity is approximated by

$$\frac{\partial \mathbf{U}(x_1, t_0, \alpha_1)}{\partial \alpha} \approx \frac{\mathbf{U}(x_1, t_0; \alpha_1 + \Delta\alpha) - \mathbf{U}(x_1, t_0; \alpha_1)}{\Delta\alpha}. \tag{7.1}$$

Of course, if the flow is smooth and $\Delta\alpha$ is small, then both the numerator and the denominator in Eq. 7.1 will be small, and in fact, as $\Delta\alpha \longrightarrow 0$, both approach zero in such a way

that their ratio converges to $\partial \mathbf{U}/\partial\alpha(x_1, t_0; \alpha_1)$. Now, suppose that the points (x_1, t_0, α_1) and $(x_1, t_0, \alpha_1 + \Delta\alpha)$ lie on opposite sides of the shock wave as in Fig. 7.2. Then even if $\Delta\alpha$ is small, the numerator in Eq. 7.1 is relatively large. Hence, the solution of the finite difference sensitivity is large and a spike occurs when differencing across a shock.

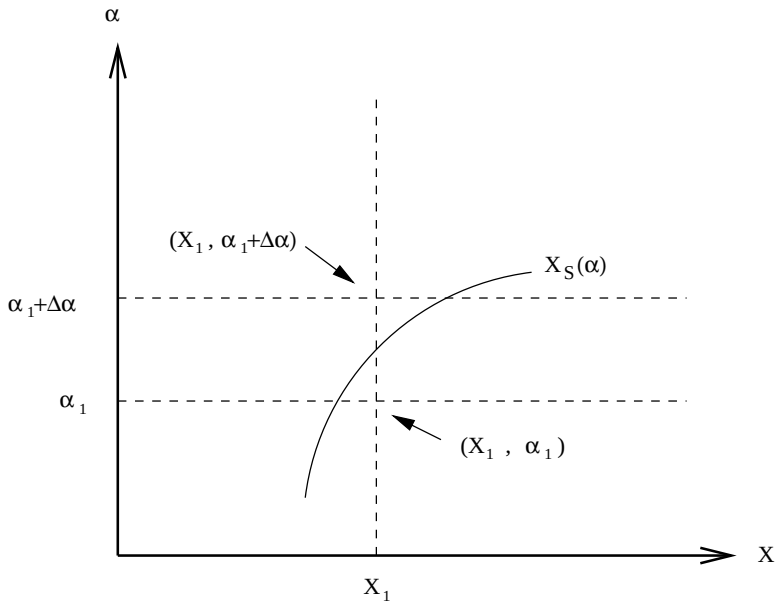

Figure 7.2: The points (x_1, α_1) and $(x_1, \alpha_1 + \Delta\alpha)$ are on opposite sides of the shock wave in the (x, t_0, α)-plane. The variables at the two points differ significantly even if the two points are close together, *i.e.*, even if $\Delta\alpha$ is small.

In the sensitivity equation approach, the same spikes develop. To understand this, consider Eq. 4.1. Again suppose one parameter α determines the flow, $\mathbf{U}(x, t; \alpha)$. The equation for the sensitivity $\mathbf{S} = \partial\mathbf{U}/\partial\alpha$, is determined by differentiating Eq. 4.1 with respect to α

$$\begin{aligned}
\mathbf{0} &= \frac{\partial}{\partial\alpha}\left(\frac{\partial \mathbf{U}}{\partial t} + \frac{\partial \mathbf{F}(\mathbf{U})}{\partial x}\right) && (7.2)\\
&= \frac{\partial^2 \mathbf{U}}{\partial\alpha\partial t} + \frac{\partial^2 \mathbf{F}(\mathbf{U})}{\partial\alpha\partial x} && (7.3)\\
&= \frac{\partial}{\partial t}\left(\frac{\partial \mathbf{U}}{\partial\alpha}\right) + \frac{\partial}{\partial x}\left(\frac{\partial \mathbf{F}(\mathbf{U})}{\partial\alpha}\right) && (7.4)\\
&= \frac{\partial \mathbf{S}}{\partial t} + \frac{\partial}{\partial x}\mathbf{F}^{\mathbf{s}}(\mathbf{U}, \mathbf{S}) && (7.5)
\end{aligned}$$

where the flux function $\mathbf{F}^{\mathbf{s}}(\mathbf{U}, \mathbf{S})$ of the sensitivity equation is defined by

$$\mathbf{F}^{\mathbf{s}}(\mathbf{U}, \mathbf{S}) = \frac{\partial \mathbf{F}(\mathbf{U})}{\partial\alpha} = \frac{d\mathbf{F}}{d\mathbf{U}}(\mathbf{U})\mathbf{S}.$$

In deriving this equation, it is important to notice that the orders of differentiation have been interchanged.

In smooth regions of the flow, there is no difficulty in interchanging derivatives; however, at a shock wave the derivation embodied in Eq. 7.4 is not allowable due to the non-existence of the appropriate derivatives at that location.

Theorem 1 (Orders of Differentiation) *Let* $\mathbf{F}(\mathbf{x}) : \Re^n \longrightarrow \Re^m$ *be given where*

$$\mathbf{F}(\mathbf{x}) = \begin{bmatrix} f_1(x_1, x_2, \ldots, x_n) \\ f_2(x_1, x_2, \ldots, x_n) \\ \vdots \\ f_m(x_1, x_2, \ldots, x_n) \end{bmatrix}$$

and suppose that

$$f_k(\mathbf{x}), \quad \frac{\partial f_k}{\partial x_i}(\mathbf{x}), \quad \frac{\partial}{\partial x_j}\left(\frac{\partial f_k}{\partial x_i}(\mathbf{x})\right), \quad \text{and} \quad \frac{\partial}{\partial x_i}\left(\frac{\partial f_k}{\partial x_j}(\mathbf{x})\right)$$

are continuous for $k = 1, 2, \ldots, m$ *and* $i, j = 1, 2, \ldots, n$ *at the point* $\mathbf{x}_0$*. Then*

$$\frac{\partial}{\partial x_j}\left(\frac{\partial}{\partial x_i}\mathbf{F}(\mathbf{x}_0)\right) = \frac{\partial}{\partial x_i}\left(\frac{\partial}{\partial x_j}\mathbf{F}(\mathbf{x}_0)\right).$$

Thus, one should not use the flux function $\mathbf{F^s}$ as defined above or realize that the derivation has a certain amount of error built in and deal with this in the numerical scheme.

It can also be seen that the same spikes arise in the ADIFOR automatic differentiation sensitivities. Since the ADIFOR sensitivity is considered to be the *exact* discrete sensitivity, it has been reasoned that these spikes are the correct solution. It can be seen though that as the grid spacing is refined, the shape of the spike becomes thinner and taller. Thus, the spikes and their shape have become an artificial phenomena introduced by the numerical methods used and are dependent upon the artificial mesh used. These spikes arise using the automatic differentiation method because even though the solution is discontinuous, it becomes a "continuous" function in the discrete space. Hence, ADIFOR has no problem differentiating the function and the result is spikes at the discontinuity.

7.1.2 Contact Discontinuities

Contact discontinuities are another source of error in the sensitivity calculations. Across a contact discontinuity, the velocity, u and the pressure, P, are continuous while the density,

ρ and hence other conserved quantities experience a jump discontinuity. Thus, for the conserved quantities the same problems, as are described above, arise and spikes arise in the conserved quantities sensitivities at the contact discontinuity.

7.2 Flow Sensitivities and Rarefaction Waves

The final source of error considered here is the rarefaction wave. Previously, it has been believed that since the flow within the rarefaction wave is smooth then the sensitivities will also be continuous and of little problem computationally. Although the sensitivities are continuous in the rarefaction wave, they still present computational difficulties. A new problem arises at either end of the rarefaction wave. The flow sensitivities introduce a jump condition at both ends of the wave making it difficult to capture the correct sensitivity. The numerical methods used are designed to correctly capture jump discontinuities for the flow and it would be reasonable to expect a similar behavior for the flow sensitivities. In effect, a smearing of the discontinuity takes place at both ends of the rarefaction wave. This is very noticeable in the density sensitivity. For more accurate solutions, this must be dealt with numerically.

7.3 Solutions to Sensitivity Calculation Problems

In the preceding sections, the sensitivity calculation problems caused by discontinuous flow were discussed. Although solutions to the problems were not explicitly given, the discussion of the problems lead into several different methods to overcome these sensitivity problems.

The first problem to discuss is the development of the spikes arising at the discontinuities. The simplest "fix" to this problem is a post processing method which will be referred to as chopping. In the chopping method, the flow sensitivities are calculated with no special attention to the discontinuities in the fluid flow. As is seen in Chapter 5 and discussed here, these flow sensitivities will introduce spikes approximating the δ-functions arising at the discontinuities. The chopping method then loops over the flow sensitivity and when ever a spike is encountered it is chopped off, *i.e.*, the sensitivity value at a point in the spike is reassigned to be the new predicted value using the points outside of the spike region. The first important aspect is how to determine where the spikes arise automatically. One possible method is to check the gradient of the flow sensitivity solution. If the gradient is large at a point $(x_1, x_2, \ldots, x_n)$, then the flow sensitivity at this point is probably in a spike and should be reassigned. Likewise, there are other methods that can be used, such

as checking for the corners that arise at either end of the spike. Methods can be used in conjunction with each other. The second important aspect is to determine how to reassign the values. This could be accomplished using a simple Taylor approximation using a point outside of the spike region and its gradient to reassign the value. The chopping method is probably the crudest method available and has several deficiencies. First of all, the chopping method is very expensive as gradients have to be calculated for the flow sensitivities and every point has to be checked. Secondly, for the detection and reassignment phase to work well, usually something must be known about the flow sensitivities *a priori*. Finally, it has been seen that the spikes may corrupt the solution outside of the spike region and thus reassigning the solution using these points may still result in a poor solution. Although the chopping method may seem crude, it may be the only solution to calculate sensitivities without spikes for the automatic differentiation methods unless one knows how to internally change the differentiation program.

Another possible method is to limit the development of the spikes on the fly, *i.e.*, the flow sensitivities are hindered from developing spikes during the calculation process. This method is discussed for the sensitivity equation method using the Roe scheme in Section 8.4.1.

The other problem to consider is the smearing of the jump discontinuities arising in the flow sensitivities at either end of the rarefaction waves. At this point, the most viable approach is to refine the grid. In Chapter 5, it was seen that as the grid was refined, the flow sensitivities captured these jumps more accurately. The problem is that there is a second level of approximation going on. The exact flow solution is approximated using a numerical routine and then this approximate flow solution is used in the approximation of the flow sensitivities. Hence, the inaccuracies in the flow solution are magnified in the flow sensitivity calculations. It may not always be possible to refine the grid due to time and cost considerations. Therefore, numerical schemes for calculating the flow sensitivities of rarefaction waves should be developed.

Chapter 8

Systems of Conservation Laws and Hyperbolic Equations

One of the largest difficulties in flow sensitivity approximation is the formation of large δ-spikes at points where the flow is discontinuous. This chapter will take a more theoretical look at the development and possible removal of spikes from the sensitivities. The focus will be on the sensitivity equation method because it seems to provide the best opportunity for building "spike limiters" into the numerical scheme. The finite difference sensitivities can be calculated without spikes by ensuring that the finite difference quotient is never taken across the shock. This only requires knowing the shock position. With the automatic differentiation approaches, on the other hand, there may not be any way to stop the development of the spikes without knowing *a priori* the shock position and building this into the code so that when the code is differentiated this information will be taken into account. For these reasons, and the fact that the sensitivity equation method can be very efficient, the focus here will be on the continuous sensitivity equations and the sensitivity equation method.

8.1 Definitions and Notation

In this section, definitions and notation for conservation laws and hyperbolic equations are discussed. This background information is included both for completeness and because it is needed in the discussion of weak solutions.

8.1.1 Hyperbolic Systems of Conservation Laws

The Euler equations studied in the previous chapters are an example of a system of conservation laws. The general form for a system of p conservation laws in n space variables is given in Definition 1.

Definition 1 *Let Ω be an open subset of $\Re^p$ and let $\mathbf{F}_j$, $j = 1, \ldots, n$, be n smooth functions from Ω into $\Re^p$; the general form of a system of conservation laws in several space variables is*

$$\frac{\partial \mathbf{U}}{\partial t} + \sum_{j=1}^{n} \frac{\partial}{\partial x_j} \mathbf{F}_j(\mathbf{U}) = \mathbf{0}, \quad \mathbf{x} = (x_1, x_2, \ldots, x_n) \in \Re^n, \quad t > 0 \tag{8.1}$$

where

$$\mathbf{U} = \begin{bmatrix} u_1 \\ u_2 \\ \vdots \\ u_p \end{bmatrix}$$

is a vector-valued function from $\Re^n \times [0, +\infty)$ into Ω. The set Ω is called the set of states and the functions

$$\mathbf{F}_j = \begin{bmatrix} f_{1j} \\ f_{2j} \\ \vdots \\ f_{pj} \end{bmatrix}$$

are called the flux-functions. One says that the system of equations, Eq. 8.1, is written in conservative form. The system of conservation laws is nonlinear if any of the $\mathbf{F}_j$ depend nonlinearly on $\mathbf{U}$ [21].

The one-dimensional Euler equations, Eq. 4.1, are a system of nonlinear conservation laws with $n = 1$, $p = 3$,

$$\mathbf{U} = \begin{bmatrix} \rho \\ m \\ e \end{bmatrix}, \qquad \text{and} \qquad \mathbf{F}(\mathbf{U}) = \begin{bmatrix} m \\ (\frac{m^2}{\rho}) + P \\ (\frac{m}{\rho})(e + P) \end{bmatrix}.$$

The study of sensitivities for discontinuous fluid flow further restricts these systems of conservation laws to be hyperbolic systems of conservation laws, Definition 2.

Definition 2 *For all $j = 1, 2, \ldots, n$ let*

$$A_j(\mathbf{U}) = \left(\frac{\partial f_{ij}}{\partial u_k}(\mathbf{U}) \right)_{1 \leq i,k \leq p} \tag{8.2}$$

be the Jacobian matrix of $\mathbf{F}_j(\mathbf{U})$; the system of equations, Eq. 8.1, is called hyperbolic if for any $\mathbf{U} \in \Omega$ and any $\omega = (\omega_1, \omega_2, \ldots, \omega_n) \in \Re^n$, $\omega \neq 0$, the matrix

$$A(\mathbf{U}, \omega) = \sum_{j=1}^{n} \omega_j A_j(\mathbf{U})$$

has p real eigenvalues, $\lambda_k(\mathbf{U}, \omega)$, and p linearly independent eigenvectors, $\mathbf{r}_k(\mathbf{U}, \omega)$. In addition, if the eigenvalues, $\lambda_k(\mathbf{U}, \omega)$ are all distinct, the system of equations, Eq. 8.1, is called strictly hyperbolic [21].

The one-dimensional Euler equations are a strictly hyperbolic system of nonlinear conservation laws where the distinct eigenvalues are

$$\lambda_1(\mathbf{U}, \omega) = u, \quad \lambda_2(\mathbf{U}, \omega) = u + a, \quad \lambda_3(\mathbf{U}, \omega) = u - a,$$

with $a^2 = \frac{\gamma P}{\rho}$ and the corresponding eigenvectors

$$\mathbf{r}_1(\mathbf{U}, \omega) = \begin{bmatrix} 1 \\ u \\ \frac{u^2}{2} \end{bmatrix}, \quad \mathbf{r}_2(\mathbf{U}, \omega) = \begin{bmatrix} \frac{\rho}{2a} \\ \frac{\rho}{2a}(u + a) \\ \frac{\rho}{2a}\left(\frac{u^2}{2} + ua + \frac{a^2}{\gamma - 1} \right) \end{bmatrix},$$

and

$$\mathbf{r}_3(\mathbf{U}, \omega) = \begin{bmatrix} -\frac{\rho}{2a} \\ -\frac{\rho}{2a}(u - a) \\ -\frac{\rho}{2a}\left(\frac{u^2}{2} - ua + \frac{a^2}{\gamma - 1} \right) \end{bmatrix}.$$

The Riemann problem studied in the previous chapters is an example of the classical initial value problem, Definition 3.

Definition 3 (Initial Value Problem (IVP)) *Find a function*

$$\mathbf{U} : (\mathbf{x}, t) \in \Re^n \times [0, +\infty) \longrightarrow \mathbf{U}(\mathbf{x}, t) \in \Omega$$

that is a solution of the system of equations, Eq. 8.1, satisfying the initial conditions

$$\mathbf{U}(\mathbf{x}, 0) = \mathbf{U}_0(\mathbf{x}), \quad \mathbf{x} \in \Re^n \tag{8.3}$$

where $\mathbf{U}_0 : \Re^n \longrightarrow \Omega$ is a given function [21].

In the case of the Riemann problem, the initial value problem is given by Example 3.

Example 3 (Initial Value Riemann Problem) *Find a function*

$$\mathbf{U} : (x,t) \in \Re \times [0,+\infty) \longrightarrow \mathbf{U}(x,t) \in \Omega = (-\infty,+\infty) \times [0,+\infty)$$

that is a solution of Eq. 8.4 satisfying the initial conditions, Eq. 8.5

$$\mathbf{U}_t + \mathbf{F}(\mathbf{U})_x = \mathbf{0} \tag{8.4}$$

$$\mathbf{U}(x,0) = \mathbf{U}_0(x) = \begin{cases} \begin{bmatrix} \rho_4 \\ m_4 \\ e_4 \end{bmatrix} & x < c = \textit{Diaphragm position} \\ \begin{bmatrix} \rho_1 \\ m_1 \\ e_1 \end{bmatrix} & x > c = \textit{Diaphragm position} \end{cases} \tag{8.5}$$

where

$$\mathbf{U} = \begin{bmatrix} \rho \\ m \\ e \end{bmatrix}, \qquad \textit{and} \qquad \mathbf{F}(\mathbf{U}) = \begin{bmatrix} m \\ (\frac{m^2}{\rho}) + P \\ (\frac{m}{\rho})(e+P) \end{bmatrix}$$

and $\mathbf{U}_0(x)$ *is discontinuous at the diaphragm.*

8.1.2 Linear Systems of Hyperbolic Equations

The other system of equations arising in sensitivity calculations is the continuous sensitivity equations for the sensitivity equation method which are derived by differentiating the Euler equations with respect to a parameter, α. The system of continuous sensitivity equations is a linear, hyperbolic, system of equations with discontinuous coefficients. In this section, the general theory for systems of linear hyperbolic discontinuous coefficient equations is discussed. Consider the following first-order, linear, variable coefficient, hyperbolic system of equations in m unknowns and two independent variables, (x,t),

$$\frac{\partial s_i}{\partial t} + \sum_{j=1}^{p} c_{i,j}(x,t)\frac{\partial s_j}{\partial x} + b_i(x,t,s_1,\ldots,s_p) = 0, \qquad i = 1,2,\ldots,p \tag{8.6}$$

where each b_i is linear in $\mathbf{S}$. The system can be written in matrix-vector form as

$$\frac{\partial \mathbf{S}}{\partial t} + C(x,t)\frac{\partial \mathbf{S}}{\partial x} + \mathbf{b}(x,t,\mathbf{S}) = \mathbf{0}. \tag{8.7}$$

This is exactly the form of the continuous sensitivity equations, Eq. 5.17, with

$$\begin{aligned} C(x,t) &= C(\mathbf{U}) = A(\mathbf{U}) \\ &= \begin{bmatrix} 0 & 1 & 0 \\ -(3-\gamma)\frac{u^2}{2} & (3-\gamma)u & \gamma-1 \\ (\gamma-1)u^3 - \frac{\gamma u e}{\rho} & \frac{\gamma e}{\rho} - \frac{3}{2}(\gamma-1)u^2 & \gamma u \end{bmatrix} \end{aligned} \tag{8.8}$$

and

$$\begin{aligned} &\mathbf{b}(x,t,\mathbf{S}) = \mathbf{b}(\mathbf{U}(x,t),\mathbf{S}(x,t)) = [A(\mathbf{U})]_x \mathbf{S} \\ = &\begin{bmatrix} 0 & 0 & 0 \\ -(3-\gamma)uu_x & (3-\gamma)u_x & 0 \\ (\gamma-1)3u^2u_x - \frac{\gamma u_x e\rho + u e_x \rho - u e \rho_x}{\rho^2} & \frac{\gamma e_x \rho - e\rho_x}{\rho^2} - 3(\gamma-1)uu_x & \gamma u_x \end{bmatrix} \cdot \begin{bmatrix} \rho' \\ u' \\ e' \end{bmatrix}. \end{aligned} \tag{8.9}$$

Clearly, the reference to the two independent variables has not been included in both the coefficient matrix C and the right hand side vector $\mathbf{b}$ to increase readability, but all the flow variables and sensitivity variables are functions of (x,t).

Definition 4 *The system of equations, Eq. 8.7, is* hyperbolic at the point (x,t)*, if* $C(x,t)$ *has* m *real and distinct eigenvalues* $\lambda_1(x,t), \lambda_2(x,t), \ldots, \lambda_m(x,t)$*. The system is said to be* hyperbolic in a domain Ω *of* $\Re^2$ *if it is hyperbolic at every point of* Ω*. [47]*

The fact that each of the m eigenvalues $\lambda_k(x,t)$ are real and distinct assures that there will also be m linearly independent eigenvectors,

$$\mathbf{r}_k(x,t) = \begin{bmatrix} r_{1,k}(x,t) \\ r_{2,k}(x,t) \\ \vdots \\ r_{m,k}(x,t) \end{bmatrix}, \qquad k = 1,2,\ldots,m. \tag{8.10}$$

Each eigenvector $\mathbf{r}_k(x,t)$ corresponds to the eigenvalue $\lambda_k(x,t)$ and is unique only up to a multiplicative constant. In terms of the continuous sensitivity equations, Eq. 5.17, the equations are hyperbolic and the distinct eigenvalues are given by

$$\lambda_1 = u, \quad \lambda_2 = u + a, \quad \lambda_3 = u - a,$$

where $a^2 = \frac{\gamma P}{\rho}$ and the corresponding eigenvectors are

$$\mathbf{r}_1 = \begin{bmatrix} 1 \\ u \\ \frac{u^2}{2} \end{bmatrix}, \quad \mathbf{r}_2 = \begin{bmatrix} \frac{\rho}{2a} \\ \frac{\rho}{2a}(u+a) \\ \frac{\rho}{2a}\left(\frac{u^2}{2} + ua + \frac{a^2}{\gamma-1}\right) \end{bmatrix}, \quad \mathbf{r}_3 = \begin{bmatrix} -\frac{\rho}{2a} \\ -\frac{\rho}{2a}(u-a) \\ -\frac{\rho}{2a}\left(\frac{u^2}{2} - ua + \frac{a^2}{\gamma-1}\right) \end{bmatrix}.$$

Note, these are the same eigenvalues and eigenvectors as for the Euler equations since both the Jacobian of the flux function, $\mathbf{F}(\mathbf{U})$ and the matrix $C(x,t)$ in the continuous sensitivity equations are the same. Hence, the continuous sensitivity equations for the Euler equations are a linear hyperbolic system of equations [24]. The coefficient matrix C is not only variable in the domain, *i.e.*, depends on both the independent variables (x,t), but is also discontinuous in the domain. The coefficient matrix has discontinuities in space and time because it is a function of the flow vector, $\mathbf{U}$. The flow vector is in turn a discontinuous function in the xt-plane, *i.e.*, contains shock waves and contact discontinuities. Thus, the coefficient matrix and right hand side vector, $\mathbf{b}$ are both discontinuous. Due to these discontinuities, the solution to the continuous sensitivity equations involve δ-functions and discontinuities. This not only increases the complexity of the theory, but also the difficulty in developing a new numerical method for these types of equations.

8.2 Weak Solutions and Weak Forms

In the previous chapters, it has been seen that the solutions of the Euler equations and the continuous sensitivity equations involve discontinuities in the flow and both discontinuities and δ-functions in the flow sensitivities. Clearly, these solutions are not classical solutions to the corresponding initial value problems.

Definition 5 *The function* $\mathbf{U} : \Re^n \times [0,+\infty) \longrightarrow \Omega$ *is a classical solution of the initial value problem, (IVP), if* $\mathbf{U}$ *is a* C^1 *function that satisfies Eq. 8.1 and the initial conditions,* $\mathbf{U}(\mathbf{x},0) = \mathbf{U}_0(\mathbf{x})$ *pointwise [21].*

The most important feature of hyperbolic systems of nonlinear conservation laws is that, in general, this classical solution will not exist, even if the initial condition, $\mathbf{U}_0(\mathbf{x})$, is a smooth function. For this reason, a different set of solutions must be defined. These solutions are referred to as weak solutions and discussed in detail in Godlewski and Raviart [21], LeVeque [28] and Rogers and Renardy [39]. In the next few paragraphs, the idea of a weak solution is developed and defined. The development follows directly from Godlewski and Raviart [21] and more information can be found there.

Definition 6 *Let* $\psi \in C_0^1(\Re^n \times [0,+\infty))^p$*, then* ψ *is a* C^1 *function with compact support in* $(\Re^n \times [0,+\infty))^p$ *which means that* ψ *is the restriction to* $(\Re^n \times [0,+\infty))^p$ *of a* C^1 *function with compact support in an open set containing* $(\Re^n \times [0,+\infty))^p$ *[21].*

If $\mathbf{U} \in C_0^1$ and satisfies Eq. 8.1 and $\phi \in C_0^1(\Re^n \times [0, +\infty))^p$, and the conservation law, Eq. 8.1, is multiplied by ϕ and integrated over $(\Re^n \times [0, +\infty))^p$, the following weak form, Eq. 8.11, is arrived at after integration by parts and simplification.

$$\int_0^\infty \int_{\Re^n} \left\{ \mathbf{U} \cdot \frac{\partial \phi}{\partial t} + \sum_{j=1}^{n} \mathbf{F}_j(\mathbf{U}) \cdot \frac{\partial \phi}{\partial x_j} \right\} d\mathbf{x}dt + \int_{\Re^n} \mathbf{U}_0(\mathbf{x}) \cdot \phi(\mathbf{x}, 0) d\mathbf{x} = 0, \tag{8.11}$$

where the dot $\cdot$ denotes the Euclidean inner product on $\Re^p$. This equation can now be used to define the weak solutions.

Definition 7 *Assume that* $\mathbf{U}_0 \in \mathbf{L}_{loc}^\infty(\Re^n)^p$*, that is* $\mathbf{U}_0$ *is in the space of locally bounded measurable functions. A function* $\mathbf{U} \in \mathbf{L}_{loc}^\infty(\Re^n \times [0, +\infty))^p$ *is called a* <u>*weak solution*</u> *to the initial value problem, (IVP), if* $\mathbf{U} \in \Omega$ *almost everywhere and satisfies Eq. 8.11 for any function* $\phi \in C_0^1(\Re^n \times [0, +\infty))^p$ *[21].*

Clearly, any classical solution of the initial value problem satisfies Eq. 8.11 for all $\phi \in C_0^1(\Re^n \times [0, +\infty))^p$. Thus, all classical solutions are weak solutions, but not vice versa.

One of the most obvious outcomes is the nonuniqueness of weak solutions. There are several different solutions that will satisfy the weak form, Eq. 8.11. Hence the most "physically relevant" solution must be obtained. This is not the focus of the present research but it does present problems in the numerical solutions of hyperbolic systems of conservation laws. Further discussions of this can be found in to Godlewski and Raviart [21], LeVeque [28], and Rogers and Renardy [39]. In most cases, the "correct" solution is chosen using the concept of entropy.

In Section 8.2.1 and Section 8.2.2, the weak form for the continuous sensitivity equations will be derived using two different approaches. The first is a weak form derived starting from the continuous sensitivity equations and the second is the differentiation of the weak form of the Euler equations with respect to a parameter α to get a new weak form. In calculating the continuous sensitivity equations, error has already been built into the equations by switching the orders of differentiation of a discontinuous function (See Chapter 7). Since, it is the weak solutions that are of interest, the weak form for the continuous sensitivity equations will be compared to the differentiated weak form of the Euler equations. Even though the solution of the Euler equations involves discontinuities, the weak form is an integral equation and the differentiation of this weak form should not cause any problems.

8.2.1 Derived Weak Form

Consider the one-dimensional sensitivity equations for the flow sensitivity with respect to a parameter α for a one-dimensional Riemann problem involving only a single shock.

$$\mathbf{S}_t(x,t) + \left[\mathbf{F^s}(\mathbf{U}(x,t),\mathbf{S}(x,t))\right]_x = \mathbf{0} \tag{8.12}$$

Let $\phi \in C_0^1(\Re \times [0,\infty))^3$, that is any function in $\Re^3 \times \Re^2$ that has compact support and is continuously differentiable in each component. Multiplying both sides of the continuous sensitivity equations by $\phi(x,t)$ and integrating both sides of the equation over the domain, $(-\infty,\infty)\times[0,\infty)$ results in

$$\int_o^\infty \int_{-\infty}^\infty \left\{\phi(x,t)\mathbf{S}_t(x,t) + \phi(x,t)\left[\mathbf{F^s}(\mathbf{U}(x,t),\mathbf{S}(x,t))\right]_x\right\} dxdt = \mathbf{0}. \tag{8.13}$$

The next step is to move the derivatives off of the sensitivity variables and flux vectors and onto the test functions. It is necessary to integrate by parts, but it is known that both $\mathbf{U}$ and $\mathbf{S}$ are discontinuous at the shock wave where the shock position or shock surface is given by $x_s(t,\alpha)$. Each of the integrals must be split up into pieces where the integrand is continuous, for a specific value of the parameter $\alpha = \alpha_0$.

$$\begin{aligned} & \int_0^\infty \int_{-\infty}^{x_s(t,\alpha_0)} \phi(x,t)\mathbf{S}_t(x,t)dxdt + \int_0^\infty \int_{-\infty}^{x_s(t,\alpha_0)} \phi(x,t)\left[\mathbf{F^s}(\mathbf{U}(x,t),\mathbf{S}(x,t))\right]_x dxdt \\ + & \int_0^\infty \int_{x_s(t,\alpha_0)}^{\infty} \phi(x,t)\mathbf{S}_t(x,t)dxdt + \int_0^\infty \int_{x_s(t,\alpha_0)}^{\infty} \phi(x,t)\left[\mathbf{F^s}(\mathbf{U}(x,t),\mathbf{S}(x,t))\right]_x dxdt \\ = & \mathbf{0}. \end{aligned} \tag{8.14}$$

Since the integrands are smooth on $[0,\infty)\times(-\infty,x_s(t,\alpha_0)]$ and $[0,\infty)\times[x_s(t,\alpha_0),\infty)$, the orders of integration can be changed on the $\phi(x,t)\mathbf{S}_t(x,t)$ terms. First of all, it is assumed that the shock position, $x_s(t,\alpha_0)$, is a monotonically increasing function, *i.e.*, the shock is continuously moving to the right. This is a physically relevant assumption and is exactly the case in the Riemann problems at hand where the shock moves from the diaphragm to the right at a constant speed through time. The following arguments will also work if the shock function is a monotonically decreasing function such as the case where the shock moves to the left. To switch the orders of integration, the integral

$$\int_0^\infty \int_{-\infty}^{x_s(t,\alpha_0)} \phi(x,t)\mathbf{S}_t(x,t)dxdt, \tag{8.15}$$

must be broken up into two regions. Region (1) is the rectangle $(-\infty, x_s(0,\alpha_0)\times[0,+\infty)$ where $x_s(0,\alpha_0)$ is the position of the diaphragm. Region (2) is the area bounded by the line $x = x_s(0,\alpha_0)$ and the shock surface $\{(x_s(t,\alpha_0),t) : t = 0 \longrightarrow +\infty\}$. The integral

$$\int_0^\infty \int_{x_s(t,\alpha_0)}^{\infty} \phi(x,t)\mathbf{S}_t(x,t)dxdt \tag{8.16}$$

is defined over a single region that does not need to be broken up to switch the orders of integration. Region (3) is the area bounded by the shock surface $\{(x_s(t,\alpha_0),t) : t = 0 \longrightarrow +\infty\}$ and the line $\{(x,0) : x = x_s(0,\alpha_0) \longrightarrow +\infty\}$. The three regions are shown in Fig. 8.1. In the situation where the shock is moving to the left, Eq. 8.16 will have to be broken up into two different regions and Eq. 8.15 will not have to be broken up into different regions. Changing the limits of integration on these integrals results in

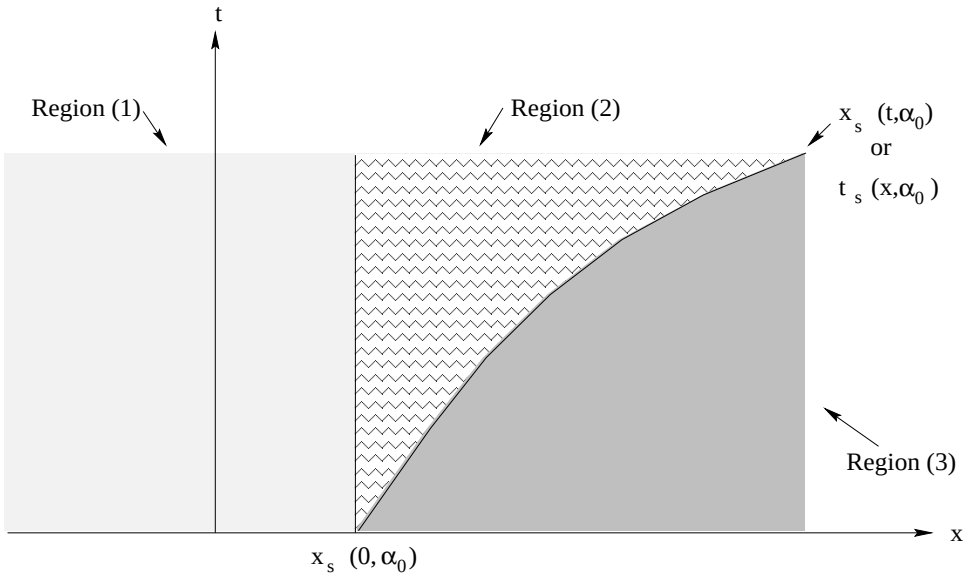

Figure 8.1: Definition of integration regions needed in order to change orders of integration.

$$\begin{aligned}
&\int_{-\infty}^{x_s(0,\alpha_0)}\int_0^{\infty}\phi(x,t)\mathbf{S}_t(x,t)dtdx + \int_{x_s(0,\alpha_0)}^{+\infty}\int_{t_s(x,\alpha_0)}^{\infty}\phi(x,t)\mathbf{S}_t(x,t)dtdx \\
+ &\int_0^{\infty}\int_{-\infty}^{x_s(t,\alpha_0)}\phi(x,t)\left[\mathbf{F^s}(\mathbf{U}(x,t),\mathbf{S}(x,t))\right]_x dxdt + \int_{x_s(0,\alpha_0)}^{\infty}\int_0^{t_s(x,\alpha_0)}\phi(x,t)\mathbf{S}_t(x,t)dtdx \\
+ &\int_0^{\infty}\int_{x_s(t,\alpha_0)}^{\infty}\phi(x,t)\left[\mathbf{F^s}(\mathbf{U}(x,t),\mathbf{S}(x,t))\right]_x dxdt = \mathbf{0} \qquad (8.17)
\end{aligned}$$

where $t_s(x,\alpha_0)$ is again the shock surface, but the parameterization is a function of x instead of a function of t. Since the shock surface is a monotonically increasing function, $t_s(x,\alpha_0)$ is just the inverse function of $x_s(t,\alpha_0)$. The point $x_s(0,\alpha_0)$ is the initial shock position, *i.e.*, the diaphragm position. Consider, the following identities

$$\begin{aligned}
\frac{\partial}{\partial t}[\phi\mathbf{S}] &= \phi_t\mathbf{S} + \phi\mathbf{S}_t, \\
\phi\mathbf{S}_t &= \frac{\partial}{\partial t}[\phi\mathbf{S}] - \phi_t\mathbf{S}, \qquad (8.18)
\end{aligned}$$

$$\begin{aligned}\frac{\partial}{\partial x}[\phi \mathbf{F^s}(\mathbf{U},\mathbf{S})] &= \phi_x \mathbf{F^s}(\mathbf{U},\mathbf{S}) + \phi \mathbf{F^s}_x(\mathbf{U},\mathbf{S}),\\ \phi \mathbf{F^s}_x(\mathbf{U},\mathbf{S}) &= \frac{\partial}{\partial x}[\phi \mathbf{F^s}(\mathbf{U},\mathbf{S})] - \phi_x \mathbf{F^s}(\mathbf{U},\mathbf{S}).\end{aligned} \tag{8.19}$$

Using the above equalities and integrating by parts gives

$$\begin{aligned}&\int_{-\infty}^{x_s(0,\alpha_0)} \phi(x,t)\mathbf{S}^L(x,t)\,|_0^\infty\, dx - \int_{-\infty}^{x_s(0,\alpha_0)}\int_0^{+\infty} \phi_t(x,t)\mathbf{S}^L(x,t)dtdx\\ +\ &\int_{x_s(0,\alpha_0)}^{+\infty} \phi(x,t)\mathbf{S}^L(x,t)\,\Big|_{t_s(x,\alpha_0)}^{\infty} dx - \int_{x_s(0,\alpha_0)}^{+\infty}\int_{t_s(x,\alpha_0)}^{+\infty} \phi_t(x,t)\mathbf{S}^L(x,t)dtdx\\ +\ &\int_0^{\infty} \phi(x,t)\mathbf{F^s}(\mathbf{U}^L(x,t),\mathbf{S}^L(x,t))\,\Big|_{-\infty}^{x_s(t,\alpha_0)} dt\\ -\ &\int_0^{\infty}\int_{-\infty}^{x_s(t,\alpha_0)} \phi_x(x,t)\mathbf{F^s}(\mathbf{U}^L(x,t),\mathbf{S}^L(x,t))dxdt\\ +\ &\int_{x_s(0,\alpha_0)}^{+\infty} \phi(x,t)\mathbf{S}^R(x,t)\,\Big|_0^{t_s(x,\alpha_0)} dx - \int_{x_s(0,\alpha_0)}^{+\infty}\int_0^{t_s(x,\alpha_0)} \phi_t(x,t)\mathbf{S}^R(x,t)dtdx\\ +\ &\int_0^{\infty} \phi(x,t)\mathbf{F^s}(\mathbf{U}^R(x,t),\mathbf{S}^R(x,t))\,\Big|_{x_s(t,\alpha_0)}^{\infty} dt\\ -\ &\int_0^{\infty}\int_{x_s(t,\alpha_0)}^{\infty} \phi_x(x,t)\mathbf{F^s}(\mathbf{U}^R(x,t),\mathbf{S}^R(x,t))dxdt = \mathbf{0}.\end{aligned} \tag{8.20}$$

In the above formula, $\mathbf{U}^L$ and $\mathbf{S}^R$ is used to stress that the integrands are defined on the left and right sides of the shock. Since the test functions have compact support, $\phi(\pm\infty,t) = \phi(x,\infty) = 0$. Using this fact, switching the orders of integration on the $\phi_t(x,t)\mathbf{S}(x,t)$ terms back to their original order and simplifying results in

$$\begin{aligned}&\int_0^{\infty}\int_{-\infty}^{\infty} \{\phi_t(x,t)\mathbf{S}(x,t) + \phi_x(x,t)\mathbf{F^s}(\mathbf{U}(x,t),\mathbf{S}(x,t))\}\,dxdt = -\int_{-\infty}^{\infty} \phi(x,0)\mathbf{S}(x,0)dx\\ +\ &\int_0^{\infty} \phi(x_s(t,\alpha_0),t)[[\mathbf{F^s}(\mathbf{U}(x_s(t,\alpha_0),t),\mathbf{S}(x_s(t,\alpha_0),t))]]dt\\ -\ &\int_{x_s(0,\alpha_0)}^{+\infty} \phi(x,t_s(x,\alpha_0))[[\mathbf{S}(x,t_s(x,\alpha_0))]]dx\end{aligned} \tag{8.21}$$

where $[[\cdot]]$ denotes the jump in $\mathbf{F^s}$ and $\mathbf{S}$. It should also be noted that the second integral in the above formula still has a discontinuity at $x_s(0,\alpha_0)$ and must be broken into pieces to be evaluated. The third and fourth integrals are just integrals along the shock surface $x_s(t,\alpha_0)$. The integral

$$-\int_{x_s(0,\alpha_0)}^{+\infty} \phi(x,t_s(x,\alpha_0))[[\mathbf{S}(x,t_s(x,\alpha_0))]]dx$$

is along the shock surface with the parameterization

$$\hat{x} = x \tag{8.22}$$

$$\hat{t} = t_s(x,\alpha_0). \tag{8.23}$$

An analogous parameterization of the shock surface can also be used,

$$\tilde{x} = x_s(t, \alpha_0) \tag{8.24}$$
$$\tilde{t} = t, \tag{8.25}$$

where $dx = \frac{\partial x_s}{\partial t} dt$. The integral is in terms of t and becomes

$$-\int_0^{+\infty} \phi(x_s(t,\alpha_0),t) \frac{\partial x_s}{\partial t}(t,\alpha_0)[[\mathbf{S}(x_s(t,\alpha_0),t]]dt.$$

This can be substituted into Eq. 8.21 to get

$$\begin{aligned}
&\int_0^{\infty}\int_{-\infty}^{\infty} \left\{\phi_t(x,t)\mathbf{S}(x,t) + \phi_x(x,t)\mathbf{F^s}(\mathbf{U}(x,t),\mathbf{S}(x,t))\right\} dxdt = -\int_{-\infty}^{\infty} \phi(x,0)\mathbf{S}(x,0)dx \\
+ &\int_0^{\infty} \phi(x_s(t,\alpha_0),t)[[\mathbf{F^s}(\mathbf{U}(x_s(t,\alpha_0),t),\mathbf{S}(x_s(t,\alpha_0),t))]]dt \\
- &\int_0^{+\infty} \phi(x_s(t,\alpha_0),t)\frac{\partial x_s}{\partial t}(t,\alpha_0)[[\mathbf{S}(x_s(t,\alpha_0),t]]dt.
\end{aligned} \tag{8.26}$$

To further simplify Eq. 8.26, the Rankine-Hugoniot jump conditions must be differentiated. The Rankine-Hugoniot jump conditions for the fluid flow are given by

$$\left(\mathbf{F}(\mathbf{U}^L) - \mathbf{F}(\mathbf{U}^R)\right) = s\left(\mathbf{U}^L - \mathbf{U}^R\right) \tag{8.27}$$

where $s = \frac{\partial x_s}{\partial t}(t,\alpha_0)$ is the shock speed. The assumption is also made that $\mathbf{F}(\mathbf{U})$ is not a function of α explicitly. The differentiation of Eq. 8.27 with respect to α is

$$\begin{aligned}
&[[\mathbf{F^s}(\mathbf{U}(x_s(t,\alpha_0),t),\mathbf{S}(x_s(t,\alpha_0),t))]] + [[\mathbf{F}_x(\mathbf{U}(x_s(t,\alpha_0),t))]]\frac{\partial x_s}{\partial \alpha}(t,\alpha_0) \\
= &\frac{\partial^2 x_s}{\partial t \partial \alpha}(t,\alpha_0)[[\mathbf{U}(x_s(t,\alpha_0),t)]] + \frac{\partial x_s}{\partial t}(t,\alpha_0)[[\mathbf{U}_x(x_s(t,\alpha_0),t)]]\frac{\partial x_s}{\partial \alpha}(t,\alpha_0) \\
+ &\frac{\partial x_s}{\partial t}(t,\alpha_0)[[\mathbf{S}(x_s(t,\alpha_0),t)]].
\end{aligned} \tag{8.28}$$

Using this fact and the fact that

$$[[\mathbf{F}_x(\mathbf{U}(x_s(t,\alpha_0),t))]] = -[[\mathbf{U}_t(x_s(t,\alpha_0),t)]], \tag{8.29}$$

results in

$$\begin{aligned}
&\int_0^{\infty} \phi(x_s(t,\alpha_0),t)[[\mathbf{F^s}(\mathbf{U}(x_s(t,\alpha_0),t),\mathbf{S}(x_s(t,\alpha_0),t))]]dt \\
= &\int_0^{\infty} \frac{\partial^2 x_S}{\partial t \partial \alpha}(t,\alpha_0)\phi(x_s(t,\alpha_0),t)[[\mathbf{U}(x_s(t,\alpha_0),t)]]dt \\
+ &\int_0^{\infty} \frac{\partial x_s}{\partial \alpha}(t,\alpha_0)[[\mathbf{U}_t(x_s(t,\alpha_0),t)]]\phi(x_s(t,\alpha_0),t)dt \\
+ &\int_0^{\infty} \phi(x_s(t,\alpha_0),t)\frac{\partial x_s}{\partial t}(t,\alpha_0)[[\mathbf{U}_x(x_s(t,\alpha_0),t)]]\frac{\partial x_s}{\partial \alpha}(t,\alpha_0)dt \\
+ &\int_0^{\infty} \phi(x_s(t,\alpha_0),t)\frac{\partial x_s}{\partial t}(t,\alpha_0)[[\mathbf{S}(x_s(t,\alpha_0),t)]]dt.
\end{aligned} \tag{8.30}$$

Using this result and substituting into Eq. 8.26 gives

$$\begin{aligned}
&\int_0^\infty \int_{-\infty}^\infty \{\phi_t(x,t)\mathbf{S}(x,t) + \phi_x(x,t)\mathbf{F^s}(\mathbf{U}(x,t),\mathbf{S}(x,t))\}\, dxdt \\
= \; & -\int_{-\infty}^\infty \phi(x,0)\mathbf{S}(x,0)dx + \int_0^\infty \frac{\partial^2 x_S}{\partial t \partial \alpha}(t,\alpha_0)\phi(x_s(t,\alpha_0),t)[[\mathbf{U}(x_s(t,\alpha_0),t)]]dt \\
+ \; & \int_0^\infty \frac{\partial x_s}{\partial \alpha}(t,\alpha_0)(t,\alpha_0)[[\mathbf{U}_t(x_s(t,\alpha_0),t)]]\phi(x_s(t,\alpha_0),t)dt \\
+ \; & \int_0^\infty \phi(x_s(t,\alpha_0),t)\frac{\partial x_s}{\partial t}(t,\alpha_0)[[\mathbf{U}_x(x_s(t,\alpha_0),t)]]\frac{\partial x_s}{\partial \alpha}(t,\alpha_0)dt. \qquad (8.31)
\end{aligned}$$

The third and fourth integrals on the right hand side of Eq. 8.31 can be combined to be just the integral along the shock surface, $x_s(t,\alpha_0)$. This can be easily seen considering the following directional derivative in the direction of $(x_s(\tau,\alpha_0),\tau)$

$$\left(\mathbf{U}_t(x_s(t,\alpha_0),t) + \frac{\partial x_s}{\partial t}(t,\alpha_0)\mathbf{U}_x(x_s(t,\alpha_0),t)\right) = \frac{\partial \mathbf{U}}{\partial \tau}(\tau). \qquad (8.32)$$

Combining these integrals and substituting, the final version of the weak form of the continuous sensitivity equations becomes

$$\begin{aligned}
&\int_0^\infty \int_{-\infty}^\infty \{\phi_t(x,t)\mathbf{S}(x,t) + \phi_x(x,t)\mathbf{F^s}(\mathbf{U}(x,t),\mathbf{S}(x,t))\}\, dxdt \\
= \; & -\int_{-\infty}^\infty \phi(x,0)\mathbf{S}(x,0)dx + \int_0^\infty \frac{\partial^2 x_S}{\partial t \partial \alpha}(t,\alpha_0)\phi(x_s(t,\alpha_0),t)[[\mathbf{U}(x_s(t,\alpha_0),t)]]dt \\
+ \; & \int_0^\infty \phi(\tau)\frac{\partial x_s}{\partial \alpha}(\tau)[[\mathbf{U}_\tau(\tau)]]d\tau. \qquad (8.33)
\end{aligned}$$

8.2.2 Differentiated Weak Form of the Euler Equations

The weak form of the Euler equations can also be differentiated with respect to the parameter α to derive a new weak form. Using the same set of test functions $\phi(x,t)$, the weak form for the Euler equations is given by

$$\int_0^\infty \int_{-\infty}^\infty \{\phi_t(x,t)\mathbf{U}(x,t) + \phi_x(x,t)\mathbf{F}(\mathbf{U}(x,t))\}\, dxdt = -\int_{-\infty}^\infty \phi(x,0)\mathbf{U}(x,0)dx. \qquad (8.34)$$

Again, it is assumed that the Riemann problem involves a single shock at $x_s(t,\alpha)$ so the integral must be broken up into pieces where the integrand is continuous, for a specific

value of the parameter $\alpha = \alpha_0$, before it is differentiated with respect to α

$$\begin{aligned} & \frac{\partial}{\partial \alpha}\left\{\int_0^\infty \int_{-\infty}^{x_s(t,\alpha_0)} \phi_t(x,t)\mathbf{U}(x,t)dxdt + \int_0^\infty \int_{-\infty}^{x_s(t,\alpha_0)} \phi_x(x,t)\mathbf{F}(\mathbf{U}(x,t))dxdt \right. \\ + & \int_0^\infty \int_{x_s(t,\alpha_0)}^\infty \phi_t(x,t)\mathbf{U}(x,t)dxdt + \int_0^\infty \int_{x_s(t,\alpha_0)}^\infty \phi_x(x,t)\mathbf{F}(\mathbf{U}(x,t))dxdt \\ = & \left. -\int_{-\infty}^{x_s(0,\alpha_0)} \phi(x,0)\mathbf{U}(x,0)dx - \int_{x_s(0,\alpha_0)}^\infty \phi(x,0)\mathbf{U}(x,0)dx \right\}. \end{aligned} \tag{8.35}$$

Since, the limits of integration involve the parameter α, Leibnitz's Rule must be used in the differentiation.

Theorem 2 (Leibnitz's Rule: [37]) *Let* $\mathbf{F} : \Re^2 \longrightarrow \Re^n$ *be the vector-valued function*

$$\mathbf{F}(x,\alpha) = \begin{bmatrix} f_1(x,\alpha) \\ f_2(x,\alpha) \\ \vdots \\ f_n(x,\alpha) \end{bmatrix}.$$

Suppose that each f_j *and* $\frac{\partial f_j}{\partial \alpha}$, $j = 1, 2, \ldots, n$ *are continuous on* $R = \{(x,\alpha) : a \le x \le b, c \le \alpha \le d\}$ *and that* h_0 *and* h_1 *both have continuous first derivatives. If* $\varphi(\alpha)$ *is defined by*

$$\varphi(\alpha) = \int_{h_0(\alpha)}^{h_1(\alpha)} \mathbf{F}(x,\alpha)dx \tag{8.36}$$

then

$$\varphi(\alpha)' = \mathbf{F}(h_1(\alpha),\alpha)h_1'(\alpha) - \mathbf{F}(h_0(\alpha),\alpha)h_0'(\alpha) + \int_{h_0(\alpha)}^{h_1(\alpha)} \mathbf{F}_\alpha(x,\alpha)dx. \tag{8.37}$$

Calculating the derivatives using Leibnitz's rule and combining integrals results in

$$\begin{aligned} & \int_0^\infty \int_{-\infty}^\infty \left\{\phi_t(x,t)\mathbf{S}(x,t) + \phi_x(x,t)\mathbf{F^s}(\mathbf{U}(x,t),\mathbf{S}(x,t))\right\} dxdt \\ + & \int_0^\infty \frac{\partial x_s}{\partial \alpha}(t,\alpha_0)\phi_t(x_s(t,\alpha_0),t)[[\mathbf{U}(x_s(t,\alpha_0),t)]]dt \\ + & \int_0^\infty \frac{\partial x_s}{\partial \alpha}(t,\alpha_0)\phi_x(x_s(t,\alpha_0),t)[[\mathbf{F}(\mathbf{U}(x_s(t,\alpha_0),t))]]dt \\ = & -\int_{-\infty}^\infty \phi(x,0)\mathbf{S}(x,0)dx - \frac{\partial x_s}{\partial \alpha}(0,\alpha_0)\phi(x_s(0,\alpha_0),0)[[\mathbf{U}(x_s(0,\alpha_0),0)]]. \end{aligned} \tag{8.38}$$

It should be noted that the first and fourth integrals above still involve discontinuities at the shock surface, $x_s(t,\alpha_0)$, that must be taken care of before the integrals can be evaluated.

Using the fact $[[\mathbf{F}(\mathbf{U})]] = \frac{\partial x_s}{\partial t}[[\mathbf{U}]]$ results in

$$\begin{aligned}
&\int_0^\infty \int_{-\infty}^\infty \{\phi_t(x,t)\mathbf{S}(x,t) + \phi_x(x,t)\mathbf{F^s}(\mathbf{U}(x,t),\mathbf{S}(x,t))\}\, dxdt \\
+ &\int_0^\infty \frac{\partial x_s}{\partial \alpha}(t,\alpha_0)\left(\phi_t(x_s(t,\alpha_0),t) + \phi_x(x_s(t,\alpha_0),t)\frac{\partial x_s}{\partial t}(t,\alpha_0)\right)[[\mathbf{U}(x_s(t,\alpha_0),t)]]dt \\
= &-\int_{-\infty}^\infty \phi(x,0)\mathbf{S}(x,0)dx - \frac{\partial x_s}{\partial \alpha}(0,\alpha_0)\phi(x_s(0,\alpha_0),0)[[\mathbf{U}(x_s(0,\alpha_0),0)]]. \qquad (8.39)
\end{aligned}$$

The second integral in Eq. 8.39 is just the directional derivative of ϕ in the direction $(x_s(\tau,\alpha_0),\tau)$, or the derivative along the shock surface. The directional derivative is given by

$$\frac{\partial \phi}{\partial \tau} = D_{(x_s(\tau,\alpha_0),\tau)}\phi = \phi_t(x_s(t,\alpha_0),t) + \phi_x(x_s(t,\alpha_0),t)\frac{\partial x_s}{\partial t}(t,\alpha_0). \qquad (8.40)$$

Thus, the second integral reduces to

$$\int_0^\infty \frac{\partial x_s}{\partial \alpha}(\tau)\phi_\tau(\tau)[[\mathbf{U}(\tau)]]d\tau. \qquad (8.41)$$

This equation can be integrated by parts to get

$$\begin{aligned}
&\int_0^\infty \frac{\partial x_s}{\partial \alpha}(\tau)\phi_\tau(\tau)[[\mathbf{U}(\tau)]]d\tau = -\frac{\partial x_s}{\partial \alpha}(0,\alpha_0)\phi(x_s(0,\alpha_0),0)[[\mathbf{U}(x_s(0,\alpha_0),0)]] \\
- &\int_0^\infty \frac{\partial^2 x_s}{\partial \tau \partial \alpha}(\tau)\phi(\tau)[[\mathbf{U}(\tau)]]d\tau - \int_0^\infty \frac{\partial x_s}{\partial \alpha}(\tau)\phi(\tau)[[\mathbf{U}_\tau(\tau)]]d\tau. \qquad (8.42)
\end{aligned}$$

Substituting into Eq. 8.39 and using the Rankine-Hugoniot jump conditions yields the final form of the differentiated weak form

$$\begin{aligned}
&\int_0^\infty \int_{-\infty}^\infty \{\phi_t(x,t)\mathbf{S}(x,t) + \phi_x(x,t)\mathbf{F^s}(\mathbf{U}(x,t),\mathbf{S}(x,t))\}\, dxdt \\
= &-\int_{-\infty}^\infty \phi(x,0)\mathbf{S}(x,0)dx + \int_0^\infty \frac{\partial^2 x_s}{\partial \tau \partial \alpha}(\tau)\phi(\tau)[[\mathbf{U}(\tau)]]d\tau \\
+ &\int_0^\infty \frac{\partial x_s}{\partial \alpha}(\tau)\phi(\tau)[[\mathbf{U}_\tau(\tau)]]d\tau. \qquad (8.43)
\end{aligned}$$

It is important to note that the equations Eq. 8.33 and Eq. 8.43 are the same weak form. The weak form involves the terms $[[\mathbf{U}(\tau)]]$ and $[[\mathbf{U}_\tau(\tau)]]$. The first term is the jump in the flow at each point, τ, along the shock surface and the second term is the spatial derivative of the flow at each point, τ, along the shock surface. The spikes arising in the weak solution of the continuous sensitivity equations are probably resulting from the $[[\mathbf{U}_\tau(\tau)]]$ term. It may be possible to develop numerical methods that will limit or eliminate the effects of this term in the weak solution.

8.3 Modified Equations

In this section the idea of modified equations are explored. The idea is to model the finite difference equations using a partial differential equation. The finite difference equation, of course, is derived by approximating the PDE and could be viewed as the model for the difference equation. But, is there a better differential equation that will model the finite difference equation? It is the hope that this modified equation will give insight to the behavior of the numerical solution [28, 46]. The problem arising in this method is that the modified equations are very complex and difficult to calculate. For this reason, the finite difference scheme considered is the Lax-Friedrichs scheme.

8.3.1 Lax-Friedrichs Modified Equations

The Lax-Friedrichs scheme as described in LeVeque [28] is given as

$$\mathbf{S}_j^{n+1} = \frac{1}{2}\left(\mathbf{S}_{j-1}^n + \mathbf{S}_{j+1}^n\right) - \frac{\Delta t}{2\Delta x}\left[\mathbf{F}^{\mathbf{s}}(\mathbf{U}_{j+1}^n, \mathbf{S}_{j+1}^n) - \mathbf{F}^{\mathbf{s}}(\mathbf{U}_{j-1}^n, \mathbf{S}_{j-1}^n)\right], \tag{8.44}$$

or the finite difference scheme can be written as

$$\frac{1}{\Delta t}\left[\mathbf{S}_j^{n+1} - \frac{1}{2}\left(\mathbf{S}_{j-1}^n + \mathbf{S}_{j+1}^n\right)\right] + \frac{1}{2\Delta x}\left[A(\mathbf{U}_{j+1}^n)\mathbf{S}_{j+1}^n - A(\mathbf{U}_{j-1}^n)\mathbf{S}_{j-1}^n\right] = \mathbf{0} \tag{8.45}$$

where $A(\mathbf{U})$ is the Jacobian matrix. The first step is to modify the notation, *i.e.*, $\mathbf{S}_{j\pm1}^{n\pm1} = \mathbf{S}(x \pm \Delta x, t \pm \Delta t)$.

$$\begin{aligned}&\frac{1}{\Delta t}\left[\mathbf{S}(x, t+\Delta t) - \frac{1}{2}\left(\mathbf{S}(x-\Delta x, t) + \mathbf{S}(x+\Delta x, t)\right)\right] + \\ &\frac{1}{2\Delta x}\left[A(\mathbf{U}(x+\Delta x, t))\mathbf{S}(x+\Delta x, t) - A(\mathbf{U}(x-\Delta x, t))\mathbf{S}(x-\Delta x, t)\right] = 0.\end{aligned} \tag{8.46}$$

The next step in deriving the modified equations is to expand everything in terms of Taylor series.

$$\begin{aligned}\mathbf{S}(x, t+\Delta t) &= \mathbf{S}(x,t) + \Delta t\mathbf{S}_t(x,t) + \frac{(\Delta t)^2}{2}\mathbf{S}_{tt}(x,t) + \frac{(\Delta t)^3}{6}\mathbf{S}_{ttt}(x,t) \\ &+ O((\Delta t)^4) \qquad (8.47)\\ \mathbf{S}(x+\Delta x, t) &= \mathbf{S}(x,t) + \Delta x\mathbf{S}_x(x,t) + \frac{(\Delta x)^2}{2}\mathbf{S}_{xx}(x,t) + \frac{(\Delta x)^3}{6}\mathbf{S}_{xxx}(x,t) \\ &+ O((\Delta x)^4) \qquad (8.48)\\ \mathbf{S}(x-\Delta x, t) &= \mathbf{S}(x,t) - \Delta x\mathbf{S}_x(x,t) + \frac{(\Delta x)^2}{2}\mathbf{S}_{xx}(x,t) - \frac{(\Delta x)^3}{6}\mathbf{S}_{xxx}(x,t)\end{aligned}$$

$$
\begin{aligned}
&+ \quad O((\Delta x)^4) && (8.49)\\
\mathbf{U}(x+\Delta x,t) &= \mathbf{U}(x,t)+\Delta x\mathbf{U}_x(x,t)+\frac{(\Delta x)^2}{2}\mathbf{U}_{xx}(x,t)+\frac{(\Delta x)^3}{6}\mathbf{U}_{xxx}(x,t)\\
&+ \quad O((\Delta x)^4) && (8.50)\\
\mathbf{U}(x-\Delta x,t) &= \mathbf{U}(x,t)-\Delta x\mathbf{U}_x(x,t)+\frac{(\Delta x)^2}{2}\mathbf{U}_{xx}(x,t)-\frac{(\Delta x)^3}{6}\mathbf{U}_{xxx}(x,t)\\
&+ \quad O((\Delta x)^4) && (8.51)
\end{aligned}
$$

To expand the Jacobian matrices, $A(\mathbf{U}(x\pm\Delta x,t))$, the following definitions are required,

$$
\begin{aligned}
\Delta\mathbf{U}_\pm &= \mathbf{U}(x\pm\Delta x,t)-\mathbf{U}(x,t) && (8.52)\\
\Delta\mathbf{U}_+ &= \Delta x\mathbf{U}_x(x,t)+\frac{(\Delta x)^2}{2}\mathbf{U}_{xx}(x,t)+\frac{(\Delta x)^3}{6}\mathbf{U}_{xxx}(x,t)+O((\Delta x)^4) && (8.53)\\
\Delta\mathbf{U}_- &= -\Delta x\mathbf{U}_x(x,t)+\frac{(\Delta x)^2}{2}\mathbf{U}_{xx}(x,t)-\frac{(\Delta x)^3}{6}\mathbf{U}_{xxx}(x,t)+O((\Delta x)^4). && (8.54)
\end{aligned}
$$

Hence the expansions of the matrix A become

$$
\begin{aligned}
A(\mathbf{U}(x+\Delta x,t))=A(\mathbf{U}+\Delta\mathbf{U}_+) &= A(\mathbf{U}(x,t))+\Delta\mathbf{U}_+A_{\mathbf{U}}(\mathbf{U}(x,t))\\
&+ \quad \frac{(\Delta\mathbf{U}_+)^2}{2}A_{\mathbf{UU}}(\mathbf{U}(x,t))+O((\Delta\mathbf{U}_+)^3), && (8.55)\\
A(\mathbf{U}(x-\Delta x,t))=A(\mathbf{U}+\Delta\mathbf{U}_-) &= A(\mathbf{U}(x,t))+\Delta\mathbf{U}_-A_{\mathbf{U}}(\mathbf{U}(x,t))\\
&+ \quad \frac{(\Delta\mathbf{U}_-)^2}{2}A_{\mathbf{UU}}(\mathbf{U}(x,t))+O((\Delta\mathbf{U}_-)^3). && (8.56)
\end{aligned}
$$

Multiplying out these equations results in

$$
\begin{aligned}
A(\mathbf{U}(x+\Delta x,t)) &= A(\mathbf{U}(x,t))+\frac{\partial A}{\partial\mathbf{U}}\Delta x\mathbf{U}_x(x,t)+\frac{(\Delta x)^2}{2}\frac{\partial A}{\partial\mathbf{U}}\mathbf{U}_{xx}(x,t)\\
&+ \quad \frac{1}{2}\frac{\partial^2 A}{\partial\mathbf{U}\partial\mathbf{U}}(\Delta x)^2(\mathbf{U}_x)^2+O((\Delta x)^3,(\Delta\mathbf{U})^3) && (8.57)\\
A(\mathbf{U}(x-\Delta x,t)) &= A(\mathbf{U}(x,t))-\frac{\partial A}{\partial\mathbf{U}}\Delta x\mathbf{U}_x(x,t)+\frac{(\Delta x)^2}{2}\frac{\partial A}{\partial\mathbf{U}}\mathbf{U}_{xx}(x,t)\\
&+ \quad \frac{1}{2}\frac{\partial^2 A}{\partial\mathbf{U}\partial\mathbf{U}}(\Delta x)^2(\mathbf{U}_x)^2+O((\Delta x)^3,(\Delta\mathbf{U})^3) && (8.58)
\end{aligned}
$$

and

$$
\begin{aligned}
A(\mathbf{U}(x+\Delta x,t))\mathbf{S}(x+\Delta x,t) &= A(\mathbf{U}(x,t))\mathbf{S}(x,t)+\Delta x\left[A(\mathbf{U}(x,t))\mathbf{S}(x,t)\right]_x\\
&+ \quad \frac{(\Delta x)^2}{2}\left[A(\mathbf{U}(x,t))\mathbf{S}(x,t)\right]_{xx}\\
&+ \quad O((\Delta x)^3,(\Delta\mathbf{U})^3) && (8.59)
\end{aligned}
$$

$$\begin{aligned} A(\mathbf{U}(x-\Delta x,t))\mathbf{S}(x-\Delta x,t) &= A(\mathbf{U}(x,t))\mathbf{S}(x,t) - \Delta x\left[A(\mathbf{U}(x,t))\mathbf{S}(x,t)\right]_x \\ &+ \frac{(\Delta x)^2}{2}\left[A(\mathbf{U}(x,t))\mathbf{S}(x,t)\right]_{xx} \\ &+ O((\Delta x)^3,(\Delta \mathbf{U})^3). \end{aligned} \tag{8.60}$$

Each of these quantities can be substituted back into Eq. 8.46 and simplified to get

$$\mathbf{S}_t(x,t) + \left[A(\mathbf{U}(x,t))\mathbf{S}(x,t)\right]_x + \frac{\Delta t}{2}\mathbf{S}_{tt}(x,t) - \frac{(\Delta x)^2}{2\Delta t}\mathbf{S}_{xx}(x,t) = O((\Delta x)^2,(\Delta t)^2,(\Delta \mathbf{U})^2). \tag{8.61}$$

The resulting modified equation for the Lax-Friedrichs method is given by

$$\begin{aligned} \mathbf{S}_t(x,t) + \left[A(\mathbf{U}(x,t))\mathbf{S}(x,t)\right]_x &= -\frac{\Delta t}{2}\mathbf{S}_{tt}(x,t) \\ + \frac{(\Delta x)^2}{2\Delta t}\mathbf{S}_{xx}(x,t) &+ O((\Delta x)^2,(\Delta t)^2,(\Delta \mathbf{U})^2). \end{aligned} \tag{8.62}$$

This can be further simplified by considering the term $\mathbf{S}_{tt}$. It is known that $\mathbf{S}_t$ is given by

$$\mathbf{S}_t(x,t) = -\left[A(\mathbf{U}(x,t))\mathbf{S}(x,t)\right]_x - \frac{1}{2}\left(\Delta t\mathbf{S}_{tt}(x,t) - \frac{(\Delta x)^2}{2\Delta t}\mathbf{S}_{xx}(x,t)\right) + HOT. \tag{8.63}$$

This equation can be differentiated with respect to t to get

$$\begin{aligned} \mathbf{S}_{tt}(x,t) &= -\left\{\left[A(\mathbf{U}(x,t))\mathbf{S}(x,t)\right]_t\right\}_x - \frac{1}{2}\left(\Delta t\mathbf{S}_{ttt}(x,t) - \frac{(\Delta x)^2}{2\Delta t}\mathbf{S}_{xxt}(x,t)\right) + HOT \\ &= -\left\{\frac{\partial A}{\partial \mathbf{U}}\mathbf{U}_t(x,t)\mathbf{S}(x,t) + A(\mathbf{U}(x,t))\mathbf{S}_t(x,t)\right\}_x + HOT. \end{aligned} \tag{8.64}$$

It is known from the Euler and continuous sensitivity equations that

$$\mathbf{S}_t(x,t) = -\left[A(\mathbf{U}(x,t))\mathbf{S}\right]_x \tag{8.65}$$

$$\mathbf{U}_t(x,t) = -\left[A(\mathbf{U}(x,t))\mathbf{U}\right]_x. \tag{8.66}$$

These quantities are substituted into Eq. 8.64 to get

$$\begin{aligned} \mathbf{S}_{tt}(x,t) &= \left[\left(\frac{\partial A}{\partial \mathbf{U}}\right)^2\mathbf{U}_x(x,t)\mathbf{U}(x,t)\mathbf{S}(x,t)\right. \\ &+ \left. 2\frac{\partial A}{\partial \mathbf{U}}A(\mathbf{U}(x,t))\mathbf{U}_x(x,t)\mathbf{S}(x,t) + \left(A(\mathbf{U}(x,t))\right)^2\mathbf{S}_x(x,t)\right]_x \\ &+ HOT. \end{aligned} \tag{8.67}$$

Plugging back into Eq. 8.62, the modified equation for the Lax-Friedrichs method is

$$\begin{aligned}\mathbf{S}_t(x,t) &+ [A(\mathbf{U}(x,t))\mathbf{S}(x,t)]_x = -\left[\left(\frac{\partial A}{\partial \mathbf{U}}\right)^2 \mathbf{U}_x(x,t)\mathbf{U}(x,t)\mathbf{S}(x,t)\right. \\ &+ \left. 2\frac{\partial A}{\partial \mathbf{U}}A(\mathbf{U}(x,t))\mathbf{U}_x(x,t)\mathbf{S}(x,t) + (A(\mathbf{U}(x,t)))^2\,\mathbf{S}_x(x,t)\right]_x + \frac{(\Delta x)^2}{2\Delta t}\mathbf{S}_{xx}(x,t) \\ &+ HOT. \end{aligned} \tag{8.68}$$

The modified equation for the Lax-Friedrichs method can now be used to analyze the numerical solution. As with all the other methods, the Lax-Friedrichs method also develops large spikes at the discontinuities. The modified equations have terms on the right hand side involving $\mathbf{U}_x$, $\mathbf{S}_x$ and $\frac{\partial A}{\partial \mathbf{U}}$; each of these derivatives involves the flow solution or sensitivities which are discontinuous. Differentiation across these discontinuities will result in the δ-spikes seen previously. One possible solution is to subtract these terms in the numerical method and cancel out their effect. Although this seems like a good approach, it will greatly increase both the complexity of the implementation and the cost of the method. Likewise, in some of the more complex methods used in computational fluid dynamics, such as the Roe scheme, the modified equations are nearly impossible to calculate. Another attempt to eliminate the spikes by considering the nonconservation law form of the continuous sensitivity equations is considered in Section 8.4.

8.4 Calculation of Sensitivities Without Spikes

The nonconservation law form of the continuous sensitivity equations is given by

$$\mathbf{S}_t + A(\mathbf{U})S_x = -\frac{\partial \mathbf{F^s}(\mathbf{U},\mathbf{S})}{\partial \mathbf{U}}\mathbf{U}_x, \tag{8.69}$$

where $A(\mathbf{U})$ is the same Jacobian as in the Euler equations and is given by

$$A(\mathbf{U}) = \begin{bmatrix} 0 & 1 & 0 \\ -(3-\gamma)\frac{u^2}{2} & (3-\gamma)u & \gamma-1 \\ (\gamma-1)u^3 - \frac{\gamma u e}{\rho} & \frac{\gamma e}{\rho} - \frac{3}{2}(\gamma-1)u^2 & \gamma u \end{bmatrix} \tag{8.70}$$

and $\frac{\partial \mathbf{F^s}(\mathbf{U},\mathbf{S})}{\partial \mathbf{U}} =$

$$\begin{bmatrix} 0 & 0 & 0 \\ (\gamma-3)\frac{mm_\alpha}{\rho^2} - (\gamma-3)\frac{m^2\rho_\alpha}{\rho^3} & -(\gamma-3)\frac{m_\alpha}{\rho} + (\gamma-3)\frac{m\rho_\alpha}{\rho^2} & 0 \\ \frac{-\gamma m_\alpha e - \gamma m e_\alpha}{\rho^2} + \frac{2\gamma me\rho_\alpha + 3(\gamma-1)m^2 m_\alpha}{\rho^3} & \frac{\gamma e_\alpha}{\rho} - \frac{\gamma e\rho_\alpha + 3(\gamma-1)mm_\alpha}{\rho^2} & \frac{\gamma m_\alpha}{\rho} - \frac{\gamma m\rho_\alpha}{\rho^2} \\ -3(\gamma-1)\frac{m^3\rho_\alpha}{\rho^4} & +3(\gamma-1)\frac{m^2\rho_\alpha}{\rho^3} & \end{bmatrix}. \quad (8.71)$$

Solving Eq. 8.69 using the Strang Splitting method for the Roe scheme described in Chapter 5, may lead to a viable approach for limiting the formation of the δ-function spikes. In the implementation of the Strang splitting method, the quantities ρ_x, m_x and e_x must be calculated where

$$\mathbf{U}_x = \begin{bmatrix} \rho_x \\ m_x \\ e_x \end{bmatrix}.$$

The simplest implementation of this method is to approximate these derivatives using a simple forward difference, *i.e.*, $\rho_x \approx \frac{\rho(x+h)-\rho(x)}{h}$. If the points, x and $x+h$ lie on opposite sides of the shock wave then the terms ρ_x, m_x, and e_x will be very large and spikes will arise in the sensitivity calculations (See Chapter 7). One possible remedy is to limit the size of these derivatives. This idea is explored using the Roe scheme for the continuous sensitivity method.

8.4.1 Derivative Limiting

In this section, the continuous sensitivity equations are solved using the Roe scheme via Strang splitting. Several different examples are calculated imposing different limits on the $\mathbf{U}_x$ term arising in Eq. 8.69. The first problem considered is a modified Riemann problem. The problem is modified in the sense that the initial pressures and densities are chosen so the solution will only involve a shock moving through the tube. This problem and the specific details are discussed in Chapter 9. The $\mathbf{U}_x$ term is limited using two different methods. The first method is a component limit which allows each individual component to be checked and limited individually;

$$abs(\rho_x) > tol \longrightarrow \rho_x = 0.0 \quad (8.72)$$

$$abs(m_x) > tol \longrightarrow m_x = 0.0 \quad (8.73)$$

$$abs(e_x) > tol \longrightarrow e_x = 0.0. \quad (8.74)$$

If the value of any derivative is greater than the tolerance, then that derivative value is set to zero because the flow sensitivities to the left and right of the shock position are constant.

The second method is a vector limit based on any of the individual components;

$$abs(\rho_x) > tol \longrightarrow \mathbf{U}_x = \mathbf{0} \tag{8.75}$$
$$abs(m_x) > tol \longrightarrow \mathbf{U}_x = \mathbf{0} \tag{8.76}$$
$$abs(e_x) > tol \longrightarrow \mathbf{U}_x = \mathbf{0}. \tag{8.77}$$

The vector limit requires that the derivative vector be set to zero if any of the components are greater than the tolerance.

In the implementation of the Roe scheme for the continuous sensitivity equations, there are three terms that may present problems, $\mathbf{U}_x$, $A(\mathbf{U})$ and $\frac{\partial \mathbf{F^s}(\mathbf{U},\mathbf{S})}{\partial \mathbf{U}}$. These terms can present problems because they each involve the discontinuous fluid flow. The Jacobian term, $A(\mathbf{U})$, does not involve any differentiation and it is the hope that the discontinuities in the flow, $\mathbf{U}$, will set up the different flow sensitivity regions. The spatial derivative term, $\mathbf{U}_x$, will be limited using one of the methods above in an attempt to fix the differentiation problems at the shock. This leaves the pseudo-Jacobian term, $\frac{\partial \mathbf{F^s}(\mathbf{U},\mathbf{S})}{\partial \mathbf{U}}$. The examination of this term reveals that it is the derivative of a flux function, $\mathbf{F^s}(\mathbf{U},\mathbf{S})$, with respect to the discontinuous flow $\mathbf{U}$, or the derivative of a discontinuous function with respect to a discontinuous vector. It is unclear what effects these discontinuities will have on the differentiation. For this reason, an averaged pseudo-Jacobian is used in the calculation of the sensitivities, *i.e.*,

$$\left[\frac{\partial \mathbf{F^s}}{\partial \mathbf{U}}\right]_i^n = \frac{\left[\frac{\partial \mathbf{F^s}(\mathbf{U}_i^n,\mathbf{S}_i^n)}{\partial \mathbf{U}} + \frac{\partial \mathbf{F^s}(\mathbf{U}_{i+1}^n,\mathbf{S}_{i+1}^n)}{\partial \mathbf{U}}\right]}{2}.$$

The averaging should help control the effects of the discontinuous flow on the derivative. It should be noted that this averaging has virtually no affect on the flow sensitivities unless the exact flow solution is used, *i.e.*, the flow contains sharp discontinuities.

The component limiting and the vector limiting has been applied to the sensitivity equation method using the Roe scheme which is implemented using Strang splitting and the averaged pseudo-Jacobian. The results for the flow sensitivities with and without component limiting are shown in Fig. 8.2, Fig. 8.3 and Fig. 8.4 for $tol = 0$, $tol = 1$, and $tol = 10$, respectively. Likewise, the results of the flow sensitivities with and without vector limiting are shown in Fig. 8.5, Fig. 8.6 and Fig. 8.7 for $tol = 0$, $tol = 1$, and $tol = 10$, respectively.

In Fig. 8.2-8.7, the spikes have been removed from the flow sensitivities, but a loss of information occurs at other points of the flow sensitivities. In each of the examples, Fig. 8.2-8.7, it appears as though the limiting of the derivative forces the flow sensitivities to a different weak solution. This is best seen in the density sensitivities as there are three obvious preshock regions including a contact discontinuity. It is interesting to note that in Fig. 8.4, the sensitivities with component limiting and $tol = 10$, the pressure and velocity

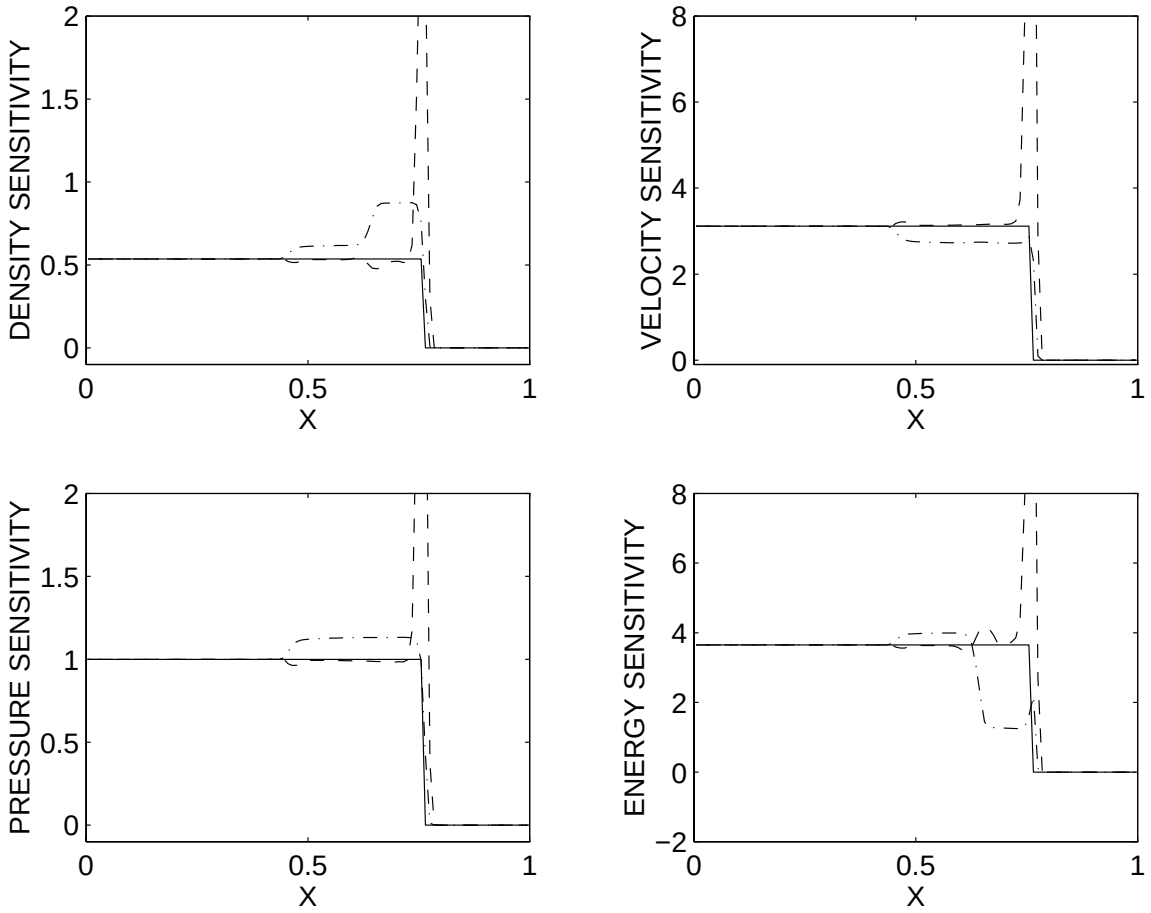

Figure 8.2: Comparison of the exact continuous sensitivities to the sensitivities with and without component limiting and $tol = 0$. The solid line (—) denotes the exact continuous sensitivities, the dashed line (- -) denotes the sensitivities without component limiting and the dot-dash line (-·-) denotes the sensitivities with component limiting.

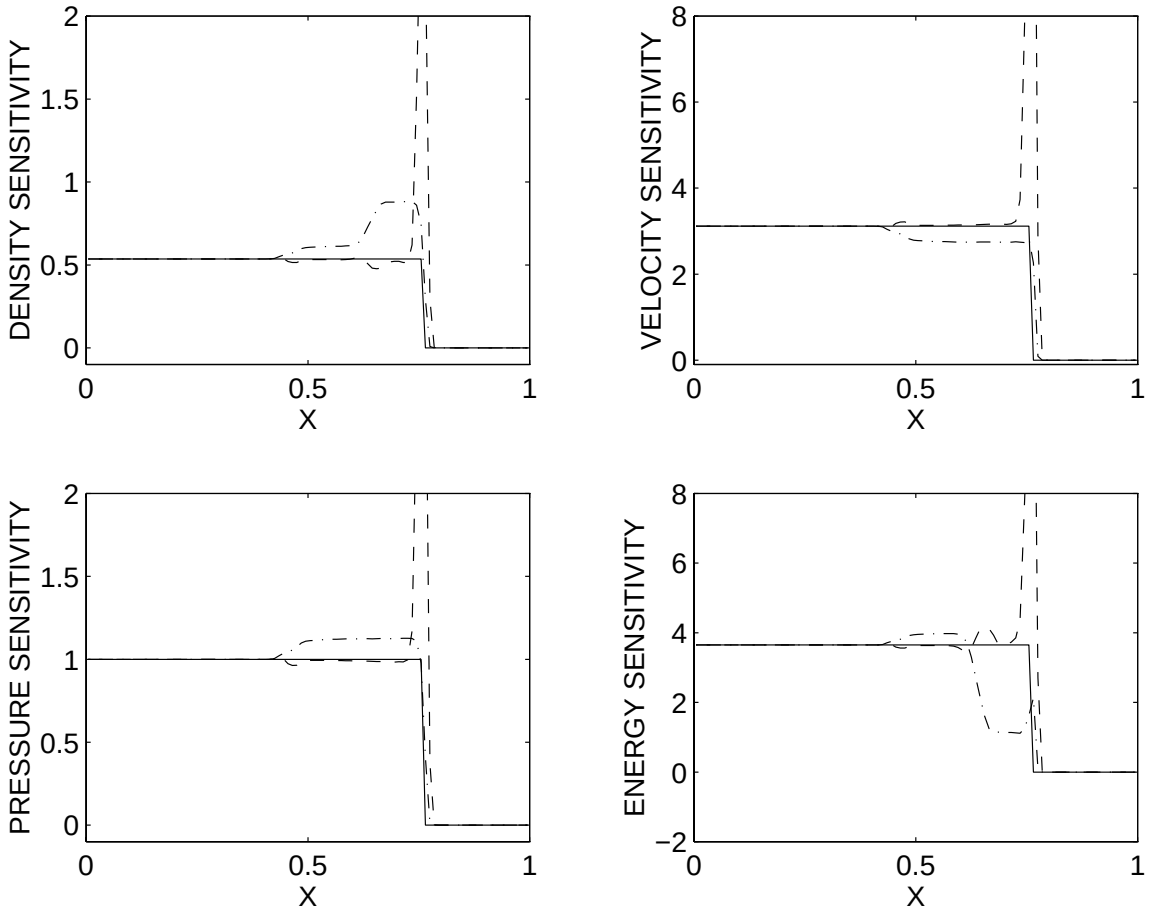

Figure 8.3: Comparison of the exact continuous sensitivities to the sensitivities with and without component limiting and $tol = 1$. The solid line (—) denotes the exact continuous sensitivities, the dashed line (- -) denotes the sensitivities without component limiting and the dot-dash line (-·-) denotes the sensitivities with component limiting.

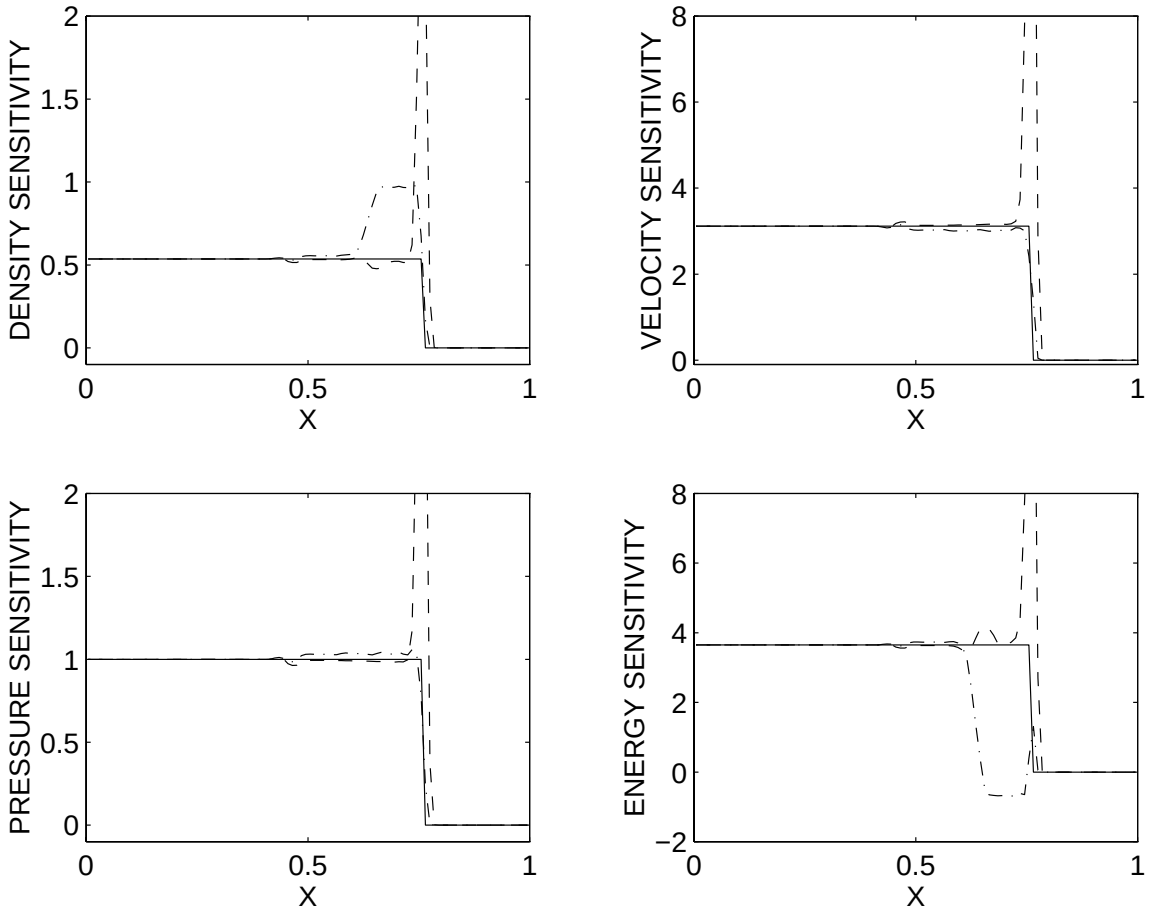

Figure 8.4: Comparison of the exact continuous sensitivities to the sensitivities with and without component limiting and $tol = 10$. The solid line (—) denotes the exact continuous sensitivities, the dashed line (- -) denotes the sensitivities without component limiting and the dot-dash line (·-·) denotes the sensitivities with component limiting.

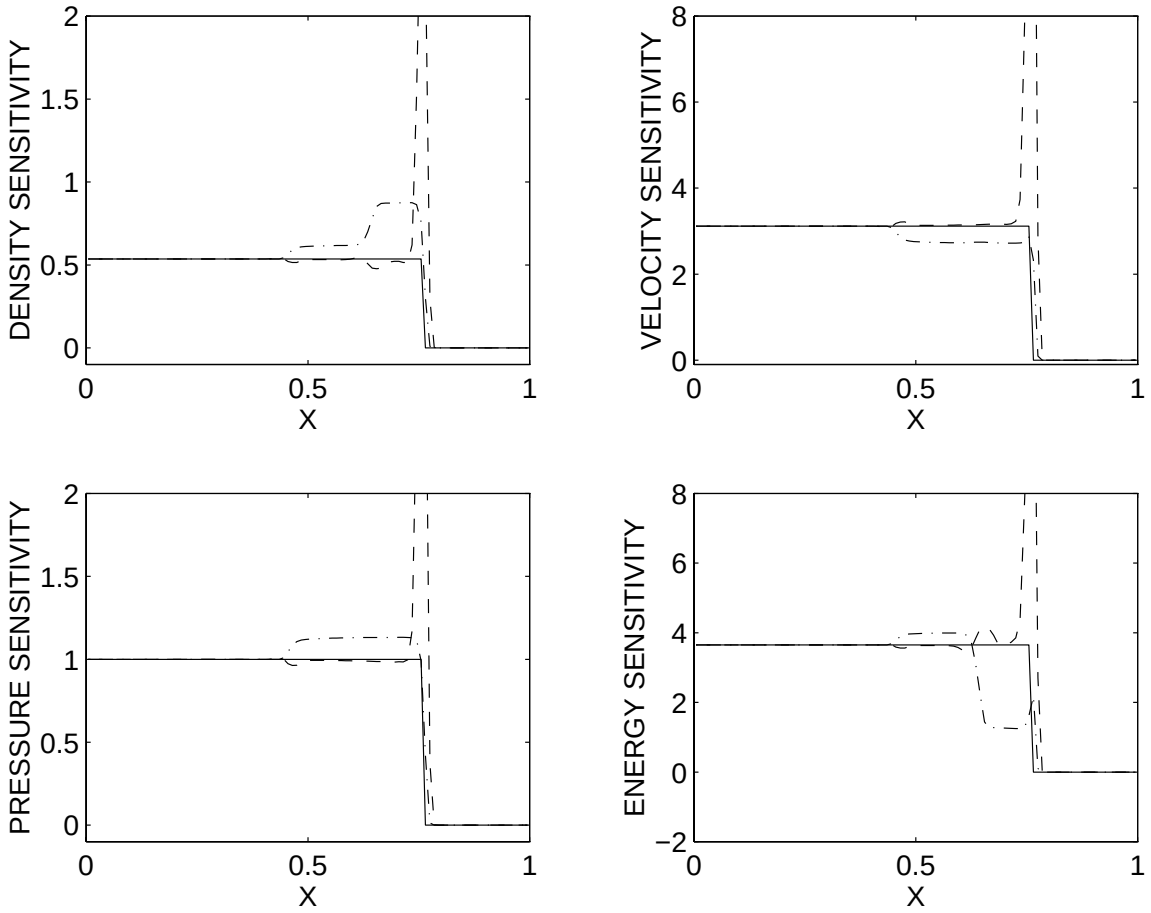

Figure 8.5: Comparison of the exact continuous sensitivities to the sensitivities with and without vector limiting and $tol = 0$. The solid line (—) denotes the exact continuous sensitivities, the dashed line (- -) denotes the sensitivities without vector limiting and the dot-dash line (-·-) denotes the sensitivities with vector limiting.

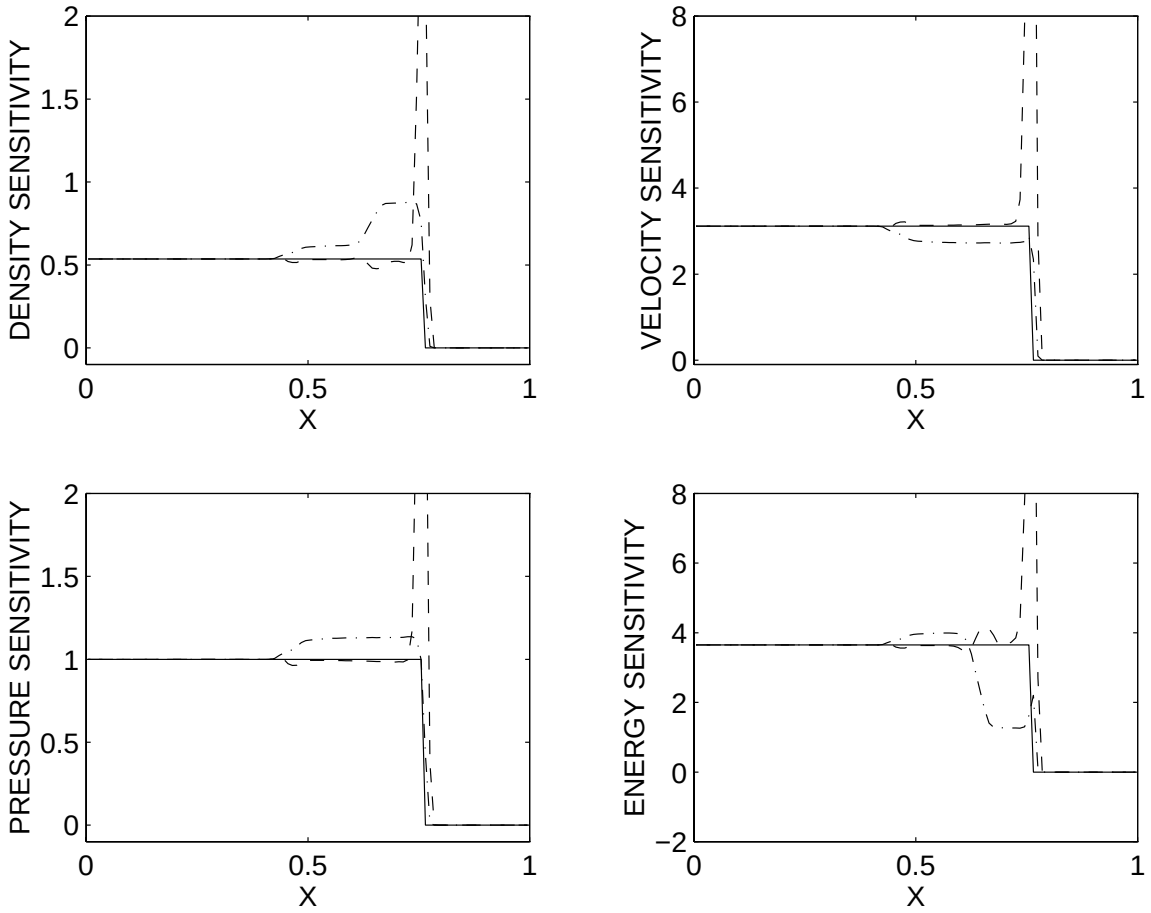

Figure 8.6: Comparison of the exact continuous sensitivities to the sensitivities with and without vector limiting and $tol = 1$. The solid line (—) denotes the exact continuous sensitivities, the dashed line (- -) denotes the sensitivities without vector limiting and the dot-dash line (-·-) denotes the sensitivities with vector limiting.

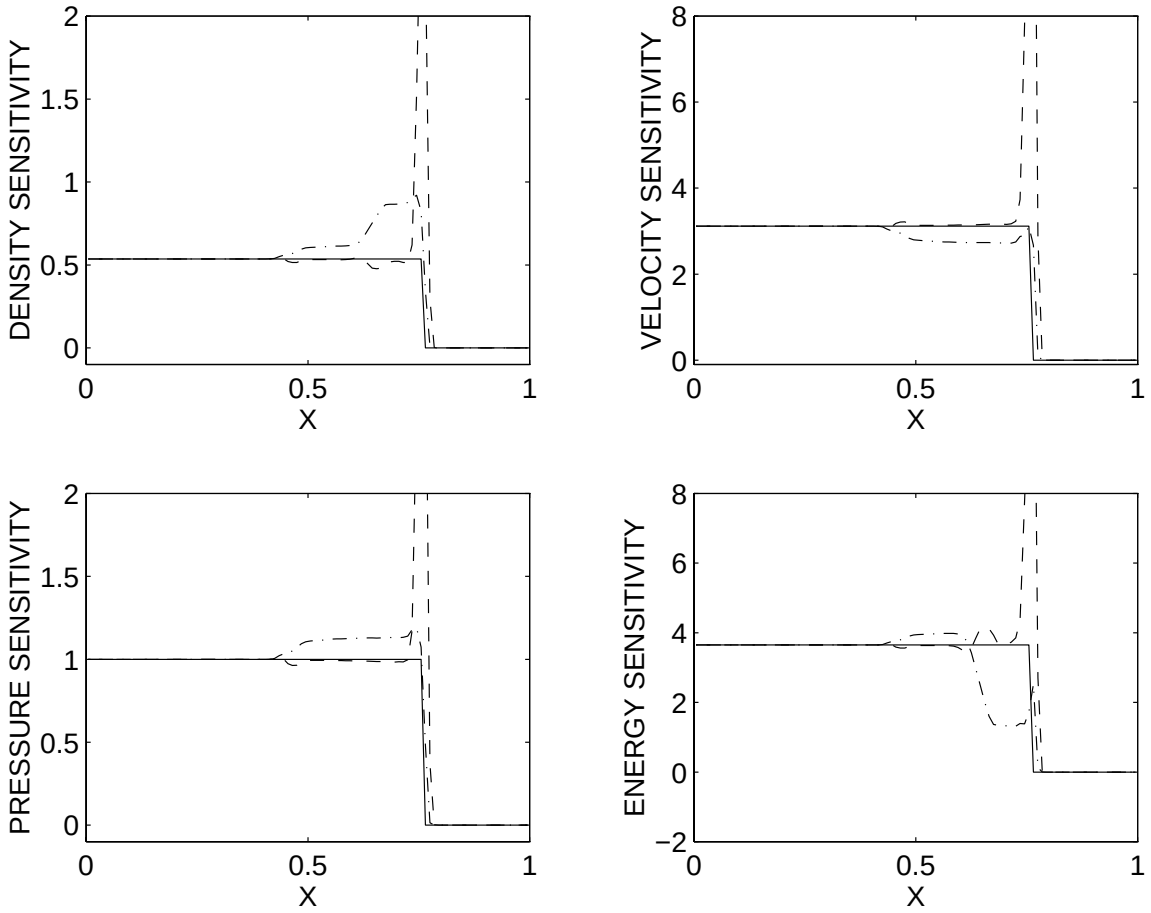

Figure 8.7: Comparison of the exact continuous sensitivities to the sensitivities with and without vector limiting and $tol = 10$. The solid line (—) denotes the exact continuous sensitivities, the dashed line (- -) denotes the sensitivities without vector limiting and the dot-dash line (-·-) denotes the sensitivities with vector limiting.

sensitivities are captured without a spike. This seems to indicate that small changes in the flow derivative, $\mathbf{U}$, due to the approximate nature of the flow are needed to drive the flow sensitivities to the correct weak form. The density and energy sensitivities in these graphs still present problems by imposing a contact discontinuity. The effect of the approximate flow is studied by implementing the same component and vector limits but using the exact flow solution in the calculation of the flow sensitivities. The exact flow is calculated so a single point is in the shock and this solution is used in the continuous sensitivity equations. The results for the for the flow sensitivities, via the exact flow solution , with and without component limiting are shown in Fig. 8.8, Fig. 8.9 and Fig. 8.10 for $tol = 0$, $tol = 1$, and $tol = 10$, respectively. The results of the flow sensitivities, via the exact solution, with and without vector limiting are only shown in Fig. 8.11 for $tol = 10$ since flow sensitivities at other tolerances are virtually identical.

The Fig. 8.8-8.11, where the exact flow solution was used in the calculation of the flow sensitivities, similar results to the sensitivities calculated using the approximate flow were achieved. In each of the two limiting methods, the sensitivities with the limits on the derivatives seemed to force the flow sensitivities to a different weak solution. It would appear that the information embodied in the $\frac{\partial \mathbf{F^s}(\mathbf{U},\mathbf{S})}{\partial \mathbf{U}}\mathbf{U}_x$ is necessary in forcing the flow sensitivities to the correct weak solution. It should be noted that examples were run where each component had a different tolerance and basically the same results were achieved. It might also be possible that the flow derivative across the shock might be necessary to force the correct weak solution. Examples were run where the derivatives were set to a variety of values other than zero and each time, the same solution was achieved.

If the tolerance is gradually increased, then the flow sensitivities move from the incorrect weak form to the correct weak form involving the spike at the shock position. The sensitivities with component limiting are shown in Fig. 8.12 and the sensitivities with vector limiting is shown in Fig. 8.13 with $tol = 0, 10, 25, 100$. Clearly, in Fig. 8.12 and Fig. 8.13 the flow sensitivities move from the imposed weak form to the correct weak form as the tolerance increases.

The next problem to consider is the Riemann problem. This problem is much harder because it also involves a contact discontinuity and a rarefaction wave. Hence, $\mathbf{U}_x$ is not zero everywhere in the flow and the tolerance must be set so that it limits the derivatives at discontinuities, but not in the rarefaction wave. The results for the sensitivities of the Riemann problem with and without component limiting and vector limiting are shown in Fig. 8.14 and Fig. 8.15, respectively for $tol = 10$. Again, the limited sensitivities have problems at the contact discontinuities and force the solution to a new weak form.

Clearly, the method of limiting the δ-spikes by limiting the derivative, $\mathbf{U}_x$, on the right hand side of Eq. 8.69, does not provide an accurate enough approximation to be used

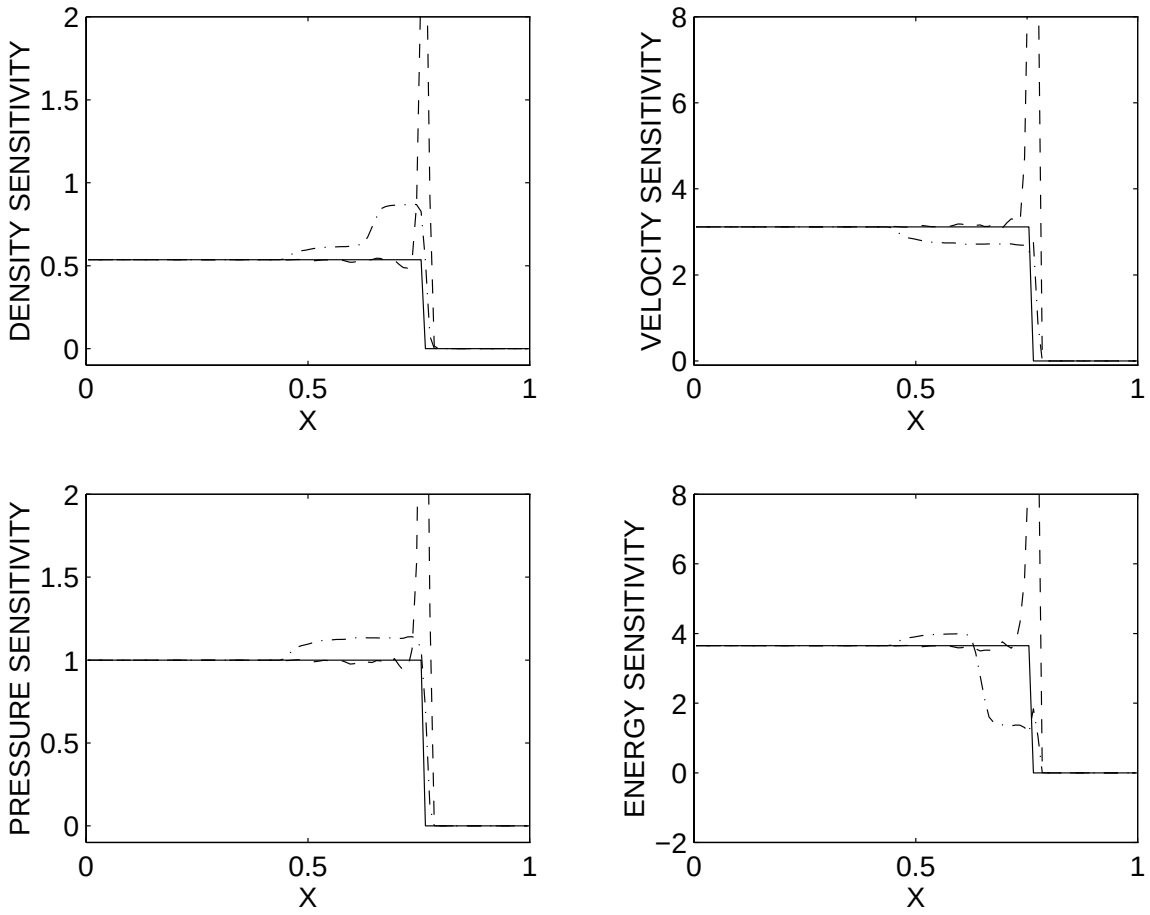

Figure 8.8: Comparison of the exact continuous sensitivities to the sensitivities, via the exact flow solution, with and without component limiting and $tol = 0$. The solid line (—) denotes the exact continuous sensitivities, the dashed line (- -) denotes the sensitivities without component limiting and the dot-dash line (·-·) denotes the sensitivities with component limiting.

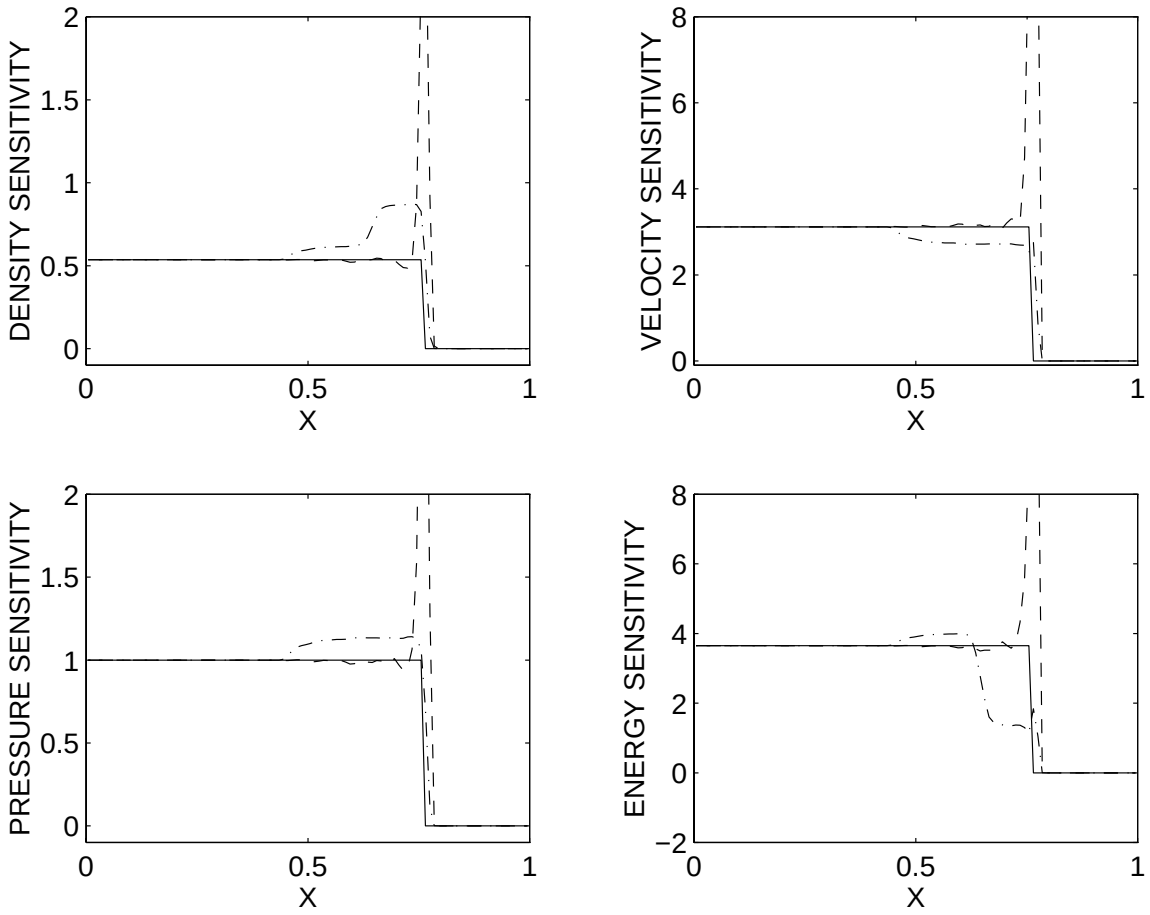

Figure 8.9: Comparison of the exact continuous sensitivities to the sensitivities, via the exact flow solution, with and without component limiting and $tol = 1$. The solid line (—) denotes the exact continuous sensitivities, the dashed line (- -) denotes the sensitivities without component limiting and the dot-dash line (·-·) denotes the sensitivities with component limiting.

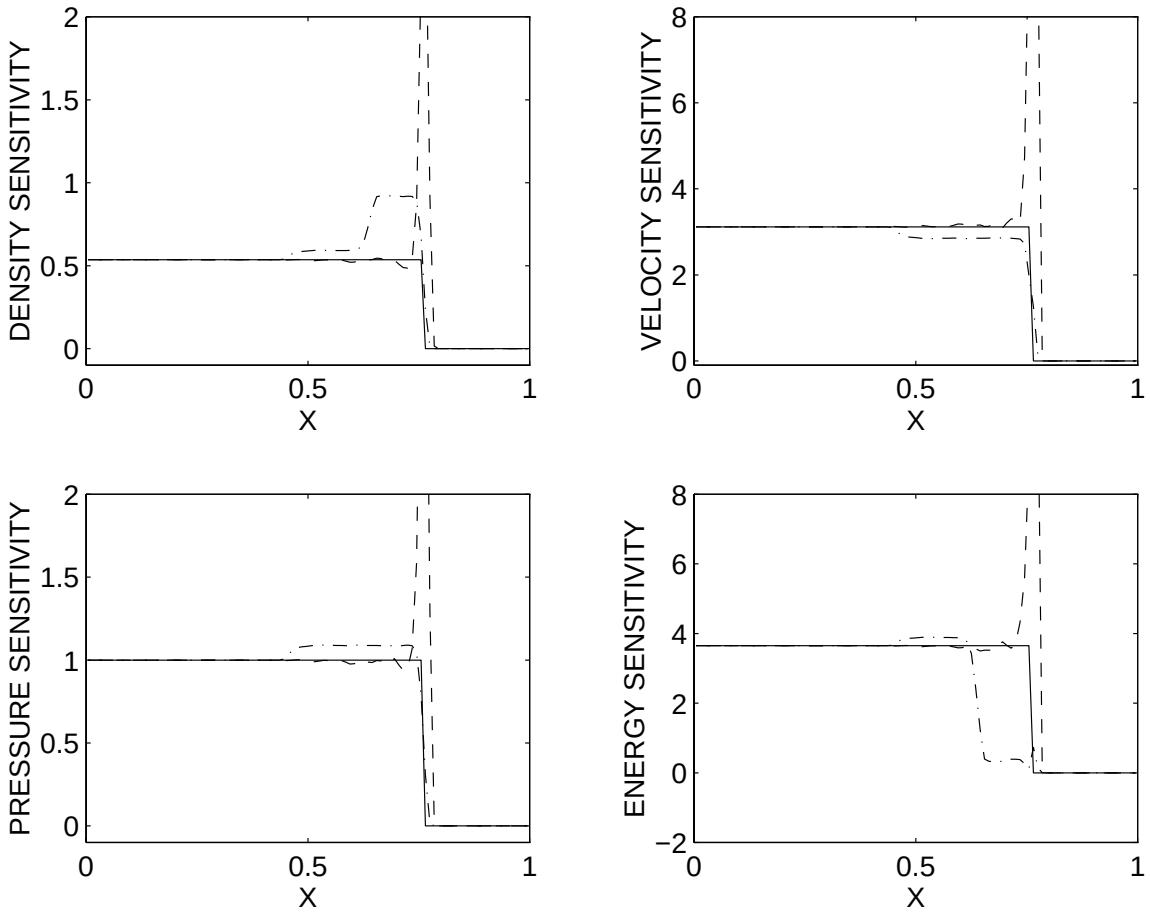

Figure 8.10: Comparison of the exact continuous sensitivities to the sensitivities, via the exact flow solution, with and without component limiting and $tol = 10$. The solid line (—) denotes the exact continuous sensitivities, the dashed line (- -) denotes the sensitivities without component limiting and the dot-dash line (·-·) denotes the sensitivities with component limiting.

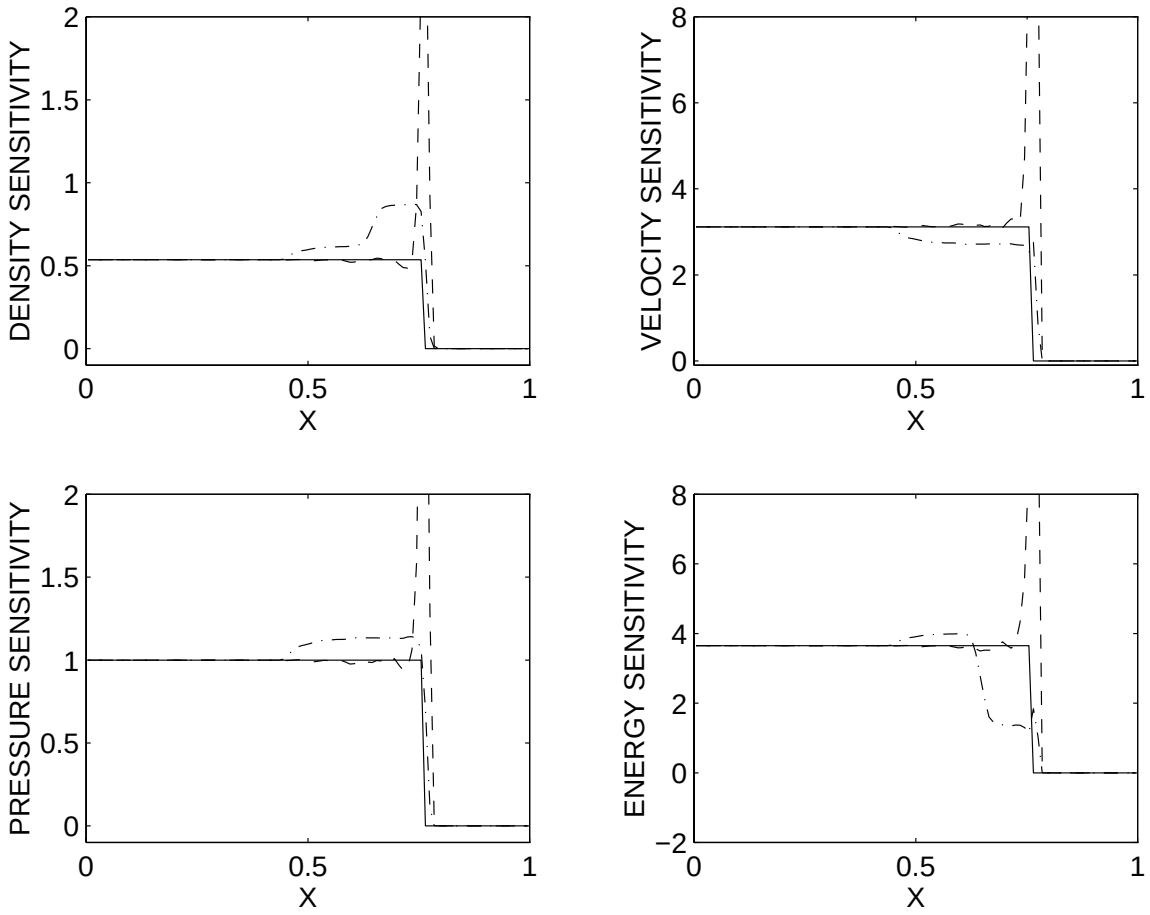

Figure 8.11: Comparison of the exact continuous sensitivities to the sensitivities, via the exact flow solution, with and without vector limiting and $tol = 10$. The solid line (—) denotes the exact continuous sensitivities, the dashed line (- -) denotes the sensitivities without vector limiting and the dot-dash line (-·-) denotes the sensitivities with vector limiting.

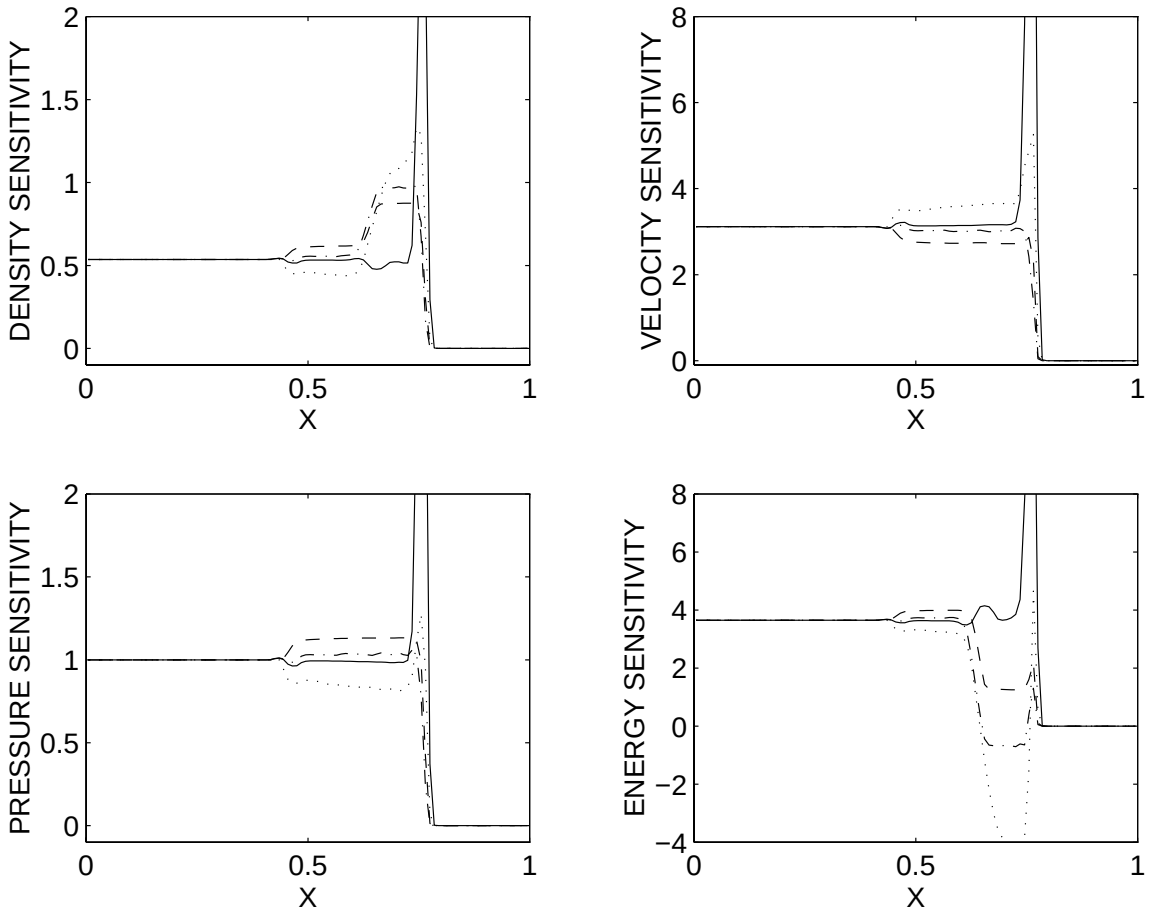

Figure 8.12: Comparison of the flow sensitivities with component limiting for different tolerances. The dashed line (- -) denotes $tol = 0$, the dot-dash line (-·-) denotes $tol = 10$, the dotted line ($\cdots$) denotes $tol = 25$ and the solid line (—) denotes $tol = 100$.

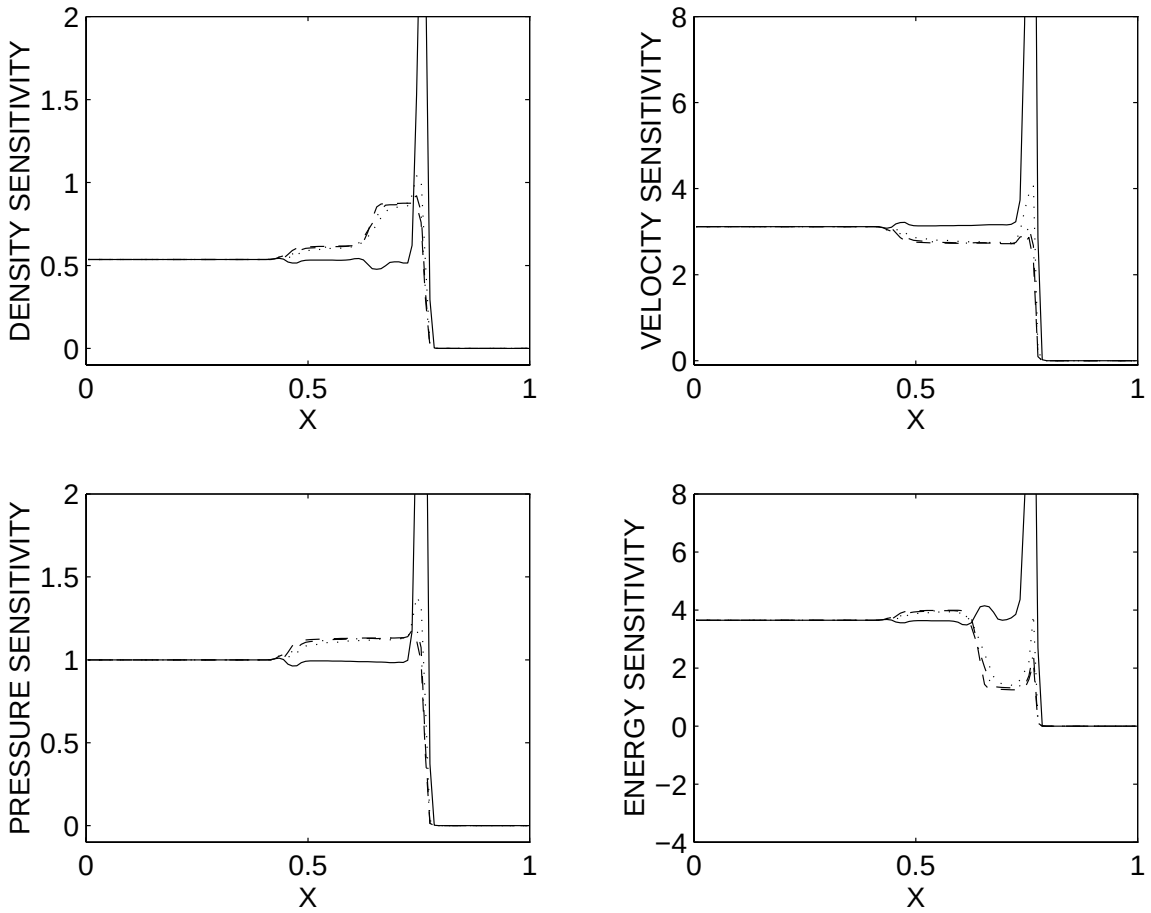

Figure 8.13: Comparison of the flow sensitivities with vector limiting for different tolerances. The dashed line (- -) denotes $tol = 0$, the dot-dash line (-·-) denotes $tol = 10$, the dotted line ($\cdots$) denotes $tol = 25$ and the solid line (—) denotes $tol = 100$.

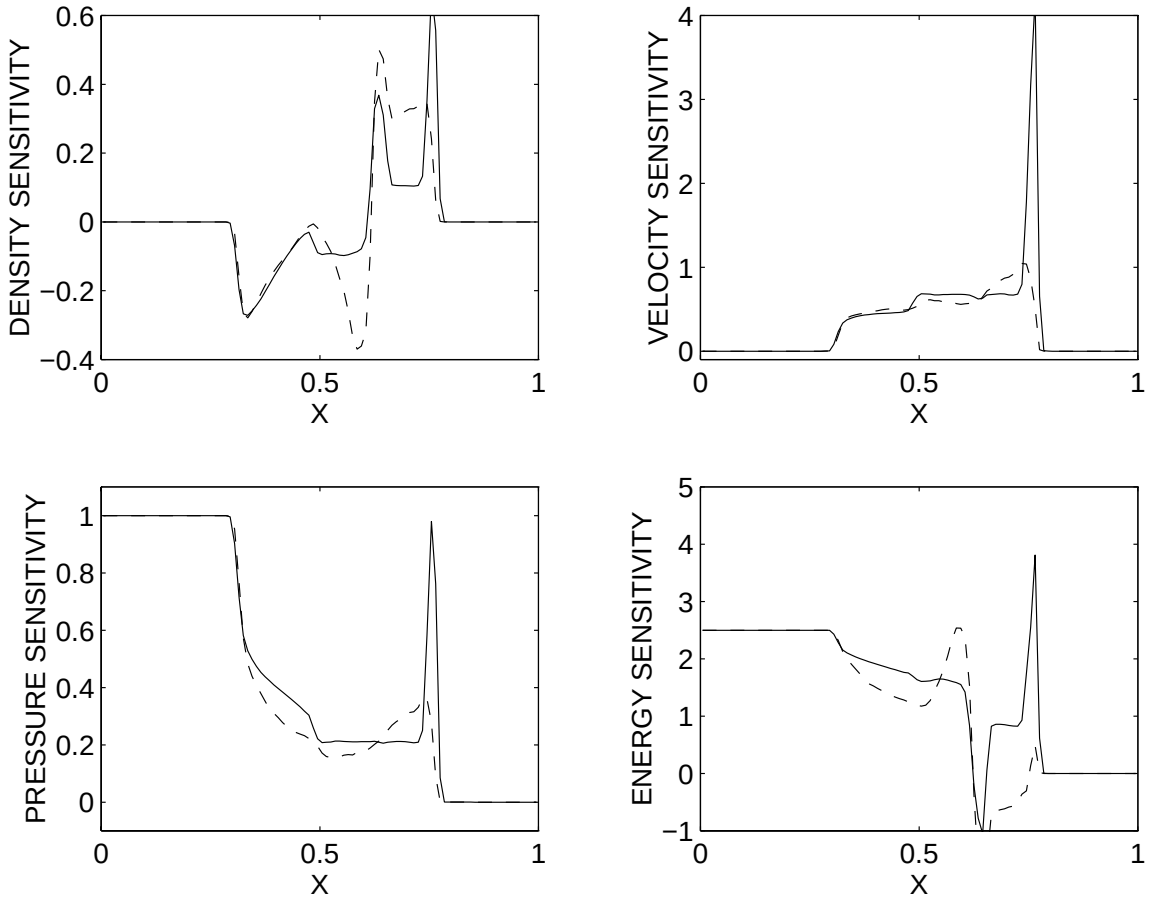

Figure 8.14: Comparison of the flow sensitivities for the Riemann problem with and without component limiting and $tol = 10$. The solid line (—) denotes the sensitivities without component limiting and the dashed line (- -) denotes the sensitivities with component limiting.

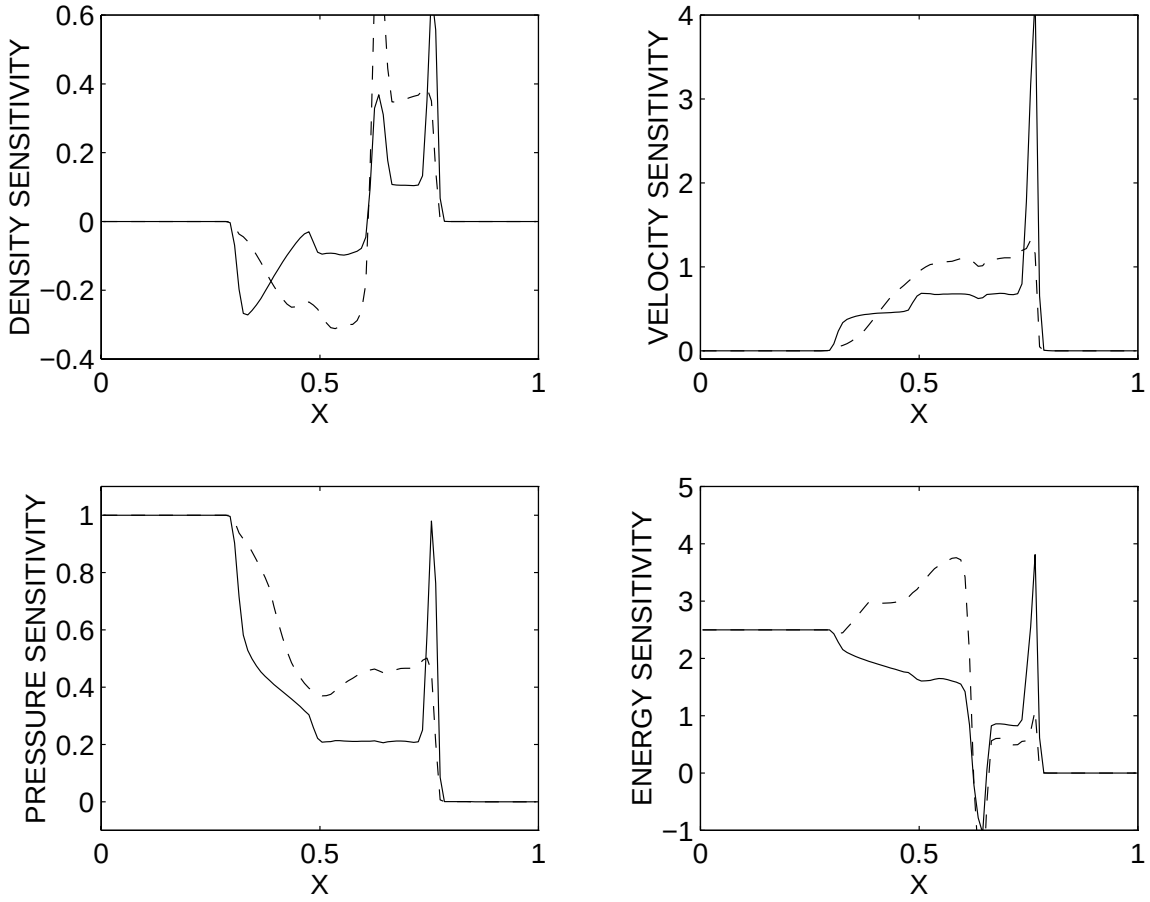

Figure 8.15: Comparison of the flow sensitivities for the Riemann problem with and without vector limiting and $tol = 10$. The solid line (—) denotes the sensitivities without vector limiting and the dashed line (- -) denotes the sensitivities with vector limiting.

in a practical application. Considering that with some methods such as the automatic differentiation methods, it may not be possible to remove the spikes. This approach is a step in the right direction and may provide information that will be used to develop methods that more accurately remove the spikes from the sensitivities.

8.5 Conclusions

In this chapter, the development of the spikes arising at the discontinuities using the sensitivity method was studied from a more theoretical point of view. First, the weak form for the continuous sensitivity equations and the differentiated weak form of the flow equations was compared and were found to be identical. A term was identified that may contribute to the formation of the δ-spikes. Second, a modified equation was derived for the Lax-Friedrichs numerical method to determine where the spikes were coming from. The modified equation gave good insight into the development of the spikes, but the derivation of the modified equation and the increased complexity of the implementation limits the use of this approach. Finally, the nonconservation law form of the continuous sensitivity equations were considered and a method was developed that limited the derivatives arising on the right hand side. This method was able to eliminate the spikes, but it effectively forced the flow sensitivities to a new weak solution. More analysis and variation of the above methods will be needed to accurately calculate flow sensitivities without spikes.

Chapter 9

Perturbed Flow Calculation Deficiencies

The solutions of computational fluid dynamics problems are both computationally expensive and time consuming. Often these problems involve tens of thousands of variables and hours of CPU time to achieve a single flow solution. Many industrial and research applications such as flow optimization-based design require multiple flows solutions at different values of the parameters that determine the flow. If the flow at certain values of the parameters is known and the flow at new values of the parameters is desired, then the flow solver must start over and calculate another complete flow solution at the new values of the parameters, not taking into account any information from the flow solution at the original values of the parameters. Flow sensitivities are used to approximate perturbed flow solutions without calculating the complete flow solution at the new values of the parameters. The development of the approximation of the perturbed flow focuses on the discontinuities in the flow which adversely affect the sensitivity calculations.

9.1 Sample Perturbed Flow Calculation

The simple supersonic ramp of Section 3.3 is again considered. The flow solution is calculated at an inflow Mach number of $M = 1.6$ and a ramp angle of 14.03° and a new flow solution is desired at an inflow Mach number of $M = 1.7$. The usual method is to completely solve the flow equations again, but this time using an inflow Mach number of $M = 1.7$. This approach can become very costly and time consuming if many different flow solutions are desired. An alternative method is to use a single variable Taylor

approximation for the inflow Mach number,

$$\mathbf{U}(x, y; M + \Delta M) \approx \mathbf{U}(x, y; M) + \Delta M \frac{\partial \mathbf{U}}{\partial M}(x, y; M) \tag{9.1}$$

where $M = 1.6$ and $\Delta M = 0.1$. The Taylor approximation involves the flow solution at the original value of the parameter along with $\frac{\partial \mathbf{U}}{\partial \alpha}(x, y; M)$, the flow sensitivity with respect to the inflow Mach number. In the above example the flow sensitivity is approximated using a forward difference quotient,

$$\mathbf{U}_M(x, y; M) = \frac{\partial \mathbf{U}}{\partial M}(x, y; M) \approx \frac{\mathbf{U}(x, y; M + \Delta \hat{M}) - \mathbf{U}(x, y; M)}{\Delta \hat{M}} \tag{9.2}$$

where $M = 1.6$ and $\Delta \hat{M} = 0.05$. The flow sensitivity of the flow density with respect to the inflow Mach number is shown in Fig. 3.1. The Taylor approximation not only must be efficient, but it must also correspond well with the calculated solution at an inflow Mach number of $M = 1.7$. The comparison of these two methods is given in Fig. 3.3. The difference between the Taylor approximation and the calculated flow solution at the new parameter is graphed in Fig. 3.4. Clearly, the Taylor approximation is not a good enough approximation to the perturbed flow, especially in the region around the shock wave. The error is partially due to two specific flow sensitivity calculation problems. Note, there is a certain amount of error already because the perturbed flow has been calculated using the Taylor approximation, in addition to, the flow sensitivity error being introduced. Also computationally, the method discussed is too expensive. These three deficiencies are discussed in Section 9.2.

9.2 Deficiencies in the Perturbed Flow Calculation

The example in Section 9.1 exhibits three different deficiencies in the perturbed flow calculations. The first is the computational cost of approximating the flow sensitivities. In this example, the sensitivities were approximated by using finite difference quotients which involved the calculation of a second flow solution. Hence, it costs more to approximate the perturbed flow than to calculate a new flow solution (See Section 2.3). The second deficiency is the inaccurate numerical approximation of the sensitivity near the shock wave. Since the shock wave is a discontinuity in the flow, if the sensitivity (or derivative) of the flow with respect to a parameter α is taken, then it will result in a δ-function at the shock wave as described in Chapter 5 and Chapter 7. The numerical schemes used to approximate the flow sensitivities have a difficult time approximating this δ-function and large spikes arise that affect the perturbed flow calculations (See Chapter 5). The third deficiency is

the incorrect placement of the shock in the perturbed flow approximation. In general, if a parameter α is perturbed by $\alpha + \Delta\alpha$, then the position of the shock will also change. In the single variable Taylor approximation, this change of shock position will not be correctly determined. Each of theses deficiencies are discussed in more detail in the Sections 9.3-9.5.

9.3 Flow Sensitivity Costs and Perturbed Flows

The computational cost of approximating flow sensitivities can make the Taylor approximation method useless from a numerical standpoint. For example, in the supersonic ramp problem it costs more to approximate the sensitivities than to recalculate the new perturbed flow with the flow solver. Some methods for calculating the sensitivities will allow the perturbed flow to be calculated at less cost than the new flow solution.

In terms of cost, the finite difference approach requires at least one more complete flow solve for each perturbed parameter, α. Likewise, the cost of the ADIFOR approach can be of the same order as for the finite difference approach. It would appear that both the ADIFOR and the finite difference approaches are not very useful in perturbed flow calculations since it would cost more to approximate the perturbed flow than to just calculate the perturbed flow. This is true in a setting where one flow sensitivity calculation is however used for one perturbed flow calculation. If a single flow sensitivity is used to calculate multiple perturbed flows, then both the finite difference and ADIFOR approaches can become cost efficient. This will depend on the number of perturbed flows desired, the number of parameters varied and the size of the fluid flow problem. In this case, these methods should be considered since their implementation is straightforward. However, if multiple parameters are used, or if a single flow sensitivity is used for a single perturbed flow, then another more cost efficient approach must be used. The sensitivity equation method provides a viable approach for calculating sensitivities for use in perturbed flows. Due to the linearity of the continuous sensitivity equations, the sensitivity equation method provides cheap approximations of the flow sensitivities. The sensitivity equation method also lends itself well in the calculation of flow sensitivities for multiple parameters. The different sensitivity calculation methods and their attributes were discussed in Chapter 2.

9.4 Sensitivity Deficiencies at the Shock Wave

In Section 7.1.1, several reasons for the development of spikes in each of the different approximate sensitivity calculation methods were discussed. It should also be pointed out

that as the resolution of the method decreases, *i.e.*, as the grid spacing increases, the numerical approximation of the δ-function grows increasingly worse. The shock wave or contact discontinuity becomes a larger fat hump and all pertinent information, such as the position of the shock wave or contact discontinuity, is effectively lost. In Section 7.3 and Chapter 8, possible methods to eliminate the spikes were discussed for the different sensitivity calculation methods. It may be difficult to avoid the spikes in the ADIFOR method in an efficient manner. The accuracy of the perturbed flow calculations relies on the ability to calculate flow sensitivities without spikes. Even if the efficiency and shock position problems are corrected, but the spikes still arise in the flow sensitivities, the error in the Taylor approximations will be unacceptable.

9.5 Incorrect Placement of Shock

The correct placement of the shock in the approximate perturbed flow is both a difficult and important enterprise. In discussions with professionals in the Aerospace/CFD community, the single most important aspect of efficient perturbed flow calculations, is the correct placement of the shock in the perturbed flow. To study this, a modified one-dimensional Riemann or shock tube problem is considered. This problem is considered because it is both computationally simple and because the exact solution and exact continuous sensitivities are known. The problem is modified in the sense that the initial data is chosen so there will only be a single shock wave moving through the tube and no rarefaction waves or contact discontinuities. Hence, the perturbed flow can be approximated without focusing on problems involved in calculating flow sensitivities, but merely focusing on the incorrect placement of the shock.

The physical set up of the Riemann problem is such that there is a tube with two gasses initially separated by a diaphragm. One gas is moving with a high density and pressure and one gas is at rest with a low density and pressure as is seen in Fig. 9.1. The problem is to calculate the flow solution when the diaphragm is instantaneously broken. The flow is governed by the one-dimensional Euler equations, Eq. 4.1, and the initial conditions are given in Fig. 9.1.

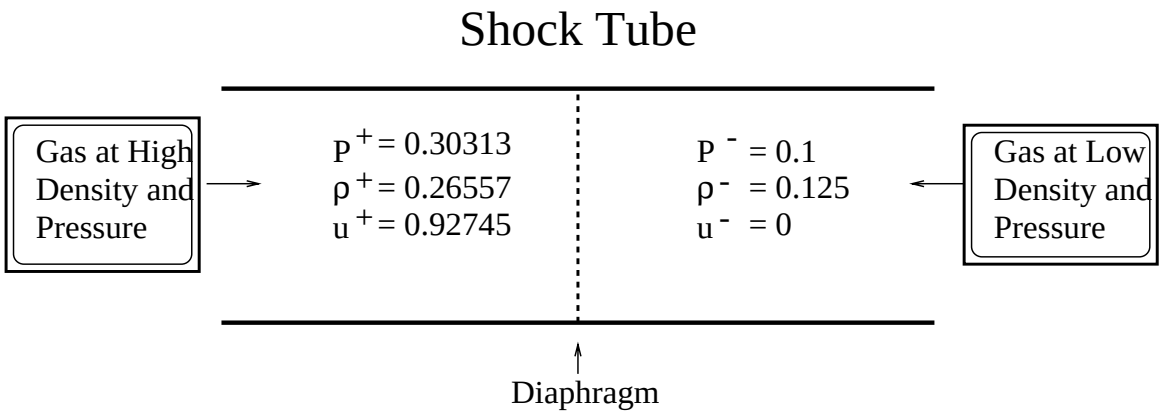

Figure 9.1: Physical setting and initial conditions for the modified Riemann problem.

The exact solution of the problem is well known and is given by

$$\mathbf{U}(x,t) = \begin{cases} \begin{bmatrix} \rho^+ \\ m^+ \\ e^+ \end{bmatrix} = \begin{bmatrix} 0.26557 \\ 0.24630 \\ 0.87204 \end{bmatrix}, & x < x_s(P^+) = s(P^+)t + c \\ \begin{bmatrix} \rho^- \\ m^- \\ e^- \end{bmatrix} = \begin{bmatrix} 0.125 \\ 0.00 \\ 0.25 \end{bmatrix}, & x > x_s(P^+) = s(P^+)t + c \end{cases} \tag{9.3}$$

where $a^- = \sqrt{\frac{\gamma P^-}{\rho^-}}$, $s(P^+) = a^- \sqrt{\frac{\gamma-1}{2\gamma} + \frac{\gamma+1}{2\gamma}\frac{P^+}{P^-}}$ is the shock speed and c is the position of the diaphragm. The position of the shock at a time, t, is denoted by $x_s(t, P^+)$. (Note: The shock position and speed is written in terms of P^+ for use in later contexts.) The exact solution of the Riemann problem is shown in Fig. 9.2.

In this example, perturbed flows are calculated with respect to the initial left pressure, P^+. That is, the parameter P^+ will be perturbed by an amount ΔP^+ and a perturbed flow will be determined at this new value. The initial left density, ρ^+, and the initial left velocity, u^+, are functions of P^+ and will also vary. This ensures that when P^+ is perturbed, the exact flow solution will only contain a single shock and not a more complex solution. The variables ρ^+ and u^+ as functions of P^+ are given by

$$\rho^+ = \rho^- \left(\frac{1 + \frac{\gamma+1}{\gamma-1}\frac{P^+}{P^-}}{\frac{\gamma+1}{\gamma-1} + \frac{P^+}{P^-}} \right), \tag{9.4}$$

$$u^+ = a^- \left(\frac{P^+}{P^-} - 1 \right) \sqrt{\frac{2/\gamma}{(\gamma+1)\frac{P^+}{P^-} + (\gamma-1)}}. \tag{9.5}$$

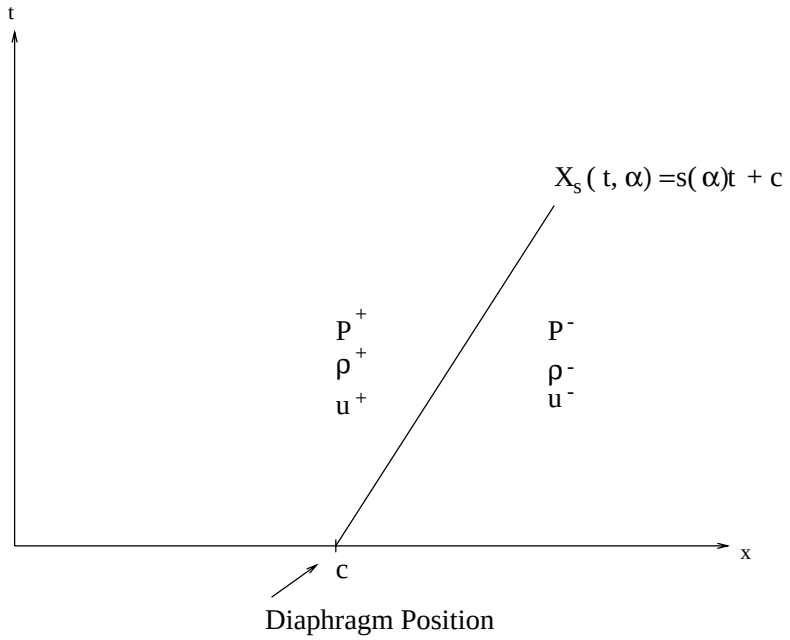

Figure 9.2: Exact solution of the modified Riemann problem in the xt-domain.

To approximate the perturbed flow for P^+, it is necessary to calculate the flow sensitivity with respect to the parameter $\alpha = P^+$. Usually, this is done approximately using one of the methods mentioned in Chapter 2. In this example, the exact continuous sensitivities are known and it is not necessary to approximate them. The exact continuous flow sensitivities with respect to P^+ are given by

$$\mathbf{S}(x,t) = \begin{cases} \begin{bmatrix} (\partial\rho/\partial P^+) \\ (\partial m/\partial P^+) \\ (\partial e/\partial P_+) \end{bmatrix} = \begin{bmatrix} \rho_\alpha^+ \\ m_\alpha^+ \\ e_\alpha^+ \end{bmatrix} & x < x_s(t,P^+) = s(P^+)t + c \\ \begin{bmatrix} (\partial\rho/\partial P^+) \\ (\partial m/\partial P^+) \\ (\partial e/\partial P^+) \end{bmatrix} = \begin{bmatrix} 0 \\ 0 \\ 0 \end{bmatrix} & x > x_s(t,P^+) = s(P^+)t + c \end{cases} \tag{9.6}$$

where

$$m_\alpha^+ = \rho_\alpha^+ u^+ + \rho^+ u_\alpha^+, \qquad e_\alpha^+ = \frac{P_\alpha^+}{\gamma - 1} + \frac{1}{2}\rho_\alpha^+ (u^+)^2 + \rho^+ u^+ u_\alpha^+,$$

and

$$P_\alpha^+ = 1, \qquad \rho_\alpha^+ = \frac{\rho^-}{P^-}\left(\frac{1 - \left(\frac{\gamma-1}{\gamma+1}\right)^2}{\left(1 + \frac{\gamma-1}{\gamma+1}\frac{P^+}{P^-}\right)^2}\right),$$

$$u_\alpha^+ = \frac{a^-}{2P^-}\sqrt{\frac{2/\gamma}{(\gamma+1)\frac{P^+}{P^-} + (\gamma-1)}}\left(\frac{(\gamma+1)\frac{P^+}{P^-} + (3\gamma-1)}{(\gamma+1)\frac{P^+}{P^-} + (\gamma-1)}\right).$$

9.5.1 Single Variable Taylor Approximation

Given both the exact flow solution and the exact continuous flow sensitivities, it is possible to approximate the perturbed flow with respect to $\alpha = P^+$. In the first example, the flow solution is calculated for $P^+ = 0.30313$ and the flow solution is desired at a 20% increase for P^+. The perturbed flow is calculated using a single variable Taylor approximation

$$\mathbf{U}(x,t;P^+ + \Delta P^+) \approx \mathbf{U}(x,t;P^+) + \Delta P^+ \mathbf{U}_{P^+}(x,t;P^+), \tag{9.7}$$

where $P^+ = 0.30313$ and $\Delta P^+ = 0.060626$. This is the same Taylor approximation used in the supersonic ramp example and the same "bad" results near the shock are expected. Since the exact solution and sensitivities are known, it is possible to compare the exact solution at $P^+ = 0.363756$ with the Taylor approximation at that point. The comparison of the exact solution with the Taylor approximation is shown in Fig. 9.3 and the error is shown in Fig. 9.4. It is important to point out that the error arising in the single variable Taylor approximation is due solely to the inaccuracy of the approximation method and not due to any sensitivity calculation errors since the exact continuous sensitivities were used in the Taylor approximation. The error in the Taylor approximation is of two basic types. The solution to the left of the shock has a small amount of error because the Taylor approximation is just an approximation and is not supposed to exactly capture the correct solution. If the perturbation, ΔP^+, was not as large, this error should decrease.

The second error in the Taylor approximation is the error due to the incorrect placement of the shock in the perturbed flow. Clearly, the Taylor approximation has not correctly placed the new shock, but instead has kept the shock position fixed from the original flow solution. Perturbations in the parameter P^+ will alter the position of the shock wave as shown in Fig. 9.5. Ideally, the perturbed flow calculation should predict the shock position for the new value of the parameter $P^+ + \Delta P^+$. If the point (x,t) is to the left or right of both shocks, then the single variable Taylor approximation does a good job of calculating the perturbed flow, but if the point, (x_0,t_0) is between the shock for the original value of P^+ and the shock for the new value of the parameter, then large errors arise. The error is due to the fact that the single variable Taylor approximation is not predicting a new shock position, but just imposing the shock position of the original parameter onto the perturbed flow. This can be seen by examining the single variable Taylor approximation,

$$\mathbf{U}(x,t;P^+ + \Delta P^+) \approx \mathbf{U}(x,t;P^+) + \Delta P^+ \mathbf{U}_{P^+}(x,t;P^+). \tag{9.8}$$

The perturbed flow is calculated using the flow at the original value of P^+ and the flow sensitivity at the original value of the parameter P^+. Both of these quantities will inherit the shock position for the original value of the parameter, e.g., Eq. 9.3 and Eq. 9.6. Therefore, there is no possible way to update to a new shock position using this Taylor approximation.

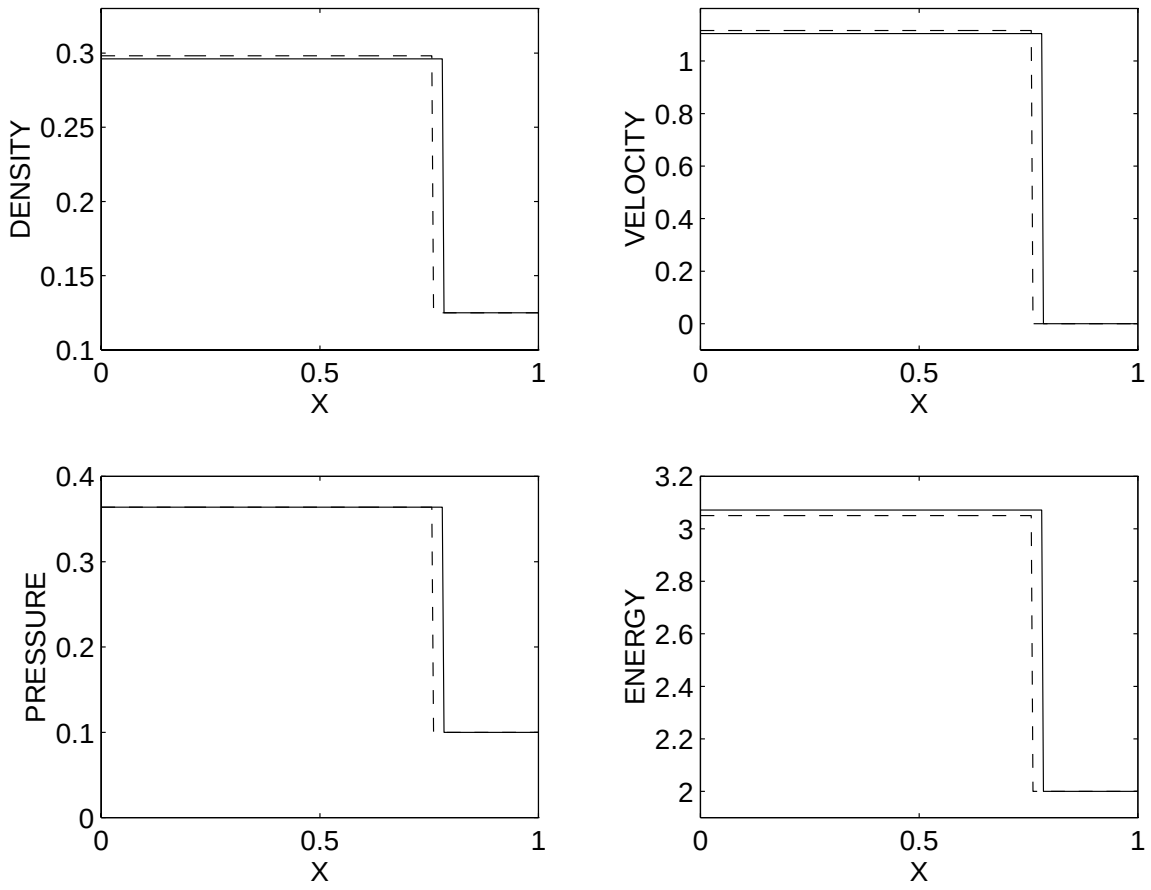

Figure 9.3: Comparison of the exact solution, solid line (—), to the single variable Taylor approximation, dashed line (- -).

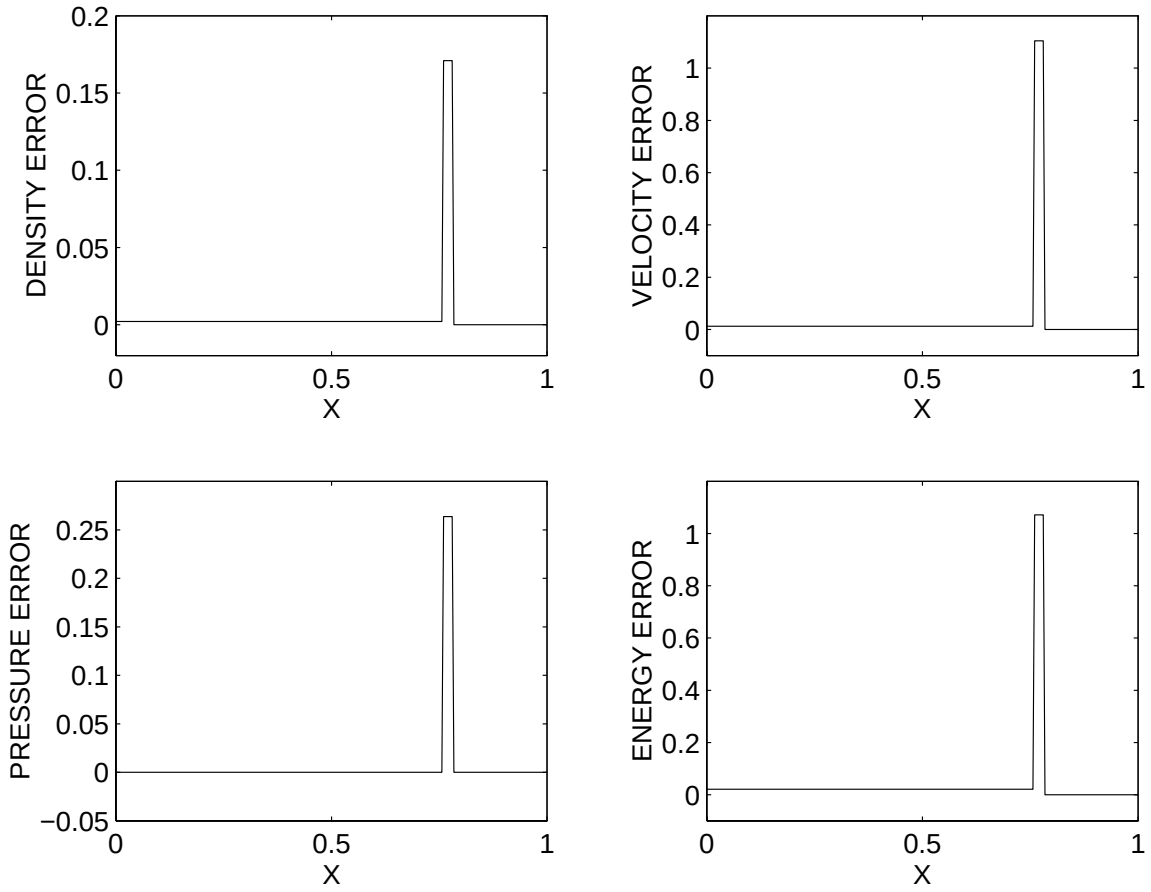

Figure 9.4: Error in the single variable Taylor approximation.

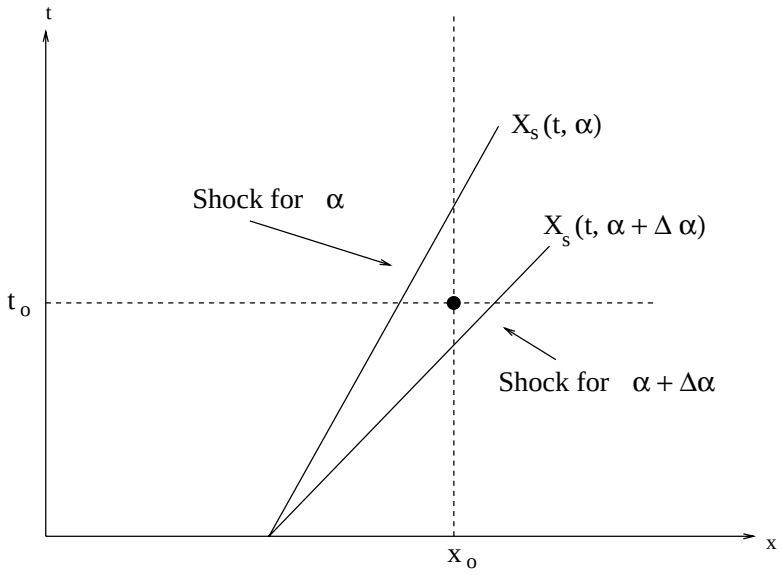

Figure 9.5: Shock positions for two different values of a parameter α.

In the analysis of the error, it has been determined that points, (x, t), that lie in the region between the two shocks are incorrectly updated. The points in this region are to the right of the original shock, but to the left of the new shock. The single variable Taylor approximation assumes the points are to the right of both shocks and updates based on this information. Hence, an incorrect shock placement is given. In reality, the Taylor approximation needs to update the perturbed flow in this region by information from the same side of both shocks. For example, if (x, t, P^+) lies between the shocks, then the Taylor approximation at $P^+ + \Delta P^+$ can be updated from $(x - \Delta x, t - \Delta t, P^+)$ as in Fig. 9.6.

9.5.2 Multivariable Taylor Approximations

To accomplish this, the single variable Taylor approximation must be expanded to include both spatial and temporal variables. This is done using the following multivariable Taylor approximation

$$\begin{aligned} \mathbf{U}(x,t;P^+ + \Delta P^+) &\approx \mathbf{U}(x - \Delta x, t - \Delta t; P^+) + \Delta P^+ \mathbf{U}_{P^+}(x - \Delta x, t - \Delta t; P^+) \\ &+ \Delta x \mathbf{U}_x(x - \Delta x, t - \Delta t; P^+) + \Delta t \mathbf{U}_t(x - \Delta x, t - \Delta t; P^+). \end{aligned} \tag{9.9}$$

The comparison of the multivariable Taylor approximation and the exact solution is shown in Fig. 9.7. The multivariable Taylor approximation gives the added dimension that the new shock position is captured exactly. A comparison between the error in the multivariable

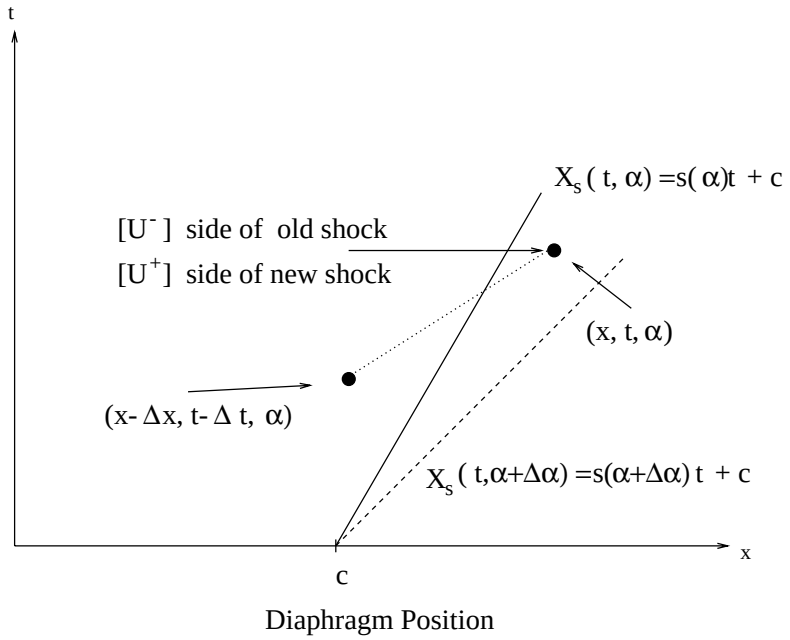

Figure 9.6: Taylor approximation updates should come from the same side of the shock for the parameter α and the shock for the perturbed parameter $\alpha + \Delta\alpha$.

Taylor approximation and the error in the single variable approximation, Fig. 9.8, shows the advantages of the correct placement. Note, there is still error in perturbed flow due to the approximation nature of the Taylor approximation formula. Thus, the multivariable Taylor approximation provides a viable method to correctly predict the new shock position. It is important to note that it is not the single variable versus the multivariable Taylor approximation that is of importance. It is the added use of both the spatial and the temporal variables in the Taylor approximation that is important. For example, if two parameters, α_1 and α_2, are perturbed, then the multivariable Taylor approximation

$$\begin{aligned}\mathbf{U}(x,t,\alpha_1+\Delta\alpha_1,\alpha_2+\Delta\alpha_2) &\approx \mathbf{U}(x,t,\alpha_1,\alpha_2)+\Delta\alpha_1\mathbf{U}_{\alpha_1}(x,t,\alpha_1,\alpha_2)\\ &+ \Delta\alpha_2\mathbf{U}_{\alpha_2}(x,t,\alpha_1,\alpha_2) \qquad (9.10)\end{aligned}$$

will not correctly place the new shock. A five term multivariable Taylor approximation using spatial and temporal variables, Eq. 9.11, must be used

$$\begin{aligned}&\mathbf{U}(x,t,\alpha_1+\Delta\alpha_1,\alpha_2+\Delta\alpha_2)\approx\mathbf{U}(x-\Delta x,t-\Delta t,\alpha_1,\alpha_2)\\ &+\Delta\alpha_1\mathbf{U}_{\alpha_1}(x-\Delta x,t-\Delta t,\alpha_1,\alpha_2)+\Delta\alpha_2\mathbf{U}_{\alpha_2}(x-\Delta x,t-\Delta t,\alpha_1,\alpha_2)\\ &+\Delta x\mathbf{U}_x(x-\Delta x,t-\Delta t,\alpha_1,\alpha_2)+\Delta t\mathbf{U}_t(x-\Delta x,t-\Delta t,\alpha_1,\alpha_2). \qquad (9.11)\end{aligned}$$

The algorithm for a general multivariable Taylor approximation in terms of parameters, spatial variables and temporal variables is discussed in the Section 9.6.

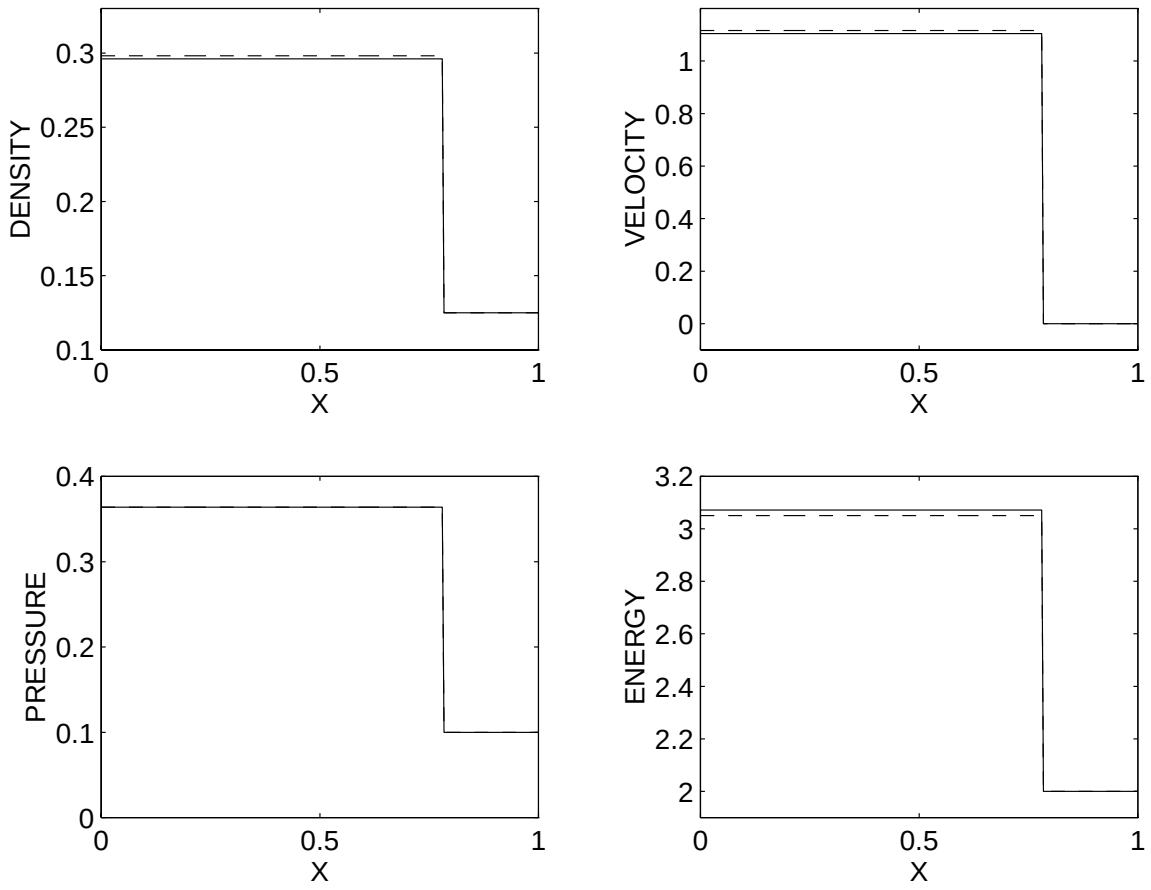

Figure 9.7: Comparison of the exact solution, solid line (—), to the multivariable Taylor approximation, dashed line (- -).

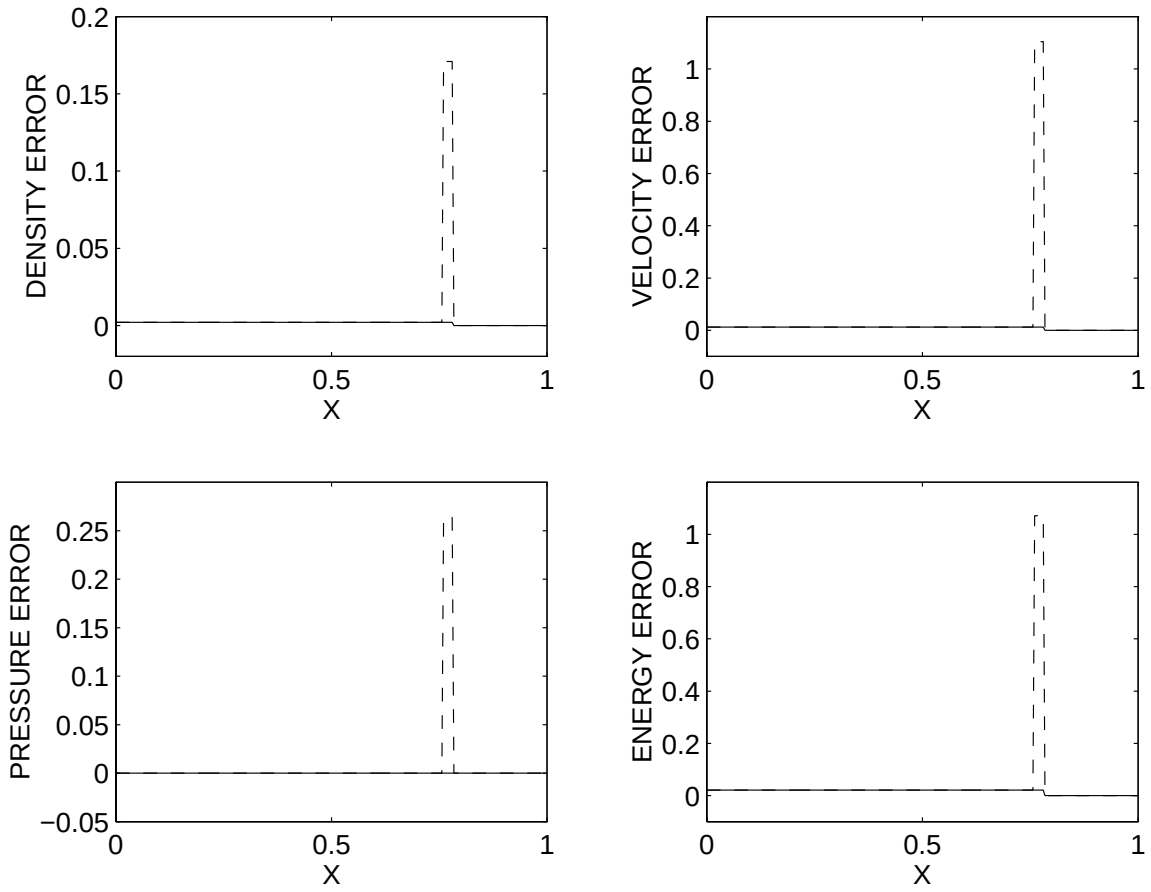

Figure 9.8: Comparison between the error in the single variable Taylor approximation, dashed line (- -) and the error in the multivariable Taylor approximation, solid line (—).

9.6 Spatial and Temporal Multivariable Taylor Approximation

The general method for calculating the perturbed flow solution, $\mathbf{U}$, at $\alpha + \Delta\alpha$ using the multivariable Taylor approximation is more complex than its definition implies. There is additional information that must be supplied or calculated to correctly implement this method. The first information that is needed is the position of the original shock and an approximation for the new shock position. Since the flow solution at the original values of the parameter is known, the original shock position can be found from this solution by checking pressure gradients or from information built into the structure of the numerical scheme. The approximate position of the new shock is more difficult to calculate. This position can be approximated by

$$x_s(t, \alpha + \Delta\alpha) \approx x_s(t, \alpha) + \Delta\alpha \frac{\partial x_s}{\partial \alpha} \tag{9.12}$$

where $\frac{\partial x_s}{\partial \alpha}$ is the shock position sensitivity. In the modified Riemann problem of Section 9.5, the shock position for the flow at $P^+ + \Delta P^+$ was approximated by

$$x_s(t, P^+ + \Delta P^+) \approx \left[s(P^+) + \Delta P^+ \frac{\partial s}{\partial P^+}(P^+) \right] t + c. \tag{9.13}$$

The calculation of the shock position sensitivity is discussed in Section 9.7 and Chapter 10.

Next, it is important to determine if each point, (x, t), is between the shocks. If a point is to the left or right of both shocks, then there is no need to apply the costlier multivariable Taylor approximation and a single variable Taylor approximation should be used. If the point, (x, t), is between the shocks, then a multivariable Taylor approximation must be used to ensure the correct shock placement. It is assumed that $\Delta\alpha$ is fixed or predetermined *a priori*. The values for Δt and Δx must then be determined on the fly. If the value of Δt is chosen arbitrarily, although it should not be excessively large or small, then the value of Δx should be set to

$$\Delta x = \frac{\partial x_s(t, \alpha)}{\partial t} \Delta t + \frac{\partial x_s(t, \alpha)}{\partial \alpha} \Delta\alpha. \tag{9.14}$$

This effectively ensures that the new point $(x - \Delta x, t - \Delta t, \alpha)$ locally lies on the tangent plane to the $xt\alpha$-shock surface, Fig. 9.9, at the point (x, t, α). Thus, if Δt is sufficiently small, the new point will lie on the same side of both shocks. Clearly, if x and t are held fixed and α is perturbed, then at some time, (x, t, α) and $(x, t, \alpha + \Delta\alpha)$ will lie on different sides of the $xt\alpha$-shock surface as is seen in Fig. 9.9. Restricting Δx, as in Eq. 9.14, will remedy this problem.

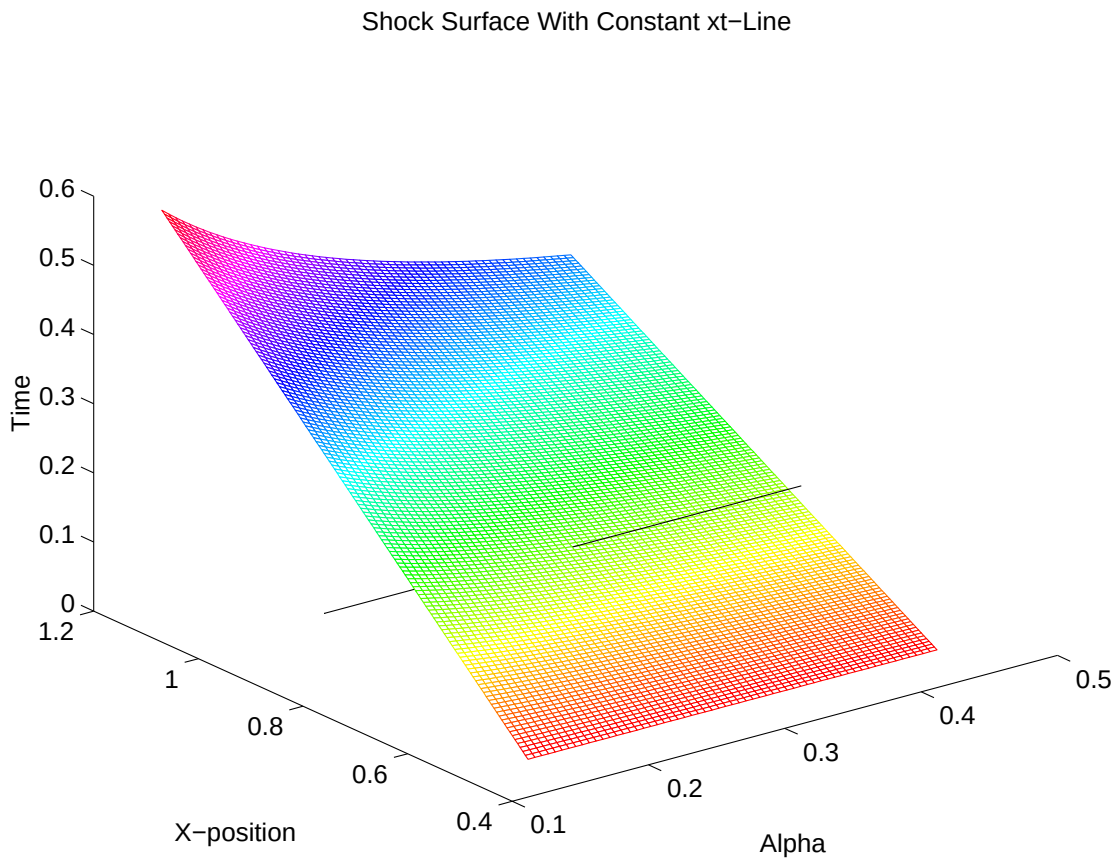

Figure 9.9: Perturbing α and moving along the xt-line will move from one side of the $xt\alpha$-shock surface to the other side of the $xt\alpha$-shock surface.

Again, in the modified Riemann problem of Section 9.5, Δx was found from

$$\Delta x = \frac{\partial x_s(t, P^+)}{\partial t}\Delta t + \left(\left[\frac{\partial s}{\partial P^+}(P^+)\right] t\right)\Delta P^+. \tag{9.15}$$

The multivariable Taylor approximation also requires the spatial and temporal derivatives of the flow solution for points lying between the shocks. The quantities $\mathbf{U}_x(x - \Delta x, t - \Delta t, \alpha)$ and $\mathbf{U}_t(x - \Delta x, t - \Delta t, \alpha)$ are calculated from the flow solutions using simple finite difference quotients. The flow sensitivities, $\mathbf{U}_\alpha(x - \Delta x, t - \Delta t, \alpha)$, are calculated using the sensitivity equation method. The quantities $\mathbf{U}_t$ and $\mathbf{U}_x$ should only be calculated for points in between the two shocks to help reduce the computational costs of the method. It should be mentioned that the flow sensitivities should be calculated so that there is no spikes or δ-functions in the solutions, since the Taylor approximation is now restricted to smooth regions of the flow. These spikes, if they arose would alter the accuracy of the method. The perturbed flow can then be updated using the spatial and temporal multivariable Taylor approximation. The implementation of this approximation requires additional information, most of which can be approximated directly from the flow solution. The algorithm for a spatial and temporal multivariable Taylor approximation is given by:

Spatial and Temporal Multivariable Taylor Approximation

Approximate the flow solution, U, at (x, t, α)**.**

Locate position of shock wave.

Approximate flow sensitivities, $\frac{\partial \mathbf{U}}{\partial \alpha}$**, at** (x, t, α)**.**

Eliminate spikes from sensitivities.

Approximate shock position sensitivity, $\frac{\partial x_s}{\partial \alpha}$**.**

$\Delta\alpha$ is fixed.

Δt is set arbitrarily.

$\frac{\partial x_s}{\partial t}$ is approximated from flow solution.

Δx is set to be $\Delta x = \frac{\partial x_s(t,\alpha)}{\partial t}\Delta t + \frac{\partial x_s(t,\alpha)}{\partial \alpha}\Delta\alpha$.

Approximate the new shock position by $x_s(t, \alpha + \Delta\alpha) \approx x_s(t, \alpha) + \Delta\alpha\frac{\partial x_s}{\partial \alpha}$**.**

Loop over grid points.

Check to see if the point, (x, t), is between the two shocks.

If (x, t) is between the shocks then

Use multivariable Taylor approximation.

Approximate $\mathbf{U}_x(x - \Delta x, t - \Delta t, \alpha)$ from flow solution.

Approximate $\mathbf{U}_t(x - \Delta x, t - \Delta t, \alpha)$ from flow solution.

Update $\mathbf{U}(x, t, \alpha + \Delta\alpha)$ using Eq. 9.9.

Else

Use single variable Taylor Approximation.

Update $\mathbf{U}(x, t, \alpha + \Delta\alpha)$ using Eq. 9.7

Endif

Continue loop.

9.7 Shock Position Sensitivity

The approximation of the new shock position and the determination of the tangent plane to the $xt\alpha$-shock surface required the calculation of the shock position sensitivity, $\frac{\partial x_s}{\partial \alpha}$. In the modified Riemann problem of Section 9.5, the exact solution and exact continuous flow sensitivities were known. Likewise, the exact shock position and speed were known and the exact shock position sensitivity was calculated. The exact shock position sensitivity with respect to $\alpha = P^+$ was

$$\frac{\partial x_s(t, P^+)}{\partial P^+} = \frac{\partial}{\partial \alpha}\left\{s(P^+)t + c\right\} = \frac{\partial s}{\partial P^+}(P^+)t \tag{9.16}$$

where

$$\frac{\partial s}{\partial P^+}(P^+) = \frac{\gamma + 1}{4\gamma}\frac{a^-}{P^-}\left(\frac{\gamma - 1}{2\gamma} + \frac{\gamma + 1}{2\gamma}\frac{P^+}{P^-}\right)^{-\frac{1}{2}}.$$

This special example was chosen so that the research could focus on the algorithms and shock positions without having to worry about the errors in calculating the sensitivities. In most cases, the exact solution and exact continuous flow sensitivities will not be available. In these cases the shock position sensitivity must be calculated numerically using information such as the Rankine-Hugoniot jump conditions. The Rankine-Hugoniot jump conditions state $[[\mathbf{F}]] = s[[\mathbf{U}]]$ where $[[\cdot]]$ denotes jump, $\mathbf{F}$ is the flux function and $\mathbf{U}$ is the flow solution; or that there is a function $\mathbf{R}(\mathbf{U})$ that is continuous across the shock wave.

$$\mathbf{R}(\mathbf{U}^+(x = x_s(t, P^+), t; P^+); P^+) = \mathbf{R}(\mathbf{U}^-(x = x_s(t, P^+), t; P^+); P^+) \tag{9.17}$$

The Rankine-Hugoniot function $\mathbf{R}(\mathbf{U})$ has been written out with full dependence on the parameter P^+. The Rankine-Hugoniot jump conditions can be differentiated with respect to the variable P^+ to derive the system of equations, Eq. 9.18.

$$\begin{aligned}\left(\frac{\partial \mathbf{R}}{\partial P^+}\right)^+ &+ \left(\frac{\partial \mathbf{R}}{\partial \mathbf{U}}^+ \left(\left(\frac{\partial \mathbf{U}}{\partial x}\right)^+ \left(\frac{\partial x_s}{\partial P^+}\right) + \frac{\partial \mathbf{U}}{\partial P^+}\right)^+\right) \\ &= \left(\frac{\partial \mathbf{R}}{\partial P^+}\right)^- + \left(\frac{\partial \mathbf{R}}{\partial \mathbf{U}}^- \left(\left(\frac{\partial \mathbf{U}}{\partial x}\right)^- \left(\frac{\partial x_s}{\partial P^+}\right) + \frac{\partial \mathbf{U}}{\partial P^+}\right)^-\right). \end{aligned} \tag{9.18}$$

The differentiated Rankine-Hugoniot jump conditions not only involve the sensitivities on either side of the shock, but also involve the shock position sensitivity. If the flow solution and flow sensitivities are known on both sides of the shock, then Eq. 9.18 may be used to solve for the shock position sensitivity. It is necessary to calculate the sensitivities without spikes to correctly approximate the sensitivities on both sides of the shock. In the modified Riemann problem, the differentiated Rankine-Hugoniot jump conditions reduced to a system of three equations in the three unknowns. Substituting the values of the different variables and solving the system resulted in the correct shock position sensitivity. This case and the shock position sensitivity are studied in greater detail in Chapter 10.

Chapter 10

Shock Position Sensitivity

The calculation of perturbed flows using the spatial and temporal multivariable Taylor approximation requires the calculation of a shock position sensitivity. In this chapter, a method is developed for calculating the shock position sensitivity by differentiating the Rankine-Hugoniot jump conditions for the Riemann problem to derive a new set of jump conditions for the continuous sensitivity equations. The shock position sensitivity can then be extracted from these new jump conditions.

10.1 Problem Definition

The development of the shock position sensitivity will use the modified version of the Riemann problem. The initial conditions are chosen so the solution only contains a single shock wave moving through the tube, see Fig 9.1, and no contact discontinuity or rarefaction wave. The flow is governed by the Euler equations

$$\mathbf{U}_t + [\mathbf{F}(\mathbf{U})]_x = \mathbf{0} \tag{10.1}$$

where

$$\mathbf{U} = \begin{bmatrix} \rho \\ m \\ e \end{bmatrix}, \quad \mathbf{F}(\mathbf{U}) = \begin{bmatrix} m \\ \frac{m^2}{\rho} + P \\ \frac{m}{\rho}(e+P) \end{bmatrix}.$$

The conservative and primitive variables are again related through the expressions $m = \rho u$ and $e = \frac{P}{\gamma - 1} + \frac{1}{2}\frac{m^2}{\rho}$. The flow across the shock wave is governed by the Rankine-Hugoniot

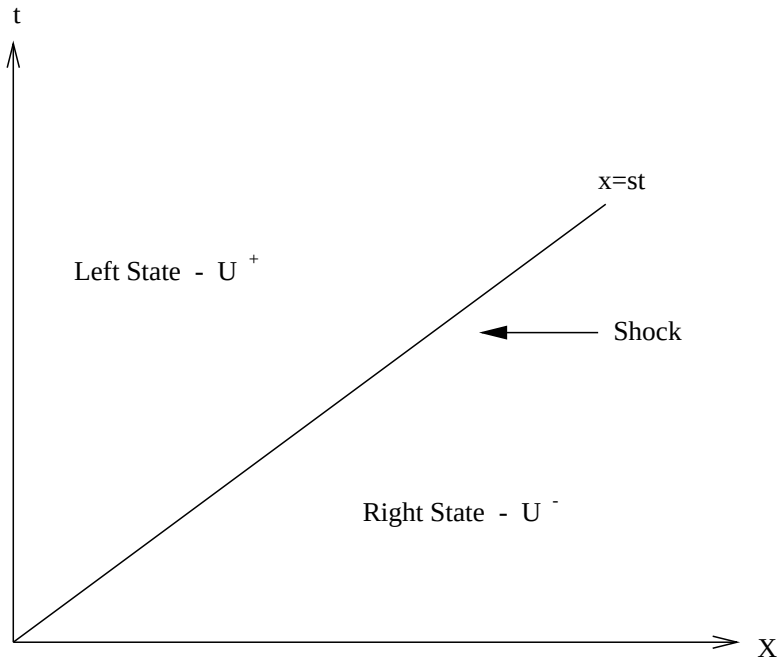

Figure 10.1: Left and Right States across a Shock

jump conditions. This states that the jump in $\mathbf{F}$ is equal to the shock speed, s, times the jump in $\mathbf{U}$, where $[[\cdot]]$ denotes jump.

$$[[\mathbf{F}(\mathbf{U})]] = s[[\mathbf{U}]] \tag{10.2}$$

or

$$\begin{bmatrix} m^+ \\ \frac{(m^+)^2}{\rho^+} + P^+ \\ \frac{m^+}{\rho^+}(e^+ + P^+) \end{bmatrix} - \begin{bmatrix} m^- \\ \frac{(m^-)^2}{\rho} + P^- \\ \frac{m^-}{\rho^-}(e^- + P^-) \end{bmatrix} = s \begin{bmatrix} \rho^+ - \rho^- \\ m^+ - m^- \\ e^+ - e^- \end{bmatrix}. \tag{10.3}$$

In Eq. 10.3, the $+$ and $-$ denote the flow value on the left and right sides of the shock respectively, as in Fig. 10.1. Simplification of Eq. 10.3 results in a system of three equations.

$$\rho^+(u^+ - s) = \rho^-(u^- - s) \tag{10.4}$$
$$m^+(u^+ - s) + P^+ = m^-(u^- - s) + P^- \tag{10.5}$$
$$e^+(u^+ - s) + u^+P^+ = e^-(u^- - s) + u^-P^- \tag{10.6}$$

where $m^{\pm} = \rho^{\pm} u^{\pm}$, $e^{\pm} = \frac{P^{\pm}}{\gamma - 1} + \frac{1}{2}\frac{(m^{\pm})^2}{\rho^{\pm}}$ and

$$s = a^{-}\left(\frac{\gamma - 1}{2\gamma} + \frac{\gamma + 1}{2\gamma}\frac{P^{+}}{P^{-}}\right)^{\frac{1}{2}}, \qquad a^{-} = \sqrt{\frac{\gamma P^{-}}{\rho^{-}}}.$$

The one-dimensional Euler equations, Eq. 10.1, and the Rankine-Hugoniot jump conditions, Eq. 10.4-10.6 completely describe the flow solution.

10.2 Differentiation of the Rankine-Hugoniot Jump Conditions

Consider calculating a perturbed flow for the Riemann problem with respect to the parameter α. This will require the calculation of the flow sensitivities and the shock position sensitivity. It will be assumed that the fluid flow equations have already been differentiated with respect to a parameter, α, to get the continuous sensitivity equations. The flow sensitivities can then be solved via the sensitivity equation method (see Chapter 2). To calculate the shock position sensitivity, the Rankine-Hugoniot jump conditions can be differentiated with respect to a parameter α. The jump conditions can be written as a continuous function across the shock noting all dependences on the parameter α.

$$\mathbf{R}(\mathbf{U}^{+}(t, x_s(t;\alpha);\alpha);\alpha) = \mathbf{R}(\mathbf{U}^{-}(t, x_s(t;\alpha);\alpha);\alpha) \tag{10.7}$$

Both sides of the equation can be differentiated with respect to the parameter α resulting in Eq. 10.8.

$$\begin{aligned}\left(\frac{\partial \mathbf{R}}{\partial \alpha}\right)^{+} &+ \left(\frac{\partial \mathbf{R}}{\partial \mathbf{U}}\right)^{+}\left[\left(\frac{\partial \mathbf{U}}{\partial x_s}\right)^{+}\left(\frac{\partial x_s}{\partial \alpha}\right) + \left(\frac{\partial \mathbf{U}}{\partial \alpha}\right)^{+}\right] \\ &= \left(\frac{\partial \mathbf{R}}{\partial \alpha}\right)^{-} + \left(\frac{\partial \mathbf{R}}{\partial \mathbf{U}}\right)^{-}\left[\left(\frac{\partial \mathbf{U}}{\partial x_s}\right)^{-}\left(\frac{\partial x_s}{\partial \alpha}\right) + \left(\frac{\partial \mathbf{U}}{\partial \alpha}\right)^{-}\right]\end{aligned} \tag{10.8}$$

Here, x_s is a parameterization of the shock position as a function of time and α, as is seen in Fig. 7.1.

The Rankine-Hugoniot jump conditions have effectively been differentiated with respect to an arbitrary parameter α resulting in a system of equations, Eq. 10.8. This differentiation not only involves a spatial derivative, $\frac{\partial \mathbf{U}}{\partial x_s}$, but also involves a shock position sensitivity, $\frac{\partial x_s}{\partial \alpha}$. It is the goal of this chapter to show that the differentiated Rankine-Hugoniot jump

conditions result in a unique system of equations for the flow sensitivities and the shock position sensitivities. For this reason, the parameter, α, is chosen to be the initial left pressure, $\alpha = P^+$. The continuous Rankine-Hugoniot function is then defined as

$$\mathbf{R}(\mathbf{U}) = \begin{bmatrix} \rho(u-s) \\ m(u-s)+P \\ e(u-s)+uP \end{bmatrix}. \tag{10.9}$$

Since x_s merely denotes the position of the shock, it is clear that the term $\left(\frac{\partial \mathbf{U}}{\partial x_s}\right)^{\pm}$ is just a one-sided spatial derivative of the flow variables. In the problem at hand, the flow to the left and right of the shock is a constant. Therefore, $\left(\frac{\partial \mathbf{U}}{\partial x_s}\right)^{\pm} = 0$. (If the flow to the left and right of the shock is not constant, then $\left(\frac{\partial \mathbf{U}}{\partial x_s}\right)^{\pm} \neq 0$, as is seen in Fig. 10.2.) If $\frac{\partial \mathbf{U}^{\pm}}{\partial x_s} = 0$,

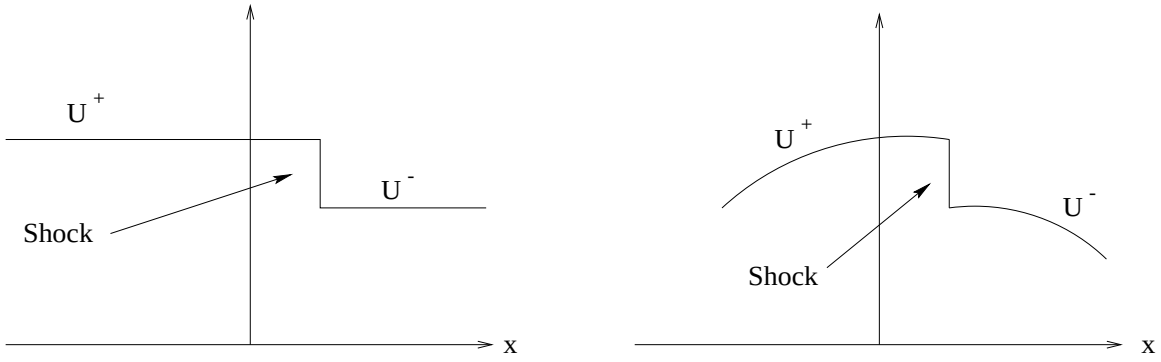

Figure 10.2: Two possible flow conditions across a shock.

then Eq. 10.8 reduces to

$$\left(\frac{\partial \mathbf{R}}{\partial \alpha}\right)^{+} + \left(\frac{\partial \mathbf{R}}{\partial \mathbf{U}}\right)^{+}\left[\left(\frac{\partial \mathbf{U}}{\partial \alpha}\right)^{+}\right] = \left(\frac{\partial \mathbf{R}}{\partial \alpha}\right)^{-} + \left(\frac{\partial \mathbf{R}}{\partial \mathbf{U}}\right)^{-}\left[\left(\frac{\partial \mathbf{U}}{\partial \alpha}\right)^{-}\right]. \tag{10.10}$$

This is the same as differentiating Eq. 10.9 with respect to α using the chain rule. The differentiation of Eq. 10.9 results in the following three equations

$$\rho^+_\alpha(u^+ - s) + \rho^+(u^+_\alpha - s_\alpha) = -\rho^- s_\alpha \tag{10.11}$$

$$m^+_\alpha(u^+ - s) + m^+(u^+_\alpha - s_\alpha) + P^+_\alpha = -m^- s_\alpha \tag{10.12}$$

$$e^+_\alpha(u^+ - s) + e^+(u^+_\alpha - s_\alpha) + u^+_\alpha P^+ + u^+ P^+_\alpha = -e^- s_\alpha \tag{10.13}$$

where $m^+_\alpha = \rho^+_\alpha u^+ + \rho^+ u^+_\alpha$, $e^+_\alpha = \frac{P^+_\alpha}{\gamma - 1} + \frac{1}{2}\rho^+_\alpha (u^+)^2 + \rho^+ u^+ u^+_\alpha$. The flow sensitivities to the right of the shock have been incorporated into Eq. 10.11-10.13, since it is known that they

are all zero, *i.e.*,

$$\rho_\alpha^- = 0 \tag{10.14}$$
$$u_\alpha^- = 0 \tag{10.15}$$
$$P_\alpha^- = 0 \tag{10.16}$$
$$m_\alpha^- = 0 \tag{10.17}$$
$$e_\alpha^- = 0. \tag{10.18}$$

Assuming the flow solution is known, the solution to the system of equations, Eq. 10.11-10.13, must be calculated for the shock position sensitivity.

10.3 Solution of the Differentiated Rankine-Hugoniot System

It is necessary to verify that the differentiated Rankine-Hugoniot system of equations, Eq. 10.11-10.13, can be solved for the flow sensitivities and shock position sensitivity and that this solution is unique. Using the fact that the sensitivities to the right of the shock are zero and the sensitivity of the left initial pressure with respect to itself is, $P_\alpha^+ = 1$, results in a system of three equations in three unknowns: ρ_α^+, u_α^+, and s_α. Assuming a solution exists to this system, two questions arise. First, is the solution to the system unique? Second, how does the solution compare to the exact continuous sensitivities and the exact shock position sensitivity given in Section 9.5 and Section 9.7, respectively? It would be nice, if the exact sensitivities and the unique solution of the system were the same. To verify this, the exact sensitivities are plugged into the system and shown to be a solution to the system. This will verify that the exact continuous sensitivities and the exact shock position sensitivity are a solution to the differentiated Rankine-Hugoniot system of equations, Eq. 10.11-10.13. If the system can then be shown to have a unique solution, then it will be verified that the unique solution exists and, in fact, is the exact continuous sensitivities and the exact shock position sensitivity.

10.3.1 Verification of the Solution

The exact continuous sensitivities calculated from differentiating the exact flow solution in each region are substituted into the differentiated Rankine-Hugoniot conditions to see whether or not they are a solution. The exact solution on the left side of the shock is given

as a function of P^+, P^-, u^-, and ρ^- by

$$\rho^+ = \rho^- \frac{P^+}{P^-}\left(\frac{1+\frac{\gamma-1}{\gamma+1}\frac{P^-}{P^+}}{1+\frac{\gamma-1}{\gamma+1}\frac{P^+}{P^-}}\right) \tag{10.19}$$

$$u^+ = a^-\left(\frac{P^+}{P^-}-1\right)\sqrt{\frac{2/\gamma}{(\gamma+1)\frac{P^+}{P^-}+(\gamma-1)}} \tag{10.20}$$

where $a^- = \sqrt{\frac{\gamma P^-}{\rho^-}}$, $m^\pm = \rho^\pm u^\pm$, and $e^\pm = \frac{P^\pm}{\gamma-1}+\frac{1}{2}\rho^\pm(u^\pm)^2$. The corresponding shock speed is given by

$$s = a^-\sqrt{\frac{\gamma-1}{2\gamma}+\frac{\gamma+1}{2\gamma}\frac{P^+}{P^-}}. \tag{10.21}$$

Each of these quantities can be differentiated with respect to $\alpha = P^+$ to obtain the exact continuous sensitivities,

$$P^+_\alpha = 1 \tag{10.22}$$

$$\rho^+_\alpha = \frac{\rho^-}{P^-}\left(\frac{1-\left(\frac{\gamma-1}{\gamma+1}\right)^2}{\left(1+\frac{\gamma-1}{\gamma+1}\frac{P^+}{P^-}\right)^2}\right) \tag{10.23}$$

$$u^+_\alpha = \frac{1}{2}\frac{a^-}{P^-}\sqrt{\frac{2/\gamma}{(\gamma+1)\frac{P^+}{P^-}+(\gamma-1)}}\left(\frac{(\gamma+1)\frac{P^+}{P^-}+(3\gamma-1)}{(\gamma+1)\frac{P^+}{P^-}+(\gamma-1)}\right) \tag{10.24}$$

$$P^-_\alpha = 0 \tag{10.25}$$

$$u^-_\alpha = 0 \tag{10.26}$$

$$\rho^-_\alpha = 0 \tag{10.27}$$

where again $m^\pm_\alpha = \rho^\pm_\alpha u^\pm + \rho^\pm u^\pm_\alpha$, $e^\pm_\alpha = \frac{P^\pm_\alpha}{\gamma-1}+\frac{1}{2}\rho^\pm_\alpha(u^\pm)^2+\rho^\pm u^\pm u^\pm_\alpha$. Likewise, the shock speed must be differentiated with respect to $\alpha = P^+$ to calculate the exact shock position sensitivity,

$$s_\alpha = \frac{1}{4}\frac{a^-}{P^-}\frac{\gamma+1}{\gamma}\frac{1}{\sqrt{\frac{\gamma-1}{2\gamma}+\frac{\gamma+1}{2\gamma}\frac{P^+}{P^-}}}. \tag{10.28}$$

The exact continuous sensitivities, Eq. 10.22-10.27, and the exact shock position sensitivity, Eq. 10.28 are substituted into the differentiated Rankine-Hugoniot system, Eq. 10.11-10.13. It can be shown after an intense exercise in algebra that these exact quantities satisfy the differentiated Rankine-Hugoniot jump conditions. Thus, this verifies that the exact continuous sensitivities and the exact shock position sensitivity are a solution to the system of equations. Since, the system is square, *i.e.*, three equations in three unknowns: ρ^+_α, u^+_α, and s_α, and a solution exists, the system will have either a unique solution or infinitely many solutions.

10.3.2 Uniqueness of the Solution

The uniqueness of the system can be determined by checking whether or not the coefficient matrix is singular or nonsingular. The determinant of the coefficient matrix of the differentiated Rankine-Hugoniot equations, Eq. 10.11-10.13 can again be calculated using a little algebra . This determinant is given in Eq. 10.29.

$$Det = (P^- - P^+) \left\{ \frac{(P^-)^2 + 2\left(\frac{\gamma^2+1}{\gamma^2-1}\right) P^- P^+ + (P^+)^2}{P^+ \left(\frac{\gamma-1}{\gamma+1}\right) P^-} \right\} \tag{10.29}$$

Physically, the problem requires the left and right initial pressures to be positive, *i.e.*, $P^+ > 0$ and $P^- > 0$. There is also a physical restriction on the ratio of specific heats, γ. This ratio is always greater than or equal to one and since there is no gas with a ratio of specific heats equal to one, $\gamma > 1$. Using these inequalities, it is reasoned that

$$\left\{ \frac{(P^-)^2 + 2\left(\frac{\gamma^2+1}{\gamma^2-1}\right) P^- P^+ + (P^+)^2}{P^+ \left(\frac{\gamma-1}{\gamma+1}\right) P^-} \right\} > 0.$$

Thus, the determinant of the coefficient matrix can only be zero if the left and right initial pressures are equal, *i.e.*, $(P^- - P^+) = 0$. In the modified Riemann problem being studied, it was stated that the single shock arose and moved through the tube based on the assumption that the left and right initial pressures were different values. Hence, the determinant is always nonzero and the system is nonsingular and has a unique solution. The unique solution of the differentiated Rankine-Hugoniot jump conditions system, Eq. 10.11-10.13, is the exact continuous sensitivities and the exact shock position sensitivity.

10.4 Conclusions

The shock position sensitivity is necessary in the calculation of perturbed flows using the spatial and temporal multivariable Taylor approximation. This quantity can be approximated by differentiating the Rankine-Hugoniot jump conditions with respect to a parameter α. The unique solution to this set of equations is the exact continuous sensitivities and the exact shock position sensitivity. Hence, if the approximate flow solution and the approximate flow sensitivities are known, the shock position sensitivity can be approximated using any of the differentiated Rankine-Hugoniot jump conditions, Eq. 10.11-10.13 and substituting in the approximate flows and sensitivities from both sides of the shock.

Chapter 11

Summary and Conclusions

11.1 Summary of Methods

The preceding work presented an in depth study of the intersection of flow sensitivities and discontinuous fluid flow. The focus was on the calculation of flow sensitivities for flows involving discontinuities, but the work can be generalized to the calculation of sensitivities for any physical system governed by a system of hyperbolic conservation laws. Chapter 2 was devoted to the development and definition of flow sensitivities as well as the definition of several sensitivity calculation methods. Approximate sensitivity calculation methods included were finite difference methods, the sensitivity equation methods and semi-analytic methods such as the automatic differentiation methods. Flow sensitivities gain most of their importance due to their applications in other areas. Chapter 3 provided several examples of applications of sensitivities. These applications included optimization and control, the calculation of perturbed flows, and the use of flow sensitivities as information tools.

Chapter 4 and Chapter 5 developed an understanding of the effects of discontinuities and complexities in the flow on the approximate flow sensitivity calculations. Here, flow sensitivities were calculated for the Riemann or shock tube problem from gas dynamics using finite differences, the sensitivity equation method and ADIFOR, an automatic differentiation method. The numerical methods used to calculated to flow solutions and flow sensitivities included the Roe scheme [24, 28], the Godunov scheme [40] and the two-step Lax-Wendroff scheme [40]. The artificial viscosity term of Lapidus [40] was added to both the Godunov and Lax-Wendroff scheme. Chapter 6 studied the effects of poor sensitivity calculations on the optimization process by comparing optimizations using exact and approximate sensitivities on the Riemann problem. Likewise, Chapters 9 and 10 studied and

developed correct and efficient methods for calculating perturbed flows via flow sensitivities and Taylor approximations.

Chapter 7 and Chapter 8 were concerned with the theory of flow sensitivities, hyperbolic equations and numerical approximation. Deficiences in the sensitivity calculation methods were explored and exposed and solutions were proposed.

11.2 Results and Conclusions

The conclusion is that discontinuities arising in the flow solution have a large effect on the calculation of flow sensitivities that should not be ignored. The exact flow sensitivities include δ-functions at the points where the flow discontinuities arise. The numerical approximation of these δ-functions by all sensitivity calculation methods result in large spikes that corrupt the flow sensitivities. The removal of these spikes from the flow sensitivities is necessary for the accuracy of the perturbed flow solutions and can greatly speed up the optimization process. Results compare the finite difference method, the sensitivity equation method and the automatic differentiation method for a variety of numerical schemes and grid sizes.

A new numerical method for calculating the sensitivity equation method sensitivities using the Roe method is developed. This method lends itself well to the calculation of sensitivities without spikes. The perturbed flow calculations are improved using a Taylor approximation in both spatial and temporal variables. In this method, a new shock position is calculated by differentiating the Rankine-Hugoniot jump conditions across the shock and solving the corresponding linear system.

11.3 Directions for Future Work

Future work should include the development of more efficient and accurate numerical methods for calculating flow sensitivities in the presence of discontinuities and complexities. The new methods should rely on solving the problems in the different subregions between the discontinuities. This will result in a coupled set of problems where the discontinuities provide the boundary conditions for the different subproblems. The focus should be on automatically setting up the subregions and interior discontinuity boundary conditions.

Bibliography

[1] Appel, J.R., Godfrey, A.G., Gunzburger, M.D., and Cliff, E.M., "Optimization-Based Design In High-Speed Flows," *Proceedings 1995 ASME Mechanical Engineering Congress And Exposition*, Fed-Vol. 232, CFD for Design and Optimization, San Francisco, CA, 195, pp. 61-68.

[2] Applebaum, M.P. and Walters, R.W., *UCFD, An Unstructured Computational Fluid Dynamics Package*, Virginia Tech, Blacksburg, VA, 1995.

[3] Baysal, O., Editor, *Proceedings 1995 ASME International Mechanical Engineering Congress and Exposition*, FED-Vol. 232, CFD for Design and Optimization, San Francisco, CA, 1995, pp. 1-91.

[4] Bischof, C., Carle, A., Khademi, P., Mauer, A., and Hovland, P., *ADIFOR 2.0 User's Guide*, Center for Research on Parallel Computation, Technical Report CRPC-95516-S, August, 1995.

[5] Bischof, C., Khademi, P., Mauer, A. and Carle, A., "Adifor 2.0: Automatic Differentiation of Fortran 77 Programs," *Computational Science and Engineering*, Vol. 3, Num. 3, 196, pp. 18-32.

[6] Bischof, C., Jones, W., Mauer, A., and Samareh, J., "Application of Automatic Differentiation to 3-D Volume Grid Generation Software," *Proceedings 1995 ASME Mechanical Engineering Congress And Exposition*, Fed-Vol. 232, CFD for Design and Optimization, San Francisco, CA, 1995, pp. 17-22.

[7] Borggaard, J.T., "The Sensitivity Equation Method for Optimal Design," Ph.D. Dissertation, Virginia Polytechnic Institute and State University, 1994.

[8] Borggaard, J.T., Burns, J.A., Cliff, E.M. and Gunzburger, M.D., "Sensitivity calculations for a 2D, inviscid, supersonic forebody problem," *Identification and Control of Systems Governed by Partial Differential Equations*, H.T. Banks *et al.*, ed., SIAM Publications, Philadelphia, PA, 1993.

[9] Burgreen, G.W., "Three-Dimensional Aerodynamic Shape Optimization Using Discrete Sensitivity Analysis," Ph.D. Thesis, Old Dominion University, May 1994, pp. 18-19.

[10] Burkardt, J.V., "Sensitivity Analyses and Computational Shape Optimization of Incompressible Flows," Ph.D. Dissertation, Virginia Polytechnic Institute and State University, 1995.

[11] Cliff, E.M., Heinkenschloss, M., and Shenoy, A.R., "On The Optimality System For A 1-D Euler Flow Problem," AIAA Paper 96-3933, Sept. 1996.

[12] Cliff, E.M., Heinkenschloss, M., and Shenoy, A.R., "An Optimal Control Problem for Flows with Discontinuities," *Journal of Optimization Theory and Applications*, Vol. 94, August 1997.

[13] Cliff, E.M. and Shenoy, A.R., "An Optimal Control Formulation For A Flow Matching Problem," *Proceedings 5th AIAA/USAF/NASA/ISSMO Symposium of Multidisciplinary Analysis and Optimization*, 1994, pp. 520-528.

[14] Courant, R. and Friedrichs, K.O., *Supersonic Flow and Shock Waves*, Springer-Verlag, New York, 1948.

[15] Dennis, J.E. and Schnabel, R.B., *Numerical Methods for Unconstrained Optimization and Nonlinear Equations*, Prentice Hall, Englewood Cliffs, NJ, 1983.

[16] Dennis, J. and Torczon, V., "Direct Search Methods on Parallel Machines," *SIAM Journal on Optimization*, Vol. 1, No. 4, Nov. 1991, pp. 448-474.

[17] Dongarra, J. and Grosse, E., "Distribution of Mathematical Software Via Electronic Mail," *Communications of the ACM*, Vol. 30, 1987, pp. 403-407.

[18] Eyi, S. and Lee, K.D., "Effects of Sensitivity Analysis on Aerodynamic Design Optimization," *Proceedings 1995 ASME International Mechanical Engineering Congress and Exposition*, FED-Vol. 232, CFD for Design and Optimization, ASME, San Francisco, CA, 1995, pp. 1-8.

[19] Gay, D.M., "Algorithm 611 Subroutines for Unconstrained Minimization Using a Model/Trust-Region Approach," *ACM Transactions on Mathematical Software*, Vol. 9, No. 4, December 1983, pp. 503-524.

[20] Glowinski, R., Pan, T.-W, Kearsley, A.J., and Periaux, J., "Numerical Simulation and Optimal Shape for Viscous Flow by a Fictitious Domain Method," *International Journal for Numerical Methods in Fluids*, Vol. 20, 1995, pp. 695-711.

[21] Godlewski, E. and Raviart, P., *Numerical Approximation of Hyperbolic Systems of Conservation Laws*, Springer-Verlag, New York, 1996.

[22] Griewank, A., and Corliss, G. (Eds), *Automatic Differentiation of Algorithms: Theory, Implementation, and Applications*, SIAM Publications, Philadelphia, PA, 1991.

[23] Hirsch, C., *Numerical Computation of Internal and External Flows, Vol. 1*, John Wiley and Sons, New York, NY, 1990.

[24] Hirsch, C., *Numerical Computation of Internal and External Flows, Vol. 2*, John Wiley and Sons, New York, NY, 1990.

[25] Huddleston, D., "Development of a free-jet forebody simulator design optimization method," *Tech. Rept. AEDC-TR-90-22*, Arnold Engineering Development Center, Arnold AFB, TN, 1990.

[26] Jameson, A., "Optimum Aerodynamic Design Using CFD and Control Theory," AIAA Paper 95-1729, June 1995.

[27] Kowalik, J. and Osborne, M., *Methods for unconstrained Optimization Problems*, American Elsevier Publishing Co., New York, 1968.

[28] LeVeque, R.J., *Numerical Methods for Conservation Laws*, Birkhäuser Verlag, Basel, Germany, 1991.

[29] LeVeque, R.J., 1995, "CLAWPACK Users Notes", (available: **http://www. netlib. org/pdes/claw/doc/**).

[30] LeVeque, R.J., and Zhang, C., "The Immersed Interface Method For Acoustic Wave Equations with Discontinuous Coefficients", to appear *Wave Motion*.

[31] Liepmann, H.W. and Roshko, A., *Elements of Gas dynamics*, John Wiley and Sons, New York, NY, 1965.

[32] McGrory, W., Slack, D.C., Applebaum, M.P. and Walters, R.W., $\mathcal{GASP}$ *: The General Aerodynamic Simulation Package*, Version 2.2, User's Guide, AeroSoft Inc., Blacksburg, VA, 1993.

[33] Narducci, R.P., "Selected Optimization Procedures for CFD-Based Shape Design Involving Shock Waves or Computational Noise," Ph.D. Dissertation, Virginia Polytechnic Institute and State University, May 1995.

[34] Narducci, R.P., Grossman, B., and Haftka, R.T., "Sensitivity Algorithms for an Inverse Design Problem Involving a Shock Wave," *Inverse Problems in Engineering*, Vol. 2 Overseas Publishers Association, Amsterdam, 1995, pp. 49-83.

[35] Newman III, J.C. and Taylor III, A.C., "Three-Dimensional Aerodynamic Shape Sensitivity Analysis and Design Optimization Using the Euler Equations on Unstructured Grids," AIAA Paper 96-2464, June 1996.

[36] Newman III, J.C. and Taylor III, A.C., "An Unstructured Grid Approach to Sensitivity Analysis and Shape Optimization Using the Euler Equations," AIAA Paper 95-1646, June 1995.

[37] Protter, M.H. and Morrey, C.B., *A First Course in Real Analysis*, Springer-Verlag, New York, 1977.

[38] Reuther, J. and Jameson, A. "Supersonic Wing and Wing-Body Shape Optimization Using an Adjoint Formulation," *Proceedings 1995 ASME International Mechanical Engineering Congress and Exposition*, FED-Vol. 232, CFD for Design and Optimization, San Francisco, CA, 1995, pp. 45-52.

[39] Renardy, M. and Rogers, R.C., *An Introduction to Partial Differential Equations*, Texts in Applied Mathematics, Vol. 13, Springer Verlag, New York, 1993.

[40] Sod, G.A., "A Survey of Several Finite Difference Methods for Systems of Nonlinear Hyperbolic Conservation Laws," *Journal of Computational Physics*, Vol. 27, 1978, pp. 1-31.

[41] Strang, G., "On the Construction and Comparison of Difference Schemes," *SIAM Journal of Numerical Analysis*, Vol. 5, 1968, pp. 506-517.

[42] Taylor III, A.C., Hou, G.W., and Korivi, V.M., "An Efficient Method For Estimating Neighboring Steady-State Numerical Solutions To The Euler Equations," AIAA Paper 91-1680, June 1991.

[43] Taylor III, A.C., Hou, G.W., and Korivi, V.M., "A Methodology for Determining Aerodynamic Sensitivity Derivatives with Respect to Variation of Geometric Shape," AIAA Paper 91-1101, 1991.

[44] Taylor III, A.C., Hou, G.W., and Korivi, V.M., "Sensitivity Analysis Applied to the Euler Equations: A Feasibility Study with Emphasis on Variation of Geometric Shape," *Proceedings of 29th Aerospaces Sciences Meeting*, AIAA Paper 91-0173, 1991.

[45] Taylor III, A.C., Hou, G.W., and Korivi, V.M., "Sensitivity Analysis, Approximate Analysis and Design Optimization for Internal and External Viscous Flows," *Proceedings of AIAA Aircraft Design Systems and Operations Meeting*, AIAA Paper 91-3083, 1991.

[46] Warming, R.F. and Hyett, B.J., "The modified Equation Approach to the Stability and accuracy Analysis of Finite-Difference Methods," *Journal of Computational Physics*, 14, 1974, pp. 159-179.

[47] Zachmanoglou, E.C. and Thoe, D.W., *Introduction to Partial Differential Equations with Application*, Dover, Toronto, Ontario, Canada, 1976.

VITA

Justin Ronald Appel was born in Miles City, Montana. He graduated in May 1988 from Shepherd High School in Shepherd, Montana and went on to the University of Montana to pursue studies in preLaw. Justin soon learned he was more scientifically and analytically inclined and transferred to Montana State University where he graduated in May 1992 with a Bachelor of Science in Mathematics. He then moved to Blacksburg, Virginia where he began pursuing a Doctorate of Philosophy in Mathematics at Virginia Polytechnic Institute and State University. Justin received his Master of Science in Mathematics from Virginia Polytechnic Institute and State University in December of 1994. He spent the next several years conducting research on flow sensitivities under the advisement of Dr. Max Gunzburger. This dissertation concludes the requirements for his Ph.D. degree and Justin will graduate in May of 1997 from Virginia Polytechnic Institute and State University.